POLITECNICO DI TORINO

Corso di Laurea Magistrale

in Ingegneria Civile

Tesi di Laurea Magistrale

High-rise buildings in Turin between the 20th and 21st centuries

- Historical background and structural analysis using the General Algorithm -

Relatore

prof. Giuseppe Lacidogna

Correlatori

ing. Giuseppe Nitti

prof. Alberto Carpinteri

Candidato

Ilario Attisano

Marzo 2025

Alla mia famiglia,

A mia madre.

Sommario (Italiano)

La presente tesi si propone di analizzare cinque edifici alti situati nella città di Torino, selezionati per il loro interesse strutturale.

Nella prima parte del lavoro viene esaminata l'evoluzione urbanistica della città, con particolare attenzione al XX secolo, a partire dal 1934, anno della costruzione della Torre Littoria, e al XXI secolo, concludendo l'analisi nel 2022, anno in cui è stato completato il Grattacielo della Regione Piemonte. Successivamente, vengono illustrati i principi fondamentali dell'ingegneria strutturale applicata agli edifici alti, con un approfondimento sui principali sistemi di stabilizzazione strutturale, quali nuclei rigidi, controventi e altri dispositivi progettati per contrastare le azioni esterne, quali il carico del vento e gli effetti sismici.

La seconda parte della tesi è dedicata alla trattazione teorica dell'Algoritmo Generale, un modello analitico finalizzato alla determinazione degli spostamenti trasversali degli elementi costituenti il sistema resistente degli edifici alti. Inoltre, vengono esaminate la teoria di Vlasov, utile per la valutazione della torsione esterna, del warping e delle sollecitazioni indotte dal momento torsionale secondario, e la teoria di Capurso, impiegata per lo studio della distribuzione dei carichi orizzontali tra le sezioni sottili dell'edificio.

L'ultima parte del lavoro è dedicata all'analisi dei casi studio selezionati: la Torre Littoria, la Torre BBPR, il Grattacielo RAI, il Grattacielo Intesa Sanpaolo e il Grattacielo della Regione Piemonte. Per ciascun edificio è stata condotta un'analisi statica e dinamica, dapprima mediante l'applicazione dell'Algoritmo Generale e successivamente attraverso un software di analisi agli elementi finiti (FEM), al fine di confrontare i risultati ottenuti tramite i due metodi.

L'obiettivo della presente ricerca è duplice: da un lato, indagare il processo di modernizzazione urbana della città di Torino e il suo confronto con le grandi metropoli internazionali, quali ad esempio Chicago e New York; dall'altro, verificare la validità e l'efficacia dell'Algoritmo Generale come strumento per la progettazione preliminare degli edifici alti.

Parole chiave: Edifici alti, Torino, Comportamento strutturale, Algoritmo Generale, Teoria di Vlasov, Teoria di Capurso.

Abstract (English)

This thesis examines the structural analysis of five tall buildings in the city of Turin, selected for their architectural and engineering significance.

The initial section provides a historical and urban development context, with a particular focus on the 20th and the 21th centuries, spanning from 1934 — the year of the construction of the Littoria Tower — to 2022, when the Piedmont Region Headquarters Tower was completed.

Subsequently, the fundamental principles of structural engineering relevant to tall buildings are discussed, with an emphasis on structural stabilization systems (e.g. cores, bracing, etc.), which play a crucial role in counteracting external forces such as wind loads and seismic actions.

The following section explores the theoretical foundations of the General Algorithm, an analytical model designed to determine the transverse displacements of the structural elements forming the resisting system of a tall building.

Additionally, Vlasov's theory is presented for evaluating external torsion, warping, and stresses induced by the secondary torsional moment, along with Capurso's theory, which is employed to analyze the distribution of horizontal loads across the thin sections of a building.

Finally, a comprehensive static and dynamic analysis of the selected buildings is conducted, first utilizing the General Algorithm and subsequently employing the Finite Element Method (FEM) software. The results obtained from these two approaches are then compared to assess their consistency and reliability.

The primary objectives of this thesis are twofold: first, to evaluate Turin's potential to evolve into a modern metropolis comparable to major international cities such as Chicago or New York; and second, to highlight the relevance and applicability of the General Algorithm as a valuable tool for the preliminary design of tall buildings.

Keywords: Tall Buildings, Turin, Structural Behaviour, General Algorithm, Vlasov's Theory, Capurso's Theory.

Contents

1 Introduction to Turin's urban history

This chapter provides a concise reconstruction of the urban planning history of Turin, drawing upon the Faraggiana's book [14] and the articles by Rolando [18] and by Martini & Rolfo [19].

The city of Turin was originally established as an ancient Roman castrum, or military citadel. The layout of the city exhibited a nearly square configuration, with sides measuring approximately 720 meters and 660 meters, respectively. The urban plan featured a checkerboard pattern, with streets arranged according to a square-mesh grid, with a spacing of approximately 75 meters. The width of the streets exhibited a range from a minimum of approximately 4-5 meters to a maximum of 8 meters. The two primary street axes, the *Decumanus Maximus* and the *Cardo Maximus*, constituted the two central streets orthogonal to each other, with the four city gates positioned at their extremities (Figure 1.1).

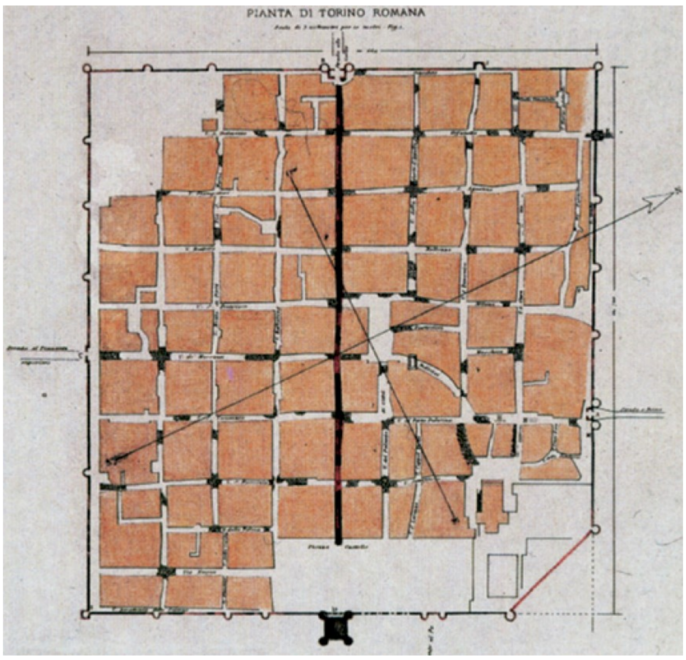

Figure 1.1: Plan of Roman Turin

The urban perimeter along which the walls were erected roughly corresponds to the following present-day streets:

- to the south, via Santa Teresa and via Cernaia;
- to the west, Corso Giuseppe Siccardi and Via della Consolata;
- to the north, via Carlo Ignazio Giulio, piazza Emanuele Filiberto and Porta Palatina;
- to the east, the wing of the Royal Palace toward Piazza Castello and the line between the blocks of Via Roma and Via Accademia delle Scienze.

The two axes of the city were oriented one according to the level line and the other according to the line of maximum slope, directions roughly parallel to the beds of the two rivers Po and Dora Riparia. The decumanus, corresponding to the present-day Via Garibaldi, aligned with the direction of maximum slope, which is found to be parallel to the riverbed of the Dora. The layout of the city is such that its sides are oriented parallel to the riverbeds, and the directions of the streets are tilted at an angle of approximately 26 degrees relative to the cardinal points.

In the 16th century, Turin became the capital of the Duchy of Savoy. Consequently, an urban renewal and expansion of the city ensued, resulting in the creation of a more grandiose and functional urban landscape suited to its new role as the capital. A notable transformation involved the strategic positioning of Piazza Castello at a central point within the urban grid. Additionally, Via Po was integrated into the urban infrastructure, positioned at an angle to the decumanus, thereby creating a direct connection between Piazza Castello and the bridge over the Po River.

The expansion of 1620 extended southward, involving the demolition of a section of the Roman wall, the creation of Piazza Reale (now Piazza San Carlo), the extension of Via Nuova, and the construction of Porta Nuova, located at the southern end of the city. The architectural design of the blocks featured increased dimensions, and the buildings situated along the primary thoroughfares were required to have continuous fronts and a minimum height of three stories above ground. This approach resulted in a more regular and orderly urban layout, accentuating the effect of line escapes to the horizon.

A subsequent phase of expansion toward the east occurred in 1673, marked by the construction of Via Po and the significant rise in importance of the Via contrada di Santa Teresa (presently Via Santa Teresa and Via Maria Vittoria), which connected the Cittadella with the embankments toward the Po. In order to endow the city with the requirements that would elevate it to a European capital, Amedeo di Castellamonte designed the urban layout and architecture of the buildings in such a way that there were wide, straight streets, wide squares, arcades, and regularity in the façades of the buildings.

The third expansion, which took place in 1702, involved the interior of the new fortifications on the west side of the old city. The primary artery, conceived by Filippo Juvarra, was the Via di Susa (presently Via del Carmine), which traversed the newly constructed Porta Susina. Subsequently, the Via Dora Grossa (today Via Garibaldi) was rebuilt, thereby reassuming the pivotal function of the ancient decumanus. The urban landscape underwent a transformation, transitioning from a square configuration, characteristic of the castrum, to an oval shape encircled by the newly constructed ramparts. Additionally, the orientation of the streets was strategically designed to create a focal point, offering views of the Royal Palace and Piazza Castello, symbols of authority and power (Figure 1.2).

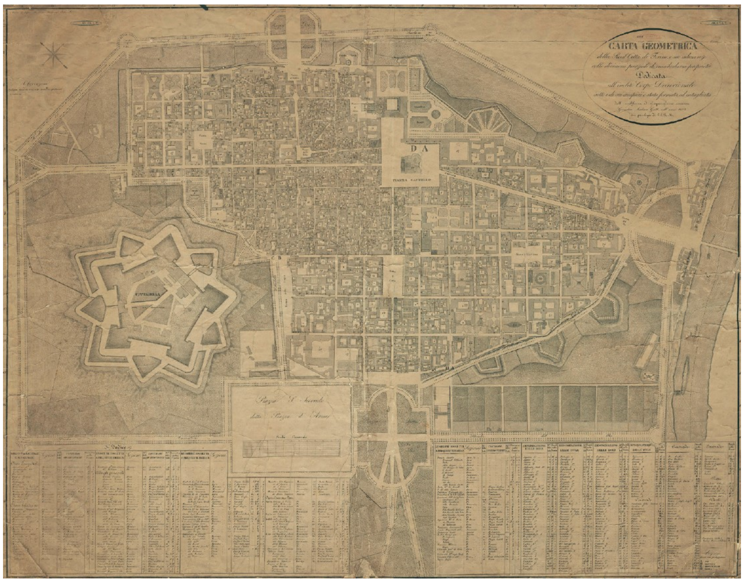

Figure 1.2: Plan of Turin designed in 1823

In the early 19th century, following a Napoleonic edict, the walls surrounding the city were demolished. In addition, the city was free to expand in every direction except westward, where the citadel fortification was located, which was dismantled only in 1856. During the Napoleonic era, significant urban planning initiatives were proposed; however, the only notable construction that was completed was the new bridge over the Po, which was finished in 1813.

Following the restoration of monarchical power and the return of King Vittorio Emanuele, the initial areas of expansion included Piazza Vittorio Emanuele I (presently known as Piazza Vittorio Veneto), extending southward to the newly constructed Viale del Re (today known as Corso Vittorio Emanuele II).

By the late 1840s, the development of the city had expanded to encompass the area between the major ring roads, which are now known as Corso Cairoli, Corso Vittorio Emanuele II, Corso Inghilterra, Corso Principe Eugenio, Corso Regina Margherita, and Corso San Maurizio. The city maintained a centralist arrangement, with the center of power identified through the convergence of the city rectorial axes. These axes, emanating from Piazza Castello and Piazza Palazzo di Città, intersected with the primary entry points to the city, thereby forming four squares: Piazza Vittorio Veneto, Piazza della Repubblica, Piazza Statuto, and Piazza Carlo Felice.

During this period, the city began to expand due to population growth, which resulted in the formation and development of the neighborhoods outside the circuit of the main boulevards: Borgo San Salvario, Borgo Nuovo, Borgo San Donato, Valdocco, Borgo Dora, Vanchiglia, and Borgo Po.

Between 1864 and 1868, the enlargement plans, known as the *"Pecco Plans"*, marked the beginning of the abandonment of the orthogonal grid oriented according to the original axes. The formation of outer aggregations resulted in the emergence and growth of outer townships, characterized by less stringent building constraints and street layouts that deviated from the rigid patterns prevalent within the customs ring (Figure 1.3).

By the early 20th century, the city had saturated the spaces within the perimeter of the city walls, and since 1887, growth outside them had also been regulated. Throughout the century, Turin successfully preserved its distinctive *"Sabaud"* character, maintaining a compact, strongly *"horizontal"*, and *"perspective machine"* at the urban scale, keeping pace with newness and modernity.

The vertical growth of Turin has occurred over the past century and a half, marked by a "push" upward, with various attempts to deviate from the uniformity of the urban grid. The main features of this grid are its recognizability, continuity, and clarity.

Turin first real tall building, the *Mole Antonelliana*, was constructed in 1863 as the city first synagogue, commissioned by the Israelite University. Standing at 167.5 meters in height, it was the most elevated masonry edifice constructed up to that time. In 1877, the edifice was acquired by the city of Turin, initially serving as a monument dedicated to Vittorio Emanuele II and subsequently as a

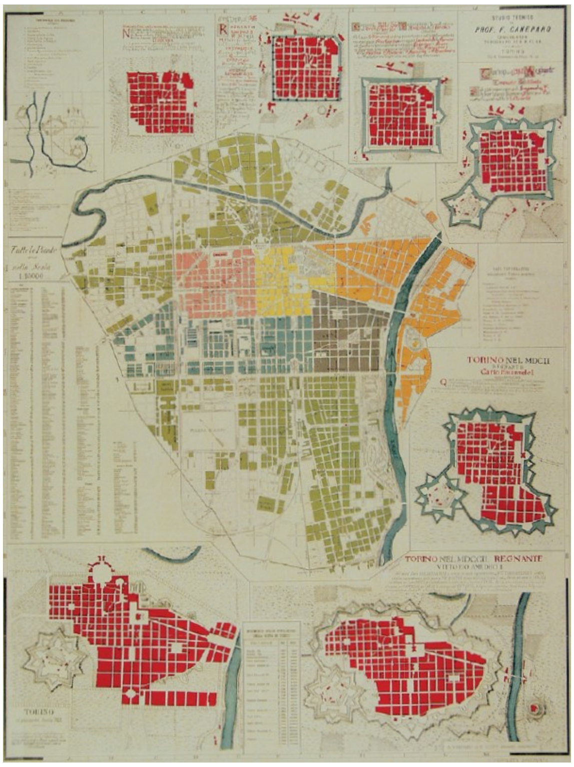

Figure 1.3: Plan of Turin designed in 1892, showing the different stages of urban development since medieval times

museum of Italian Independence. The edifice underwent further alterations with the construction of the conical spire with the Winged Genius at its summit (replaced in 1904 with a star), and it was rebuilt with a metal structure following the 1953 hurricane that demolished the entire spire.

Another notable example of a tall building are the *Rivella Towers*, constructed in 1929 behind the Giardini Reali, at the entrance with Corso Regio Parco. These two buildings, each seven stories in height, including the spire, are designed as "twin" structures, intended for residential and commercial use on the ground floors. The architectural style of these buildings can be characterized as geometrized Art Deco, a term used to describe a style characterized by horizontal bands of exposed brick and light plaster. These bands serve to reinterpret the "urban gateway" motif, which is a point of access to the urban *boulevard*.

The first skyscraper in Turin, the *Littoria Tower* (today knows as Reale Mutua Tower), was constructed in 1935. The Fascist regime authorized the construction of this building as a symbol of its newly asserted power and the culmination of the renovation of Via Roma. The Littoria Tower interrupted the homogeneity of the city skyline, which was characterized by an essentially flat pattern of architecture, from which the bell towers and domes of sacred buildings emerged, with the exception of the Mole Antonelliana. The Littoria Tower, a testament to 20th-century urban renewal, stands as a 19-story structure, measuring 87 meters in height (109 meters with the top metal antenna). It embodies rationalist architecture, a style associated with the international Modern Movement. The tower's design features a steel load-bearing structure, where the horizontal course of the lower portion of the block, accentuated by travertine moldings and the system of windows constricted within wide brick banded fields, contrasts with the markedly verticalized course of the upper volume. The Littoria Tower, a structure whose construction was originally intended to serve as the headquarters for the Fascist National Party, was instead designed to house offices and luxury residential units.

In the post-World War II era, spanning from the 1950s to the 1960s, Italy witnessed a substantial expansion of its large-scale facilities sector. This development was driven by several factors, including postwar reconstruction efforts, the implementation of a comprehensive highway infrastructure plan, and the hosting of significant events such as the 1960 Olympics in Rome and the 1961 Turin celebrations.

In Turin, the adoption of the new master plan, drafted by Annibale Rigotti and approved in 1959, marked the phase of postwar reconstruction, during which thousands of building applications were authorized and a number of small skyscrapers were permitted in the historic center, which had been damaged by bombing.

A notable example of this period is the *Lancia Palace*, constructed in 1957 to house the offices of the Turin-based automobile company. This structure, with its 16 floors and a height of 73 meters, is distinguished by its distinctive bridge-like shape, spanning Via Lancia, made possible by the use of reinforced concrete truss beams resting on two dihedral bases, with the vertical connections strategically positioned. The office spaces are distributed along the two glazed façades, while the services, stairways, and elevators are situated in the two trapezoidal plan ends. Both primary façades are adorned with expansive mirrored windows, while the side elevations feature recessed windows that extend along the full height of the building.

In 1961 the *BBPR Tower* was built, a building complex comprising residential and office spaces for Reale Mutua Assicurazioni. The complex consists of five to ten stories, with a tower reaching 14 stories, situated at the intersection of Corso Francia and Piazza Statuto. The complex, designed by the BBPR firm, is an example of brutalist architecture, an architectural current named after the French term *"béton brut"* meaning reinforced concrete left exposed, and which aims to show the roughness of things simply for what they are. The integration of the building with the surrounding urban environment is achieved through the ground attachment, which features a high porch designated for commercial use, including a mezzanine. The roofs, due to the setback of the top floor, visually rest lightly on the bodies below. A set-back loggia ensures continuity along the uppermost line of the lower body, situated between the tower and the body of intermediate height, thereby subdividing the more substantial volume into two overlapping components. The structure is composed of reinforced concrete, which is either sprayed, hammered, or trachyte-covered, depending on the specific technique employed. The foundation of the structure is the pillars of the portico, which remain visible, creating a contrast with the infilled areas of face brick.

The *SIP Palace*, now the building of the Province of Turin, was constructed in the area of the new Porta Susa station on Corso Inghilterra in 1962. The edifice, conceptualized as a"horizontal skyscraper", with its 18 floors reaches a height of 65 meters; moreover, the main façade is punctuated by the dense repetition of pilasters, between which large windows open.

In 1968, the *Rai skyscraper*, which houses the offices of the public service corporation, was constructed on the southeastern side of Piazza XVIII Dicembre. The 19-story, 72-meter-high building is attached to two lower structures that align with and maintain the proportions of the porticoes of Via Cernaia. The vertical development of the structure is accentuated by the façade partitions, and is concluded with a large canopy on the top terrace that forms a "shutter rebate" proportionate to the scale of the entire building.The steel structure is covered by aluminum and glass curtain walls, whose regular and proportionate scanning, together with the attention to detail exhibited in the iron and stone works, evokes New York precedents.

The advent of the 2000s witnessed the onset of a transformative epoch in urban landscapes, marked by the availability of substantial industrial areas that had been left unoccupied and the allocation of considerable capital for major public construction projects. The impetus for this transformation was the approval of the new Master Plan in 1995, which was developed by the Gregotti Associati firm. This plan was accompanied by the Strategic Plan and the Turin 2006 Olympic event, which served as the host city for the 20th Winter Olympic Games.

In particular, the Master Plan envisaged the centralization of the so-called *"Spina Centrale"* a large urban area located on the site of the old railway, which runs north-south in the municipal territory, in an almost barycentric position with respect to the city context, and which is divided into four sections starting from Largo Filippo Turati and ending in Corso Grosseto. A strip of about 4 kilometers on the edge of the railway line was thus redesigned, with the total burying of the line and the quadrupling of the tracks to allow for an integrated public transport service, including High Speed Rail. In addition, tall buildings were planned in various places because of the demand for density, which, according to administrators, would increase the value of the areas involved.

In 2006, the City Council authorized a series of variants to the Master Plan, thereby eliminating the previously established height limit for buildings. This was done in order to ensure that the tallest building in the city would be the Mole Antonelliana, the symbol of the city.

Consequently, the *Sanpaolo Tower*, a 166-meter-high structure designed by Renzo Piano for the city primary banking group, was constructed in 2012. The skyscraper's architectural style aligns with Piano's design for the headquarters of the 'New York Times', characterized by a glass prism structure that obscures the building's framework, thereby creating a traversable and transparent space. The skyscraper demonstrates a commitment to sustainability, featuring a double-glazed skin, extensive use of solar panels, and maximization of natural lighting. The skyscraper embodies Piano's philosophy that technological advancements should be designed to serve the needs of the client, the users, and the environment.

In conclusion, the year 2022 marked the completion of the *Piedmont Region Headquarters Tower*, which currently stands as the tallest building in the city, reaching a height of 209 meters. Initially, the building was to have been erected on the former Metaferro area, situated between Corso Lione and Corso Mediterraneo, at the terminus of "Spina 1", but was subsequently relocated in 2006-07 to the former ex-FIAT Avio area, located to the south of Lingotto. In this new configuration, the structure plays a pivotal role in the urban redevelopment program of the area owned by RFI (Italian railway network) around the Oval. This program envisions a mix of residential, tertiary, commercial, and hospitality activities, and the structure acts as a pivot between the Via Nizza axis and the urban space behind (Figure 1.4).

Figure 1.4: Planimetry of the city of Turin in the present day

2
Construction types of tall buildings

2.1 Definition of tall building

The definition of a *"tall building"* [32] is a relative matter that depends on the location and, in particular, the city, in which the building is located. It is therefore not possible to define a tall building according to its width or number of storeys, because, for example, in Europe a 20-storey building could be considered tall, while in America, in cities where there are several skyscrapers, the same building would not be considered tall; this is because the concept of a tall building depends on the context and therefore on people's perception. It is therefore not possible to provide a measurable definition of a tall building. The dividing line for the definition of a tall building can be the structural design.

From a structural point of view, a building is considered tall when its design and analysis are influenced by horizontal loads. The most important horizontal actions affecting a building are wind and earthquake: dynamic forces that hypothetically lie on a horizontal plane but whose direction can be entirely arbitrary. Structural elements must therefore be designed to absorb the stresses arising from these actions.

Compared to vertical loads, lateral loads acting on buildings vary greatly and increase rapidly with height. Therefore, the problem in the construction of tall buildings consists in analysing the effects of horizontal actions on the structure. Structural elements are intended to absorb horizontal forces and provide the structure with adequate strength and stiffness to ensure acceptable deformations of the building.

2.2 General design criteria

In the early design stages, it is important that all professionals in the design team cooperate to meet the functionality, safety and maintainability requirements of the building. In particular, the structural layout will be subordinate to the architectural requirements for the interior space layout and aesthetics of the building.

The main design criterion is therefore architectural, as it is essential to ensure an appropriate arrangement of the interior spaces; therefore, to meet the functional requirements of the building, the structural system must be as unobtrusive as possible.

From a structural point of view, the criteria that must be ensured are: an adequate reserve of resistance against structural failure, an adequate reserve of lateral stiffness and efficient performance during the life of the building. It is also important that these requirements are achieved as efficiently and economically as possible. In addition, it must be ensured that the entire structure and its components are designed to ensure adequate durability and to withstand with adequate safety the most unfavourable loads and deformations that may occur during the construction phases and the service life of the structure.

The primary load-bearing elements in tall buildings are columns and walls. Columns primarily transfer both gravity and lateral loads, while walls, functioning as shear walls or cores, provide structural stability by resisting lateral forces. Additionally, these walls often enclose interior spaces and may incorporate essential building services, such as elevator shafts.

In the design process, an in-depth knowledge of the structural components of high-rise buildings and their behaviour is essential in order to conceive a resistant system adequate for the loads it is subjected to. The main function of the structure is to respond to external vertical (dead loads, live loads) and horizontal (wind, earthquake) actions with sufficient stiffness and strength and to remain stable under the action of the loads. Since the system must be efficient, economical and guarantee the minimisation of structural penalties due to height, while maximising the fulfilment of maintainability requirements, a precise and correct analysis of the structure is necessary.

A first fundamental aspect concerns the position of the centre of gravity of the masses and the centre of gravity of the stiffnesses. For the determination of the latter, the spatial arrangement and dimensioning of the bracing elements play a crucial role. Furthermore, in order to reduce internal stresses in the structure, it is convenient to place the resisting elements as far as possible from the centre of gravity of the plan, thus maximising the resistant moment arm. In fact, pillars or septa tend to be positioned along the perimeter of the building in a symmetrical arrangement so that the stresses in the various elements are uniform.

In the design, a linear elastic behaviour of the structure is assumed for which the

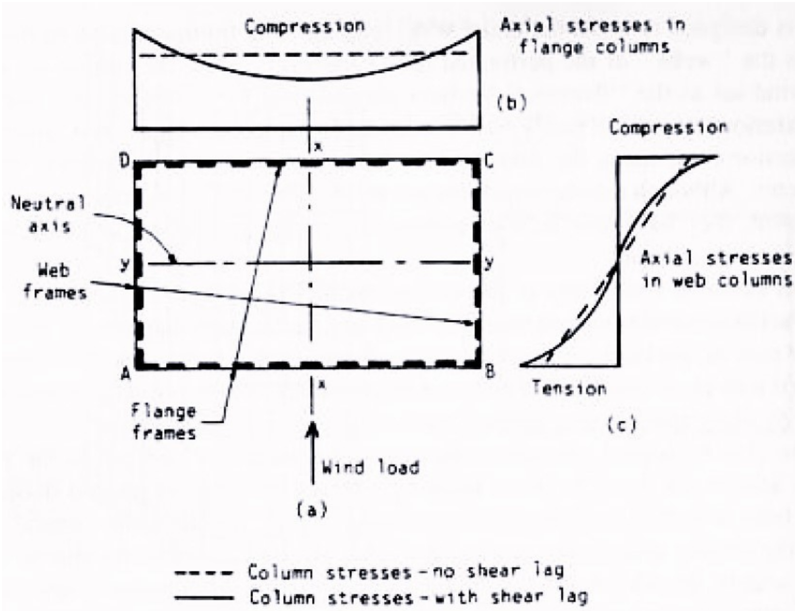

Figure 2.1: Stress development in a section with shear-lag phenomenon

assumption of preservation of flat sections applies; consequently, the stress trend in a section subject to bending is linear. In the case of slender elements, however, this statement is no longer valid and the stress distribution presents a non-linear trend on the faces parallel to the direction of force, with an increase at the edges and a reduction in the areas further away from them. This phenomenon is called *shear-lag* and it must be limited by a suitable connection of the vertical elements, so as to form rigid vertical planes and refer, to a good approximation, to the hypothesis of conservation of flat sections.

Another important aspect concerns stiffness, particularly lateral stiffness. A parameter for estimating the lateral stiffness of a building is the *drift index*, which is the ratio between the maximum displacement at the top of the building and its total height. Considering a single storey, the inter-storey drift index provides a measure of the possible local deformation.

Lateral displacements must be limited in order to prevent second-order deformation effects caused by gravitational loads. Deformations must be sufficiently small so as not to compromise the functioning of non-structural elements, to avoid excessive cracking that may lead to a loss of rigidity, to prevent redistribution of load between non-load-bearing parts and to prevent excessive movement of the structure that may compromise the comfort of persons.

A further aspect to consider is that, although the construction of large sections leads to an increase in their inertia with a consequent decrease in stresses, the sections may sometimes be too large. Therefore, it may be advantageous to construct numerous sections separate and adequately connected to each other in order to achieve behaviour similar to that of a rigid body.

Finally, a structural scheme that reduces the tension in the vertical resistance elements must be implemented to avoid uplift of the foundation and cracking of structural parts, which could compromise the stability and durability of the structure.

2.3 Main structural types

As has been noted by Taranath in [32] and by Stafford Smith in [30], the choice of structural scheme for a tall building, in addition to its ability to efficiently withstand different combinations of gravitational and horizontal loads, is influenced by other factors such as: the location and function of the building, the height and size of the building, the materials used and the nature and intensity of the horizontal load.

The main objective in choosing a structural scheme is to arrange the resisting elements in such a way that they support, with adequate strength and stiffness, the stresses induced by gravitational loads (dead loads and live loads) and horizontal loads (wind and earthquake). With respect to horizontal loads, a tall building can be considered a bracket embedded in the base. The structure may consist of one or more brackets acting individually, as shear walls or cores, or it may comprise walls and columns suitably connected by beams or braces. The stiffness and lateral resistance of the building can be further improved if the veritcal resisting elements have different free deflection characteristics and interact with each other via the slabs and connection beams.

In the following, the main structural schemes used for tall buildings are illustrated.

2.3.1 Frame system

A frame structure consists of grids of beams and columns connected by nodes that can be defined as rigid in that they have sufficient rigidity to maintain, under the action of the load, the angle at which the beam-column connection was designed. Thanks to their non-deformability, these connections provide the system with the necessary strength and stiffness (Figure 2.2).

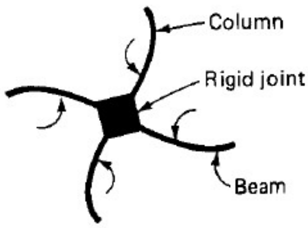

Figure 2.2: Rigid connection

The resistance to horizontal loads in a rigid frame system is given primarily by the bending resistance of the beams, columns and connections.

The total displacement caused by horizontal actions is the sum of a bending component and a shear component; in the case of tall buildings, the contributions of the two components are comparable.

The horizontal shear accumulated above each plane is counteracted by the shear of the columns in the plane under examination and the moment applied to the joint from the upper and lower columns is absorbed by the beams connected to that joint. The total deformation (Figure 2.3) shows a shear pattern with upwind concavity, maximum slope at the base and minimum slope at the top.

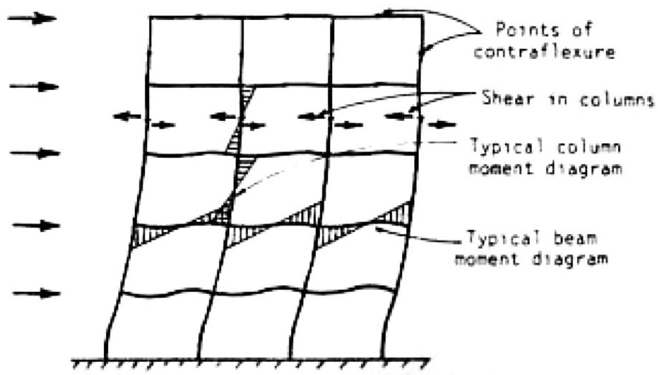

Figure 2.3: Rigid frame deformation

The total moment caused by the external horizontal load is counteracted at each storey by the torque resulting from the axial tensile and compressive forces in the columns on the opposite side of the structure. The extension and shortening of the columns determines the bending and horizontal displacements of the building; the displacement of the floors caused by the bending increases with height due to the rotation that accumulates upwards. This construction system is efficient for buildings not more than 30 storeys high; it also has the advantage of being able to create large meshes of beams and columns, which makes it possible to obtain ample space for the insertion of openings, which results in great freedom in the design of internal room distribution.

2.3.2 Braced systems

A bracing system consists of the insertion of diagonals between floors. This system increases resistance to horizontal actions as it allows the flexural component of beams and columns to be neglected by generating axial actions in its constituent elements.

The axial actions generated determine two different types of behaviour for the structural elements of the bracing: the columns show bending behaviour with maximum inclination at the top, while the beams show shear behaviour with maximum inclination at the base; the resulting behaviour of the system is therefore given by the sum of the two behaviours.

Two types of bracing exist in the literature:

- Concentric braced frames
- Eccentric braced frames

In concentric bracing, the axes of column, beam and rod intersect at a single node, so only axial action is generated; in the second type there is eccentricity between the rods and in this case shear and bending moment actions are generated in the beams.

The eccentric bracing system provides the structure with the rigidity typical of a bracing system and, at the same time, a dissipative capacity comparable to that of a frame with rigid nodes. The connection zone between the beam and the diagonals is called the *link* (Figure 2.4). Depending on the length of the latter, the behaviour is different: if the length is approximately twice the height of the beam, the link will be affected by the formation of a plastic hinge; if, on the other hand, the length is relatively short, shear yielding of the beam web will occur.

The lateral displacement of the system is the sum of several contributions:

- displacement due to axial forces in the diagonals
- displacement due to axial forces in the columns
- displacement due to bending deformation of the link

The final deformed configuration of the structure is given by the combination of the deformation of the bracing, which has a typical bending behaviour, and the deformation of the rigid node frame, which has a typical shear behaviour.

The choice of the type of bracing depends on the required stiffness, but is also influenced by the size of the openings in the architectural design, as diagonals hinder the planning of interior spaces, which is why such elements are usually incorporated into the walls.

2.3.3 Shear walls system

Shear walls are thin flat elements, generally made of reinforced concrete, which may form part of a core, a stairwell or partition walls between interior spaces (Figure 2.5). Usually, these elements are continuous up to the base to which they are rigidly attached by forming vertical brackets. Due to their high axial rigidity and strength, these construction systems are suitable for reinforcing buildings of up to approximately 40 storeys while supporting the gravitational load.

As a rule, the walls in plan are positioned in such a way that they attract a sufficient amount of their self-weight to suppress the maximum tensile bending stresses caused by the lateral load; in this way, only the minimum reinforcement of the wall is required.

Shear walls may have linear or L, T or U sections to better suit the design and to increase their flexural stiffness. The planimetric arrangement of the shear walls influences the position of the centre of stiffness, so the best positioning must be evaluated in order to reduce torsional effects as much as possible.

A shear wall system comprises a set of shear walls whose lengths and thicknesses may vary or which may be interrupted at various points along the vertical development, which results in a redistribution of moments and shear between the walls with the interacting horizontal forces in the connecting beams and floors.

It is possible to classify shear wall systems as either proportionate or non-proportionate. A proportionate system is characterised by a ratio of the bending stiffnesses of the walls that remains constant along their height. This system does not

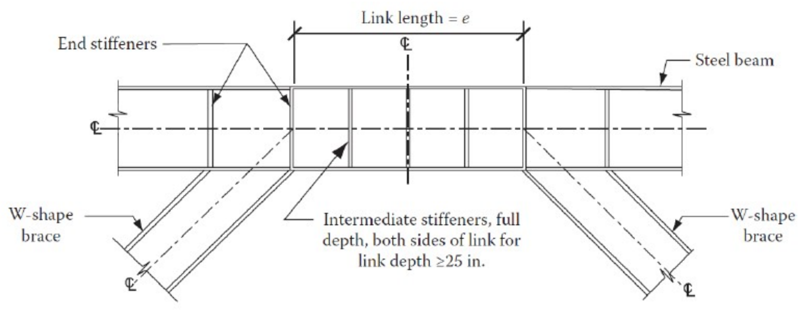

Figure 2.4: Link area in an eccentric bracing system

experience any redistribution of shear moments along the height. A non-proportional system, on the other hand, is one in which the ratio of flexural stiffnesses of the walls is not constant along the height. In planes where the stiffness changes, shear and moment redistribution occurs in the shear walls with corresponding horizontal interactions in the connection elements and there is the possibility of high local shear values occurring in the walls.

2.3.4 Coupled systems frames + shear walls

In this structural system, there is a combination of rigid frames, which tend to deform in shear, with shear walls, which tend to deform in bending, bound together in such a way that they have a common deformed configuration due to the horizontal stiffness of the beams and of the slabs (Figure 2.6). The shear walls and frames interact horizontally, especially at the top of the building, to create a more rigid and resistant structure; in particular, the walls reduce the rotations of the frames at the base of the building, while the frames reduce the rotations of the walls at the top.

In the design of tall buildings, it is assumed that the shear walls entirely resist all horizontal loads, while the frames are designed so that they only resist gravity loads.

This structural system is appropriate for buildings with between 40 and 60 storeys.

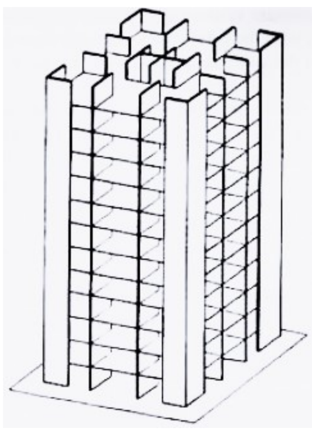

Figure 2.5: Shear walls structure

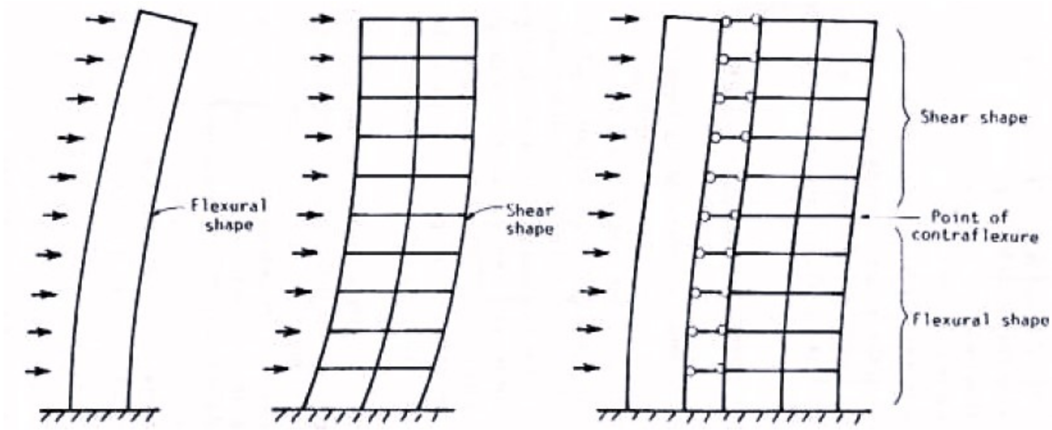

Figure 2.6: Shear wall-frame interaction

2.3.5 Tube systems

This structural solution consists of closely spaced external columns, connected around the perimeter by edge beams with high stiffness. In this type of structural solution, the elements responsible for resisting the vertical forces are located along the edges of the structure, which maximises the inertia of the building cross-section and thus its rigidity.

There are different categories of tubular structures:

- Framed tube structures
- Concentric tube structures
- Bundled structures

Framed tube structures consist of four rigid orthogonal frames, which in plan form a tube that is entirely responsible for resisting the wind load (Figure 2.7). The frames parallel to the wind direction act as the core, while the frames orthogonal to the wind action act as flanges. The vertical forces, on the other hand, are partly absorbed by the pipe itself and partly by the pillars or cores inside the plan through the floors connecting the vertical elements.

In order to obtain a sufficiently rigid tube, it is necessary for each frame to be sufficiently rigid, and this is achieved by using very tall and short beams; stiffening the latter is achieved by reducing their span, i.e. by placing the columns with a close spacing and increasing their height. Generally, columns are placed with a spacing between 1 m and 4.5 m, and height values between 60 cm and 130 cm are assumed for beams.

Due to the small spacing between the pillars, it is not possible to realise large openings; however, in some buildings it is possible to create them by using a large

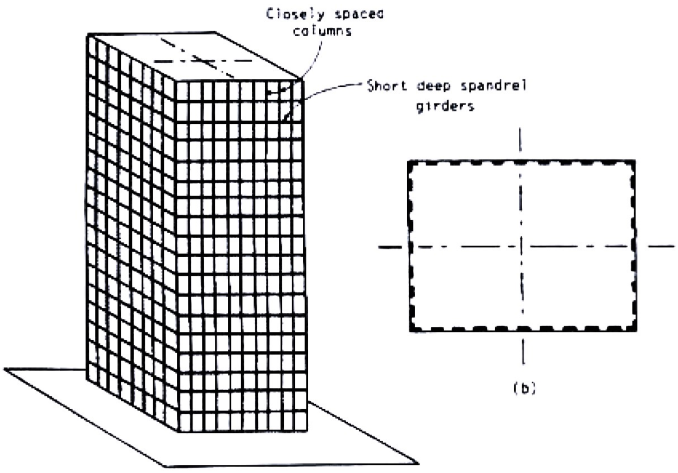

Figure 2.7: Framed-tube structure

transfer beam to receive and redistribute the vertical loads to the larger and more widely spaced pillars on the ground floor. Alternatively, several pillars can be joined by means of an inclined column arranged in such a way that fewer pillars can be placed on the lower floors.

When the structure is subjected to bending due to horizontal forces it behaves like a vertical bracket in which the upwind columns are subjected to tensile forces and the downwind columns to compressive forces. Shear action and in-plane bending, on the other hand, are mainly absorbed by the frames parallel to the lateral action. The efficiency of the system is closely linked to the geometry of the shape chosen for the building plan, such as the ratios of depth to width, and of height to width.

The deformability of the edge beams produces a *shear-lag* effect. This effect invalidates Navier's assumption of flatness of the sections after deformation has occurred and results in a non-linear stress trend along the faces parallel to the action, with increases at the edges, i.e. the edge columns, and decreases in the areas furthest from the edges themselves, i.e. the inner columns.

The main resistance is provided by the side panels which, as they deform, cause tension in the windward columns and compression in the leeward ones. The main interaction between the perimeter frames is manifested by the vertical displacements of the corner columns, corresponding to the shear of the beams of the flange frames which mobilises the normal stress in the flange columns. The deformations caused by compression are not equal in all columns, since the edge beam bends and the axial deformation of the adjacent columns is less by an amount that depends on the stiffness of the connection beam.

Since the external applied moment must be counteracted by the internal torque

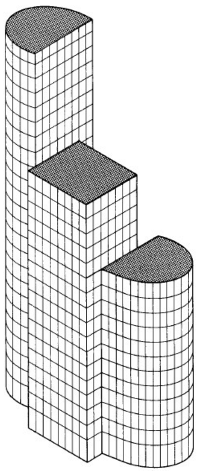

Figure 2.8: Bundled tube structure

resulting from the tensile and compressive forces on the opposite sides of the building, it follows that the stresses in the corner pillars will be greater than those resulting from purely tubular behaviour, while those in the internal pillars will be less. Since the column stresses are less effectively distributed than in a real tube, the resistant moment and flexural rigidity are reduced.

The effect of the shear-lag causes the floors to flex, as the flat cross-sections no longer remain flat, resulting in deformations of the internal partitions and secondary structural components, which increase cumulatively over the entire height of the building.

This structural system allows for buildings with more than 100 storeys.

Concentric tube structures involve the use, in addition to the outer tube, of an inner core that generally houses the lift shaft and the plant cavity.

This structural scheme therefore consists of two concentric tubes made integral with each other through the building floors; the outer shell and inner core work together to absorb horizontal and vertical forces.

Bundle structures involve the insertion of frames or shear walls coupled with inner frames that contribute to the stiffening of the outer shell. The main tube is thus subdivided into a bundle of tubes, each of which is smaller in size than the main tube, thus reducing the shear-lag effect (Figure 2.8).

When a tube bundle system is subjected to horizontal actions, the high stiffness of the floors determines the equality of the displacements of the inner frames and the outer tube. The proportion of lateral force absorbed by each inner frame is proportional to its stiffness. Consequently, columns further away from the corners

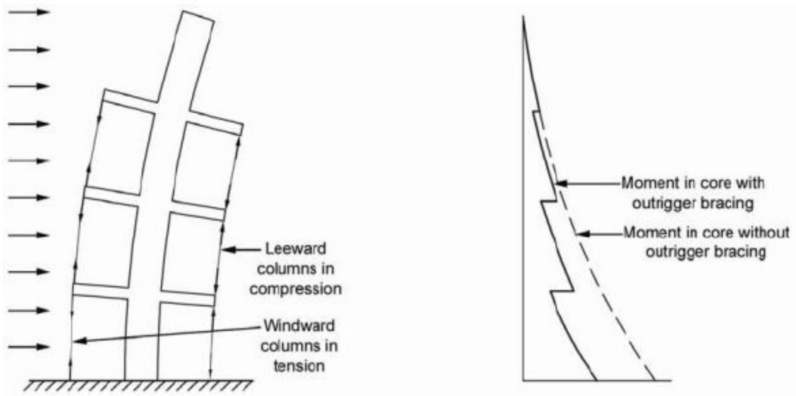

Figure 2.9: Outriggers structure behaviour

of the building are mobilised directly by the internal cores and therefore absorb a higher rate of axial action, deforming more.

The effect of shear-lag is greatly reduced and the structural behaviour approaches that of a real pipe.

This structural system allows for architectural solutions that enhance the function and form of the building.

2.3.6 Outriggers system

This structural system consists of a central core, made of reinforced concrete or a steel frame, braced and connected to the outer columns by means of bending-rigid horizontal beams, the so called *outriggers*.

When the building is subjected to horizontal forces, the columns constrained to the outriggers counteract the rotation of the core, reducing the bending moment and lateral displacements. As a result, the structure flexes as a vertical cantilever shelf, producing tension in the upwind columns and compression in the downwind columns (Figure 2.9).

Usually, edge beams with large cross-sections, also known as *belts* (Figure 2.10), are used, placed around the structure at the same level as the outriggers, which collaborate with the outriggers in resisting horizontal actions by mobilising the perimeter columns. In order to make the outriggers and belt girders sufficiently rigid in bending and shear, they are made at least one storey high, but often two. Due to their high thickness, in order to minimise their footprint, they are generally placed on the floors where the installations are located.

A building can also be effectively stiffened by means of a single level of outriggers

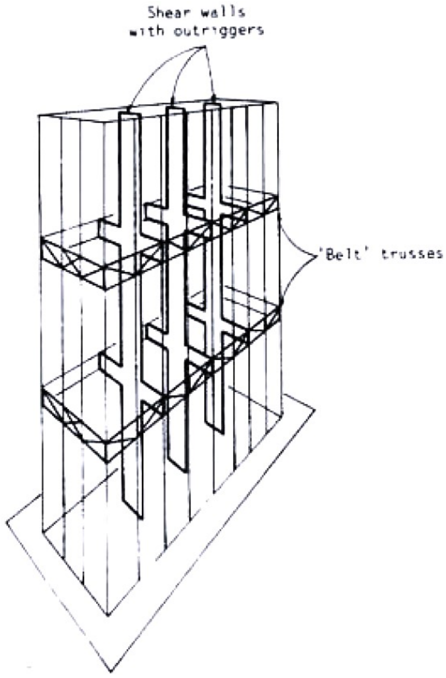

Figure 2.10: Outrigger system with belt trusses

placed at the top of the structure; in this case, the structure can be classified as a*top-hat* structure. Each level of outriggers increases the lateral stiffness of the building, but to a lesser extent than the previous level. In very tall buildings, up to four levels of outriggers can be used.

This structural system, in addition to providing resistance to horizontal loads, compensates for the differential shortening of the external columns caused by temperature action and the axial force overhang between the core and the external columns. The positioning of a truss at the top of the building eliminates the differential displacements between the external and internal columns by providing a compression restraint when the columns are in tension and a tension restraint when the columns are in compression.

3 General Algorithm

For the design of the structural system components described in Chapter 2, it is essential to determine the load-bearing capacity of each individual vertical element, as outlined in ify the amount of external load that each individual vertical element is capable of bearing, as delineated in [4], [6], [7], [8], [10], [11] and [20]. In particular, the following sections present the General Algorithm [4], an analytical method developed by Professor *A. Carpinteri et al.* This algorithm enables both static and dynamic analyses of high-rise buildings featuring various structural resistance systems, ensuring a comprehensive assessment of their reliability.

Taking into account the model of a frames-and-shear-walls system (Figure 3.1), a simplified approach assumes that the connections between the two substructures can be represented by rigid rods. This hypothesis is postulated to ensure the congruence of the horizontal displacements at each floor is satisfied.

If $\{F\}$ represents the external load vector and $\{X\}$ the redundant unknown forces transmitted through the rods, due to the congruence conditions:

$$[C_1](\{F\} - \{X\}) = [C_2]\{X\} \tag{3.1}$$

where $[C_1]$ and $[C_2]$ are the compliance matrices of the frames and shear wall, respectively. Defining[C] as the sum of matrices $[C_1]$ and $[C_2]$, the numerical solution of Equation (3.1) is

$$\{X\} = [C]^{-1}\{F\} \tag{3.2}$$

which identifies the distribution of the redundant forces exchanged (Figure 3.1).

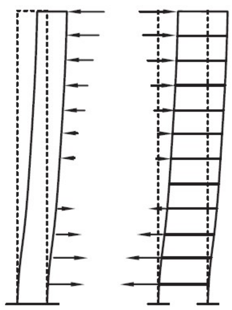

Figure 3.1: Frames+shear walls system behaviour

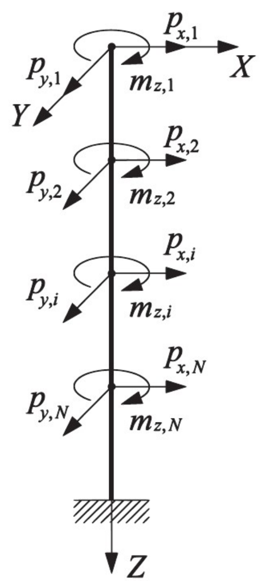

Figure 3.2: External load applied to the origin of the reference system

The limitation of this analytical approach is that it can only be applied to a restricted number of cases, defined by simple structural combinations. It is characterised by a profound lack of generality, which prevents the analysis of different and more complex structural solutions and, above all, tends to reduce a three-dimensional problem to a planar one. This limitation renders the method an inadequate solution, especially in cases involving highly complex shapes that cannot be simplified.

In the majority of buildings, the resistance system is composed of various vertical elements that form a three-dimensional structural skeleton. In this case, a more general semi-analytical approach can be proposed, taking into account three degrees of freedom per floor. This approach enables the simultaneous study of the bending and torsional behaviour of the structure. The approach is versatile, as it can be applied to any type of vertical bracing, ranging from simple frames to free-shaped tubular elements, provided that their stiffness matrix is known.

The formulation is based on the following fundamental hypotheses:

1. The structural material is homogeneous, isotropic, and obeys Hooke's law.
2. The floor slabs are rigid in their own plane but their out-of-plane rigidity is negligible.
3. In transversal analysis, the axial deformation of the structural elements due to gravity loads is negligible.

In accordance with the aforementioned hypotheses, it is hypothesised that an N-storey building is characterised by M vertical bracings, with each bracing defined by an arbitrary position in the floor plan. The right-handed system XYZ is utilised to define the global coordinate system. Since the slabs, which connect the bracings to each other, are considered to be infinitely rigid in their own planes, the degrees of freedom are represented by the transverse displacements of the single floors: ξ and η in the directions X and Y, and the torsional rotation ϑ, for each story. In a similar manner, the external load applied to the origin of the reference system is expressed by a 3N-vector $\{F\}$, in which 2N shearing forces $\{p_x\}$, $\{p_y\}$ and N torsional moments $\{m_z\}$ are included (Figure 3.2):

$$\{F_i\} = \left\{ \begin{matrix} p_i \\ m_{z,i} \end{matrix} \right\} = \left\{ \begin{matrix} p_{x,i} \\ p_{y,i} \\ m_{z,i} \end{matrix} \right\} \tag{3.3}$$

Within the right-handed system $X_i^* Y_i^* Z_i^*$, the local coordinate system of the ith bracing, the 3N-load vector $\{F^*\}$, and the 3N-displacement vector $\{\delta_i^*\}$ describe the amount of external load carried by the ith element and its transverse displacements, respectively.

The loading vector $\{F_i^*\}$ can be reduced to $\{F_i\}$, which refers to the global coordinate system XYZ, by means of the following expressions, valid for each bracing:

$$\{p_i^*\} = [N_i]\{p_i\} \tag{3.4}$$

$$m_{z,i}^* = m_{z,i} - \{\Psi_i\} \wedge \{p_i\} \times \{u_z\} \tag{3.5}$$

In matrix form:

$$\left\{ \begin{matrix} p_{x,i}^* \\ p_{y,i}^* \\ m_{z,i}^* \end{matrix} \right\} = \begin{bmatrix} [N_i] & [0] \\ -\{u_z\} \wedge \{\Psi_i\} & [I] \end{bmatrix} \left\{ \begin{matrix} p_{x,i} \\ p_{y,i} \\ m_{z,i} \end{matrix} \right\} \tag{3.6}$$

where:

$[N_i]$ represents the orthogonal rotation matrix from system XY to system $X_i^* Y_i^*$

$\{\Psi_i\}$ is the coordinate vector of the origin of the local system in the global one

$\{u_z\}$ is the unit vector associated with the direction Z

$[I]$ is the identity matrix

$[0]$ is the null matrix

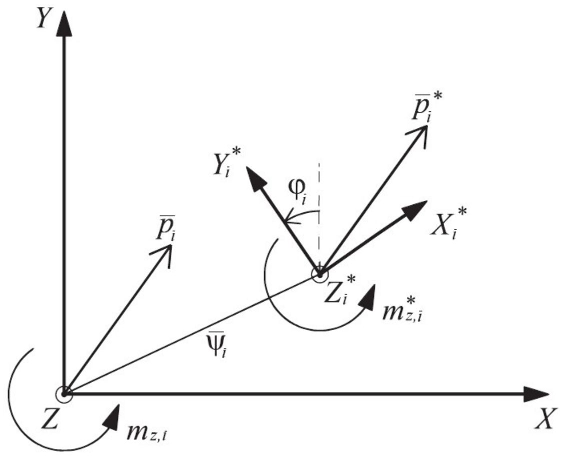

Figure 3.3: Local reference system

The orthogonal matrix $[N_i]$, extended to consider all floors, can be represented by means of the angle φ_i between the Y and Y_i^* axes (Figure 3.3):

$$[N_i] = \begin{bmatrix} [cos\varphi_i] & [sin\varphi_i] \\ -[sin\varphi_i] & [cos\varphi_i] \end{bmatrix} \tag{3.7}$$

where each term is a diagonal $(N \times N)$ submatrix:

$$[cos\varphi_i] = \begin{bmatrix} [cos\varphi_i] & 0 & \dots & 0 \\ 0 & [cos\varphi_i] & \dots & 0 \\ \vdots & \vdots & & \vdots \\ 0 & 0 & \dots & [cos\varphi_i] \end{bmatrix} \tag{3.8a}$$

$$[sin\varphi_i] = \begin{bmatrix} [sin\varphi_i] & 0 & \dots & 0 \\ 0 & [sin\varphi_i] & \dots & 0 \\ \vdots & \vdots & & \vdots \\ 0 & 0 & \dots & [sin\varphi_i] \end{bmatrix} \tag{3.8b}$$

Taking into account all floors, Equation 3.6 can be rewritten in the following form:

$$\{F_i^*\} = [A_i]\{F_i\} \tag{3.9}$$

Matrix $[A_i]$ gathers the information regarding the reciprocal rotation between the local and global coordinate systems and the location of the ith bracing in the global system XY:

$$[A_i] = \begin{bmatrix} [N_i] & [0] \\ -\{u_z\} \wedge \{\Psi_i\} & [I] \end{bmatrix} \tag{3.10}$$

The component $-\{u_z\} \wedge \{\Psi_i\}$, valid for each floor, is obtained from Equation 3.5, exploiting the fact that the scalar triple product is invariant under any cyclic permutation of its factors. For the sake of simplicity, to take into account the N floors of the structure, this vector product can be written as a (2N×N) matrix $[C_i]$ composed of two diagonal submatrices containing the coordinates $(x_i; y_i)$ of the origin of the local system $X_i^* Y_i^*$:

$$- \{u_z\} \wedge \{\Psi_i\} = - \begin{vmatrix} \bar{i} & \bar{j} & \bar{k} \\ 0 & 0 & 1 \\ x_i & y_i & 0 \end{vmatrix} = -[-y_i \quad x_i] = -[C_i]^T \tag{3.11}$$

Thus, the final expression for matrix $[A_i]$ is

$$[A_i] = \begin{bmatrix} [N_i] & [0] \\ -[C_i]^T & [I] \end{bmatrix} \tag{3.12}$$

In the same way, the vector $\{\delta_i^*\}$, constituted by 2N translations ξ_i^*, η_i^* and N rotations ϑ_i^*, can be connected to the corresponding $\{\delta_i\}$, which is referred to the global coordinate system

$$\{\delta_i^*\} = \begin{Bmatrix} \xi_i^* \\ \eta_i^* \\ \vartheta_i^* \end{Bmatrix} \tag{3.13}$$

The displacements $\{\delta_i\}$ in the global coordinate system XY are then connected to the displacements $\{\delta_i^*\}$ in the local coordinate system $X_i^* Y_i^*$ by the orthogonal matrix $[N_i]$:

$$\begin{Bmatrix} \xi_i^* \\ \eta_i^* \end{Bmatrix} = [N_i] \begin{Bmatrix} \xi_i \\ \eta_i \end{Bmatrix} \tag{3.14a}$$

$$\vartheta_i^* = \vartheta_i \tag{3.14b}$$

Taking into account all floors, Equations 3.14 can be rewritten in the following form by means of the compact (3N×3N) matrix $[B_i]$:

$$\{\delta_i^*\} = [B_i]\{\delta_i\} \tag{3.15}$$

where matrix $[B_i]$ is similar to $[A_i]$, the term $[B_i]^T$ being reduced to a null matrix:

$$[B_i] = \begin{bmatrix} [N_i] & [0] \\ [0] & [I] \end{bmatrix} \tag{3.16}$$

A relation between $\{F_i^*\}$ and $\{\delta_i^*\}$ is considered known through the condensed stiffness matrix $[K_i^*]$, referred to the local coordinate system:

$$\{F_i^*\} = [K_i^*]\{\delta_i^*\} \tag{3.17}$$

Substituting Equations 3.9 and 3.15 into Equation 3.17, the load vector $\{F_i\}$ turns out to be connected to the displacement vector $\{\delta_i\}$ through a product of matrices, which identifies the stiffness matrix $[K_i]$ of the ith bracing in the global coordinate system XY:

$$\{F_i\} = \big([A_i]^{-1}[K_i^*][B_i]\big)\{\delta_i\} = [K_i]\{\delta_i\} \tag{3.18}$$

Due to the presence of in-plane rigid slabs connecting the vertical cantilevers, the transverse displacements of each element can be computed considering only three generalized displacements, ξ, η, and ϑ, per floor. This step, extended to consider all floors, is performed through the matrix $[T_i]$ that takes into account the location of each bracing in the plan by means of the coordinates $(x_i; y_i)$ and, therefore, the matrix $[C_i]$:

$$\{\delta_i\} = \begin{bmatrix} [I] & [C_i] \\ [0] & [I] \end{bmatrix}\{\delta\} = [T_i]\{\delta\} \tag{3.19}$$

where $\{\delta\}$ is the floor displacement vector, that is, the displacement vector associated with the origin of the global reference system.

The substitution of Equation 3.19 into Equation 3.18 allows the identification of the stiffness matrix of the ith bracing, in reference to the global coordinate system XYZ and to the generalized floor displacements ξ_i, η_i, and ϑ:

$$\{F_i\} = \big([K_i][T_i]\big)\{\delta\} = \big[\bar{K}_i\big]\{\delta\} \tag{3.20}$$

For global equilibrium, the external load $\{F\}$ applied to the structure is equal to the sum of the M vectors $\{F_i\}$. In this way, a relationship between the external load and the floor displacements is obtained and the global stiffness matrix of the structure is computed. By means of this matrix, once the external load is defined, the displacements of the structure are acquired, from which the information regarding each single bracing can be deduced:

$$\{F\} = \sum_{i=1}^{M}\{F_i\} = \left(\sum_{i=1}^{M}\big[\bar{K}_i\big]\right)\{\delta\} = \big[\bar{K}\big]\{\delta\} \tag{3.21}$$

and therefore

$$\{\delta\} = \big[\bar{K}_i\big]^{-1}\{F\} \tag{3.22}$$

Recalling Equation 3.20 and comparing it with Equation 3.22, an equation connecting the vectors $\{F\}$ and $\{F_i\}$ allows the definition of the amount of the external load carried by the i-th vertical stiffening element:

$$\{\delta\} = \left[\bar{K}_i\right]^{-1}\{F\} = \left[\bar{K}_i\right]^{-1}\{F_i\} \tag{3.23}$$

from which we obtain

$$\{F_i\} = \left[\bar{K}_i\right]\left[\bar{K}\right]^{-1}\{F\} = [R_i]\{F\} \tag{3.24}$$

The load distribution matrix $[R_i]$, shown in Equation 3.24, demonstrates that each bracing is subjected to a load $\{F_i\}$ that is given by the external load F premultiplied by the own stiffness matrix and the inverse of the global stiffness matrix.

Once the generalized displacement vector $\{\delta\}$ is known, recalling Equations 3.13, 3.17, and 3.19, the displacements and the forces related to the ith bracing in its local coordinate system can be computed. Consequently, since the loads applied to each element are clearly identified, a preliminary assessment can easily be performed.

Equation 3.24 provides a solution to the problem of the external load distribution between the resistant elements employed to stiffen a three-dimensional tall building. This formulation is to be general and can be adopted with any kind of structural element, provided that their own condensed stiffness matrix $[K_i^*]$ is known. This renders the implementation of most common vertical stiffeners, including frames, braced frames, shear walls and tubular elements, straightforward within this static formulation.

The formulation offers several advantages. Firstly, it facilitates the identification of the structural parameters that govern the lateral behaviour of the building. Secondly, it is remarkably clear and concise, thereby minimising the risk of unexpected errors and ensuring relatively short times of modelling and analysis in the presence of very complex structures, when compared with finite element computations.

3.1 Vlasov's theory of thin-walled open-section beams in torsion

In the presence of torsional actions, thin-walled open-section elements demonstrate a distinct behaviour that deviates from the outcomes of Saint-Venant's theory. Upon the occurrence of torsional deformation, the section undergoes a twisting

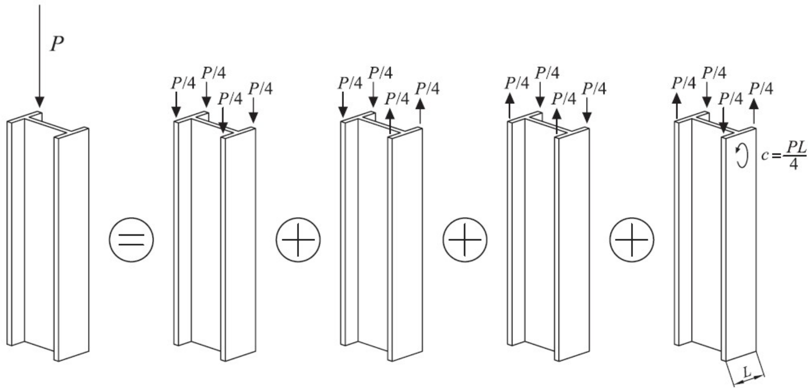

Figure 3.4: I-beam subjected to concentrated load

movement around its shear centre. Concurrently, it does not maintain its planar configuration, as it experiences various longitudinal strains, resulting in an out-of-plane distortion, otherwise referred to as *warping*, of the section. AConsequently, an additional longitudinal stress, which is not considered in the theory of primary torsion, develops in the thickness of the section.

Consider the case of a cantilever I-beam subjected to a concentrated load on one of its flanges (Figure 3.4). In accordance with the principle of superposition, this load can be reduced to the sum of four different loading cases: one is purely axial, two are purely flexural, while the remaining one is defined as flexural torsion, since the two flanges are forced to bend in opposite directions in their own planes. In the latter case, the section does not remain flat and additional normal stresses appear. These additional normal stresses give rise to a generalised action called *bimoment*, which is directly related to the deformation of the section and consists of two bending moments, each acting on a single flange, of equal magnitude but opposite sign.

In the case of compact sections, this self-equilibrating effect is only local and rapidly diminishes as the distance from the end of the beam increases. Conversely, in the case of thin-walled open-section beams, the warping stresses decrease slowly as the walls become thinner. It is imperative to note that the intensity of this stress state cannot be disregarded for these sections, as the application of Saint-Venant's theory could result in significant inaccuracies.

Vlasov's theory is based on two main geometrical hypotheses:

1. The section is considered rigid and, therefore, its shape is undeformable
2. The shearing strains on the midline of the section are assumed to vanish

Consider a free-form, thin-walled, open-section beam in a generic coordinate system where the Z axis is parallel to the beam's longitudinal axis. A specific cross-section is defined at z = constant; the X and Y axes complete the right-handed XYZ coordinate system. The coordinates (x, y) or the curvilinear coordinate s (see can be used to identify each point on the centre line (Figure 3.5).

In order to define the equations governing the structural behaviour of thin-walled open sections, it is assumed that the beam is subjected to some torsional deformations. Consequently, each point of the section is characterised by a new position in the general XYZ coordinate system. According to the first geometric hypothesis, the beam is deformable although the shape of the section remains unchanged. It therefore behaves as a perfectly rigid body whose position can be described by three independent variables corresponding to the three generalised displacements of an arbitrarily chosen point: two translations ξ and η in the X and Y directions respectively, and the rotation ϑ.

The transverse displacements ξ and η of any point belonging to the section can be determined using the well-known expressions:

$$u = \xi(z) - \vartheta(z)y \tag{3.25a}$$

$$v = \eta(z) + \vartheta(z)y \tag{3.25b}$$

The tangential displacement δ_t, related to the generic point of the section, can be computedby

$$\delta_t = \{\delta\}^T\{u_t\} = u\frac{dx}{ds} + v\frac{dy}{ds} \tag{3.26}$$

and then

$$\delta_t = \xi\frac{dx}{ds} + \eta\frac{dy}{ds} + \vartheta\, h(s) \tag{3.27}$$

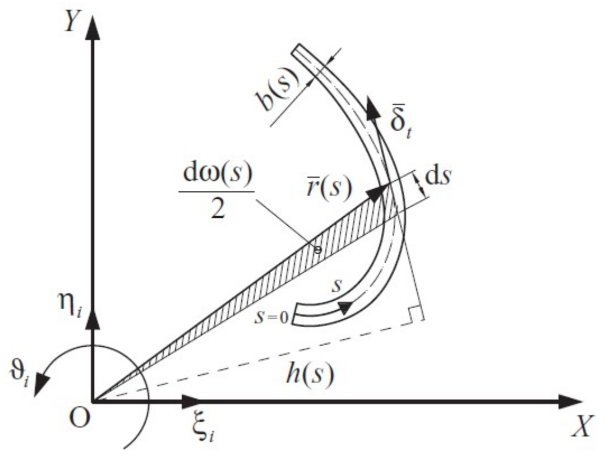

Figure 3.5: Thin-walled open-section beam

in which the term $h(s)$ represents the distance between the origin of the reference system and the tangent line to the section midline (Figure 3.5):

$$h(s) = \{r\}^T\{u_n\} = x\frac{dy}{ds} - y\frac{dx}{ds} \tag{3.28}$$

The longitudinal displacement component w can be obtained by Vlasov's second hypothesis, according to which the shearing strains on the midline are considered negligible:

$$\gamma_{zs} = \frac{\partial w}{\partial s} + \frac{\partial \delta_t}{\partial z} = 0 \tag{3.29}$$

Taking into account the following relationship:

$$\omega(s) = \int_0^s h(s)\, ds \tag{3.30}$$

the analytical expression of w is derived by integration:

$$w = \zeta(z) - \int_0^s \frac{\partial \delta_t}{\partial z} ds = \zeta(z) - \xi' x - \eta' y - \vartheta' \omega \tag{3.31}$$

The term $\zeta(z)$ is defined as an arbitrary function, depending only on z, which describes a longitudinal translation of the entire section; $\omega(s)$ is defined as the *sectorial area*, that is, double the area swept by the radius vector r from s = 0 to the current point s of the section's midline. The points O and $s = 0$ are the origin of an arbitrary reference system and the sectorial origin, respectively (Figure 3.5).

The longitudinal component w is composed of four terms: the first three are well known and arise from extension and bending in the XZ and YZ planes. The component that describes the warping of the section is expressed by the fourth term and, in particular, ϑ' can be considered as an amplification factor, whereas ω is the shape of the warped section.

By differentiating w with respect to z, it is possible to obtain the expression of the longitudinal deformation ε_z:

$$\varepsilon_z = \frac{\partial w}{\partial z} = \zeta' - \xi'' x - \eta'' y - \vartheta'' \omega \tag{3.32}$$

The fourth term of Equation 3.32 demonstrates that the hypothesis of primary torsion, according to which the unit angle of torsion should be constant, can, in general, be removed.

The general expression of the normal stresses is obtained by multiplying Equation 3.32 by the elastic modulus E:

$$\sigma_z = E\varepsilon_z = E(\zeta' - \xi'' x - \eta'' y - \vartheta'' \omega) \tag{3.33}$$

In each section of the beam, the normal stress σ_z is the sum of two contributions:

$$\sigma_z = \sigma_z^{SV} + \sigma_z^{VL} \tag{3.34}$$

where

$$\sigma_z^{VL} = -E\vartheta''\omega \tag{3.35}$$

It is evident from these expressions that normal stresses may manifest not only in the context of uniform extension and bending of the beam, but also as a consequence of non-uniform torsion of the cross section. On the other hand, this specific contribution is usually assumed to vanish in the theory of primary torsion.

Equation 3.33 allows the definition by integration of the internal actions related to the extensional and flexural behavior of the beam:

$$N = \int_A \sigma_z \, dA = E(A\zeta' - S_y\xi'' - S_x\eta'' - S_\omega\vartheta'') \tag{3.36a}$$

$$M_y = \int_A \sigma_z x \, dA = E(S_y\zeta' - I_{yy}\xi'' - I_{yx}\eta'' - I_{y\omega}\vartheta'') \tag{3.36b}$$

$$M_x = \int_A \sigma_z y \, dA = E(S_x\zeta' - I_{xy}\xi'' - I_{xx}\eta'' - I_{x\omega}\vartheta'') \tag{3.36c}$$

$$B = \int_A \sigma_z \omega \, dA = E(S_\omega\zeta' - I_{\omega y}\xi'' - I_{\omega x}\eta'' - I_{\omega\omega}\vartheta'') \tag{3.36d}$$

in which the sectorial characteristics of the section are expressed by the sectorial static moment S_ω, the sectorial moment of inertia $I_{\omega\omega}$, and the sectorial products of inertia $I_{\omega x}$ and $I_{\omega y}$, defined as follows:

$$S_y = \int_A x \, dA \tag{3.37a}$$

$$S_x = \int_A y \, dA \tag{3.37b}$$

$$S_\omega = \int_A \omega \, dA \tag{3.37c}$$

$$I_{yy} = \int_A x^2 dA \tag{3.38a}$$

$$I_{xx} = \int_A y^2 dA \tag{3.38b}$$

$$I_{\omega\omega} = \int_A \omega^2 dA \tag{3.38c}$$

$$I_{yx} = I_{xy} = \int_A xy\, dA \tag{3.39a}$$

$$I_{x\omega} = I_{\omega x} = \int_A \omega y\, dA \tag{3.39b}$$

$$I_{y\omega} = I_{\omega y} = \int_A \omega x\, dA \tag{3.39c}$$

Equation 3.36d defines the *bimoment* action, which represents a generalized self-balanced force system equivalent to two bending moments, having the same magnitude but opposite signs.

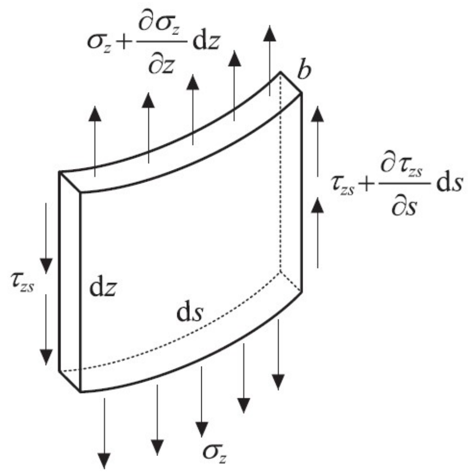

Figure 3.6: Longitudinal equilibrium of a beam portion

The tangential stresses τ_{zs}, supposed to be defined by a constant distribution on the thickness of the section, can be obtained considering the longitudinal equilibrium of an elementary portion of the beam, whose dimensions are length dz, width ds, and thickness b (Figure 3.6):

$$\left(\frac{\partial \tau_{zs}}{\partial s} ds\right) b\, dz + \left(\frac{\partial \sigma_z}{\partial z} dz\right) b\, ds = 0 \tag{3.40}$$

Dividing Equation 3.40 by $dsdz$, the following expression is obtained:

$$\frac{\partial(\tau_{zs} b)}{\partial s} + \frac{\partial(\sigma_z b)}{\partial z} = 0 \tag{3.41}$$

On the basis of Equation 3.41, three additional transverse internal actions, the shearing forces, and the secondary torsional moment, can be defined:

$$T_x = \int_A \tau_{zs} \frac{dx}{ds}\, dA \tag{3.42a}$$

$$T_y = \int_A \tau_{zs} \frac{dy}{ds}\, dA \tag{3.42b}$$

$$M_z^{VL} = \int_A \tau_{zs} h\, dA \tag{3.42c}$$

Integrating by parts and applying Equation 3.41, the following relations are obtained:

$$T_x = -\int_C \frac{\partial(\tau_{zs} b)}{\partial s} x\, ds = \int_C \frac{\partial(\sigma_z b)}{\partial z} x\, ds = \frac{d}{dz}\int_A \sigma_z x\, dA \tag{3.43a}$$

$$T_y = -\int_C \frac{\partial(\tau_{zs} b)}{\partial s} y\, ds = \int_C \frac{\partial(\sigma_z b)}{\partial z} y\, ds = \frac{d}{dz}\int_A \sigma_z y\, dA \tag{3.43b}$$

$$M_z^{VL} = -\int_C \frac{\partial(\tau_{zs} b)}{\partial s} \omega\, ds = \int_C \frac{\partial(\sigma_z b)}{\partial z} \omega\, ds = \frac{d}{dz}\int_A \sigma_z \omega\, dA \tag{3.43c}$$

Comparing Equations 3.43 with Equations 3.36, it is possible to recognize a fundamental differential relationship between the longitudinal and the transverse actions:

$$T_x = \frac{dM_y}{dz} = E(S_y\zeta'' - I_{yy}\xi''' - I_{yx}\eta''' - I_{y\omega}\vartheta''') \tag{3.44a}$$

$$T_y = \frac{dM_x}{dz} = E(S_x\zeta'' - I_{xy}\xi''' - I_{xx}\eta''' - I_{x\omega}\vartheta''') \tag{3.44b}$$

$$M_z^{VL} = \frac{dB}{dz} = E(S_\omega\zeta'' - I_{\omega y}\xi''' - I_{\omega x}\eta''' - I_{\omega\omega}\vartheta''') \tag{3.44c}$$

The last equation highlights that, due to the warping of the section, an unexpected torsional moment M_z^{VL} is generated, it being the first derivative of the bimoment action.

The secondary torsional moment M_z^{VL} is generated by the τ_{zs} stresses due to the shearing actions T_x and T_y.

A further step of differentiation leads to the equilibrium equations that take into account the distributed external loads p_x, p_y, and m_z (known terms):

$$p_x = -\frac{dT_x}{dz} = E(-S_y\zeta''' + I_{yy}\xi^{IV} + I_{yx}\eta^{IV} + I_{y\omega}\vartheta^{IV}) \tag{3.45a}$$

$$p_y = -\frac{dT_y}{dz} = E(-S_x\zeta''' + I_{xy}\xi^{IV} + I_{xx}\eta^{IV} + I_{x\omega}\vartheta^{IV}) \tag{3.45b}$$

$$m_z^{VL} = -\frac{M_z^{VL}}{dz} = E(-S_\omega\zeta''' + I_{\omega y}\xi^{IV} + I_{\omega x}\eta^{IV} + I_{\omega\omega}\vartheta^{IV}) \tag{3.45c}$$

Indeed, the thin-walled open section is subjected to an external torsional moment which can be divided into two parts: the first, according to Saint-Venant's theory, is due to a linear variation of the tangential stresses through its thickness and is equal to zero at the centre line; the second, according to Vlasov's theory, is due to a constant distribution of the tangential stresses through the thickness and is related to equilibrium, the normal stresses resulting from the differential distortion of the section.

In each section of the beam, the torsional moment M_z is the sum of the two contributions

$$M_z = M_z^{SV} + M_z^{VL} = GI_t\vartheta' + E(S_\omega\zeta'' - I_{\omega y}\xi''' - I_{\omega x}\eta''' - I_{\omega\omega}\vartheta''') \tag{3.46}$$

and, therefore, the global equilibrium Equation 3.45c becomes

$$m_z = m_z^{SV} + m_z^{VL} = -\frac{dM_z^{SV}}{dz} - \frac{dM_z^{VL}}{dz} = -GI_t\vartheta'' + E(-S_\omega\zeta''' + I_{\omega y}\xi^{IV} + I_{\omega x}\eta^{IV} + I_{\omega\omega}\vartheta^{IV}) \tag{3.47}$$

where G is the shear modulus and I_t is the torsional stiffness factor of the section.

Finally, an expression of the tangential stresses τ_{zs} can be obtained by substituting Equation 3.33 into Equation 3.41:

$$\frac{\partial(\tau_{zs}b)}{\partial s} + Eb(\zeta'' - \xi'''x - \eta'''y - \vartheta'''\omega) = 0 \tag{3.48}$$

and integrating with respect to s:

$$\tau_{zs} = -\frac{E}{b}\left[(\zeta''A(s) - \xi'''S_y(s) - \eta'''S_x(s) - \vartheta'''S_\omega(s)\right] \tag{3.49}$$

where the following geometrical expressions are used:

$$A(s) = \int_0^s b\,ds \tag{3.50a}$$

$$S_y(s) = \int_0^s xb\,ds \tag{3.50b}$$

$$S_x(s) = \int_0^s yb\,ds \tag{3.50c}$$

$$S_\omega(s) = \int_0^s \omega b\,ds \tag{3.50d}$$

The system of differential equilibrium Equations 3.45 allows the computation of the unknown displacements.

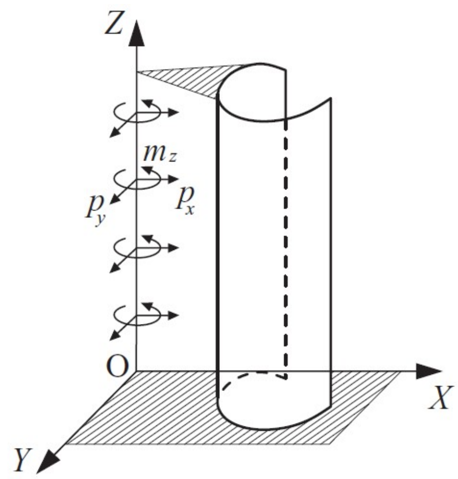

Figure 3.7: Thin-walled open-section cantilever

3.2 Capurso's method: Lateral loading distribution between the thin-walled open-section vertical cantilevers of a tall building

Thin-walled open-section shear walls are mainly used in tall buildings to enhance to their horizontal resistance and stiffness. In accordance with the previous hypotheses, the analytical formulation proposed by Vlasov can be adopted to evaluate the structural behaviour of a tall building stiffened by a single thin-walled open-section cantilever.

The calculation of the sectorial terms is carried out considering the origin of the generic right-handed system XYZ. The analysis incorporates transverse distributed actions p_x, p_y and m_z.

If the axial force in the vertical bracing is assumed to be zero, the term ζ' in Equation 3.36a can be eliminated:

$$\zeta' = \frac{S_y}{A}\xi'' + \frac{S_x}{A}\eta'' + \frac{S_\omega}{A}\vartheta'' = x_G\xi'' + y_G\eta'' + \omega_0\vartheta'' \tag{3.51}$$

The substitution of Equation 3.51 into Equations 3.36b, 3.36c, and 3.36d permits the definition of new expressions for the longitudinal actions without the term ζ':

$$M_y = -E(J_{yy}\xi'' + J_{yx}\eta'' + J_{y\omega}\vartheta'') \tag{3.52a}$$

$$M_x = -E(J_{xy}\xi'' + J_{xx}\eta'' + J_{x\omega}\vartheta'') \tag{3.52b}$$

$$B = -E(J_{\omega y}\xi'' + J_{\omega x}\eta'' + J_{\omega\omega}\vartheta'') \tag{3.52c}$$

where

$$J_{yy} = I_{yy} - Ax_G^2 \tag{3.53a}$$

$$J_{xx} = I_{xx} - Ay_G^2 \tag{3.53b}$$

$$J_{xy} = I_{xy} - Ax_G y_G \tag{3.53c}$$

$$J_{\omega\omega} = I_{\omega\omega} - A\omega_0^2 \tag{3.54a}$$

$$J_{\omega y} = I_{\omega y} - A\omega_0 x_G \tag{3.54b}$$

$$J_{\omega x} = I_{\omega x} - A\omega_0 y_G \tag{3.54c}$$

Equations 3.53 represent the implementation of the Huygens–Steiner theorem, whereby the system XYZ is transferred from the generic origin to the centroid of the section. Similarly, Equations 3.54 express the sectorial properties with respect to the baricentric axes and to the sectorial centroid.

By ignoring the torsional rigidity GI_t, Equations 3.53 and 3.54 also affect the system of Equations 3.44, which become

$$T_x = -E(J_{yy}\xi''' + J_{yx}\eta''' + J_{y\omega}\vartheta''') \tag{3.55a}$$

$$T_y = -E(J_{xy}\xi''' + J_{xx}\eta''' + J_{x\omega}\vartheta''') \tag{3.55b}$$

$$M_z^{VL} = -E(J_{\omega y}\xi''' + J_{\omega x}\eta''' + J_{\omega\omega}\vartheta''') \tag{3.55c}$$

and, similarly, the distributed external loads p_x, p_y, and m_z of the system of Equations 3.45 turn into

$$p_x = E(J_{yy}\xi^{IV} + J_{yx}\eta^{IV} + J_{y\omega}\vartheta^{IV}) \tag{3.56a}$$

$$p_y = E(J_{xy}\xi^{IV} + J_{xx}\eta^{IV} + J_{x\omega}\vartheta^{IV}) \tag{3.56b}$$

$$m_z^{VL} = E(J_{\omega y}\xi^{IV} + J_{\omega x}\eta^{IV} + J_{\omega\omega}\vartheta^{IV}) \tag{3.56c}$$

If the matrix of inertia $[J]$ and the vectors $\{\delta\}$, $\{M\}$, $\{T\}$, and $\{F\}$ are introduced, it is possible to write the systems of Equations 3.52, 3.55, and 3.56 in a compact form:

$$[J] = \begin{bmatrix} J_{yy} & J_{yx} & J_{y\omega} \\ J_{xy} & J_{xx} & J_{x\omega} \\ J_{\omega y} & J_{\omega x} & J_{\omega\omega} \end{bmatrix} \tag{3.57}$$

$$\{\delta\} = \begin{Bmatrix} \xi \\ \eta \\ \vartheta \end{Bmatrix} \tag{3.58a}$$

$$\{M\} = \begin{Bmatrix} M_y \\ M_x \\ B \end{Bmatrix} \tag{3.58b}$$

$$\{T\} = \begin{Bmatrix} T_x \\ T_y \\ M_z^{VL} \end{Bmatrix} \tag{3.58c}$$

$$\{F\} = \begin{Bmatrix} p_x \\ p_y \\ m_z \end{Bmatrix} \tag{3.58d}$$

$$\{M\} = -E[J]\{\delta''\} \tag{3.59a}$$

$$\{T\} = -E[J]\{\delta'''\} \tag{3.59b}$$

$$\{F\} = E[J]\{\delta^{IV}\} \tag{3.59c}$$

Since the matrix of inertia is symmetrical and positive definite until the geometry of the section is such that the determinant of *[J]* is not zero, it can be inverted to obtain a relationship between the fourth derivatives of the displacements and the external distributed actions:

$$\{\delta^{IV}\} = \frac{1}{E}[J]^{-1}\{F\} \tag{3.60}$$

The transverse displacements of the section are obtained by integrating Equation 3.60 and applying the boundary conditions at the base and at the top of the cantilever.

At the constrained end:

$$\{\delta\} = \{0\} \tag{3.61a}$$

$$\{\delta'\} = \{0\} \tag{3.61b}$$

$$\tag{3.61c}$$

for $z = 0$

whereas, at the top:

$$\{\delta''\} = \{0\} \tag{3.62a}$$

$$\{\delta'''\} = \{0\} \tag{3.62b}$$

$$\tag{3.62c}$$

for $z = l$.

Once ξ, η, and ϑ are known, the application of Equation 3.51 yields the uniform axial displacement ζ with the corresponding boundary condition:

$$\zeta(z = 0) = 0 \tag{3.63}$$

Eventually, the displacement components δ_t and w can be easily derived from Equations 3.27 and 3.31, as well as the internal stress state given by Equation 3.33, to which the effect of the primary torsion has to be added.

The application of this analytical formulation is precluded in circumstances where specific sections are concerned, for which the matrix [J] is singular. These are the cases of shear walls formed by a single thin rectangular plate or by several thin plates converging to a single point, as shown in Figure 3.8. In these cases the warping function vanishes.

The previous formulation can be extended to consider the case of M vertical cantilevers, which represent the resistant skeleton of a tall building, loaded by transverse actions applied to the floors with respect to the global XYZ coordinate system. The vertical bracings are interconnected by rigid slabs in the plane, whose out-of-plane stiffness can be considered negligible.

The unknown variables of the problem are the displacements of the floors, identified by the translations ξ and η in the X and Y directions respectively, and the torsional rotation ϑ. If $\{F_i\}$ indicates the vector of the transverse actions transmitted to the ith cantilever, by virtue of Equation 3.59c we have

$$\{F_i\} = E[J_i]\{\delta^{IV}\} \tag{3.64}$$

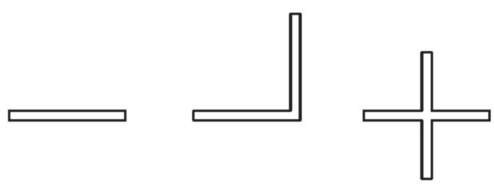

Figure 3.8: Thin plate shear walls

where matrix $[J_i]$ contains the moments of inertia with reference to the centroid of the section and to the sectorial centroid, whereas the vector $\{\delta^{IV}\}$ gathers fourth order derivatives of the floor displacements ξ, η and ϑ.

If $\{F\}$ is the vector of the external loads, the equilibrium condition imposes

$$\{F\} = \sum_{i=1}^{M}\{F_i\} = E\left(\sum_{i=1}^{M}[J_i]\right)\{\delta^{IV}\} = E[J]\{\delta^{IV}\} \tag{3.65}$$

Therefore, the combination of M cantilevers behaves as a single cantilever whose matrix of inertia is given by the sum of the M matrices related to the single cantilevers:

$$[J] = \sum_{i=1}^{M}[J_i] \tag{3.66}$$

Equation 3.65 can be solved following the procedure previously described for a single vertical bracing. Once the floor displacements are known, the displacements of each cantilever can be deduced and information on the stress state can also be obtained. Finally, it is interesting to note that, from the relationship between the vector $\{F_i\}$ of the ith cantilever and the global vector $\{F\}$, each bracing is subjected to an external load vector obtained from the product of its own inertia matrix and the inverse of the global one, analogous to what appears in the general algorithm:

$$\{F_i\} = [J_i][J]^{-1}\{F\} \tag{3.67}$$

In the case of a discrete distribution of transverse forces corresponding to the different floors, the (3×3) matrix $[J]$, which is a function of the longitudinal coordinate z, can be expanded to a $(3N \times 3N)$ stiffness matrix to be inserted in the general algorithm.

3.3 Diagonalization of Vlasov's equations

The system of Equations 3.45 can be strongly simplified by making certain choices. In fact, if a centroidal coordinate system is considered, the following conditions are all immediately satisfied:

$$S_y = \int_A x\,dA = 0 \tag{3.68a}$$

$$S_x = \int_A y\,dA = 0 \tag{3.68b}$$

In addition, if the reference system is also principal, the product of inertia is null:

$$I_{xy} = I_{yx} = \int_A xy\, dA = 0 \tag{3.69}$$

On the other hand, if the sectorial pole coincides with the shear center of the section, it can be shown that

$$I_{\omega y} = I_{y\omega} = \int_A \omega x\, dA = 0 \tag{3.70a}$$

$$I_{\omega x} = I_{x\omega} = \int_A \omega y\, dA = 0 \tag{3.70b}$$

In addition, if the sectorial origin is in the sectorial centroid, by definition it follows that the sectorial static moment is also null:

$$S_\omega = \int_A \omega\, dA = 0 \tag{3.71}$$

Taking into account Equations 3.52 and considering the principal reference system with its origin in the shear center, the internal actions can be defined as

$$M_y = -EJ_{yy}\xi'' \tag{3.72a}$$

$$M_x = -EJ_{xx}\eta'' \tag{3.72b}$$

$$B = -EJ_{\omega\omega}\vartheta'' \tag{3.72c}$$

When the centroid and shear center do not coincide, the diagonalization of Vlasov's equations, is possible only in the case $N = 0$.

The substitution of Equations 3.72 into Equation 3.33 gives an expression of the normal stress based on the corresponding internal actions:

$$\sigma_z = \frac{M_y}{J_{yy}}x + \frac{M_x}{J_{xx}}y + \frac{B}{J_{\omega\omega}}\omega \tag{3.73}$$

The first two contributions derive from the well-known Saint-Venant's theory and are based on the hypothesis of plane sections; the third describes the normal stresses due to the out-of-plane warping of the profile.

The internal actions producing tangential stresses are also diagonalized:

$$T_x = -EJ_{yy}\xi''' \tag{3.74a}$$

$$T_y = -EJ_{xx}\eta''' \tag{3.74b}$$

$$M_z^{VL} = -EJ_{\omega\omega}\vartheta''' \tag{3.74c}$$

This means that the system of Equations 3.56 is reduced to the following decoupled equilibrium equations:

$$p_x = EJ_{yy}\xi^{IV} \tag{3.75a}$$

$$p_y = EJ_{xx}\eta^{IV} \tag{3.75b}$$

$$m_z^{VL} = EJ_{\omega\omega}\vartheta^{IV} - GI_t\vartheta'' \tag{3.75c}$$

Imposing the boundary conditions, the system can be solved and functions ξ, η and ϑ can be determined together with the normal and tangential stresses.

It is interesting to observe that Equation 3.75c is formally the same as the equation of the elastic line with effects of the second order, due to a tensile axial load N:

$$q(z) = EIv^{IV} - Nv'' \tag{3.76}$$

The substitution of Equations 3.74 into Equation 3.49 gives an expression for the tangential stresses:

$$\tau_{zs} = \frac{1}{b}\left[\frac{T_x}{J_{yy}}S_y(s) + \frac{T_y}{J_{xx}}S_x(s) + \frac{M_z^{VL}}{J_{\omega\omega}}S_\omega(s)\right] \tag{3.77}$$

The initial two terms are derived from Jourawski's theory, while the final term derives from Vlasov's theory.

It is noteworthy to emphasise the formal analogy between the well-known elastic line equations, which describe the bending behaviour of a beam, and the diagonalised differential equations, which describe the torsional behaviour of thin-walled open-section beams.

As in the case of flexural curvature, in the case of torsional behaviour the term ϑ'' vanishes where the bimoment is zero or, in other words, the bimoment is zero where the line describing the rotations of the beam has an inflection point.

If the contribution due to the primary torsion $GI_t\vartheta''$ is negligible, equation 3.75c can be integrated more easily.

3.4 Dynamic analysis of tall buildings

It is well known that the higher a building is, the more sensitive it is to the dynamic effects of wind and earthquakes. At the conceptual design stage, a preliminary assessment of the free vibration frequencies is essential.

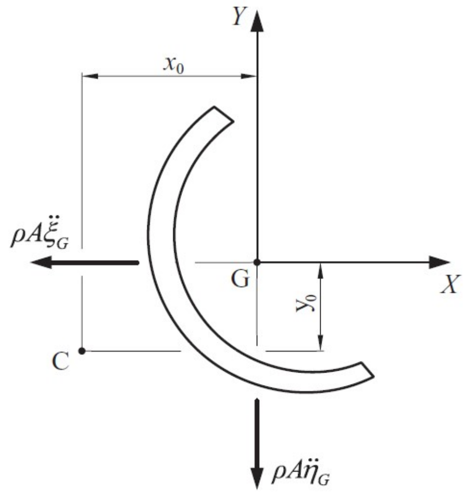

Figure 3.9: Inertial forces acting on a thin-walled open-section

As only mode shapes and natural frequencies are evaluated, external actions are not taken into account and forced ground motions are not included in the analysis.

The D'Alembert principle permits the reduction of the inertial forces of the structure to static forces, thereby enabling their inclusion in Equation 3.21. Specifically, the masses of the building floors manifest in the global equilibrium equations in conjunction with the corresponding accelerations. Conversely, the mass pertaining to the vertical elements is deemed negligible, and its effect is thus excluded. Consequently, the load vector in this case is represented by the product of a mass matrix and a vector containing the inertial accelerations of the floors.

The inertial forces are (Figure 3.9)

$$p_x = -\rho A\ddot{\xi}_G \tag{3.78a}$$

$$p_y = -\rho A\ddot{\eta}_G \tag{3.78b}$$

Let the shear center C be the origin of the local coordinate system; the transverse displacements of the centroid can be written in terms of the global floor displacements ξ, η and ϑ through the following expressions:

$$\ddot{\xi}_G = \frac{d^2}{dt^2}(\xi - y_0\vartheta) \tag{3.79a}$$

$$\ddot{\eta}_G = \frac{d^2}{dt^2}(\eta + x_0\vartheta) \tag{3.79b}$$

where x_0 and y_0 define the position of the centroid with respect to the shear center.

The actions described by Equations 3.78, applied to the centroid of the section, produce a torsional moment with respect to the shear center:

$$m_z = -\rho J_p \frac{d^2\vartheta}{dt^2} + \left[\rho A \frac{d^2}{dt^2}(\xi - y_0\vartheta)\right] y_0 - \left[\rho A \frac{d^2}{dt^2}(\eta + x_0\vartheta)\right] x_0 \tag{3.80}$$

where J_p is the polar moment of inertia of the section referred to the centroid of the section.

Substituting Equations 3.78 and 3.80 into Equations 3.75 yields

$$EJ_{yy}\frac{\partial^4\xi}{\partial z^4} + \rho A \frac{\partial^2}{\partial t^2}(\xi - y_0\vartheta) \tag{3.81a}$$

$$EJ_{xx}\frac{\partial^4\eta}{\partial z^4} + \rho A \frac{\partial^2}{\partial t^2}(\eta + x_0\vartheta) \tag{3.81b}$$

$$EJ_{\omega\omega}\frac{\partial^4\vartheta}{\partial z^4} - GI_t\frac{\partial^2\vartheta}{\partial z^2} + \rho J_p\frac{\partial^2\vartheta}{\partial t^2} - \rho A y_0\frac{\partial^2\xi}{\partial t^2} + \rho A y_0^2\frac{\partial^2\vartheta}{\partial t^2} + \rho A x_0\frac{\partial^2\eta}{\partial t^2} + \rho A x_0^2\frac{\partial^2\vartheta}{\partial t^2} \tag{3.81c}$$

Using the relationship between the polar moment of inertia in reference to the shear center, I_0, and to the center of gravity, J_p:

$$J_p = I_0 - Ay_0^2 - Ax_0^2 \tag{3.82}$$

and substituting this equation into Equation 3.81c, we have:

$$EJ_{\omega\omega}\frac{\partial^4\vartheta}{\partial z^4} - GI_t\frac{\partial^2\vartheta}{\partial z^2} + \rho I_0\frac{\partial^2\vartheta}{\partial t^2} - \rho A y_0\frac{\partial^2\xi}{\partial t^2} + \rho A x_0^2\frac{\partial^2\eta}{\partial t^2} = 0 \tag{3.83}$$

In general, the three equations are coupled to each other. Only in the case of double symmetry is the bending problem decoupled from the torsion problem.

It is possible to separate the spatial problem from the temporal, expressing the unknowns ξ, η and ϑ as the product of a spatial function *Z(z)* and a time function *T(t)*:

$$\xi = U(z)T(t) \tag{3.84a}$$

$$\eta = V(z)T(t) \tag{3.84b}$$

$$\vartheta = \Theta(z)T(t) \tag{3.84c}$$

Substituting Equations 3.84 into Equations 3.81a and b and into Equation 3.83 yields

$$\frac{EJ_{yy}U^{IV}}{-\rho AU + \rho Ay_0\Theta} = \frac{\ddot{T}}{T} = -\omega_n^2 \tag{3.85a}$$

$$\frac{EJ_{xx}V^{IV}}{-\rho AV + \rho Ax_0\Theta} = \frac{\ddot{T}}{T} = -\omega_n^2 \tag{3.85b}$$

$$\frac{EJ_{\omega\omega}\Theta^{IV} - GI_t\Theta''}{-\rho I_0\Theta + \rho Ay_0U - \rho Ax_0V} = \frac{\ddot{T}}{T} = -\omega_n^2 \tag{3.85c}$$

where ω_n^2 is the square of the angular frequency.

From the system of Equations 3.85, it is possible to obtain the time-dependent differential equation:

$$\ddot{T} + \omega_n^2 T = 0 \tag{3.86}$$

The general integral of this equation is given by

$$T(t) = A_n cos\omega_n t + B_n sin\omega_n t \tag{3.87}$$

The coefficients A_n and B_n can be obtained from the initial conditions of the problem.

Any vibrational motion of the beam can be described as a superposition effect of the mode shapes:

$$\xi = \sum_{n=1}^{\infty} U_n(z) T_n(t) \tag{3.88a}$$

$$\eta = \sum_{n=1}^{\infty} V_n(z) T_n(t) \tag{3.88b}$$

$$\vartheta = \sum_{n=1}^{\infty} \Theta_n(z) T_n(t) \tag{3.88c}$$

The boundary conditions at the constraint (z = 0) are

$$U = V = \Theta = U' = V' = \Theta' = 0 \tag{3.89}$$

while, at the top:

$$U'' = V'' = \Theta'' = U''' = V''' = GI_t\Theta' - EJ_{\omega\omega}\Theta''' = 0 \tag{3.90}$$

In the case of an N-storey building, the dead load of the floors is dominant with respect to the mass of the bracings. Consequently, the inertial forces are evaluated as the product of the mass matrix of the floors and the vector containing the accelerations of the same floors in the directions X and Y. If the viscous damping forces are neglected, the equation of motion can be expanded to a $3N \times 3N$ matrix relationship after the expansion and assembly procedures of the mass matrix and the stiffness matrix. Subsequent to the determination of the eigenvectors of the displacements of the floors $\{\delta\}$, the displacements of the i-th element and, consequently, the stresses acting in it can be calculated using the General Algorithm.

4 Analysis of the main tall buildings in Turin

This chapter provides a brief historical overview of some of the main tall buildings in Turin, followed by an examination of their structural analyses. These analyses are derived from the theses of M. De Santis [13], M. Taggio [31], M. Fiammingo [15], E. J. Paganone [28], and D. Vigorita [33], as well as from the articles of *A. Carpinteri et al.* [5] and *G. Nitti et al.* [26]. The analyses are carried out using both the Analytical Model, based on the General Algorithm, and the Numerical Model, employing the Finite Element Method.

4.1 Historical background

Any discussion of Turin's high-rise buildings must begin with the Mole Antonelliana (Figure 4.1), the emblematic building of the city, built in 1889 by the architect Alessandro Antonelli. Originally conceived as a synagogue, it was not appreciated by the Jewish community because of its architectural complexity and running costs, so it was bought by the city council to make it a monument to national unity. Until the 1930s, the Mole Antonelliana held the record for being the tallest masonry building in Europe at 167.5 meters.

The Littoria Tower (Figure 4.2), now the Reale Mutua Tower, was built in 1934 to a design by the architect Armando Melis de Villa. Located in the city centre, in Via Giovanni Battista Viotti, the Reale Mutua Tower is a residential building that is an example of rationalist architecture. It is made up of an eight-storey body and a 19-storey tower that reaches a height of 87 meters.

In 1959, the BBPR Tower (Figure 4.3) was built in Piazza Statuto, on the corner of Corso Francia. This building, with its 14 floors reaching a height of 60 meters, is an example of post-rationalist Brutalist architecture. It was built for Reale Mutua Assicurazioni to a design by Studio BBPR, a group of architects made up of Gian Luigi Banfi, Lodovico Barbiano di Belgiojoso, Enrico Peressutti and Ernesto Nathan Rogers.

In 1968, on Via Cernaia, the Rai Skyscraper (Figure 4.4), now known as the

Figure 4.1: Mole Antonelliana

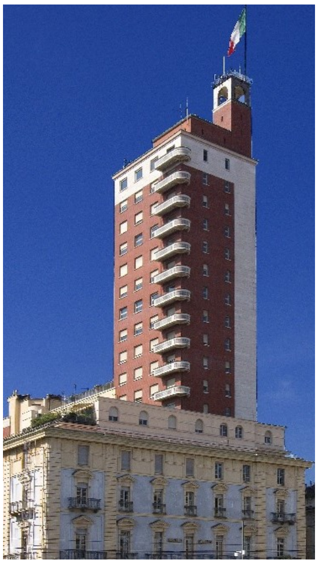

Figure 4.2: Littoria Tower

Figure 4.3: BBPR Tower

Figure 4.4: Rai skyscraper

Pietro Micca Palace, was built at the behest of architects Aldo Morbelli and Domenico Soldiero Morelli. Inspired by the American International Style, the building has 24 floors and a total height of 72 meters.

In 2015, the Sanpaolo Tower (Figure 4.5), a building of the banking group of the same name located on Corso Inghilterra, was designed by the architect Renzo Piano. At 166.26 meters, it is the third tallest building in Turin, after the Mole Antonelliana and the Piedmont Region Headquarters Tower.

In 2022, the Piedmont Region Headquarters Tower (Figure 4.6) will be completed on Via Nizza, housing the central offices and bodies of the Region. Designed by Massimiliano Fuksas, it is the tallest building in the city at 209 metres.

In Figure 4.7 is shown the location in the city of the tall buildings that were examined in the present thesis.

Figure 4.5: Sanpaolo Tower

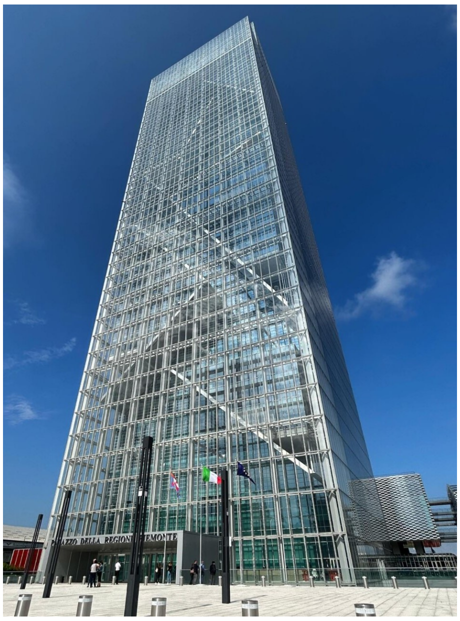

Figure 4.6: Piedmont Region Tower

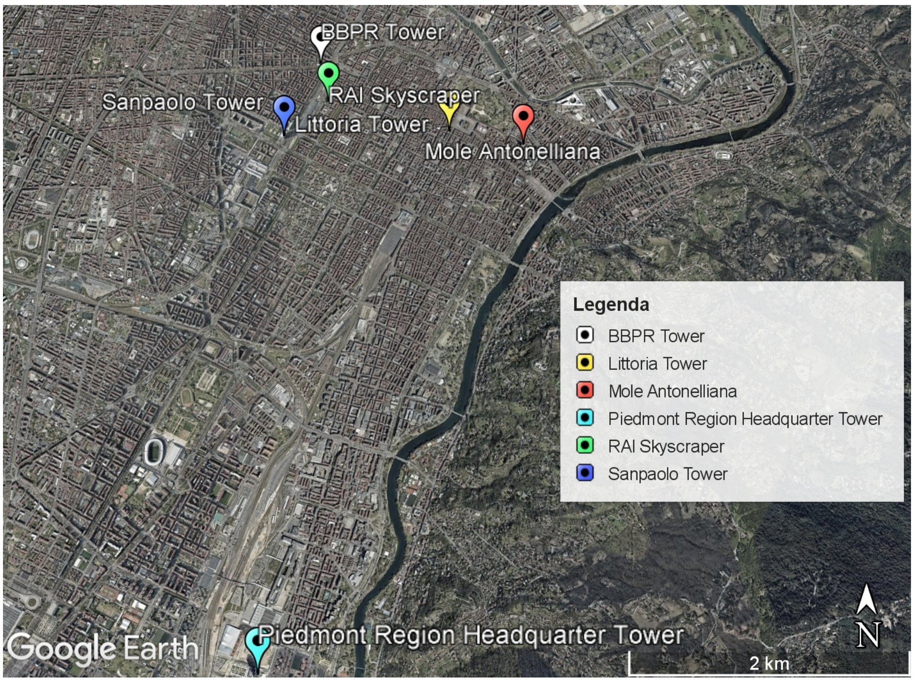

Figure 4.7: Location in the city of tall buildings

4.2 Reale Mutua Tower

The tower was completed and inaugurated in 1934, and construction took just over a year after the project was approved. Originally the building was to have been erected in Piazza XVIII Dicembre, in the area where the Rai skyscraper still stands today, but the redesign of Via Roma, which was underway at the time, suggested the current location as the best for a work of such magnitude.

Today's Via Roma is the result of profound urban changes in the last century, which transformed a simple Baroque street, whose sole purpose was to connect the ancient Piazza Castello with the modern Porta Nuova railway station, into a street with completely different characteristics. At the beginning of the 20th century, the street was lined with dilapidated 18th-century buildings and lacked basic services such as drinking water and sewerage. The idea of a possible intervention to improve the dilapidated conditions of Via Roma, in order to make this artery luxurious and elegant, began to take hold among the local administrators.

The urban desing criteria for the remaking of the new street included:

- The construction of arcades in the style of the large porticoed streets typical of Turin
- A greater width of the street, up to 15 meters
- The absence of the typical bow-windows

In 1926, with the drafting of the new Regulatory Plan by Scanagatta and Godino, the previously mentioned stated urban planning criteria were resumed. The following is what was in the Scanagatta Plan:

> *"The galleries around the churches, which were planned to be 8 meters wide, will be widened to 15 meters for aesthetic reasons and to make it easier for pedestrians to pass through them, thus avoiding the obstruction of the public passage at the churches, which is not subject to widening. These tunnels will be built in the manner that the Municipality reserves the right to prescribe with the approval of the construction projects... The corner buildings at the outlets on the squares will have to conserve their current architectural physiognomy for a depth of at least 14 meters facing the new Via Roma, starting from the squares themselves. Those in the intermediate blocks towards Via Roma must harmonise with the 18th-century style of Piazza San Carlo at least in their main lines, with recurring cornices at the same level for each block. The formation of bow windows in the buildings of the new street is forbidden. The porticoes must be supported by columns of granite or other equivalent stone,*

they must all have the same width of 5.80 meters from the inner edge of the fabrication to the street alignment and common height of the same blocks and in any case not less than 7.50 meters. The four blocks adjacent to Piazza San Carlo must only have four storeys above ground level, i.e. three storeys above the porticoes, excluding any kind of back storey, but they must not exceed a height of 21 meters, and the five storeys must be extended to the entire block."

The renovation of Via Roma began on 20 January 1931. One of the first blocks to be affected by the renovation of Via Roma was the Sant'Emanuele block, where the Reale Mutua Tower was built, owned by Società Reale Mutua Assicurazioni since its inauguration in 1934. At the beginning of the 1930s, the Società Reale Mutua Assicurazioni bought the whole block in order to take part in the reconstruction of the first section of Via Roma.

In the meantime, the City Council modified the previous restrictions on new construction, increasing the cubic meters and heights of the buildings that could be built in the block. On the basis of these new municipal regulations, Arch. Melis de Villa arrived at an estimated cubage of 60,000 m^3 in his design, as opposed to the 45,000 m^3 foreseen by the previous restrictions. On 22 January 1932, the Superior Council of Fine Arts in Rome gave its final favourable opinion on the preliminary project, and the following month Bernocco and Melis' drawings were deposited in the technical offices of the Municipality. The reasons for the client's choice of a tower are still not entirely clear. Many have speculated that Turin was a "French" city from an urbanistic point of view, as it did not have the classical medieval tower that was found in the most important Italian cities such as Bologna, Florence or Pisa, and that the work therefore represented an "Italianisation" of the city centre. The decision to build a tower therefore represented the Commission's desire to create a decisive break between "old" and "new".

The project, designed in the modern style by the architect Armando Melis de Villa, originally envisaged a ten-storey building with an eight-storey tower at the top, with a turret with four large clocks on each side. Later, the project was modified by a decree of the Turin City Council, which reduced the number of arcades facing Piazza da Castello from five to four. The reduction in the number of arcades led to the creation of an opening to Via Viotti, useful for the flow of traffic and the entrance to Via Pietro Micca, but also to a loss of cubic space. This change in cubic capacity represented a potential loss of income for the SMRA, so after an intense exchange of correspondence a simple solution was found that allowed the lost cubic meters to be converted into additional floors to be added to the tower, bringing the building to a total of 20 floors.

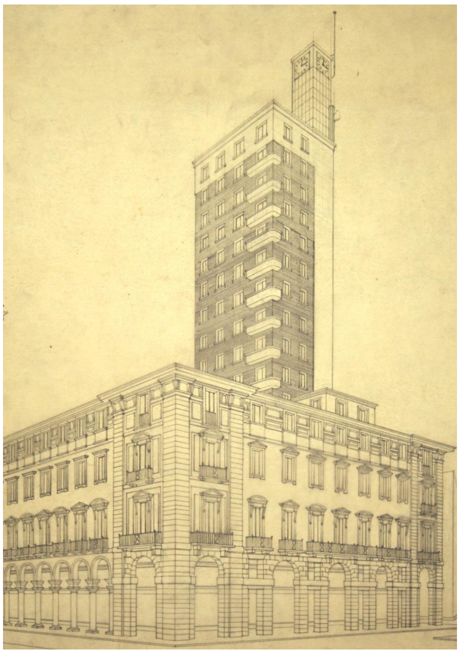

Figure 4.8: Prospect of the Reale Mutua Tower

An axonometry of the first design of the Reale Mutua Tower is shown in Figure 4.8. In this drawing it is possible to observe the five arches of the neo-baroque style building facing Piazza Castello.

Thus, in 1932, the construction of the first Italian skyscraper with an all-steel supporting structure began, designed by Melis for the Reale Mutua Assicurazioni company, at a height of 85 meters.

4.2.1 The structural system of the Reale Mutua Tower

The Melis Tower is the first skyscraper in Italy to have a supporting structure made entirely of steel.

The construction system used for the construction of the skyscraper on the Sant'Emanuele block is the braced frame, in which there is an in-framed structure with bracing systems in both X and Y directions. For the framed part, there are columns with IPN coupled profiles by means of braces, while for the beams there are simple IPN profiles. The bracing was realised using simple, coupled C-profiles, while for the low building, which is connected to the tower, there is no bracing and it too consists of double IPN caulked profiles for the columns and single IPN profiles for the beams. The tower, which has no structural function, is constructed using open profiles and is braced on all four sides.

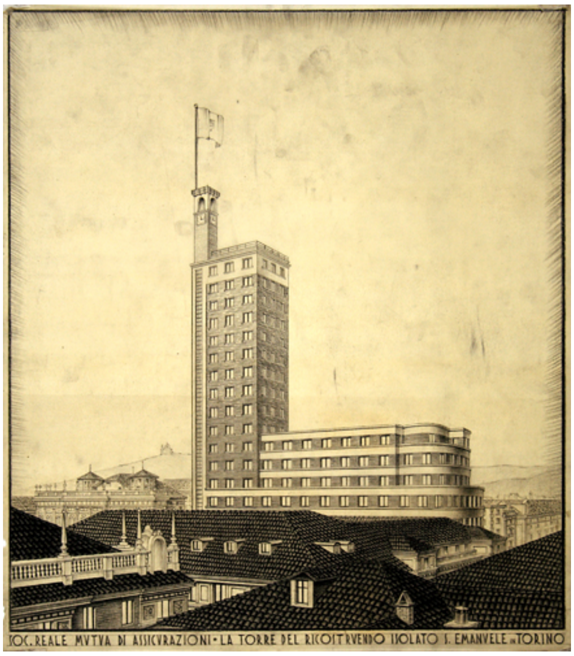

Figure 4.9: Project proposal no. 4 for the Littoria Tower - Armando Melis de Villa Foundation

Figure 4.10: Tower's metal skeleton

Figure 4.11: Detail of the tower's metal skeleton

4.2.2 Technologies and materials

The Reale Mutua Tower was not only a record in terms of height, but also in terms of the materials and construction technologies used.

The use of innovative technologies was mainly due to the choice of a steel supporting structure instead of the classic masonry or reinforced concrete solution. The realisation of a metal framework provided advantages from an architectural point of view, such as the possibility of realising large spans and thus being able to realise profound variations in use, but at the same time also presented several problems due to:

- protecting the framework from fire and oxidation without sacrificing the advantages of lightweight construction;
- building insulation;
- construction of lightweight floors and partition elements;

The solution to the first problem was realised by using the innovative pumice concrete for the time. Experimentally, the designers observed that, by creating a 5 cm layer of pumice concrete, the steel protected by it could maintain a temperature of less than 70°for four hours, considering a wood fire at a temperature of 700°. On the basis of these observations, all metal components were embedded in pumice concrete, with the following component doses:

Material	**Quantity**
Pumice in a mixed size of 6 mm to 9 mm	1 m^3
Sand	0.20 m^3
Cement	250 kg

To solve the second problem, hollow perimeter walls were used instead, with an outer wall of 12 cm thick marble or ceramic tiles and a 6 cm thick layer of porous cement on the inside. A thin brick wall was used to create the cavity. The thermal resistance of these perimeter walls is comparable to that of a 70 cm thick solid wall.

Steel beams and volterrane were used for the floors, and innovative materials such as *Eraclit* or tarred felt were added to complete the stratigraphy, as shown in Figure 4.13.

A typical roof slab stratigraphy is shown below:

- Stoneware tiles 1.0 cm;
- Cement mortar 2.0 cm;

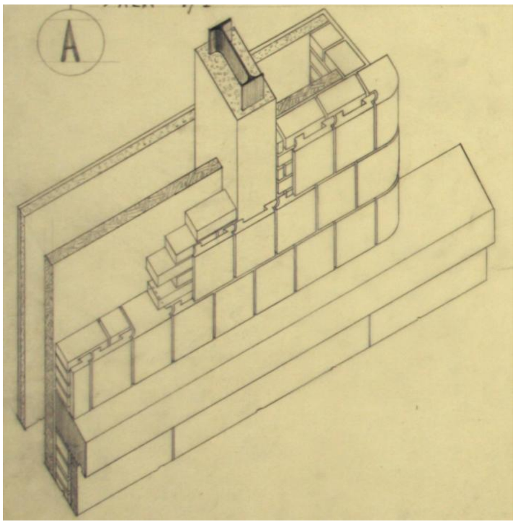

Figure 4.12: Detail of the stratigraphy of the hollow perimeter wall

- Asphalt 2.0 cm
- Tarred felts 0.5 cm
- Pumice concrete 3.0 cm;
- Heraclit 5.0 cm;
- Cement mortar 0.5 cm;
- Pumice concrete 2.0 cm;
- Volterrane 14 cm;
- Plaster 2.0 cm.

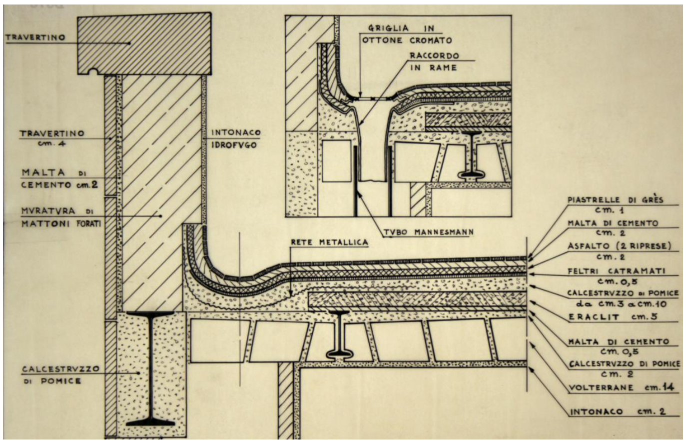

Figure 4.13: Detail of the stratigraphy of a roof slab

For the construction of the Tower, an innovative technology called *electric arc welding*, developed by the swedish Kjellberg, was adopted. The use of electric arc welding in construction had considerable advantages: it made it possible to reduce the weight of the brackets and attachment plates, to achieve high rigidity values thanks to the monolithic nature of the connected parts, to achieve better aesthetics and to achieve considerable cost and time savings.

According to the Società Nazionale Officine Savigliano in its Technical Bulletin of May-December 1933, the use of electric arc welding made it possible to reduce the weight of the construction by 20%. Using this technique, it was possible to raise the supporting structure in just 75 days by assembling 900 tonnes of steel.

4.2.3 Static and Kinematic Verification of the Reale Mutua Tower

Structure modelling

In order to perform the static and kinematic verifications of the structure, it was necessary to model the Reale Mutua Tower using the *Sap2000* software, which allows the three-dimensional calculation of its frame. On the basis of the structural drawings provided by Reale Mutua Assicurazioni, a model was created with the following characteristics:

- n°Elements: 2526
- n°Nodes: 1242
- n°of Equilibrium Equations: 4764
- n°of constrained nodes : 37
- Slab behaviour: Infinitely rigid in the plane

The modelling of the columns was carried out using the Section Designer application within the software, which allowed the presence of IPN coupled profiles to be taken into account, while the modelling of the connections was carried out considering perfect joints, as the structure is assembled using electric arc welding. Horizontal and vertical loads have been taken into account in the analyses developed, the former being represented by the self-weight of the structure, the permanent loads carried and the crowd, while the latter are represented by the effect of wind, defined according to the requirements of the Italian standard NTC18.

The following loads were considered for the subsequent analysis of the structure:

- Vertical Loads
  - Dead loads of the structure G1
  - Weight Carried by the structure G2
  - Crowd Load Q

newpage

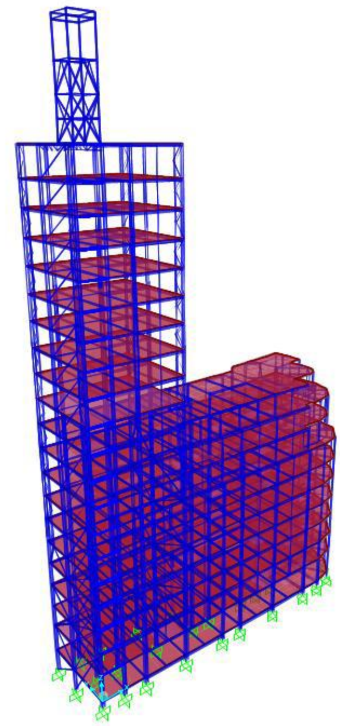

Figure 4.14: 3D model of the tower

- Horizontal Loads
  - Wind F
- Load Analysis: Roof Slab

Layer of Roof Slab	**Thickness [m]**	**Weight [kg/m^3]**	**Weight [kg/m^2]**
Stoneware Tiles	0.01	-	18.5
Cement Mortar	0.02	2100	42
Asphalt	0.02	1300	26
Bituminous Felt	0.005	-	2.7
Pumice Concrete	0.1	1000	100
Eraclit	0.05	-	45
Cement Mortar	0.005	2100	10.5
2 IPN 140 Profiles (Sec.)	-	7800	29
Pumice Concrete	0.02	1000	20
Volterrane	0.14	-	145
Plaster	0.02	1700	34
		TOTAL	**432**

- Load Analysis: Slab

Layer of Roof Slab	**Thickness [m]**	**Weight [kg/m^3]**	**Weight [kg/m^2]**
Stoneware Tiles	0.01	-	18.5
Cement Mortar	0.02	2100	42
Pumice Concrete	0.1	1000	100
Cement Mortar	0.005	2100	10.5
2 IPN 140 Profiles	-	7800	57.1
Volterrane	0.14	-	145
Plaster	0.02	1700	34
		TOTAL	**407**

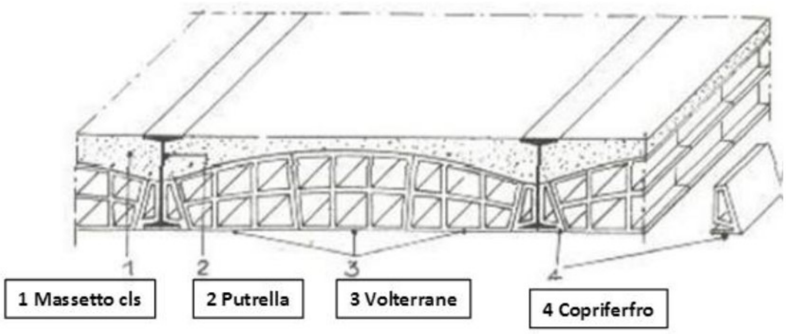

Figure 4.15: Steel slab and volterrane

In order to determine the weight of the partitions, without knowing the type of walls used and their stratigraphy, a dead weight of 150 kg/m2 is assumed. Based on the above assumptions, the vertical loads are as follows:

Load Type	**Value [kN/m^2]**
Roof Slab	4.32
Slab	4.07
Partitions	1.50
Crowd Load	2.00

Wind action calculation

Referring to the wind action calculation shown in Appendix A, where the load condition for considering twisting actions is added to the load condition where the equivalent static wind action is applied according to the two axes of symmetry of the section, two load cases are configured.

- Case 1: Wind action along the symmetry axes of the structure

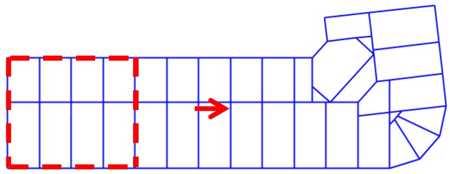

Figure 4.16: Wind action in X direction

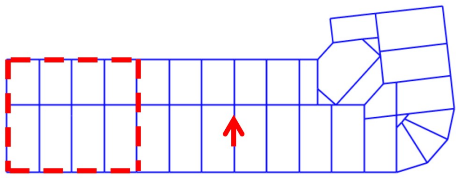

Figure 4.17: Wind action in Y direction

- Case 2: Wind action taking into account torque actions

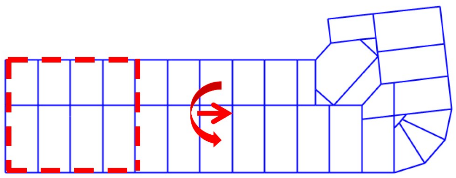

Figure 4.18: Wind action in X direction

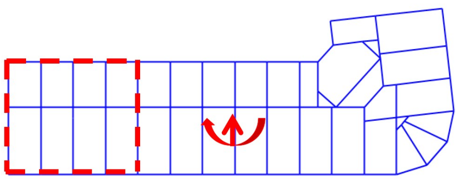

Figure 4.19: Wind action in Y direction

Calculations and results

The results of the two load cases analysed for the two directions X and Y, for the upwind and the downwind side. The complete results are presented in Appendix C, while the summary results are shown in the tables 4.1 and 4.2.

Fx [kN]	Mx,z [kNm]	Fy [kN]	My,z [kNm]
-	-	-	-
52	0	138	0
46	0	120	0
47	0	123	0
52	0	136	0
57	0	149	0
64	0	168	0
64	0	165	0
54	0	163	0
59	0	180	0
61	0	184	0
51	0	156	0
52	0	57	0
53	0	59	0
55	0	60	0
56	0	61	0
57	0	62	0
58	0	64	0
59	0	65	0
63	0	70	0
34	0	37	0

Table 4.1: Summary of results for case 1

Fx [kN]	**Mx,z [kNm]**	**Fy [kN]**	**My,z [kNm]**
-	-	-	-
26	81	69	-565
23	71	60	-491
23	72	61	-503
26	81	68	-559
28	88	74	-610
32	99	84	-689
32	100	83	-661
27	71	81	-651
30	79	90	-718
30	80	92	-733
25	55	28	-66
26	56	29	-68
27	58	29	-70
27	59	30	-71
28	60	31	-73
28	62	31	-74
29	63	32	-76
29	64	32	-77
32	69	35	-83
17	37	19	-44

Table 4.2: Summary of results for case 2

Kinematic verification of the structure according to Eurocode 3

When performing the global analysis of the structure to evaluate the actions on the elements of the structure, it is necessary to consider both the ultimate limit state conditions and the service limit state conditions, for the latter it is generally necessary to limit the horizontal displacements of the structure to ensure habitability levels and to contain any instability phenomena. Eurocode 3 and NTC18 propose limit values for the global displacement Δ and the interstory displacement δ. The values suggested by the standard and shown in Figure 4.20 should be compared with the results obtained when considering load combinations at the serviceability limit state, since for steel structures such as the Reale Mutua Tower, the combination to be applied to determine the maximum displacements is the characteristic one.

Tipologia dell'edificio	*Limiti superiori per gli spostamenti orizzontali*	
	$\frac{\delta}{h}$	$\frac{\Delta}{H}$
Edifici industriali monopiano senza carroponte	$\frac{1}{150}$	/
Altri edifici monopiano	$\frac{1}{300}$	/
Edifici multipiano	$\frac{1}{300}$	$\frac{1}{500}$
In caso di specifiche esigenze tecniche e/o funzionali tali limiti devono essere opportunamente ridotti.		

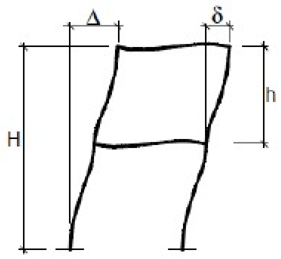

Figure 4.20: Displacement limits given by NTC18

The displacement graphs and the deformed shapes below are only for the load case named Case 1, as Case 2 only emphasises the torsional actions of the structure.

- Case 1: Wind in X direction
  The displacements of the structure due to the wind blowing in the X direction can be seen in Figure 4.21

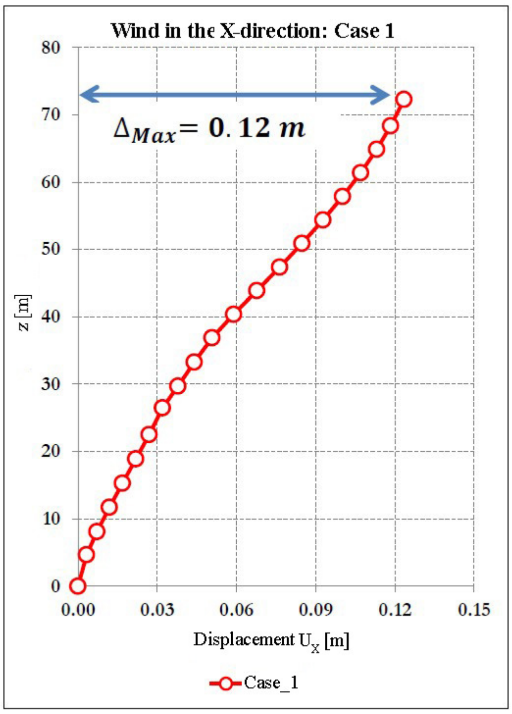

Figure 4.21: Displacement in X direction

- Maximum displacement

$$\Delta_{max} = 0.12\,m$$

- Limit displacement

$$\Delta_{lim} = \frac{1}{500} \cdot H = 0.15\,m$$

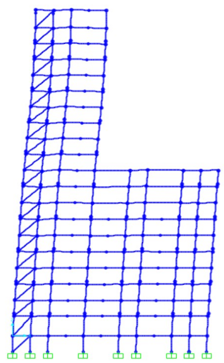

Figure 4.22: Deformation of the structure in the X-direction

- Case 1: Wind in Y direction
  The displacements of the structure due to the wind blowing in the Y direction can be seen in Figure 4.23.
  - Maximum displacement

$$\Delta_{max} = 0.19\,m$$

- Limit displacement

$$\Delta_{lim} = \frac{1}{500} \cdot H = 0.15\,m$$

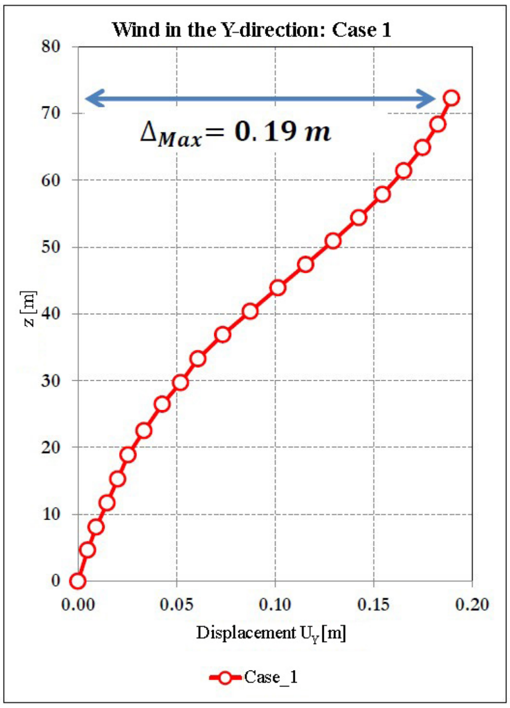

Figure 4.23: Displacement in Y direction

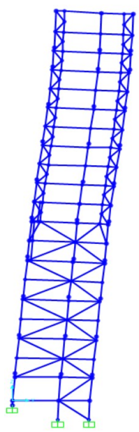

Figure 4.24: Deformation of the structure in the Y-direction

- Case 2: Wind in X direction

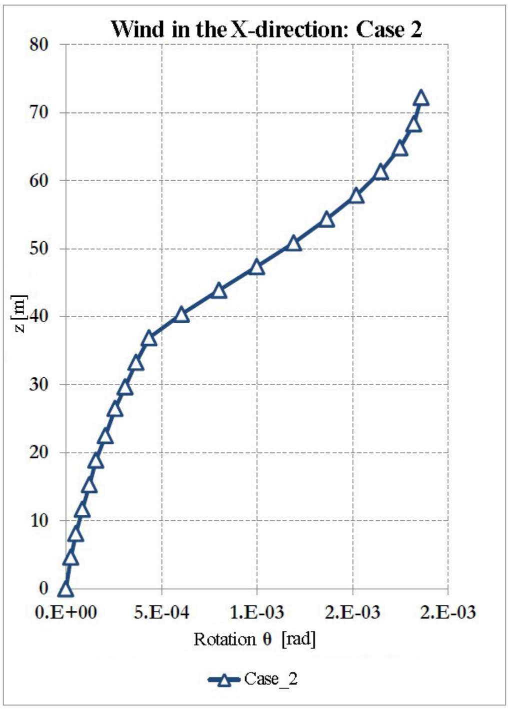

Figure 4.25: Rotation of the structure in X direction

- Case 2: Wind in Y direction

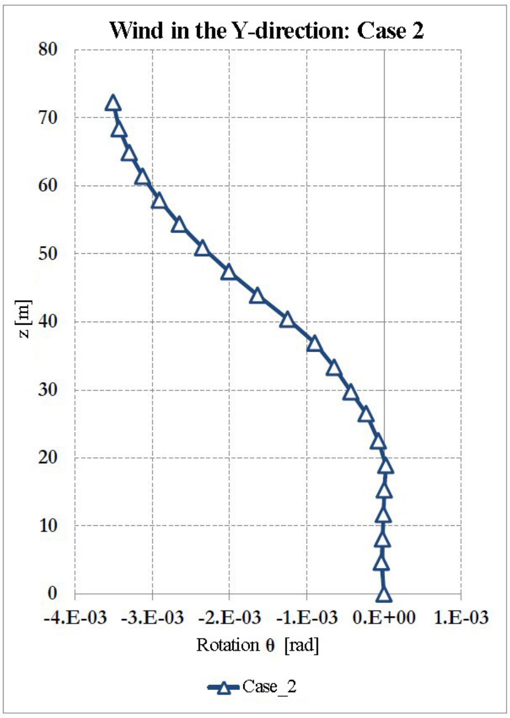

Figure 4.26: Rotation of the structure in Y direction

Conclusions

The influence of the low body on the displacements in both the X and Y directions is considerable: for the first direction, this influence is manifested in the formation of a flexure in the displacement diagram, shown in Figure 4.25, which is not present in a typical displacement diagram of a frame structure. A similar situation occurs in the Y direction: what has an important effect on the kinematic response of the structure is the presence of bracings placed on the side walls of the tower, which provide the necessary stiffness to create an inflection point in this direction as well. It is important to note that the bracings stop at the same height as the low body; above the tenth floor, the kinematic behaviour of the structure returns to that of a framed structure. In both cases, the structure remains within the limits imposed by the standard in terms of displacements, which are equal to 1/500th of the height of the tower.

The static analysis carried out showed that the solution with coupled profiles offers significant advantages, as it allows the creation of a light structure with high load resistance. The analysis of the composite member showed that, for the type of analysis carried out and for the loads considered here, it has large safety margins.

The Reale Mutua Tower, although it was designed in the 1930s, complies with the analyses I have carried out in accordance with Italian and European regulations. With its innovative solutions and the secrets it contains, the Melis Tower represents a national record that must continue to be protected, studied and improved.

4.3 BBPR Tower

The BBPR Tower (Figure 4.27), built in 1959 by the architects' studio of the same name, is located in Piazza Statuto at the corner of Corso Francia and is a residential, office and commercial building. The building has fourteen floors above ground and two underground, a reinforced concrete structure with masonry infill and a sloping roof covered with flat tiles.

The tower is part of a complex made up of three buildings of different heights; in fact, along Corso Francia, the building goes from 14 to 6 and finally to 10 floors above ground; along Via Cibrario, on the other hand, there is another building, built later, of only 5 floors.

Figure 4.27: BBPR Tower

The acronym *"BBPR"* comes from the initials of the surnames of the four architects Gian Luigi Banfi, Lodovico Barbiano di Belgiojoso, Enrico Peresutti and Ernesto Nathan Rogers, who in 1931 founded a design studio that was to become a point of reference for Milanese architecture. Driven by a strong spirit of collaboration, they never designed something that was the expression of the inspiration of a single member, but always worked as a team, agreeing on every aspect of the design, which was quite unusual at the time, as they used to associate each work with the name of the designer whose character and personality it reflected. As reported in the essay *"BBPR and Milan 1931-1976"* by Stefano Guidarini and Luca Molinari, the four architects used to publicly declare:

> *"any project done in four is still better than the one that could have been done by each one individually, [...] and we will never reveal the individual authorship of an idea, every idea is always our idea."*

The guideline that characterises the studio's projects after the Second World War, the period in which the BBPR tower was built, is the problem of the integration. It is taken from *"BBPR and Milan 1931-1976"*:

> *"In the 1950s, BBPR initiated a profound reflection on the renewal of modern architecture in relation to context, history and tradition. In this perspective, the theory of environmental pre-existences, promoted by Rogers in the pages of 'Casabella-continuity', proposed to face the problem of design in relation to a new conception of the environment, trying to represent empirically in the architectural language some significant features of places, recovering their material, chromatic and perceptive aspects."*

The architectural concept of the BBPR Tower is characterized by the presence of regularly spaced, equally sized columns that, starting from the second floor, project outward from the building's footprint before retreating inward to meet the sloping rooflines.

Since the building is located at the edge of Turin's historic center, where each building is surrounded by a wide and elegant portico, the presence of this portico serves a dual purpose. On the one hand, it echoes the surrounding buildings, thus resolving the issue of integration into the context. On the other hand, with its massive columns and imposing regular geometry, it is a clear sign of the structure's weight, an aspect that the designers did not intend to hide behind a facade cladding but, on the contrary, wished to highlight, as it is precisely the presence of weight and the way the structure resists it that is the source of the architectural emotion; this makes the building one of the few examples of post-rationalist or "brutalist" architecture in Turin.

The building was commissioned by the "Reale Mutua" insurance company, which in 1955 acquired the land at the beginning of Corso Francia, owned by the Turin-Rivoli Tramway Consortium, which decided to sell the land to raise funds for the construction of a new trolleybus station. When Reale Mutua bought the land, which initially did not include the building in via Cibrario, it announced its intention to build a new headquarters for its offices, which at the time were located in the historic building in via Corte d'Appello.

The project was entrusted to the architects of the BBPR studio in Milan, who at first thought of a large seventeen-storey tower that would occupy the entire area facing the square, divided into two bodies, one resting on the other, with a common base for the whole structure, on which a second upper body would rest where the height of the building would increase again. However, this project was not carried out, partly because of the changing needs of the client, who delayed the sale of the historic headquarters in the city centre, preferring to divide the new building into a series of different units, including shops, offices and apartments, but of a smaller size, which was more attractive to the property market of the time, and partly because the company did not own the land overlooking via Cibrario, which it would only acquire in later years. It was therefore decided to reduce the height of the tower.

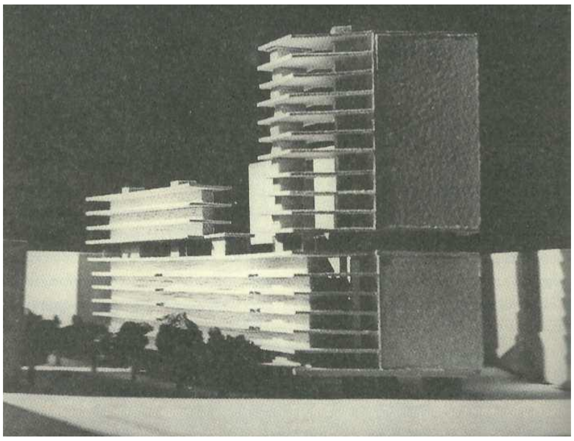

Figure 4.28: Cardboard model of the initial design of the complex for Reale Mutua Assicurazioni (from the Archives of the Central Library of Architecture of the Politecnico di Torino)

Work began without defining the internal layout of the building and its uses, which were later entrusted to the architect Gian Franco Fasana. Instead, the reinforced concrete structures were designed by engineer Giulio Pizzetti. The work was carried out by the engineer Luigi Raineri, who had already built the historic headquarters of the insurance company.

With regard to the supporting structure, in Sergio Pace's essay [27], the architects state:

> *"The structure is the unitary element of the building: the columns supporting the part above the first floor transfer the loads of the same to the ground floor through an inclination designed to divide the diagonal component of the axial forces, one horizontal, which engages the roof of the ground floor slab, and the other vertical, which is discharged on the columns of the same. In the upper part of the building, the columns, which protrude 1.2 meters above the ground from the second floor, are joined by the roof structure to form a seamless whole."*

What is most characteristic of the post-war period is the convergence between the figure of the engineer and that of the architect, who until then had worked separately, one concentrating simply on structural calculations and applying the results of theory of structures, the other on the definition of forms, in some cases ignoring the presence of a load-bearing structure. The direct consequence of this is the search for new forms, so that the function of the structure to carry loads can be seen in the form, a new reflection on form that also involves the field of industrial architecture.

Architectural choices dominate the design, and in the BBPR Tower we can see that the columns of the portico are always the same size, both below the tower, where the height is maximum, and where the building is only six or five storeys above the ground.

Again, in Sergio Pace's article:

> *"Faced with such different heights, the system of reinforced concrete beams and columns could have been modified, especially in section, to be more consistent with the principles of statics. However, this has not been done: the consistency required by structural engineering is sacrificed in the name of the building's coherence with the building typology and urban morphology. The portico along the entire ground floor, up to the mezzanines, is not affected by any variation dictated by the different heights: under the tower or under the three-storey building, the section of the column and the oblique supports are always identical, testifying more to a contemporary interpretation of the porticoes of Turin than to an aseptic constructive correctness."*

Another important aspect that must be taken into account in order to place the work in its proper context is its considerable height: in fact, the tower reached a height of 60 meters in its final configuration and, being so close to the city centre, it introduced a revolutionary element into the skyline of the city of Turin. A theme to which the inhabitants of Italy's elegant "living room", characterised by mostly low buildings and dominated by the dome of the Mole Antonelliana, have always shown great sensitivity. Although the tower was much lower than the Mole, it stood out from the surrounding buildings, comparable to the height of the Cathedral's bell tower.

4.3.1 The structural system of the BBPR Tower

At the Historical Archives of the City of Turin, it is possible to consult the drawings of the construction project, a total of 117 plates, and the report of the inspection carried out at the end of the work.

The building is divided into three parts: the tower itself, referred to in the plans as "Body C", the ten-storey "Body A", facing the corner of Corso Francia and Via Matteucci and intended for residential use, and the six-storey "Body B", between the two, intended for offices. In Piazza Statuto, the tower is flanked by the last part of the complex, which is lower and more recent. It was actually built ten years later, at the end of the 1960s, after the purchase of Via Cibrario 1, a nineteenth-century building that was demolished to make way for a four-storey building.

In the analysis that followed, the tower was considered separately from the rest of the building, since body B was not present in the original configuration, having been built at a later date. Furthermore, considering the extension in plan of both bodies A and B, if these were included in the analysis and therefore in the modelling, the height of the tower would be less relevant in terms of the longitudinal development of the complex. In addition, the plans of the various decks of B and C, i.e. where the tower joins the building in Corso Francia, indicate that a 3 cm gap should be maintained between the beams of the two buildings at every level; in this way, the end spans of the frames of B would give rise to overhangs of more than two meters in length. However, as there is no gap visible on the façade, the beams of body B must necessarily have leaned against the external columns of the tower, allowing the two structures to deform uniformly. Such separations can be considered valid for horizontal loads perpendicular to the plane of the frames.

The tower occupies the area of plot no.3, which has 14 and 16 meters sides inclined at an angle of 60 degrees. The building rises 14 storeys above the ground, reaching a height of 51 meters with the last floor. There are also two basement levels up to a height of -6.50 meters. The floor height is 3.40 meters throughout the building, except on the ground floor where the first floor is 6.80 meters high.

The supporting structure consists of frames and two open thin-section walls ("shearwalls") in reinforced concrete. The latter have a height equal to that of the building and a constant thickness throughout. The septum of the lift shaft has a C-section with a thickness of 20 cm. The stairwell, which is separate from the lift shaft, is enclosed by a septum with a horseshoe section and a thickness varying between 20 and 30 cm.

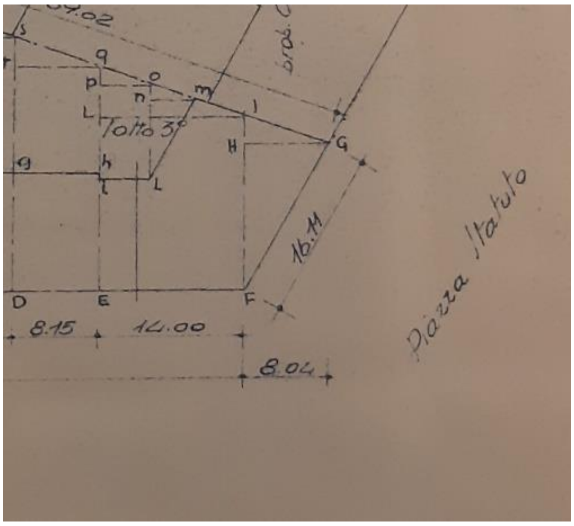

Figure 4.29: Detail of the layout (Historical Archives of Turin)

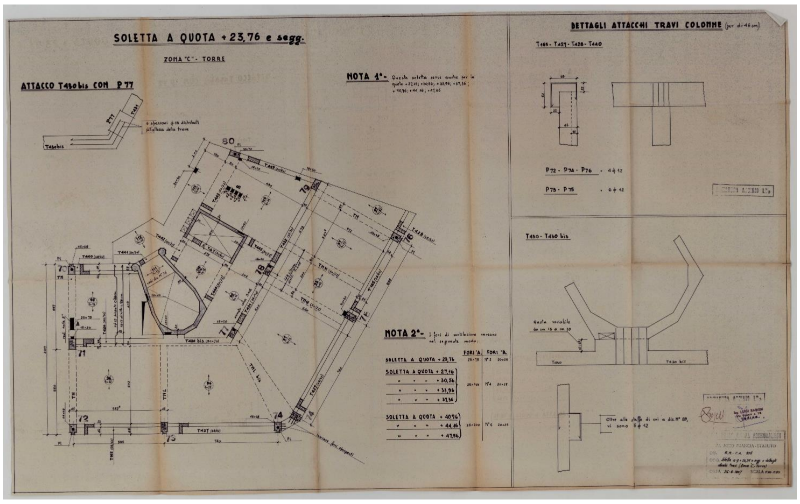

Figure 4.30: Standard deck plan (Historical Archives of Turin)

There are 11 columns (numbered 70 to 80) and they have a rectangular section, except for the corner column, which has a more complex section; its section decreases with the height of the tower. From the level of the first deck, the external piers (numbered 72 to 76) project 1 meter from the base; in addition, pier 74 is divided into two piers with a rectangular section. From the third deck, the section of the piers remains constant.

The main frames of the building are the external ones, included in the façade, and the internal ones. The external beams have an inverted L-section with a width of 68 cm and a height of 62 cm (identified as T165 and T427). The T430 beam of the central frame also has an L-section, but is squarer, with dimensions of 50 cm by 70 cm. The remaining beams of the main frames have a rectangular cross section and variable height, while the thickness of the beams described transverse to the main frames remains constant and equal to that of the slab (22 cm). The exception is beam T449, which measures 30 x 80 cm.

The roof has a double slope and crosses the walls of the lift shaft, which rises to a height of 54 meters.

4.3.2 Analytical model of the BBPR Tower

The semi-analytical calculation code *Ta.Bu. (Tall Builiding Structural system)*, based on the analytical formulation of A. Carpinteri. This code allows the study of tall buildings, even in the presence of thin section walls.

The code analyses a building consisting of N floors with, for each floor, three degrees of freedom in terms of ξ, η and ϑ, i.e. displacements along the X and Y axes respectively and rotation around the Z axis. Another unknown is the force vector F_i in each plane after the external loads have been applied.

The code also imposes constraints on the definition of the structural model:

- Frame elements are defined by the coordinates of their centre of gravity;
- The spans of the frame elements are all equal;
- The dimensions of the sections of the beams and columns that make up the frame are constant and are defined once for each frame;
- Frames are plane;
- The cross-sections of the beams and columns are all rectangular;
- It is not possible to introduce overhangs; open thin section cores *(Vlasov elements)* have a constant thickness cross-section and their shape is defined by discrete midline points;
- All vertical elements are considered embedded at the base and free at the top;
- Floors are considered infinitely rigid in their own plane and infinitely deformable outside it.

With this in mind, the structure was modelled by defining eight frames and two ‘Vlasov type’ elements, open thin section cores of constant thickness, 20 cm for the lift shaft (‘shearwall 2’) and 25 cm for the staircase (‘shearwall 1’), although in reality the latter varies in thickness between 20 and 30 cm (Figure 4.31).

For the main outer frames (frames 1 and 3), the inner frame (frame 4) and the upper left frame (frame 8), the heights of the beams have been defined as the heights of the rectangular sections of equivalent inertia to those of the existing beams, which in reality have an L-shaped cross-section. It should also be noted that a number

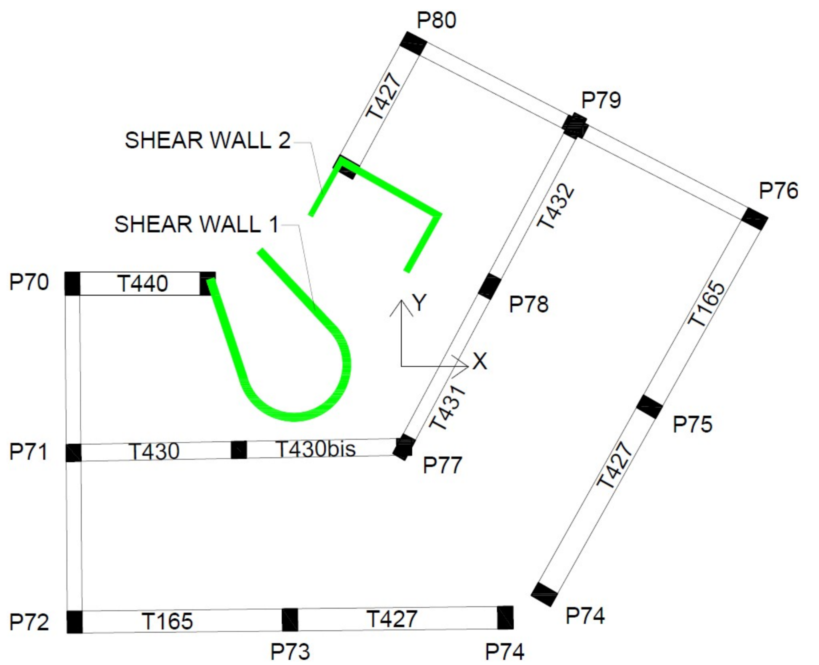

Figure 4.31: Floor plan of the analytical model

Frame	Beam dimensions		Column dimensions		Centroid coordinates		Angle	Span
	b [cm]	h [cm]	b [cm]	h [cm]	x [cm]	y [cm]	α [°]	[m]
1	45	40	45	68	-353	-778	0	6.67
2	45	20	45	68	-1019	-253	90	5.23
3	45	40	45	68	767	-128	60	6.67
4	50	66	45	50	-505	-214	-1	5.14
5	35	70	40	70	285	288	60	5.08
6	30	80	40	70	576	727	-28	6.31
7	80	22	35	70	-58	814	61	4.33
8	45	40	45	70	-808	268	0	4.21

Table 4.3: Model Frames

of columns have been introduced, such as the column of frame 8, which cannot terminate in the septum, and the central column of frame 4, in order to simulate the constraint that the T430 beam finds in the septum of the staircase at approximately half its length. The same was done for the outer frames 2 and 6. The elements introduced are not intended to faithfully reproduce the geometry of the building, but rather to simulate its global response to horizontal actions.

The shear walls were introduced by discretising their sections, the coordinates of the extreme points of which are given in Table 4.4.

Shear walls	Midpoint	Centroid Coordinates		Thickness
	med	x [cm]	y [cm]	S [cm]
1	1	-436.7	367.6	25
	2	-217.5	126.8	25
	3	-173.8	51	25
	4	-174.5	-29.8	25
	5	-221	-107.6	25
	6	-289.1	-147.8	25
	7	-379	-147	25
	8	-452.2	-102.6	25
	9	-490.8	-27.5	25
	10	-589.4	278.1	25
2	1	18.2	297.9	20
	2	117.7	471.1	20
	3	-180.6	642.4	20
	4	-278.9	471.2	20

Table 4.4: Shear walls Data

The value of the modulus of elasticity of the concrete used in the calculations is 28 GPa. This is derived from the formula provided by the Italian standard:

$$E_{cm} = 22000\left(\frac{f_{cm}}{10}\right)^{0.3}$$

with $f_{cm} = 11.2$ MPa

This value of the average characteristic compressive strength comes from a study entitled "*Statistical analysis on the dispersion of compressive strength values of concrete taken from existing buildings*", edited by M.T. Cristofaro, A. D'Ambrisi, M. De Stefano, M. Tanganelli and R. Pucinotti.

During the survey campaign, 942 structural elements belonging to 118 buildings were analysed, cylindrical samples were taken by coring, and laboratory compression tests were carried out on these samples to determine the value of the characteristic mean compressive strength. The data sample was then divided into four sub-groups based on the date of construction of the building, thus identifying the four decades:

1950s, 1960s, 1970s and 1980s. The f_{cm} value of f_{cm} relative to the 1950s construction was taken into account, which was 11.2 MPa.

Application of the investigative load

In order to carry out a preliminary study of the behaviour of the building with respect to horizontal loads, an investigative horizontal load was applied, constant for each floor, with an intensity of 100 kN, first in the X-direction and then in the Y-direction.

The concentrated force is applied at the geometric centre of gravity of the floor, where the origin of the global reference system of the model is fixed. No torque is applied, the torsion is only due to the distance between the point of application of the load and the centre of rigidity of the deck.

- Case 1: Concentrated load applied in the X-direction

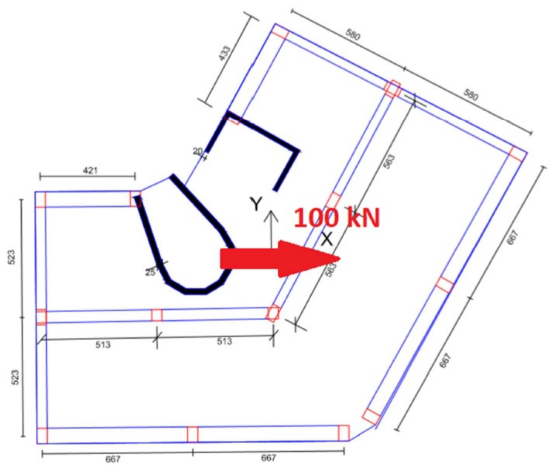

Figure 4.32: Investigative load applied in the X-direction

The displacement of the structure is qualitatively appreciable from the axonometry of the deformed shape (Figure 4.33).

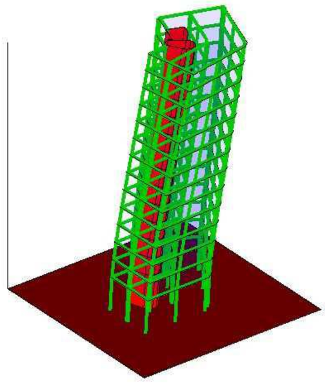

Figure 4.33: Structural deformation for the investigative load applied in the X-direction

The values of the displacements, ξ, η and ϑ, with respect to the origin of the global reference system can be deduced from the graphs shown in Figure 4.34, 4.35 and 4.36

The displacement $\xi(z)$ (Figure 4.34), in the X direction, shows a roughly linear trend, increasing with height. The maximum value reached on the last floor is 3.34 cm. At the first floor, a variation of the tangent of the graph can be seen, corresponding to the variation of the stiffness due to the different interstorey value of the first floor.

The displacement $\eta(z)$ (Figure 4.35), in the Y direction, shows a curvilinear trend following the discontinuity of the tangent to the first plane. The maximum value obtained is 2.19 mm in the 9th plane.

The rotations (Figure 4.36) of the planes vary with continuity as the height z increases, reaching a maximum value of $6.73 \cdot 10^{-4}$ rad at the last plane. The vertical tangent at zero height represents the interlocking condition at the base.

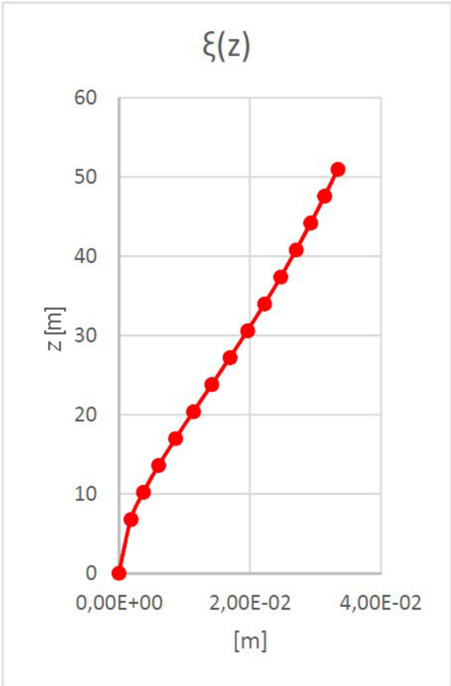

Figure 4.34: Displacement $\xi(z)$ in the X-direction

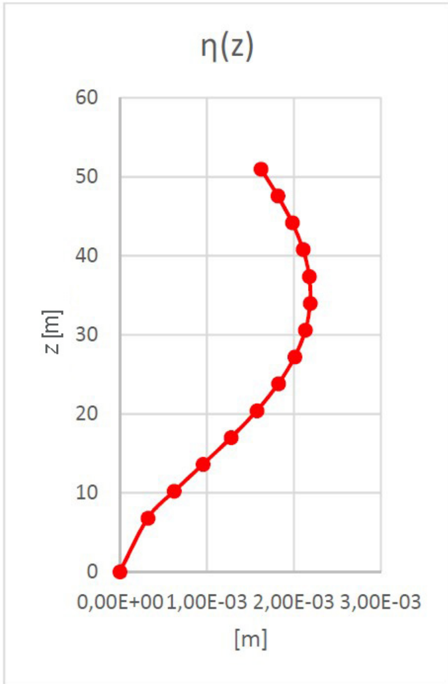

Figure 4.35: Displacement $\eta(z)$ in the Y-direction

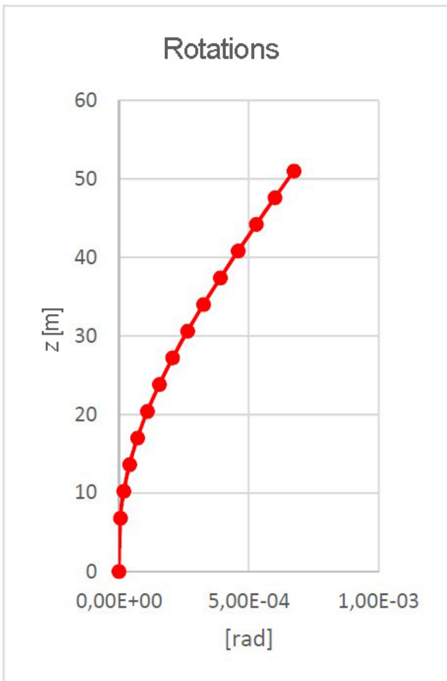

Figure 4.36: Rotation $\vartheta(z)$ about the Z-axis

- Case 2: Concentrated load applied in the Y-direction

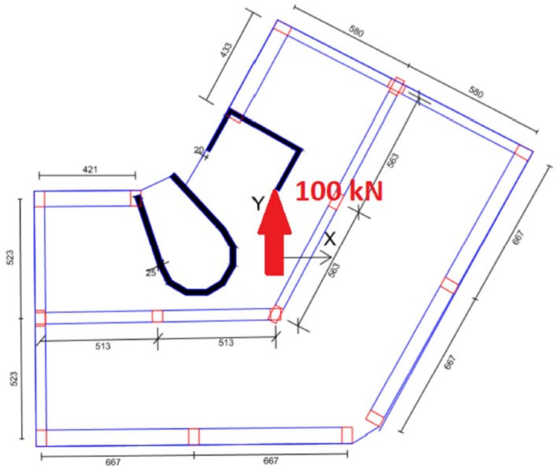

Figure 4.37: Investigative load applied in the y-direction

The deformed shape can be seen in Figure 4.38.

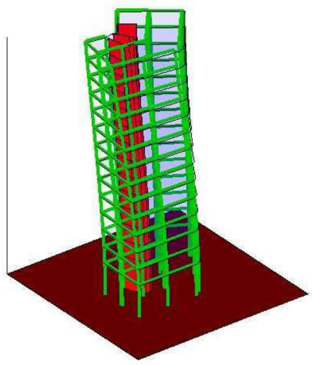

Figure 4.38: Structural deformation for the investigative load applied in the Y-direction

The graphs of the displacements, ξ, η and ϑ, are shown in Figure 4.39, 4.40 and 4.41

The displacement $\xi(z)$ in the X direction, transverse to the applied load, shows the same values as in the previous case. The maximum value is again in the ninth plane and is 2.19 mm.

The displacement $\eta(z)$ in the Y-direction represents in this case the displacement according to the direction of the load. There is a larger displacement in the Y direction, with a maximum value of 5.24 cm.

In comparison to the preceding case, the rotations $\vartheta(z)$ are more pronounced, reaching a maximum value of $1.69 \cdot 10^{-3}$ rad.

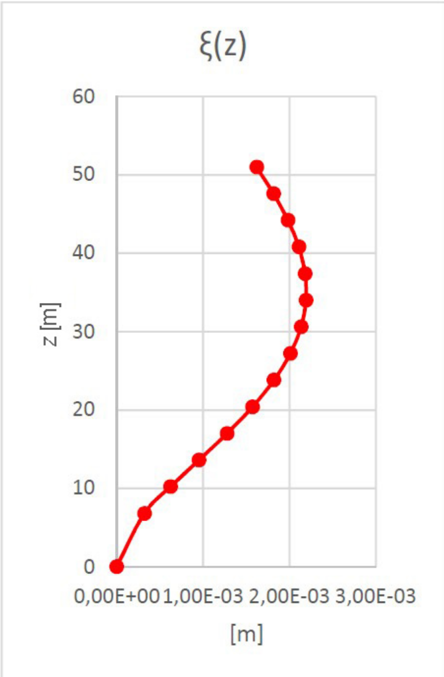

Figure 4.39: Displacement $\xi(z)$ in the X-direction

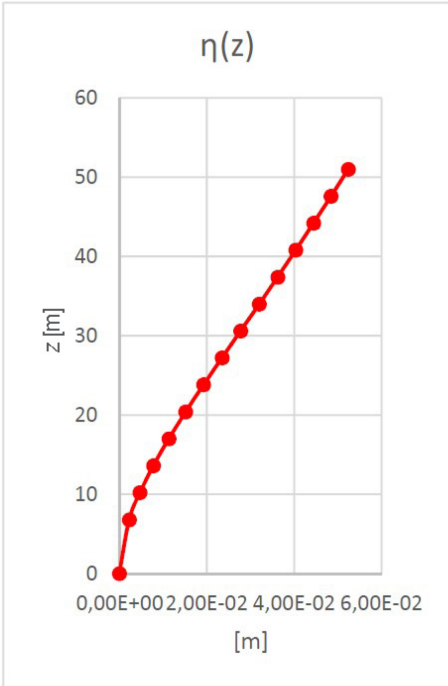

Figure 4.40: Displacement $\eta(z)$ in the Y-direction

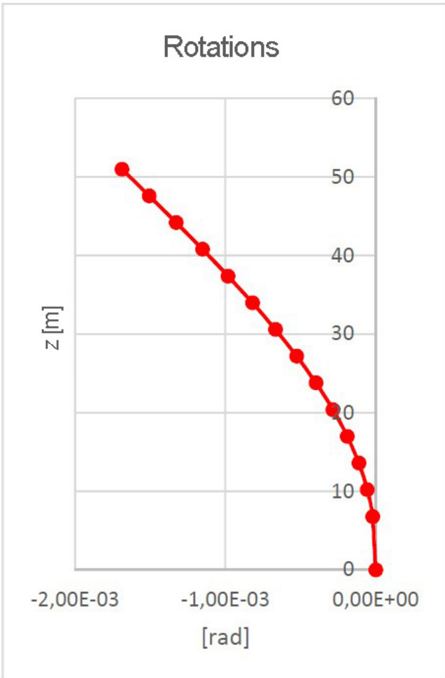

Figure 4.41: Rotation $\vartheta(z)$ about the Z-axis

Wind action calculation

Referring to Appendix A for the calculation of wind action, the values of wind pressures and relative forces per unit length are given in Table 4.5:

Storey	z (m)	c(z) [-]	p (N/m²)	p_f (N/m²)	F (N/m)	F_{fri} (N/m)	F_{tot} (N/m)
1	6.8	1.48	577.9	11.6	1964.8	39.3	2004.1
2	10.12	1.48	577.9	11.6	1964.8	39.3	2004.1
3	13.52	1.56	609.4	12.2	2072.1	41.4	2113.5
4	16.92	1.72	670.4	13.4	2279.3	45.6	2324.8
5	20.32	1.85	721.7	14.4	2453.6	49.1	2502.7
6	23.72	1.96	766.1	15.3	2604.6	52.1	2656.7
7	27.12	2.06	805.3	16.1	2738.1	54.8	2792.8
8	30.52	2.15	840.5	16.8	2857.8	57.2	2915.0
9	33.92	2.23	872.5	17.4	2966.6	59.3	3025.9
10	37.32	2.31	901.8	18.0	3066.3	61.3	3127.6
11	40.72	2.38	928.9	18.6	3158.4	63.2	3221.6
12	44.12	2.44	954.1	19.1	3244.1	64.9	3309.0
13	47.52	2.50	977.7	19.5	3324.2	66.5	3390.7
14	50.92	2.56	999.9	20.0	339.5	68.0	3467.5

Table 4.5: Wind forces

The following section presents the calculation cases for wind blowing in the X and Y directions, considered in both positive and negative directions. For each calculation case, the value of the force along the X-axis and the Y-axis were calculated for each floor of the building. These values were traced back to the centre of gravity of the deck and the value of the torsion around the Z-axis that arises from the transport of these forces in the centre of gravity was determined.

In the following results, the motions that cause a clockwise rotation of the deck, as observed in the plan view, have been considered to be positive.

- Case 1: Wind blowing in the X-direction with direction concordant with the axis

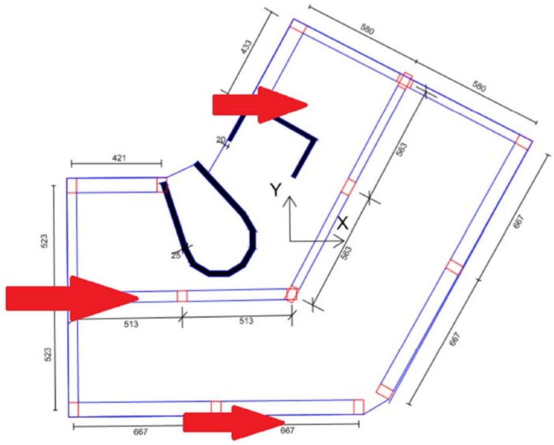

Figure 4.42: Wind load acting in the X-direction with direction concordant with the axis

F [kN]	M [kNm]
15.12036	89.89053
15.12036	89.89053
15.9459	94.79835
17.54035	104.2774
18.88218	112.2545
49.03369	45.81916
51.54598	48.16675
53.80053	50.2735
55.84796	52.1867
57.72505	53.94073
59.45944	55.56142
61.07241	57.06865
62.58075	58.4781
63.99791	59.80236

- Case 2: Wind blowing in the X-direction with direction opposite to the axis

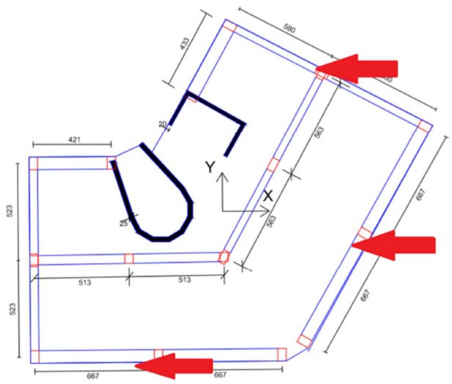

Figure 4.43: Wind load acting in the X-direction, in the opposite direction to the axis

F [kN]	M [kNm]
-24.3491	34.64574
-24.3491	34.64574
-25.6785	36.53732
-28.2461	40.19074
-30.4069	43.26532
-48.0726	-68.8979
-50.5356	-72.428
-52.746	-75.5959
-54.7533	-78.4728
-56.5936	-81.103
-58.294	-83.5473
-59.8753	-85.8137
-61.3541	-87.9331
-62.7435	-89.9244

- Case 3: Wind blowing in the Y-direction with direction concordant with the axis

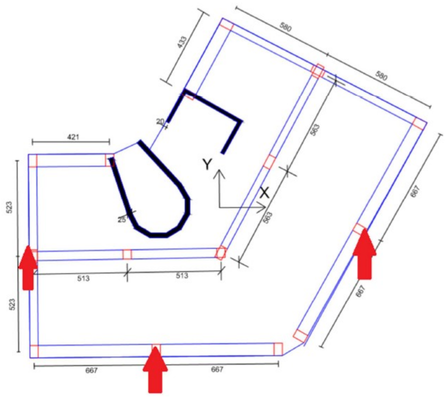

Figure 4.44: Wind load acting in the Y-direction with direction concordant with the axis

F [kN]	M [kNm]
41.00471	-11.0458
41.00471	-11.0458
43.24348	-11.6489
47.56745	-12.8137
51.20634	-13.7939
54.93734	-8.72892
57.75211	-9.17616
60.27811	-9.57751
62.57204	-9.94199
64.67514	-10.2761
66.61835	-10.5849
68.42552	-10.872
70.11546	-11.1406
71.70325	-11.3928

- Case 4: Wind blowing in the Y-direction with direction opposite to the axis

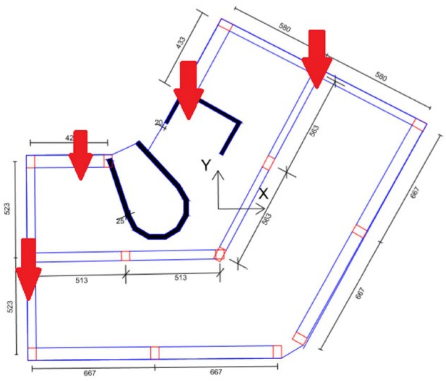

Figure 4.45: Wind load acting in the Y-direction, in the opposite direction to the axis

F [kN]	M [kNm]
-16.9661	-84.8796
-16.9661	-84.8796
-17.8924	-89.5138
-19.6815	-98.4645
-21.1871	-105.997
-52.5468	51.34829
-55.2391	53.97917
-57.6552	56.34014
-59.8493	58.48422
-61.8609	60.44992
-63.7195	62.26618
-65.4481	63.95529
-67.0645	65.53483
-68.5832	67.01888

Results

In order to examine the behaviour of the building in response to horizontal loads, the wind loads previously calculated in accordance with the current standard were introduced into the analytical model. This was done by considering the wind to be blowing once in the X-direction and once in the Y-direction.

- Case 1: Wind blowing in the X-direction

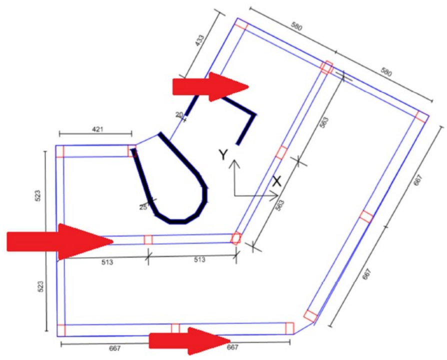

Figure 4.46: Wind load acting in the X-direction with direction concordant with the axis

The deformed shape of the structure is shown in Figure 4.47.

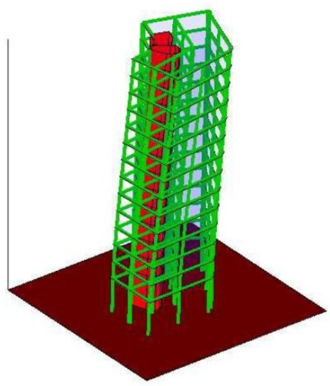

Figure 4.47: Structural deformation for the wind load applied in the X-direction

The response of the structure in terms of displacements along the X and Y axes and rotation about the Z axis are shown in Figure 4.48, 4.49 and 4.50.

The displacement $\xi(z)$ exhibits a linear trend with a change in slope at the first floor. The maximum value is observed on the final floor and is approximately 2 cm.

The displacement $\eta(z)$ is curvilinear with a change of tangent at the first plane and a maximum value of approximately 0.5 mm.

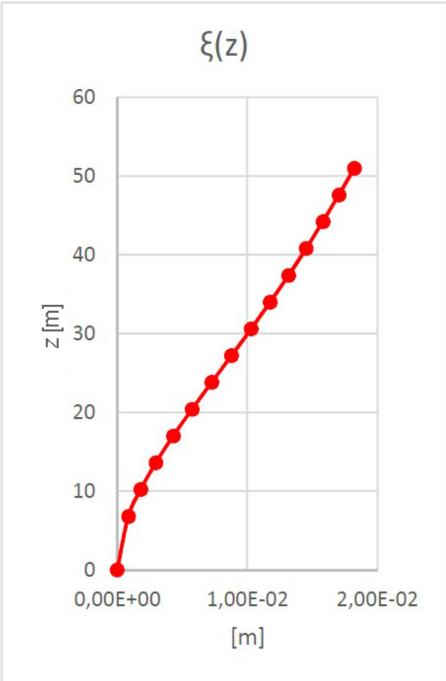

Figure 4.48: Displacement $\xi(z)$ in the X-direction

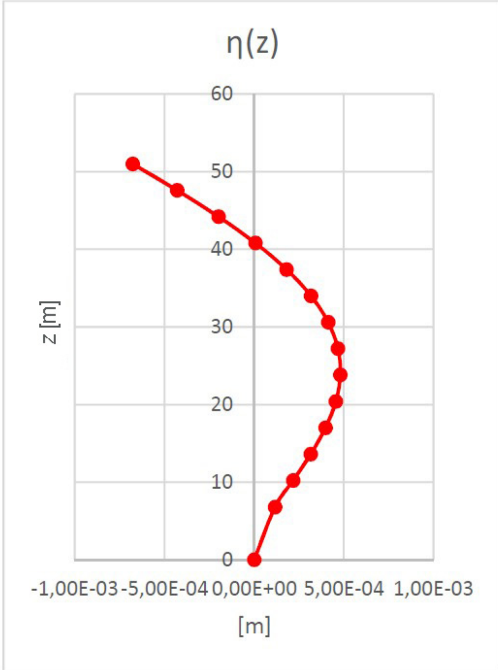

Figure 4.49: Displacement $\eta(z)$ in the Y-direction

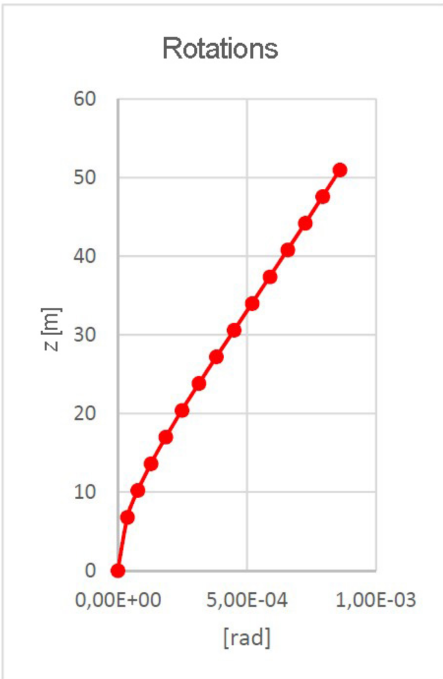

Figure 4.50: Rotation $\vartheta(z)$ about the Z-axis

It can be observed that the rotation increases linearly with height, reaching a maximum value of $9 \cdot 10^{-4} rad$ at the top floor.

It is of interest to present the results of the analysis of stairwell (shearwall 1), which has an unusual 'horseshoe' shape, in terms of bending moment (Figure 4.52 and 4.53), shear (Figure 4.54 and 4.55), bi-moment (Figure 4.56) and torsional moment (Figure 4.57). These stresses are referred to a local reference system with its origin in the shear centre of the section, and the axes are oriented according to the principal directions of inertia (Figure 4.51).

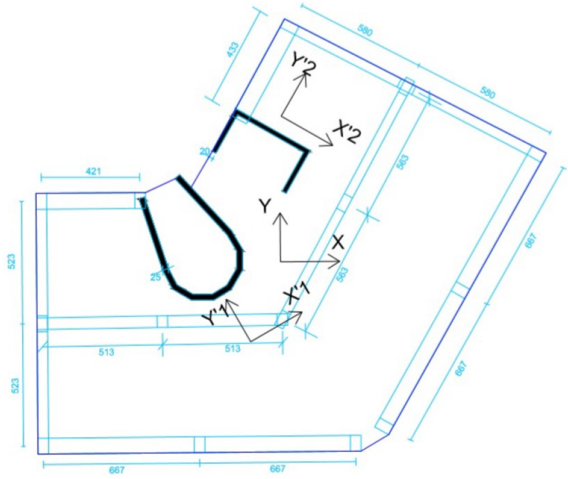

Figure 4.51: Axes of shear walls in the local reference system

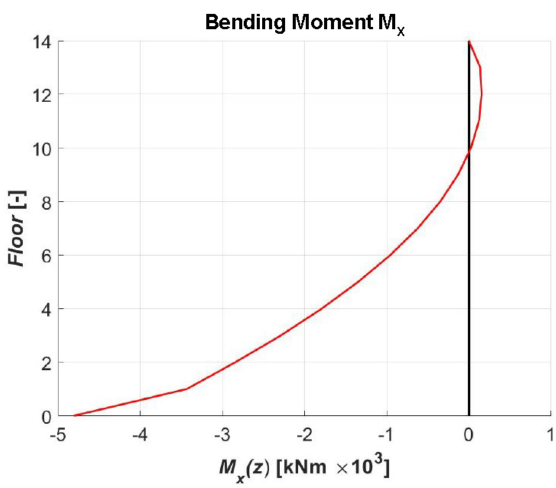

Figure 4.52: Bending moment M_x

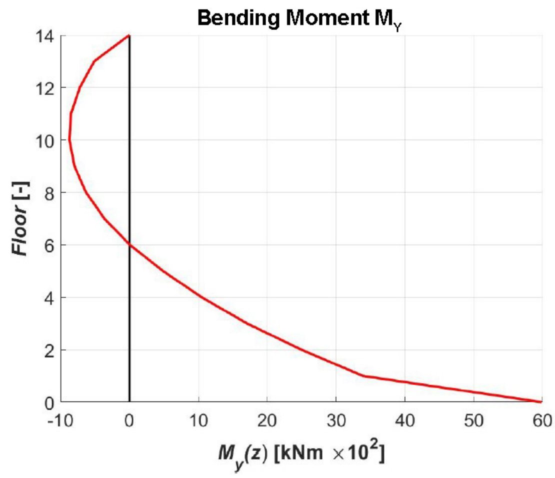

Figure 4.53: Bending moment M_y

An examination of the torsional moment graph (Figure 4.57) reveals a pattern whereby the total torsion, calculated as the sum of the contributions from the torsion at Vlasov and Saint-Venant, aligns closely with the trend observed in the torsional component at Vlasov alone.

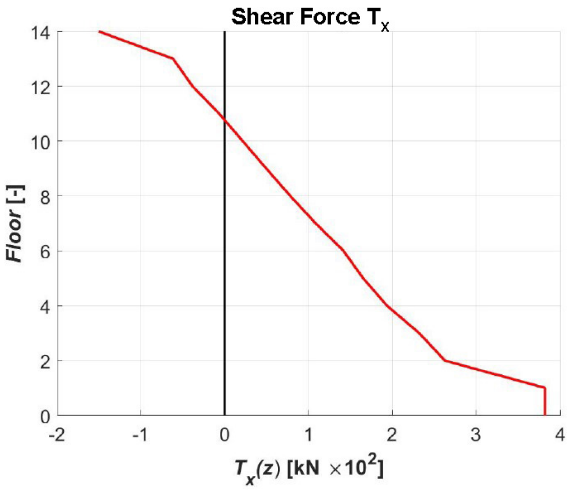

Figure 4.54: Shear force T_x

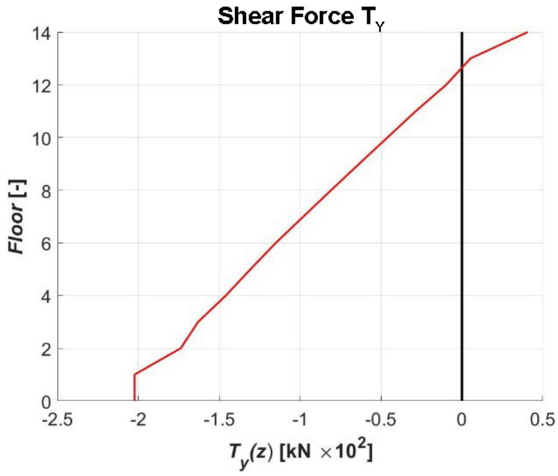

Figure 4.55: Shear force T_y

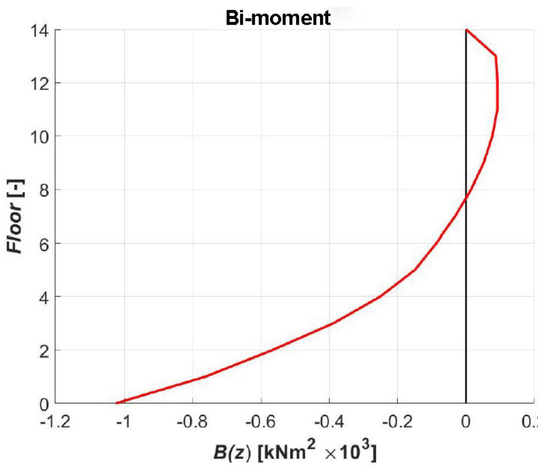

Figure 4.56: Bi-moment B

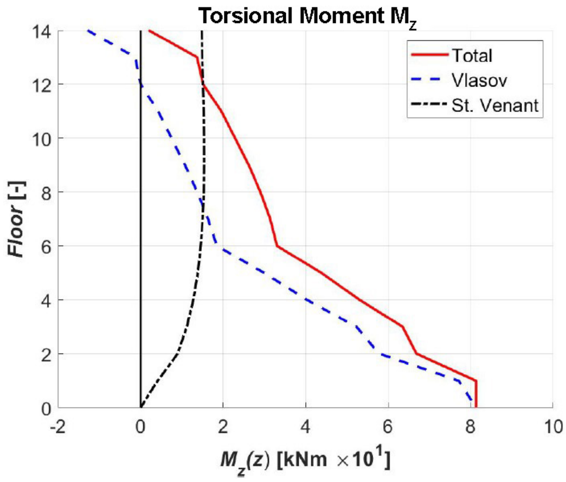

Figure 4.57: Torsional moment M_z

- Case 2: Wind blowing in the Y-direction

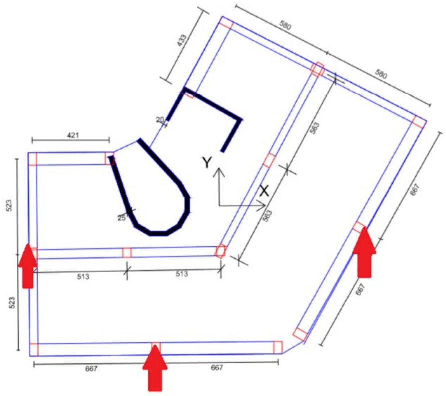

Figure 4.58: Wind load acting in the Y-direction with direction concordant with the axis

The deformed shape of the structure is shown in Figure 4.59.

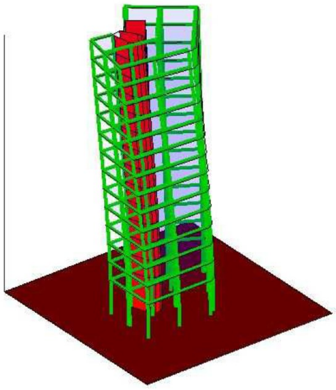

Figure 4.59: Structural deformation for the wind load applied in the Y-direction

The response of the structure in terms of displacements along the X and Y axes and rotation about the Z axis are shown in Figure 4.60, 4.61 and 4.62.

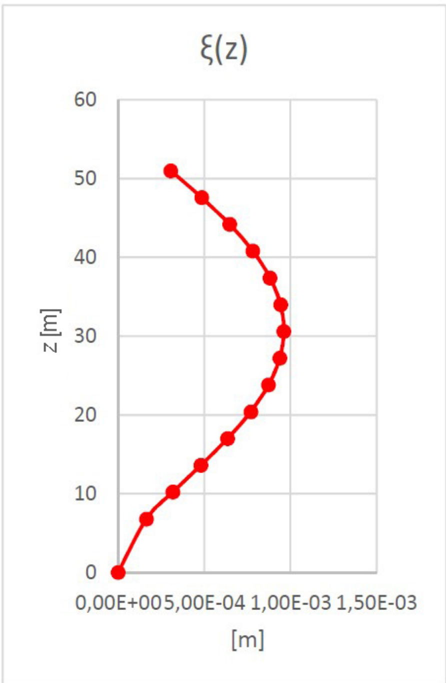

Figure 4.60: Displacement $\xi(z)$ in the X-direction

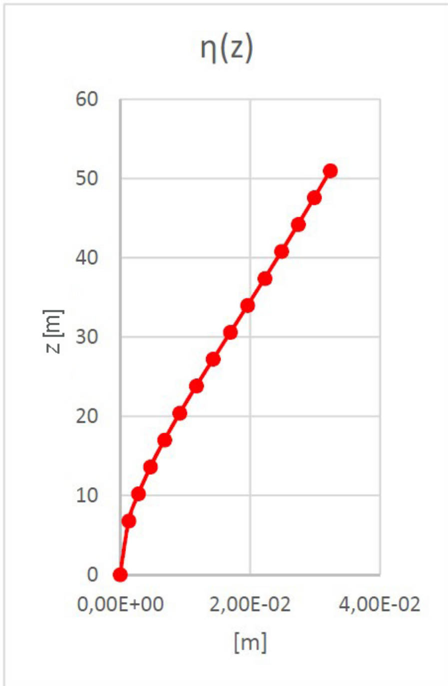

Figure 4.61: Displacement $\eta(z)$ in the Y-direction

In this case, a greater value of the displacement $\eta(z)$, concordant with the direction of the load, of approximately 3.5 cm is observed.

The graphs of the bending moment (Figure 4.63 and 4.64), shear (Figure 4.65 and 4.66), bi-momentum (Figure 4.67) and torsional moment (Figure 4.68)for the stairwell septum (shearwall 1) are also presented for this load case.

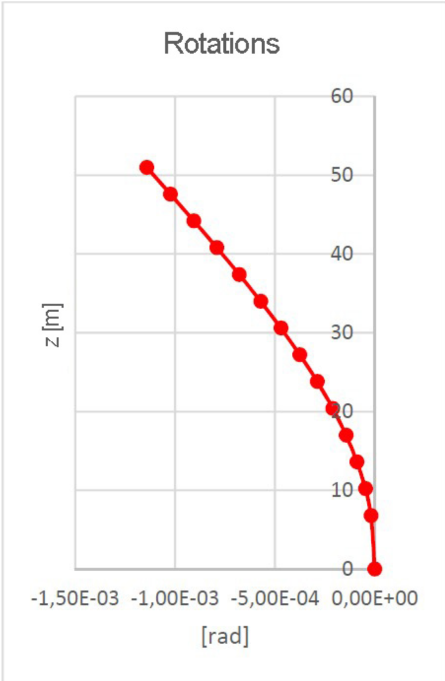

Figure 4.62: Rotation $\vartheta(z)$ about the Z-axis

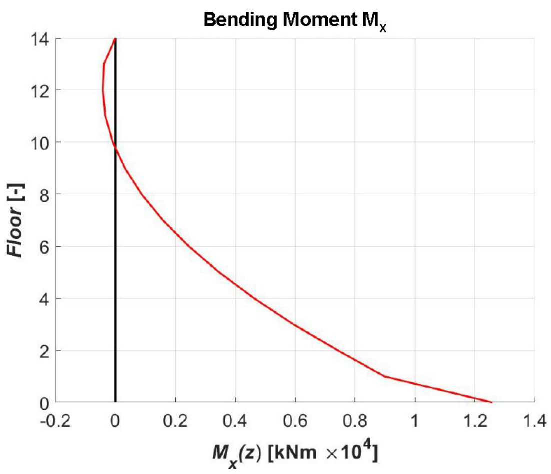

Figure 4.63: Bending moment M_x

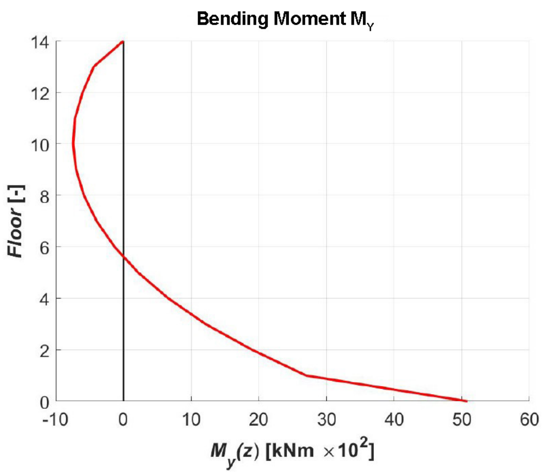

Figure 4.64: Bending moment M_y

As previously observed, the total torsional moment exhibits a trend that is closely aligned with the trend of the Vlasov torsional component on its own.

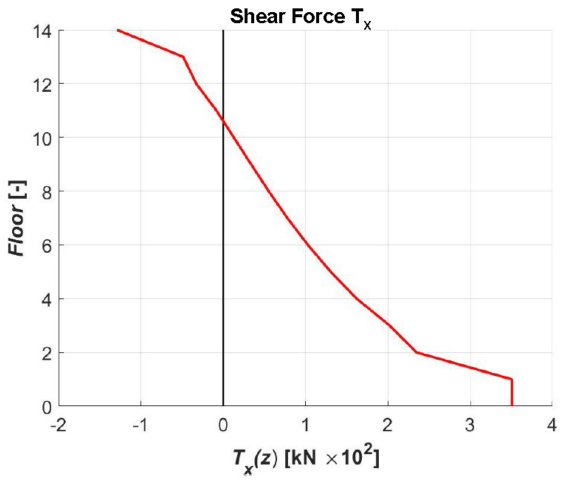

Figure 4.65: Shear force T_x

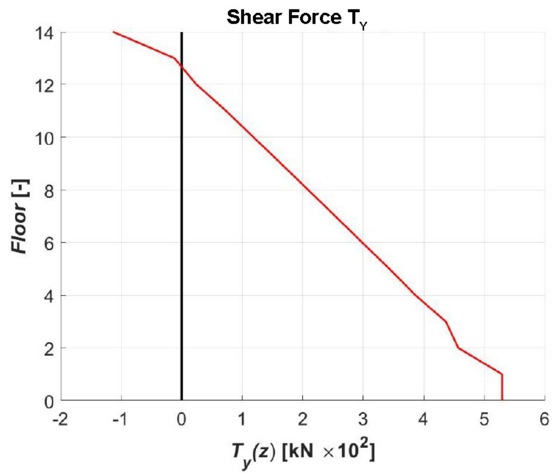

Figure 4.66: Shear force T_y

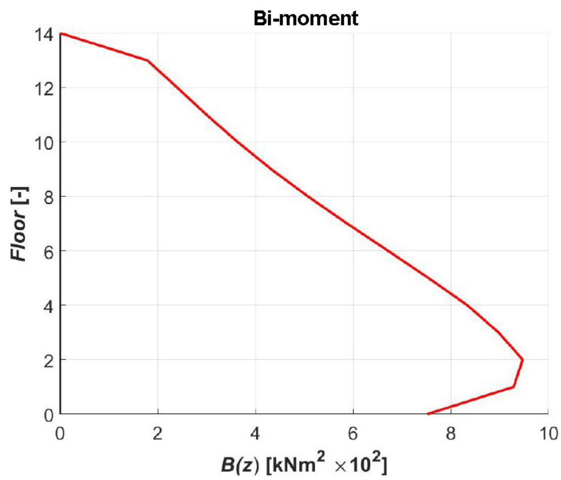

Figure 4.67: Bi-moment B

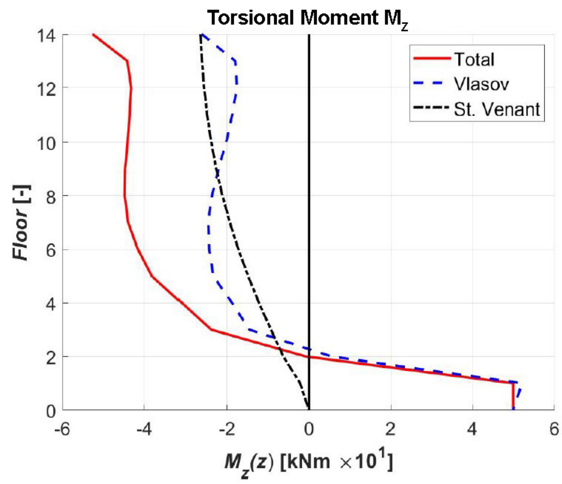

Figure 4.68: Torsional moment M_z

Comparative analysis of the actions absorbed by the two shear walls

In order to study the overall behaviour of the structure and to understand to what extent the shearwalls are involved in the absorption of external horizontal actions, a comparison of the stresses affecting the two septa is proposed for load cases considering wind blowing in the X and Y directions.

- Case 1: Wind blowing in the X-direction

With reference to Figure 4.46, it is important to note that the stresses in the two septa do not have the same direction. This is due to the fact that the local reference systems are oriented in accordance with the primary directions of inertia observed in the sections.

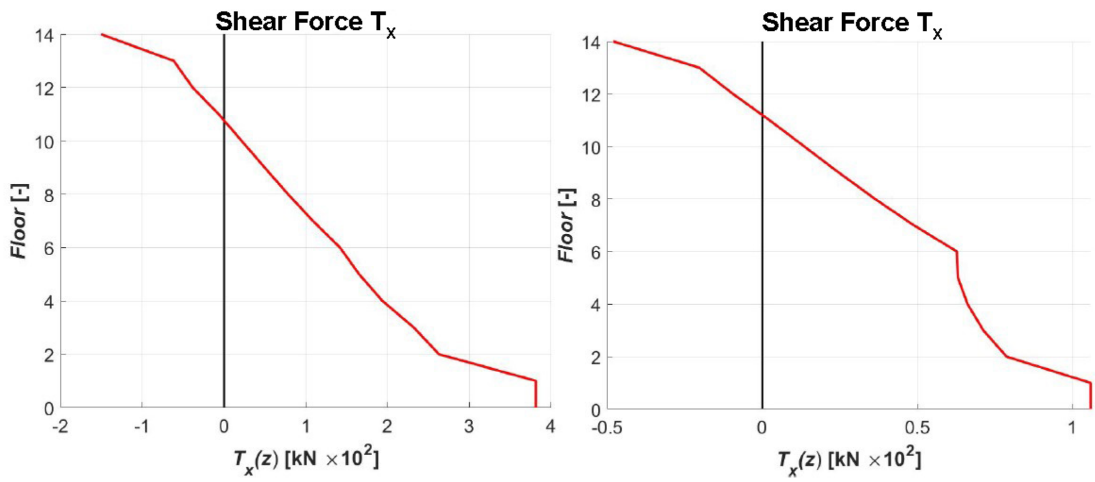

Figure 4.69: Shear T_x for the shear walls 1 and 2

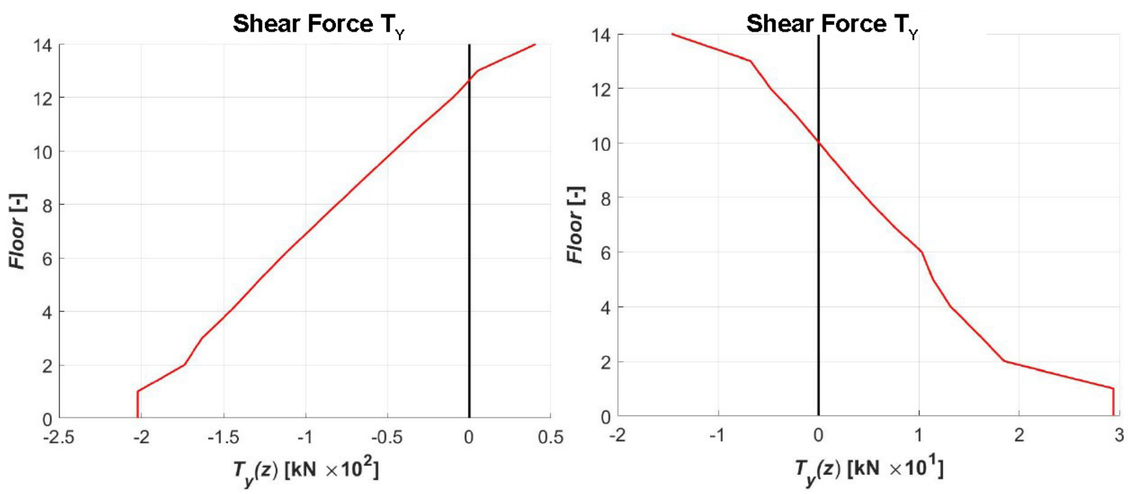

Figure 4.70: Shear T_y for the shear walls 1 and 2

A comparison of the shears T_x and T_y (Figure 4.69 and 4.70) for the two shearwalls reveals that, under this loading condition, the greatest cut is observed at the base of the stairwell shearwall (shearwall 1), which is more than three times the value at the base of the lift shaft shearwall (shearwall 2). Furthermore, it can be observed that the shear trends are analogous for the two hearwalls, exhibiting cancellation at approximately 11 m elevation.

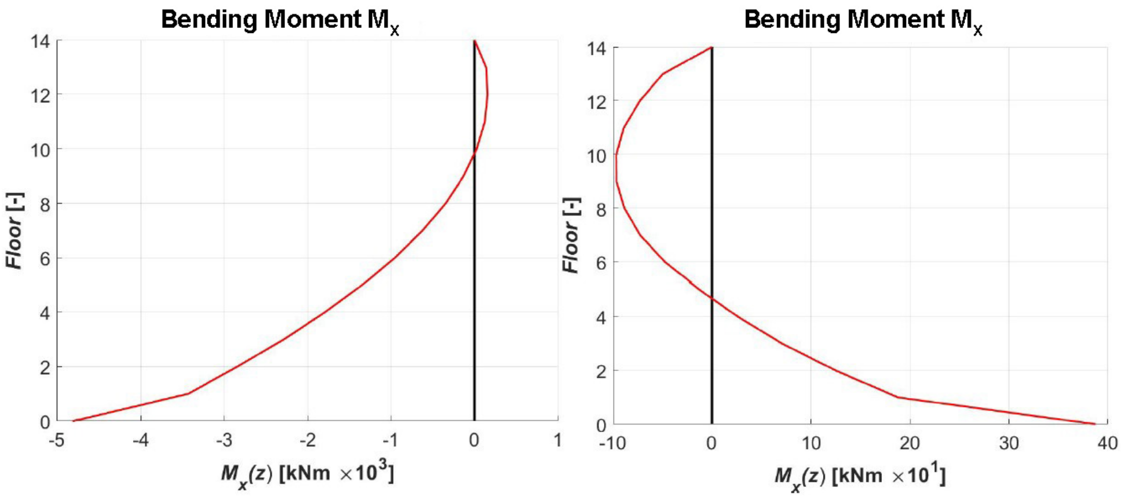

Figure 4.71: Bending moment M_x for the shear walls 1 and 2

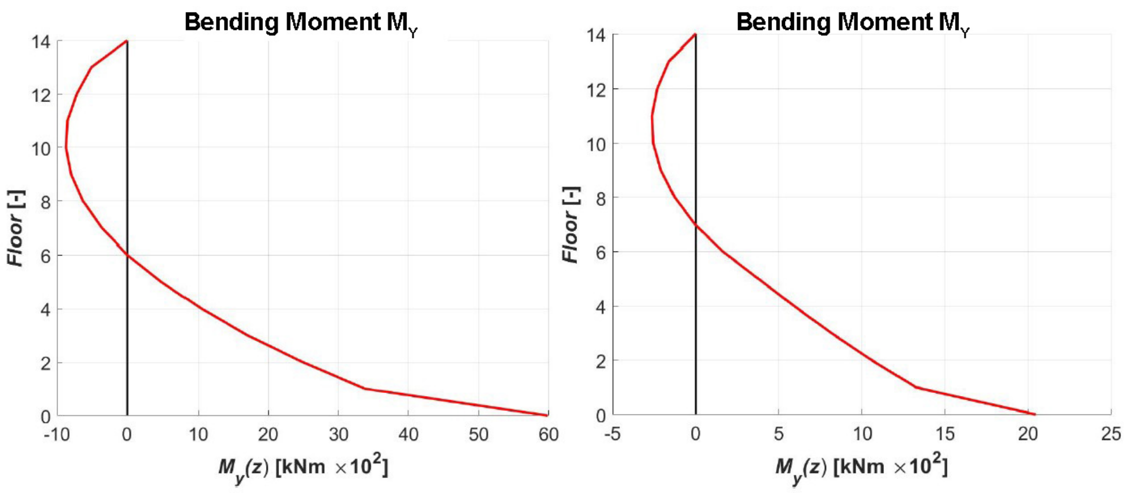

Figure 4.72: Bending moment M_y for the shear walls 1 and 2

A comparison of the bending moments M_x and M_y (Figure 4.71 and 4.72) shows that the bending behaviour in this direction is predominantly influenced by the stairwell wall (shearwall 1), with a bending moment value that is approximately three times greater than that of the lift shaft (shearwall 2).

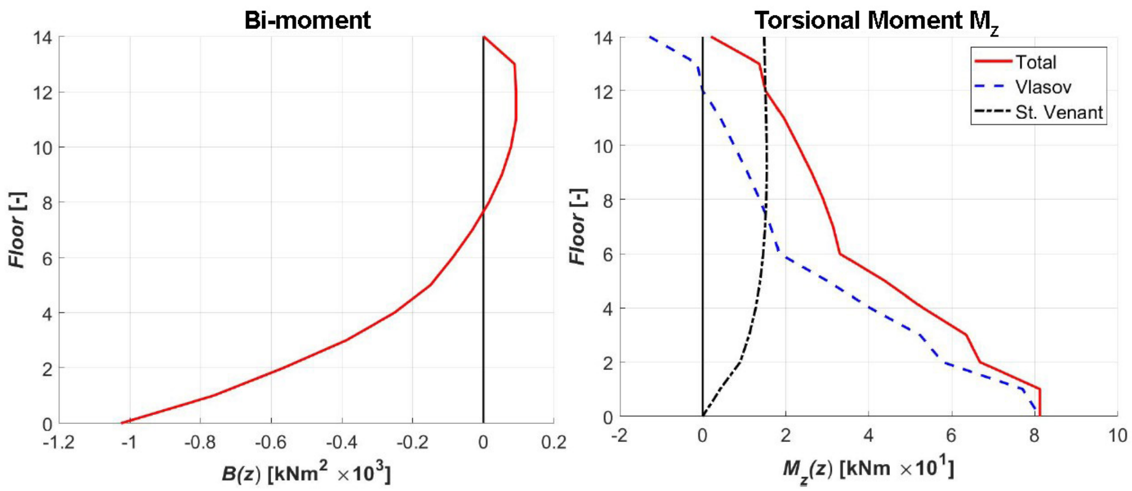

Figure 4.73: Bi-moment B and torsional moment M_z for the shear walls 1

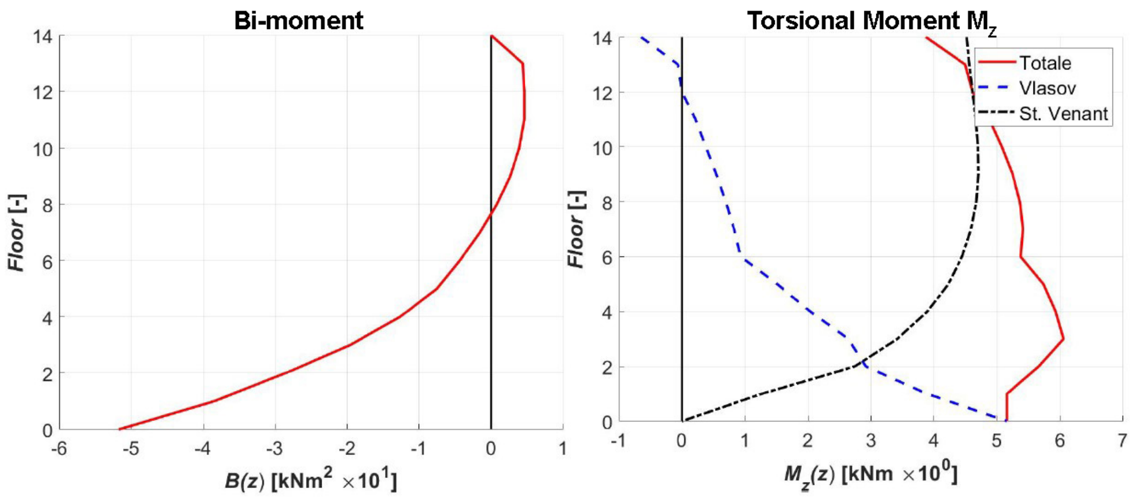

Figure 4.74: Bi-moment B and torsional moment M_z for the shear walls 2

- Case 2: Wind blowing in the Y-direction

With reference to Figure 4.58, a comparison is made between the different stresses affecting the structure.

It can be seen from Figure 4.75 and 4.76 that even in this load condition, it is shear wall 1 that absorbs the largest proportion of the load. In this case, the shear at the base is an order of magnitude greater than the shear at the base of the lift shaft shear wall (shearwall 2).

It can also be seen that with regard to bending moments (Figure 4.77 and 4.78), it is the stairwell wall (shearwall 1) that absorbs a greater proportion of the load. The bending moment M_x of the lift shaft wall (shearwall 2) is markedly lower than that of shearwall 1, by a factor of at least one order of magnitude.

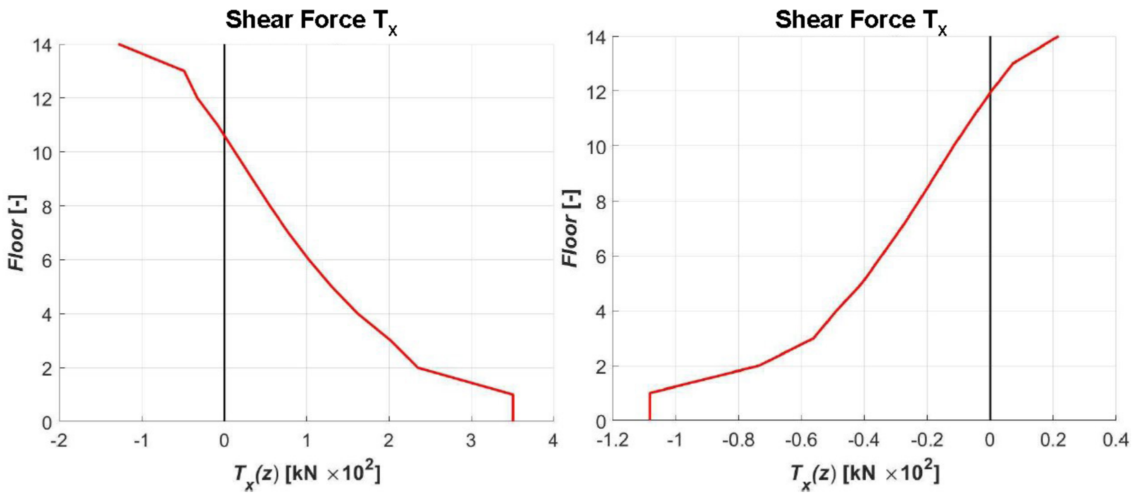

Figure 4.75: Shear T_x for the shear walls 1 and 2

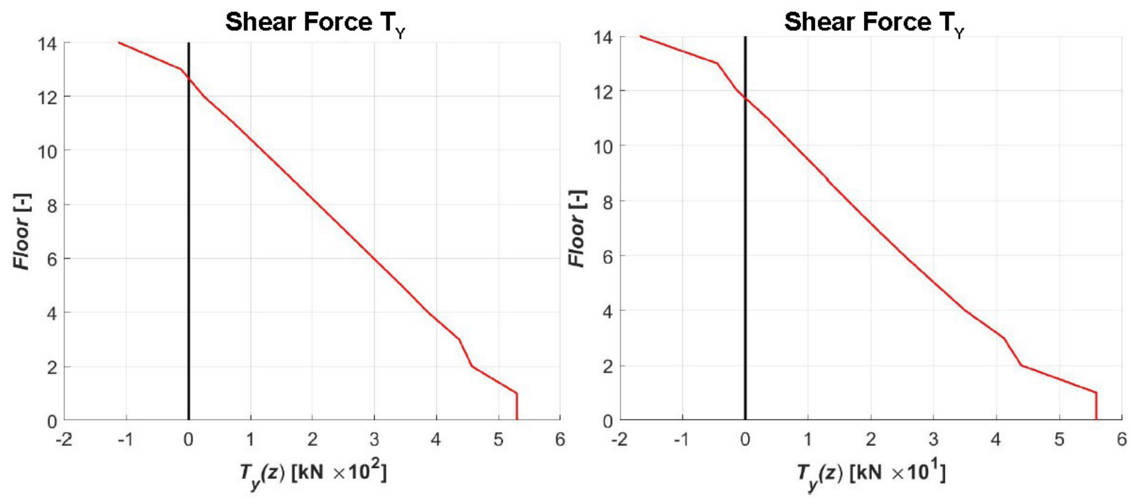

Figure 4.76: Shear T_y for the shear walls 1 and 2

With regard to the bending moment M_y, the behaviour is reversed, with shear-wall 2 absorbing a higher proportion of the load.

Furthermore, the bi-moment is observed to be higher for the stairwell wall (shear-wall 1).

An examination of the torsional moment graphs M_z reveals that, while the total torsion trend for the stairwell wall(shearwall 1) is largely analogous to the Vlasov torsional component, the total torsion trend for the lift shaft wall (shearwall 2) is more closely aligned with the Saint-Venant torsional component (Figure 4.79 and 4.80).

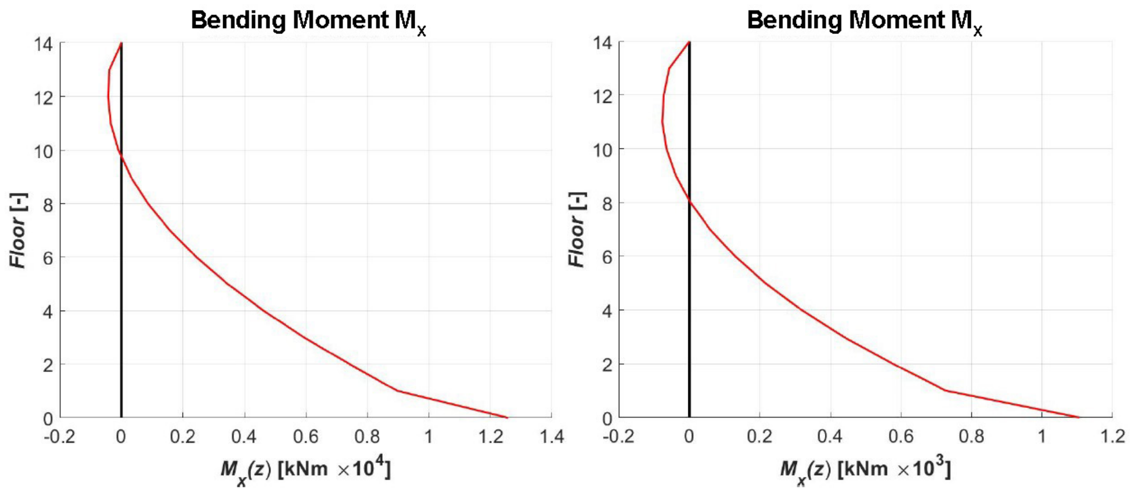

Figure 4.77: Bending moment M_x for the shear walls 1 and 2

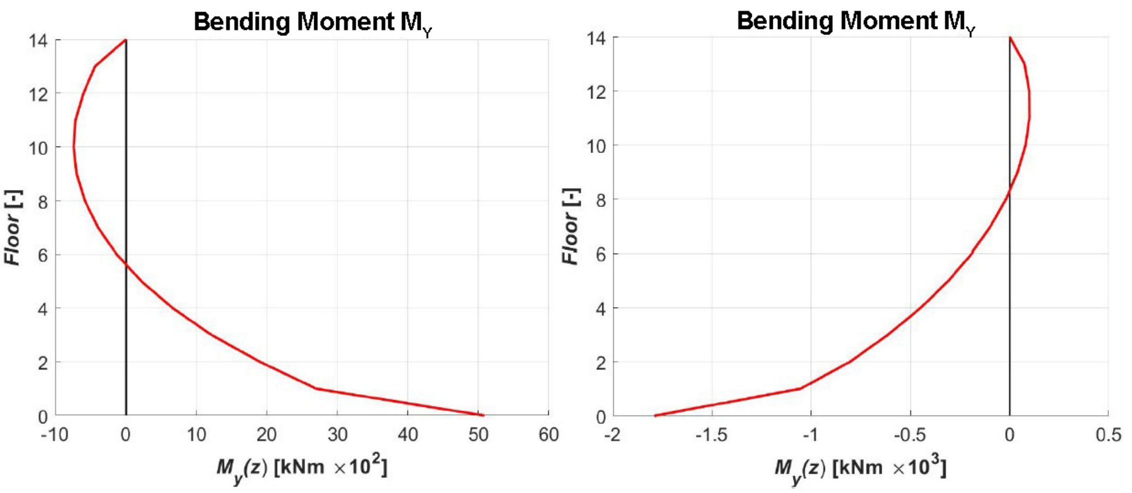

Figure 4.78: Bending moment M_y for the shear walls 1 and 2

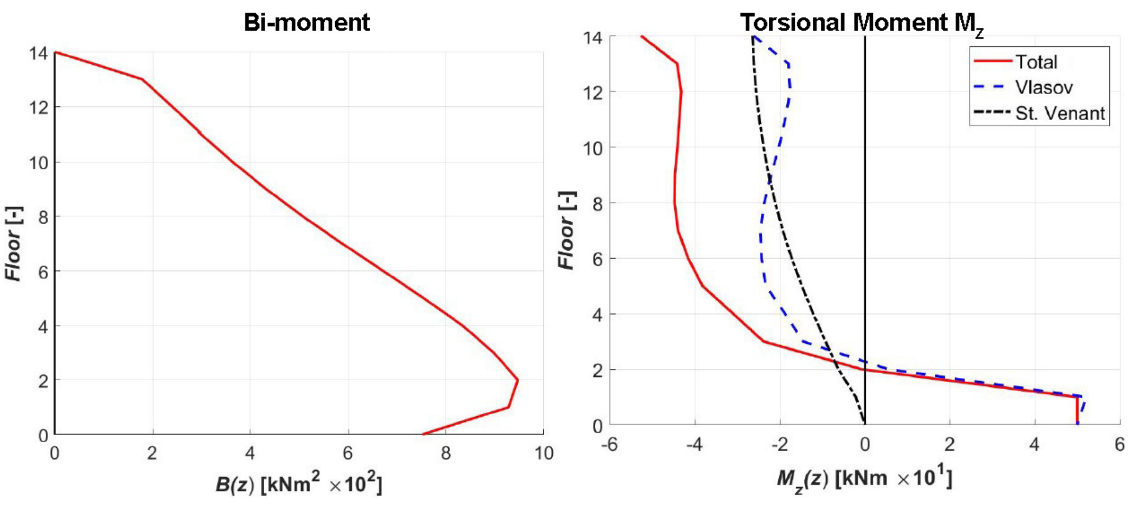

Figure 4.79: Bi-moment B and torsional moment M_z for the shear walls 1

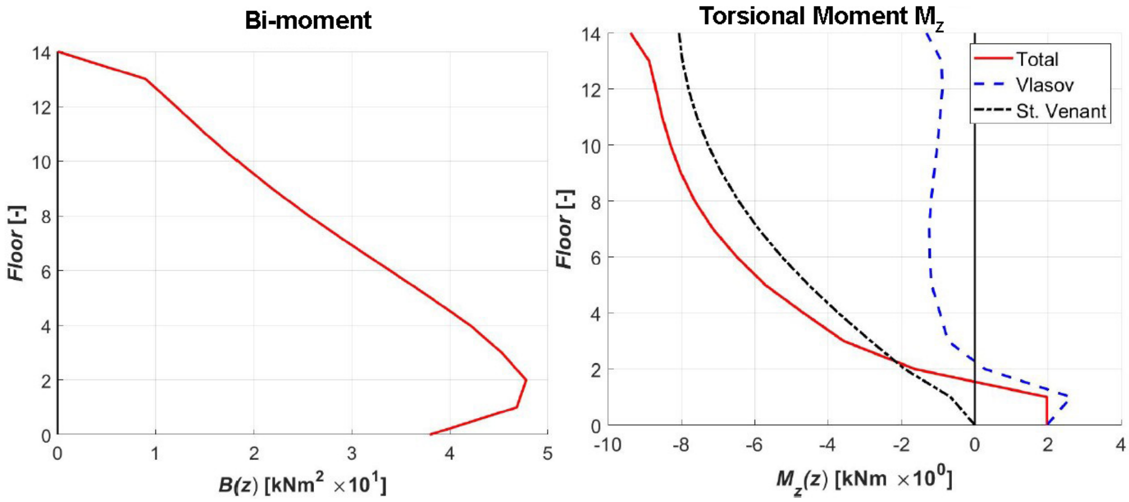

Figure 4.80: Bi-moment B and torsional moment M_z for the shear walls 2

In consideration of the presented analysis, it can be observed that in the context of the building resistance to horizontal external actions, the influence of shearwall 1 of the stairwell is particularly pronounced.

Stress calculation

Once the static analysis has been completed and the stress values determined, it is possible to proceed with the calculation of the normal and tangential stresses affecting the shear walls.

In particular, the impact of wind blowing in the X and Y directions on the stairwell walls (shearwall 1) was examined.

- Case 1: Wind blowing in the X-direction

In the present case, the stresses are reported in Table 4.6:

Stress	Unit of measure	Value
M_x	[kNm]	-4.81E+03
M_y	[kNm]	5.98E+03
B	[kNm^2]	-1.03E+03
T_x	[kN]	3.81E+02
T_y	[kN]	-2.02E+02
M_z^{VL}	[kNm]	8.13E+01
M_z^{SV}	[kNm]	1.00E-99

Table 4.6: Stresses

a. Normal stress σ_z

Using the formula 3.73:

$$\sigma_z = \frac{M_y}{J_{yy}}x + \frac{M_x}{J_{xx}}y + \frac{B}{J_{\omega\omega}}\omega$$

where the values of the moments of inertia, calculated using the formulae 3.53a, 3.53b and 3.54a, are given in the Table 4.7.

J_{xx}	[m^4]	8.29E+00
J_{yy}	[m^4]	4.69E+00
$J_{\omega\omega}$	[m^6]	2.56E+01

Table 4.7: moments of inertia

Applying the formula 3.73 at the points at the edges of the mean line of the section, numbered from 1 to 10 starting from the upper right extreme, as shown in Figure 4.81

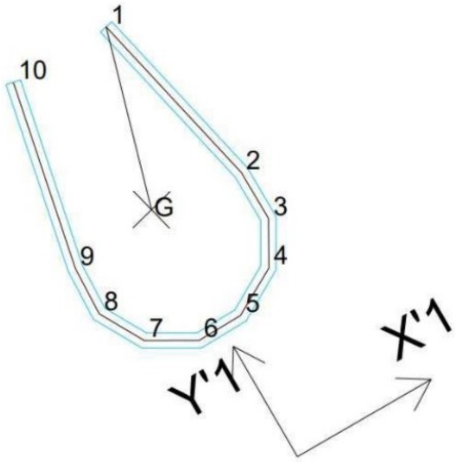

Figure 4.81: Section of shear wall - local reference system and element numbering

The coordinates *(x,y)* of the points were considered in the local reference system, with the origin situated at the section's shear centre and the axes oriented in accordance with the principal directions of inertia.

The sectorial coordinate ω was calculated by situating the pole at the centre of gravity of the section and the origin at point 1. Subsequently, the coordinates were transferred back to the principal reference system by applying the following formula:

$$\omega(s_0, s) = \omega(s_1, s) - \omega(s_1, s_0)$$

where $\omega(s_0, s)$ is the principal sectorial coordinate, $\omega(s_1, s)$ is the sectorial coordinate in the initial reference system (Figure 4.81) and $\omega(s_1, s_0)$ represents the value of ω calculated between the origins of the two reference systems using the following formula:

$$\omega(s_1, s_0) = \frac{S_\omega(s_1)}{A}$$

with:

$$S_\omega(s_1) = \int_A \omega(s_1, s)\, dA$$

The values of the sectoral coordinate ω, for the ten points considered, are reported in Table 4.8.

Finally, by substituting the values of the different terms into the formula 3.73, we obtain the values of the normal tension σ_z for the same points (Table 4.9):

ω [m^2]
-10.50655914
-5.638380829
-4.266804569
-2.717019954
-0.77707434
0.989042679
2.916087626
4.437948483
5.740665912
10.50033472

Table 4.8: Sectorial coordinate ω

σ [MPa]
-5.49
-2.95
-2.50
-2.68
-3.52
-4.59
-5.92
-6.95
-7.44
-8.59

Table 4.9: Normal stress σ_z

b. Tangential stress τ

Applying the formula 3.77, the tangential stress acting along the midline of the section due to the presence of shear stresses and the Vlasov moment is calculated:

$$\tau_{zs} = \frac{1}{b}\left[\frac{T_x}{J_{yy}}S_y(s) + \frac{T_y}{J_{xx}}S_x(s)\frac{M_z^{VL}}{J_{\omega\omega}}S_\omega(s)\right]$$

where b represents the thickness of the shear wall, which is 24 cm, and the static moments are derived from the expressions 3.68a, 3.68b and 3.71:

$$S_y = \int_A x\,dA = 0$$
$$S_x = \int_A y\,dA = 0$$
$$S_\omega = \int_A \omega\,dA = 0$$

where for each point the portion of the cross-sectional area enclosed by the considered chord was considered. Substituting the values of the different terms into 3.77, the values shown in the Table 4.10 were obtained.

τ [MPa]
0.01
-0.08
-0.16
-0.23
-0.29
-0.31
-0.30
-0.28
0.03

Table 4.10: Tangential stress σ_z

The primary tangential tension due to the presence of the Saint-Venant torsional moment is then calculated using the formula:

$$\tau(s,T) = \frac{M_z^{SV}}{J_t} b(s) \tag{4.1}$$

In the present case, the tension $\tau(s,T)$ is observed to be constant along the midline of the section, given that the thickness b is held constant, and linearly variable along the thickness of the section.

In the analysed shear wall, the value of the torsional stiffness factor J_t is calculated to be $6.48 \cdot 10^{-2} m^4$. Additionally, the Saint-Venant torsional moment M_z^{SV} is determined to be null, as the section at the base of the building was considered in the analysis.

The graphs (Figure 4.82 and 4.83)illustrate the trend of the stresses along the development of the mean line of the section (coordinate s).

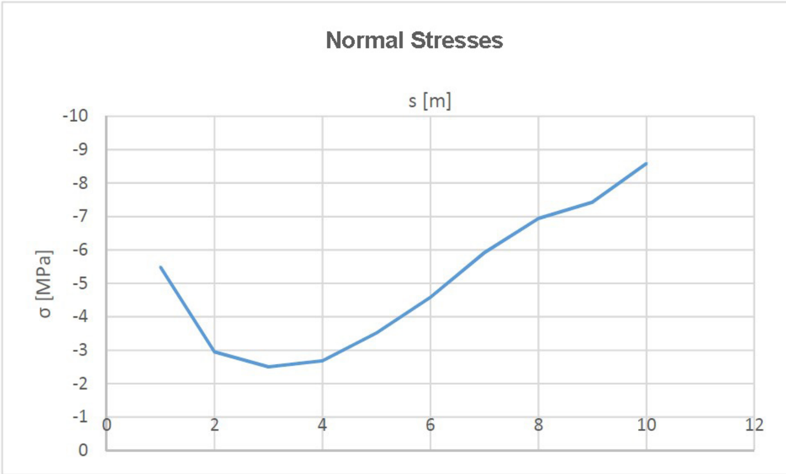

Figure 4.82: Normal stresses σ_z

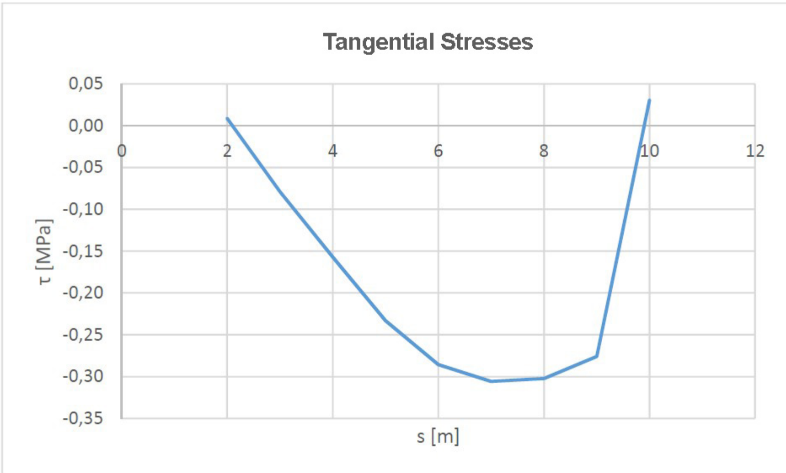

Figure 4.83: Tangential stresses $\tau_z s$

- Case 2: Wind blowing in the Y-direction

In this case, the stresses are associated with the section of the shear wall located at the second floor, as this area exhibits a higher bi-moment value. Their values are reported in Table 4.11.

Applying the formula 3.73, the values of the normal stresses σ_z are obtained (Table 4.12).

By applying the formulas 3.77, the values of the tangential stresses τ_{zs} along the mean line of the section are obtained (Table 4.13).

By means of the formula 4.1 we obtain the value of the tangential tension caused by the presence of the Saint Venant torsional moment M_z^{SV}, which in the case is different from zero.

Stress	Unit of measure	Value
M_x	[kNm]	7.42E+03
M_y	[kNm]	1.90E+03
B	[kNm^2]	9.47E+02
T_x	[kN]	2.35E+02
T_y	[kN]	4.57E+02
M_z^{VL}	[kNm]	5.483E+00
M_z^{SV}	[kNm]	-6.27E+00

Table 4.11: Stresses

σ [MPa]
7.21
4.82
4.08
3.35
2.71
2.44
2.61
3.17
3.99
7.25

Table 4.12: Normal stress σ_z

Finally, the stress trends along the mean line of the section are shown in Figure 4.84 and 4.85.

τ [MPa]
0.63
0.73
0.76
0.70
0.59
0.42
0.26
0.15
0.38

Table 4.13: Tangential stress σ_z

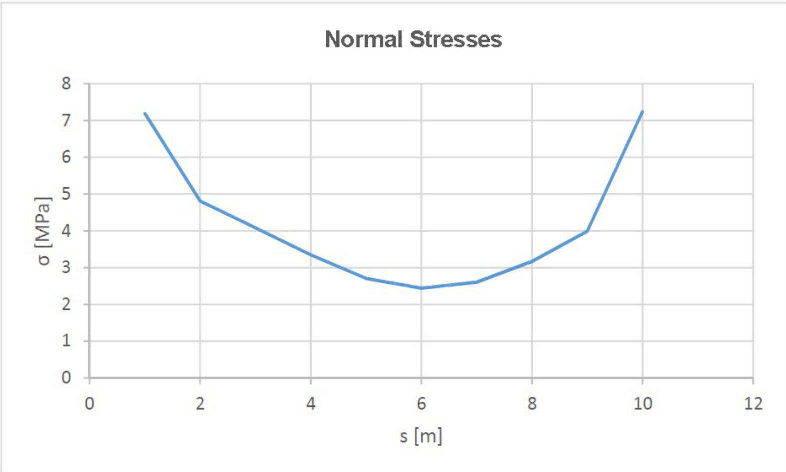

Figure 4.84: Normal stresses σ_z

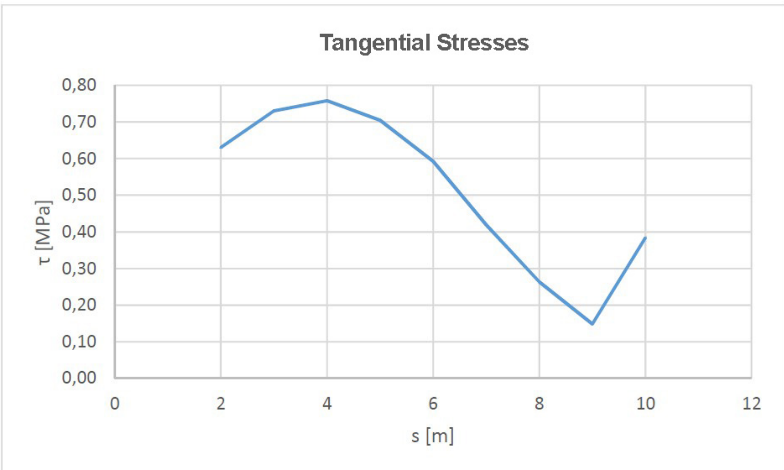

Figure 4.85: Tangential stresses $\tau_z s$

4.3.3 FEM Model

In order to perform a comparison of the results obtained from the static analysis using the analytical model, a finite element model was constructed using the software *SAP2000* (Figure 4.86).

In order to construct the model, 450 nodes were defined. A total of 530 *frame elements* were employed for the modelling of the beams and columns, while 182 *shell elements* were utilised for the modelling of the shear walls.

The sections attributed to the different frame elements are reflective of the actual characteristics of the building's load-bearing structure. The cross-sectional areas of the pillars exhibit variation along the height of the tower. In the case of beams that are not rectangular in shape, rectangular sections with moment of inertia equivalent to that of the actual beams have been defined. The sections defined for the shear walls are of the *'shell-thick' type* and have two different thicknesses (20 and 30 cm), while a generic section was defined at the base for the corner column, utilising the two moments of inertia around the two local axes contained in the plane of the section.

Ultimately, the structure was constrained by means of embedments at the base and at the end nodes of the ground floor columns. Additionally, rigid diaphragms were incorporated at each deck level to introduce the assumption of a rigid plane.

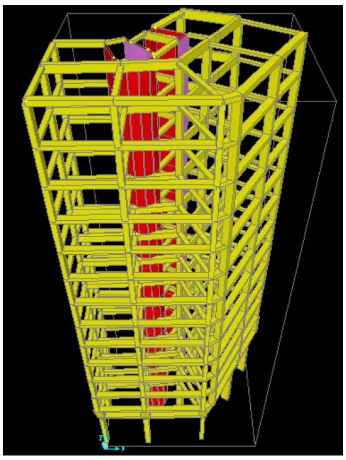

Figure 4.86: 3D FEM model

In order to apply the loads, a fictitious series of columns, modelled with 15 nodes and 14 frames, was positioned at the centre of the reference system of the analytical model, situated in the geometric centre of the deck area.

In conclusion, a fictitious material with an extremely low elastic modulus value and a circular cross-section with a diameter of 20 cm was attributed to this columns.

A comparison of the displacements in the X-axis direction of the nodes of the fictitious columns for a concentrated load of 100 kN, acting at each plane with the same axis direction, with the displacements obtained from the analytical model subjected to the same load yielded identical values (Figure 4.87).

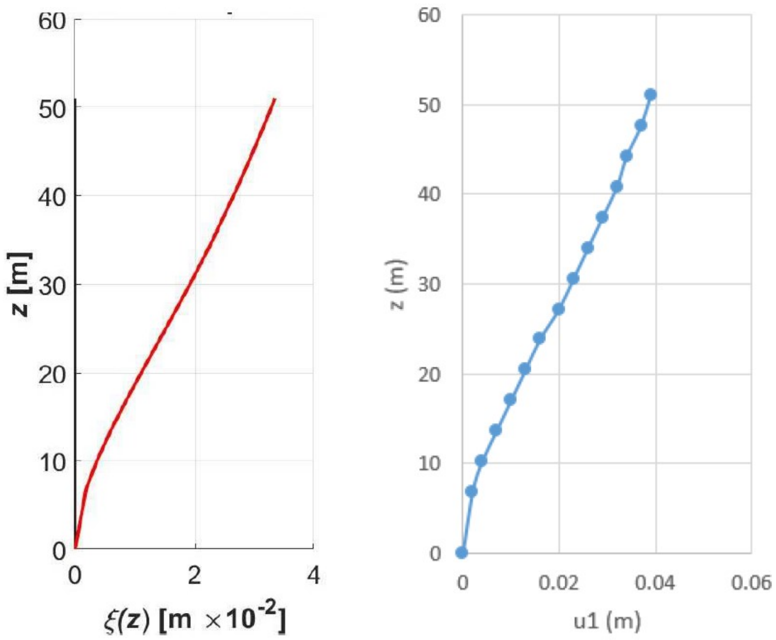

(a) Analytical model displacements

(b) FEM model displacements

Figure 4.87: Comparison of displacements between analytical model and FEM model

4.3.4 Comparison of analytical and FEM model results

In order to compare the results with the analysis using the analytical model, the FEM model was loaded at the nodes of the fictitious columns with the same horizontal loading conditions as those used in the analytical analysis.

The following comparison graphs illustrate the results of the analytical model (grey curves) and the FEM analysis (orange curves). In particular, the horizontal displacements along the X-axis ($u_1 - \xi(z)$), along the Y-axis ($u_2 - \eta(z)$) and the rotations ($r_3 - \vartheta(z)$) were compared.

- Case 1: Wind blowing in the X-direction

It can be observed from Figure 4.88 and 4.89 that the numerical model provides greater displacement values, with a maximum deviation of less than 20% at the last

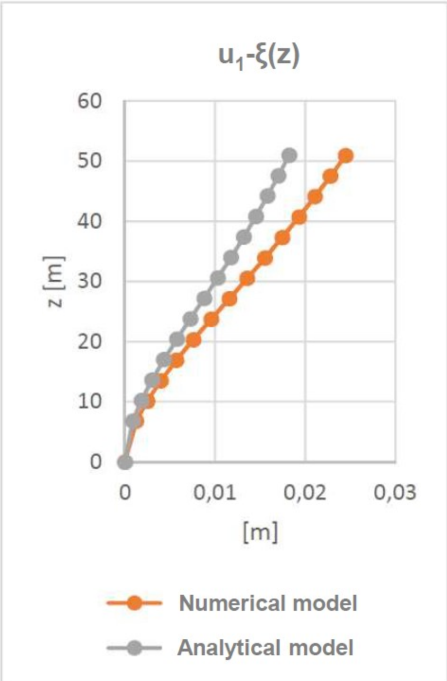

Figure 4.88: Horizontal displacements in X-direction

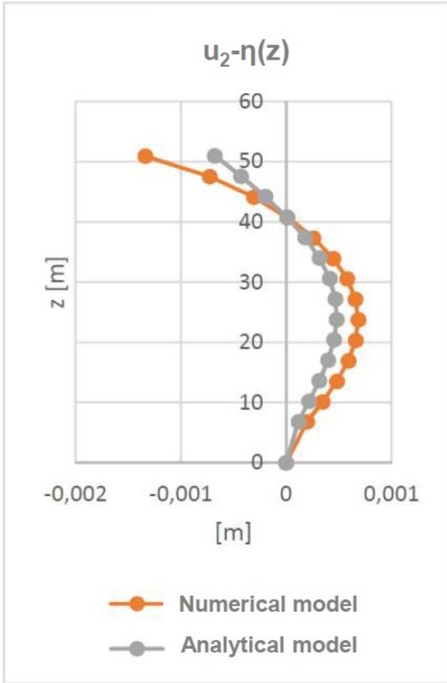

Figure 4.89: Horizontal displacements in Y-direction

plane. The displacement of the numerical model is approximately 2.4 cm against the 1.8 cm calculated by the analytical model, with a deviation of 0.14% around the mean value.

In the case of rotations (Figure 4.90), more similar values are obtained between the two models, in fact the rotation of the last plane is $7.72{\cdot}10^{-4} rad$ for the numerical model and $8.59 \cdot 10^{-4} rad$ for the analytical model. There is therefore a deviation from the mean value between the two models of about 5%.

- Case 2: Wind blowing in the Y-direction

For the displacements along X (Figure 4.91) it can be seen that the maximum displacement value occurs at the eighth plane and is 0.96 mm for the analytical model and 1.35 mm for the numerical model, with a deviation of 17%.

It can be seen that in the case of displacements along Y (Figure 4.92), the values obtained from the analytical model and the numerical model almost coincide. The maximum value occurs at the last plane and is 3.33 cm for the numerical model and 3.23 for the analytical model, with a deviation of 1.5%.

Again, as in the previous case, the maximum value of the rotations is in the last plane and the deviation between the two models is approximately 5% (Figure 4.93).

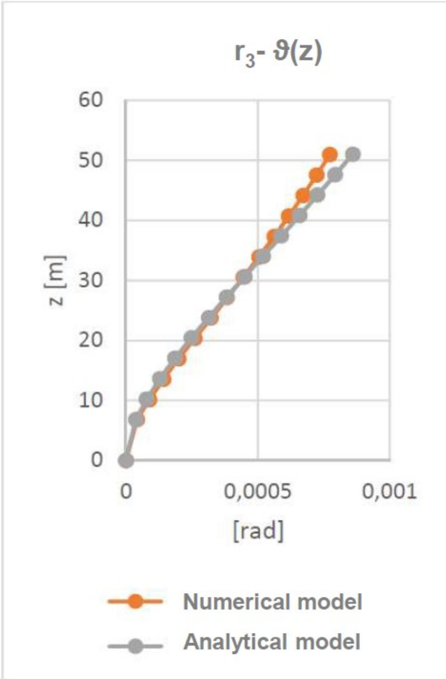

Figure 4.90: Rotations

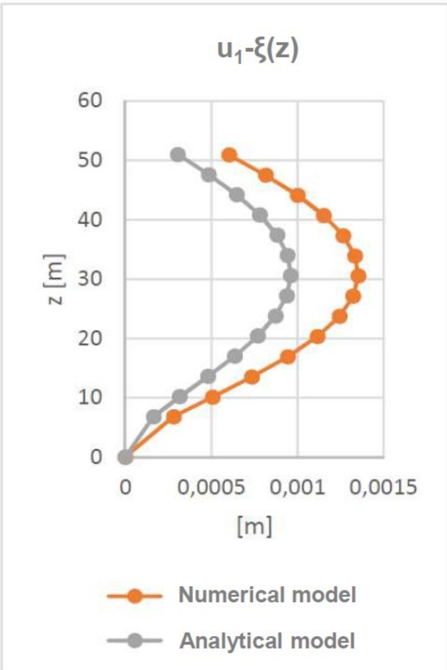

Figure 4.91: Horizontal displacements in X-direction

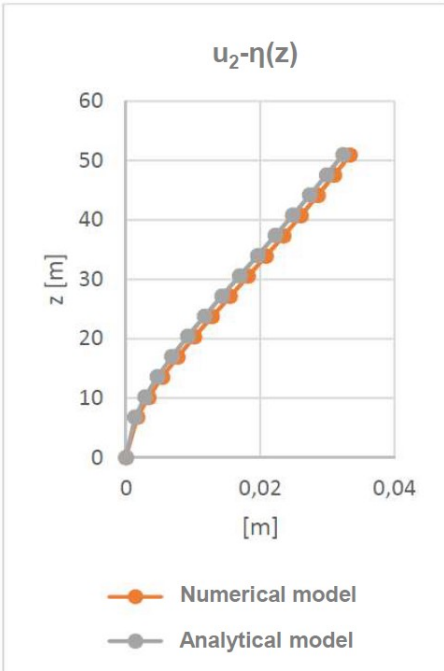

Figure 4.92: Horizontal displacements in Y-direction

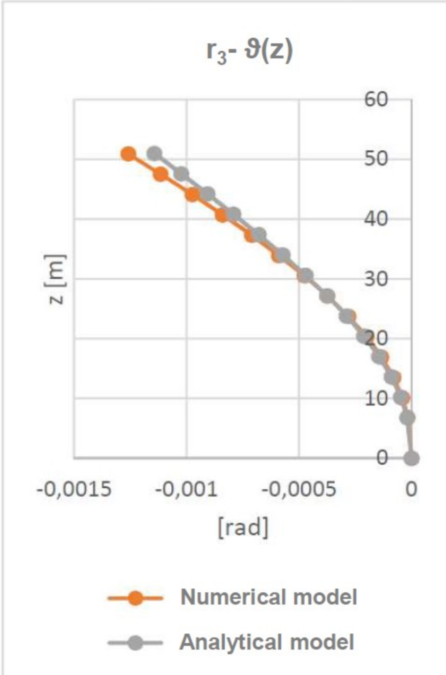

Figure 4.93: Rotations

4.3.5 Dynamic Modal analysis

As is known from the study of the dynamics of structures, dynamic modal analysis operates a decomposition of the dynamic response of the structure into the contributions of its individual vibration modes. This is achieved by moving from a system of equations with n degrees of freedom to n systems of equations with a single degree of freedom.

In order to study the intrinsic properties of the structure in response to dynamic stresses, the system without forcing was analysed. This consisted of the stiffnesses of the resistant vertical elements and the masses of the floors.

Analytical model

The mass of the typical floor was evaluated through a load analysis, with reference to a typical floor of the period in which the building was constructed. In particular, a concrete-masonry slab was considered, comprising a 6 cm high solid slab and 18 cm high block, a beam floor thickness of 10 cm and a block width of 30 cm.

In accordance with the methodology prescribed in NTC18, the weight of the non-structural permanent loads associated with the floor, plaster, screed and partitions was incorporated into the overall weight of the floor.

Typical floor					
Element	Width (m)	Heigth (m)	Incidence	γ (kN/m^3)	Total (kN/m^2)
Concrete rib	0.1	0.18	2.5	25	1.125
Slab	1	0.06	1	25	1.5
Block	0.3	0.2	2.5	6	0.9
Total					3.525

Self-weight of Non-Structural Elements			
Element	Thickness (m)	Unit weight γ (kN/m^3)	Total load (kN/m^2)
Plaster	0.015	20	0.3
Screed	0.06	21	1.26
Flooring	0.01	20	0.2
Total			**1.76**

Load from Partitions		
Element	Thickness (m)	Total load (kN/m^2)
Plaster	0.012	0.24
Brick	0.100	1.10
Plaster	0.012	0.24
Total		**1.58**

Total load per linear meter (h=280)	4.99	kN/m
G_2	2.00	kN/m^2

A typical floor weight of 7.3 kN/m^2 was thus obtained.

An extension of 205 m^2 was considered, a damping coefficient (ξ) equal to 0.05, and the moments of inertia were calculated with respect to the axes of the global reference system and the polar moment of inertia. The resulting values were as follows: The calculated values for the moments of inertia are as follows: J_{xx} = 2393.76 m^4, J_{yy} = 6626.53 m^4 and J_{xy} = 9020.29 m^4.

The results for the oscillation periods and frequencies of the first four modes of vibration are presented in Table 4.14.

T [s]	f [Hz]
1.53	0.66
1.24	0.80
1.07	0.93
0.33	3.02

Table 4.14: Analytical model - Oscillation periods and frequencies

Numerical model

In this instance, the floors were assigned a weight of 30.42 kN/m^3, a thickness of 24 cm and a damping coefficient of 0.05.

The results for the oscillation periods and frequencies of the first four vibration modes are shown in Table 4.15.

T [s]	**f** [Hz]
1.29	0.78
1.22	0.82
1.17	0.86
0.34	2.65

Table 4.15: Numerical model - Oscillation periods and frequencies

Comparison of analytical and numerical model results

There is a notable resemblance between the values of the oscillation periods and frequencies derived from the two analyses. The discrepancies between the values of the two models can be attributed to the geometric dissimilarities between them.

The discrepancies between the outcomes yielded by the two models, quantified in percentage terms, are illustrated in Table 4.16

T [s]	**f** [Hz]
8.4	8.7
1.0	1.0
4.3	4.0
1.3	6.5

Table 4.16: Percentage deviations between analytical and numerical model

4.3.6 Conclusions

A comparison of the results obtained through analytical calculation with those derived from numerical calculation demonstrated convergence in the values of the displacements, despite differences in the construction of the two models. The most significant of these is the collaboration between the primary frames and the secondary transverse frames, which is not accounted for in the analytical model. In the latter model, the frames are incorporated as discrete elements, whereas in the numerical model this feature is introduced through the ability to model a spatial frame.

In the present case, this approximation is justifiable, given that it is typical for structures of this type to exhibit warping in a single main direction.

A second discrepancy between the models is observed in the representation of the outer frames. In particular, the frames in the analytical model are represented as flat elements, whereas in the numerical model the actual geometry is followed by considering an overhang of one meter on the first floor.

4.4 Rai Skyscraper

The Rai skyscraper, now known as the Pietro Micca building, was built in 1968 by architects Aldo Morbelli and Domenico Morelli between Piazza XVIII Dicembre and Via Cernaia, on the edge of the city centre (Figure 4.94).

The building was built to house the national headquarters of RAI (Radiotelevisione Italiana), the Italian public radio and television service. Following the relocation of a large number of offices in the city of Rome, the skyscraper retained part of the offices, which were then completely relocated to CRIT in Via Cavalli in 2016 due to the high presence of asbestos in the structure. The skyscraper remains completely unused to this day.

In 2021, it was purchased by the IPI SpA Real Estate Group with the intention of cleaning it up and redeveloping it. The project, entrusted to 'CRA' (Carlo Ratti Associati), includes the preservation of the characteristic steel façade and the restoration of the interior spaces, which will be used for offices, a commercial area, apartments and a large terrace on the seventh floor.

Figure 4.94: Rai skyscraper

4.4.1 The structural system of the Rai skyscraper

The Rai skyscraper is constituted by a central parallelepiped of 18 floors above ground, with a height of 72 m, and two lower bodies that evoke the style of the

19th-century arcades of Via Cernaia.

The skyscraper is characterised by the presence of visible steel load-bearing structures, which serve to emphasise its vertical development. This is further accentuated by the facade partitions. The building is topped by an imposing canopy. The steel structure is clad with aluminium and glass, which together constitute a *'curtain wall'* of regular and proportioned arrangement. The iron and stone details evoke the style of earlier New York buildings from the 1950s.

The floor plan of the main building is rectangular in shape, with a footprint of 53×13.5 m. It comprises 11 main frames placed in the transverse direction and 4 secondary frames in the longitudinal direction.

With the exception of the first and second floors, which are 5.45 m and 3.76 m high, respectively, and the top three floors, which are 4 m and 6 m high, each floor is 3.50 m high. Additionally, two subterranean levels, each measuring 4 meters in height, are incorporated into the structure.

From *"Un nuovo palazzo a Torino"* [25], Domenico Morelli's words on the architectural design of the building are quoted:

> *"The maximum exploitation of the land had already been indicated by the Municipal Offices in a quadrilateral construction with an internal courtyard and sleeves of varying height according to the surrounding public spaces. The resulting cubage, however, was not sufficient for the RAI's needs, which had become more precise in the meantime, so that the courtyard would have to be covered over and other fallbacks would have to be made to meet them, thus worsening the layout of the complex. It was at this point that the idea arose in us, and was readily accepted by RAI, to raise a building of considerable height on the front of the square, appropriately set back, so as to be able to contain the other smaller limits than those foreseen in the regular solution: a solution that also made it possible to concentrate in the said ≪skyscraper≫all the offices and services of a normal character, reserving the other parts for special ones."*

> *"Unfortunately, further requirements of the RAI required an increase in volume, which, for various reasons, was not achieved by raising the skyscraper, but by adding a floor on Via Cernaia and Via Guicciardini, as well as forming a raised hall on one half of the large inner courtyard. These variants have altered the composition of the volumes with respect to the original project, but above all have diminished the airiness and luminosity of the courtyard and the rooms facing it, although recognising that since most of them also overlook the*

street and are fully air-conditioned, the damage has been reduced more to an aesthetic matter."

"[...] we established the following points for the design:

- *creating a structure that, i terms of materials and architecture, would clearly denote the new technical and functional requirements;*
- *to place a building in Via Cernaia that, in terms of volume and height, would fit into the composition of the street;*
- *instead, to erect an element of considerable height on the square, which would create a clear separation, but at the same time would constitute a compositional element linking the ribbon of old buildings of limited height on Via Cernaia and Piazza S. Martino and the new tall and massive blocks of State Offices; an element seen almost as a link between the skyscrapers of the Directional Centre and the old traditional fabric;*
- *keeping architectural lines within the limits of maximum compositional simplicity and traditionality, with the aim of disturbing as little as possible what little remains of value in the surrounding environment;*

It was in fact our conviction that when one intervenes in an environment that has already been established for some time, one should try to make oneself stand out as little as possible, without, however, renouncing to give the new building its current characteristics;"

"The skyscraper is built against the sleeve of Via Cernaia; on the ground floor there is the main entrance that extends, with its fully glazed atrium, under the said sleeve, to the arcades of the street. Vertical movement is ensured by four fast lifts and the external double staircase, dimensioned for rapid displacement of the building; a freight elevator, at the other end, serves all floors, including the first basement.The said double staircase is connected to the main building by a ≪bridge≫, on the sides of which are the floor toilets. At the two heads of the high-rise building there are still two metal emergency staircases. The buildings on the streets have two other staircases: one at the corner of Via Guicciardini and Via Ruffini, the other at the point where the Via Cernaia sleeve joins the skyscraper; both are equipped with double lifts. The latter staircase is essentially intended to serve the kitchen, bar, and company canteen, located on the top two floors on Via Cernaia."

"The entire complex is built in reinforced concrete in the underground part and in some elements that required isolation from the rest of the structure (lift

shafts, compartments for the numerous and complex ascending ducts, service stairs, etc.); all the remaining elevated bodies are in iron. The iron structure for the upper body was dictated by economic reasons; however, it was extended to the other buildings as well, both for reasons of aesthetic uniformity and in consideration of the considerable span of the floors. The load-bearing pillars all have a rectangular tubular cross-section; in the skyscraper they vary in size every three storeys; in the buildings on the streets they are of constant size; only the thickness changes. The beams of the floors are generally double-T beams of various types and sizes; in the buildings on the streets, those perpendicular to the external walls are instead made up of two separate and opposing C-sections, which protrude on the façade beyond the bank beam and embrace the pillars; this solution has made it possible to obtain a continuous slot for each pair of beams, the width of the pillar, through which the vertical pipes pass. The horizons in the skyscraper are all made of ≪profiled sheet ≫with a thin concrete slab overlaid; in the low buildings, on the other hand, given the considerable spans to be covered, they are made of reinforced concrete; in some parts the concrete cooperates with the iron structure and decreases its deformability. From a technical point of view, the skyscraper structure was particularly delicate. In fact, it consists of a quadruple row of pillars, connected by beams and floors; but to absorb the horizontal stresses resulting from the considerable height, three transversal diaphragms and one longitudinal diaphragm with a braced structure were used, which absorb, through the floors, the thrust exerted by the wind on the façades. The external parts are made almost entirely of ≪curtain wall ≫of natural aluminium and double crystals; ≫, an alloy of aluminium and silicon, which takes on a beautiful purplish-grey colour, has also been used in the roofing of the perimeter beams, in the joint covers and other internal parts. Only for environmental and practical reasons, the few concrete parts and the skirting boards were covered with Diorite della Balma worked with a pointed tool or with a hammering tool."

"The almost exclusive adoption of natural anodised aluminium, and of crystals, is not only the consequence of a search for lightness and simplicity, but the desire to use materials that can, with a not onerous maintenance, conserve their characteristics for a long time; in fact, almost all synthetic materials undergo a more or less marked degradation over time. Undoubtedly, constructions of this kind require very complex and sensitive air-conditioning systems, lacking thermal inertia; but if one considers that the need not to waste space inside obliges one to reduce the load-bearing structures to a minimum."

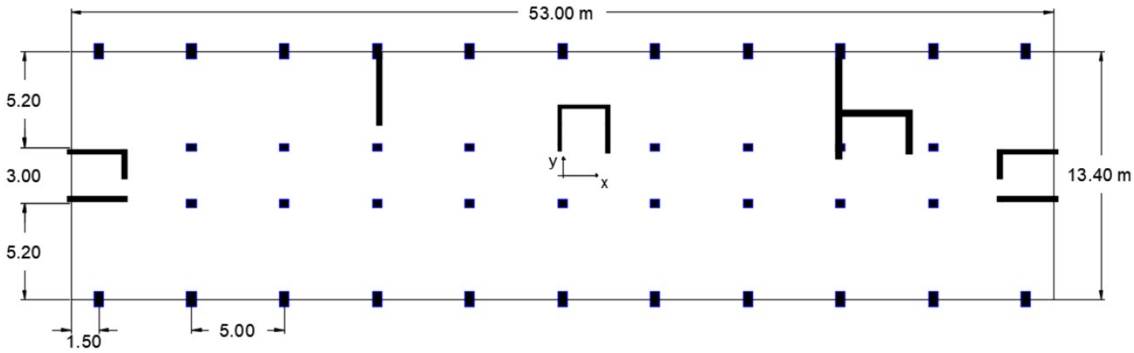

Figure 4.95: Typical floor plan

Of particular interest are the five reinforced concrete walls that extend the full height of the building (Figure 4.95).

Also from *Un nuovo palazzo a Torino*, Fabrizio De Miranda's words on structural design are quoted:

> *"The distribution study envisaged a central tower body, with a volume of about 80,000 cubic meters, to be used as offices, and a complex of lower bodies, with a volume of about 3,000 cubic meters, arranged around the skyscraper and designed to harmonise the main building with the city environment, by means of architectural recurrences and porticoes in continuation of the pre-existing ones."*
>
> *"Referring in particular to the tower body, which obviously presents the most interesting aspects from a structural point of view, here are the key points in order:*
>
> - *vertical and horizontal structural elements of limited overall dimensions, with external dimensions as uniform as possible, depending on both distributional requirements and particular unquestionable architectural constraints (e.g. façade pillars with constant overall dimensions, placed outside the perimeter wall);*
> - *maximum lightening of elevated structures to allow for direct foundations, avoiding costly piling works;*
> - *structures of rapid and continuous assembly, with the adoption of bolted joints, limiting in-situ welding to only those joints subject to particular architectural requirements;*
> - *impossibility of restoring horizontal thrusts to the foundation level by means of lattice bracing, due to the need for a free portico at street level;*
> - *study of a particular type of anchorage between steel superstructures and*

reinforced concrete substructures at the vertical, transverse and longitudinal bracings;

- *location, distribution and form of the bracing structures, determined and studied in accordance with the functional and distribution requirements of the building and in function of the limitation of elastic deformations under the action of the wind;*
- *rigid transmission of the wind thrust, at each horizon, to the vertical bracing structures: a problem that is not easy to solve in relation to the light type of slab adopted and to the numerous holes of considerable size to be provided in the same for the passage of stairs, hoists, lifts, etc. This problem appeared particularly important and delicate on the first floor where, due to the undesirable presence of diagonal bracing in the underlying portico, the transversal bracing of the tower stops: the wind thrust concentrated in said bracing must therefore, at this level, be uniformly distributed to the underlying transversal portals by means of the very high rigidity slab in the horizontal plane.*

”

Furthermore, the text provides a technical description and load analysis of the structures. In particular, the complex is comprised of a 72.56-meter-high tower building with 20 floors above ground and two basement floors, surrounded by a complex of low perimeter structures. The buildings are constructed with a steel load-bearing structure, which serves to minimise the encumbrances of the load-bearing members and the loads on the foundations. In contrast, the basement floors and foundations are constructed with reinforced concrete. The subterranean levels, due to their considerable mass, serve to stabilise the structure against overturning forces.

The load-bearing structures of the basement floors are composed of a series of flat transverse frames with a spacing of 2.50 m $\div$ 4.50 m, with a span of approximately 10 m. The frames are coupled with C-shaped composite beams that embrace the columns to which they are welded in place. The floor is constructed of profiled sheets with a reinforced concrete slab. The maximum allowable overload is 600 kg per square meter.

The floor plan of the skyscraper is rectangular in shape, with dimensions of 53 meters. It features two slight recesses of 3 meters on the gables and a large lateral appendage, which is used for the staircase and services. The structure is composed of 11 vertical transversal frames, positioned at a constant centre-to-centre distance of

5 m. The main frame beams and external columns are welded to racks of secondary beams in the workshop. The secondary beams, which run continuously parallel to the long side of the building, have a span of 5 m and a centre-to-centre distance of 2.50 m. The floor runs continuously over the secondary beams and is constructed from 10/10 mm thick profiled sheet, welded at each wave to the secondary beams with welding nails. A 4 mm diameter steel mesh is spot-welded above the profiled sheet, and a 4 cm thick concrete slab has been cast on site above the extrados of the profiled sheet. The structure is completed by the addition of vertical bracing trusses, comprising three transverse elements and one longitudinal element.

Three groups of structural elements can be identified:

a) from -0.90 to +4.50 m
b) from +4.50 m to 18°floor
c) technical volumes and roof

a) Structures from -0.90 to +4.50 m

The initial section of the edifice comprises 11 rigid node portals, each comprising four uprights positioned transversally to the façade. The two external uprights are hinged at the base, while the two internal uprights are interlocked. The crossbeams of the portals are responsible for bearing the loads transmitted directly from the slab at an elevation of +4.50 m, while the vertical loads from the upper columns and the wind loads at the braces act upon their uprights. The horizontal wind loads are conveyed at an elevation of 4.50 m by three vertical bracing beams and distributed uniformly across all the base frames via a 15 cm thick reinforced concrete solid slab with double cross reinforcement. This slab acts as an infinitely rigid element within its own plane.

The vertical posts and portal beams are constructed from plates that have been welded in a workshop setting to form rectangular caissons of consistent dimensions (290 mm $\times$ 600 mm for the piers and 290 mm $\times$ 450 mm for the stringers). However, the external piers of the three portals, which are designed to accommodate the upper bracings, exhibit a widening sectional profile as they ascend (reaching dimensions of 290 mm $\times$ 1000 mm).

b) Structures from +4.50 m to 18th floor

The structural composition of this section is comprised of eight rigid end node frames and intermediate pendulums, in addition to three braced frames.

With regard to the rigid node frames, the external columns are constructed from tubular sections with a rectangular cross-section, which undergo a reduction in size at each three floors, from 380 to 280 mm at the base, to 280 mm at the top. The welds of the segments are done on-site through the use of electric welding. The internal columns, which also have a rectangular cross-section, are interrupted at each floor. The main beams, comprising double-T sections with a height of 320 mm, traverse the building in a continuous manner and are reinforced with horizontal plates welded to the wings in proximity to the internal columns. Composite beam stub are also welded to which the secondary beams are bolted. These beams consist of double-T sections with a height of 220 mm on the internal ones and composite plates welded to a C shape with a height of 320 mm on the perimeter ones.

In the bracing frames, the external columns, which are continuous and welded every three storeys, are formed of two rectangular profiles that are joined at each storey with pieces of double-T or rectangular profiles. Similarly, the internal columns are continuous and welded together every three storeys. The main beams, comprising double-T profiles with a height of 320 mm, are affixed to the columns through the use of bolts. The diagonals are formed of ring profiles, which are also joined by bolting. In order to ensure that the deflection at the top remained within the permitted limits, two exceptionally robust connecting beams were employed, situated between the 9th and 10th floors.

c) Technical volumes and roof

The end section is characterised by portals transversal to the building, approximately 6 m high, with beams cantilevering 5.30 m over the entire building. The beams are composite and exhibit a variable cross-section, whereas the columns are characterised by a square tubular cross-section.

The roof is constructed using exposed galvanised profiled sheet of the *"Steelox type"*, over a span of 5 m. A load-bearing reinforced concrete slab is cast on top of this.

Additionally, technical volumes pertaining to the operation of lifts and other associated services are situated on the 18^{th} floor.

Foundations

The foundation comprises a reinforced concrete wall with a height of 12 meters, emerging at the foot of a slab. The anchorage at the base of the bracing frames was achieved through the use of prestressing cables, which extend throughout the full height of the wall beams.

Structural load analysis

In addition to the self-weight of the steel structures and the profiled sheet, the following loads were considered and are presented in Table 4.17.

Structural load analysis	
1st floor	
- Self-weight of slab	300 kg/m^2
- Flooring, ceiling, thermal-acoustic layer, and partition walls	220 kg/m^2
Total permanent loads	520 kg/m^2
- Live load	600 kg/m^2
Upper floors	
- Self-weight of slab	150 kg/m^2
- Flooring, ceiling, thermal-acoustic layer, and partition walls	220 kg/m^2
Total permanent loads	370 kg/m^2
- Live load	300 kg/m^2
- Live load on the 2nd floor	600 kg/m^2

Table 4.17: Structural load analysis

The stairwells and lift walls bear on the steel structure. For the calculation of the columns, the overloads were reduced according to C.N.R.-UNI standards.

On a total empty volume of 60,750 cubic meters, the unitary incidences of the structures are reported on Table 4.18.

Incidence of structures	
Columns and bracings	12.30 kg/m^3
Main beams	6.50 kg/m^3
Secondary beams	5.20 kg/m^3
Profiled sheet	4.00 kg/m^3
Total	28.00 kg/m^3

Table 4.18: Unitary incidence of structures

4.4.2 Analytical model

In order to study the building, the *Ta.Bu.* calculation code was employed, whereby a simplified model (Figure 4.96 and 4.97) of the skyscraper comprising walls of constant thickness and mechanical properties that remained consistent throughout the height of the structure was created. Furthermore, the mechanical properties of the materials were standardised in accordance with the average resistance observed across the different floors.

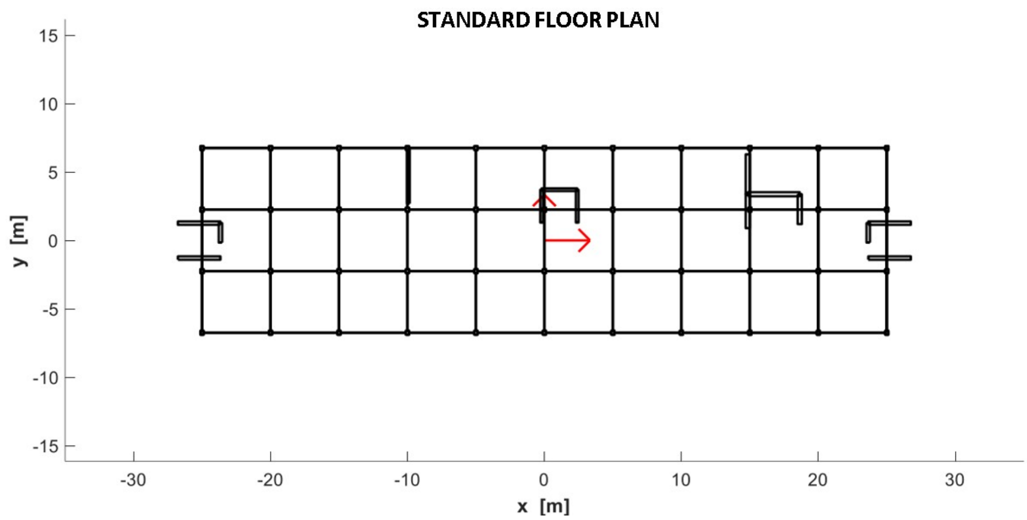

Figure 4.96: Standard floor plan

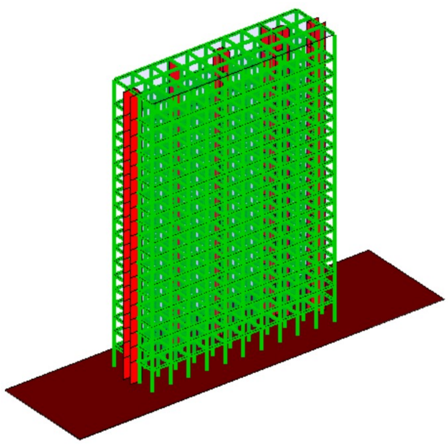

Figure 4.97: Structure 3D model

Wind action calculation

Referring to Appendix A for the calculation of the wind action, the values of the wind pressures and associated forces are given for cases where the wind blows in the direction of the Y-axis and X-axis.

- Case 1: Wind blowing in the Y-direction

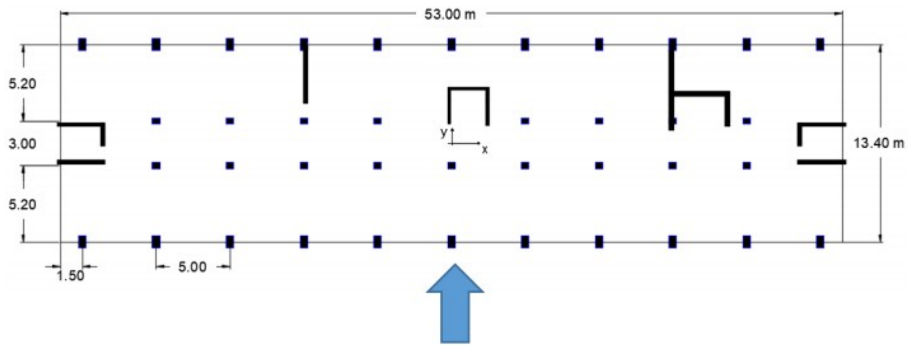

Figure 4.98: Wind blowing in the Y-direction

Floor	$\mathbf{c_e(z)}$	$\mathbf{p(z)}$ [N/m^2]	**Longitudinal force** $\mathbf{F_l(z)}$ [kN]	**Tangential force** $\mathbf{F_t(z)}$ [kN]	**Total force** $\mathbf{F(z)}$ [kN]
1	1.48	48.2	13.9	1.3	15.2
2	1.48	48.2	9.6	0.9	10.5
3	1.52	49.4	9.2	0.8	10.0
4	1.69	54.9	10.2	0.9	11.1
5	1.83	59.4	11.0	1.0	12.0
6	1.95	63.3	11.7	1.1	12.8
7	2.05	66.7	12.4	1.1	13.5
8	2.14	69.8	12.9	1.2	14.1
9	2.23	72.6	13.5	1.2	14.7
10	2.31	75.1	13.9	1.3	15.2
11	2.38	77.4	14.4	1.3	15.7
12	2.44	79.6	14.8	1.4	16.1
13	2.51	81.6	15.1	1.4	16.5
14	2.56	83.5	15.5	1.4	16.9
15	2.62	85.3	15.8	1.5	17.3
16	2.67	86.9	16.1	1.5	17.6
17	2.73	88.8	18.8	1.7	20.5
18	2.78	90.5	19.2	1.8	20.9

Floor	$c_e(z)$	$p(z)$ [N/m^2]	Longitudinal force $F_l(z)$ [kN]	Tangential force $F_t(z)$ [kN]	Total force $F(z)$ [kN]
19	2.85	92.9	29.5	2.7	16.1

Table 4.19: Wind forces for wind blowing in the Y-direction

- Case 2: Wind blowing in the X-direction

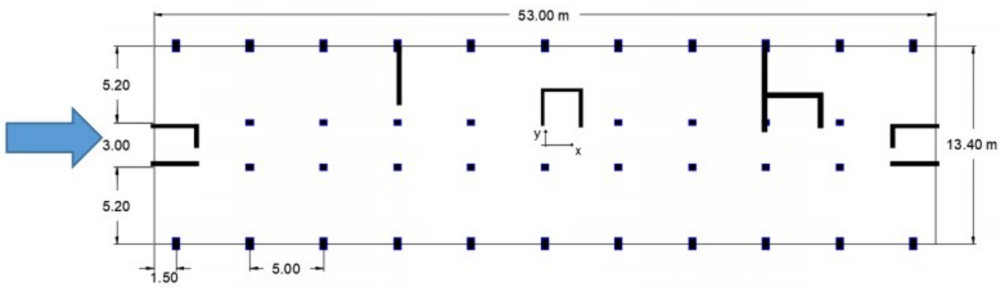

Figure 4.99: Wind blowing in the X-direction

Floor	$c_e(z)$	$p(z)$ [N/m^2]	Longitudinal force $F_l(z)$ [kN]	Tangential force $F_t(z)$ [kN]	Total force $F(z)$ [kN]
1	1.48	163.0	12.0	5.0	17.0
2	1.48	163.0	8.3	3.5	11.7
3	1.52	167.3	7.9	3.3	11.2
4	1.69	185.8	8.8	3.7	12.4
5	1.83	201.1	9.5	4.0	13.5
6	1.95	214.3	10.1	4.2	14.4
7	2.05	225.9	10.7	4.5	15.1
8	2.14	236.2	11.2	4.7	15.8
9	2.23	245.6	11.6	4.8	16.4
10	2.31	254.1	12.0	5.0	17.0
11	2.38	262.0	12.4	5.2	17.5
12	2.44	269.3	12.7	5.3	18.0
13	2.51	276.2	13.0	5.4	18.5
14	2.56	282.6	13.4	5.6	18.9
15	2.62	288.6	13.6	5.7	19.3
16	2.67	294.3	13.9	5.8	19.7
17	2.73	300.5	16.2	6.8	23.0
18	2.78	306.3	16.5	6.9	23.4

Floor	$\mathbf{c_e(z)}$	**p(z)** [N/m²]	**Longitudinal force** $\mathbf{F_l(z)}$ [kN]	**Tangential force** $\mathbf{F_t(z)}$ [kN]	**Total force** **F(z)** [kN]
19	2.85	314.5	25.5	10.6	18.1

Table 4.20: Wind forces for wind blowing in the Y-direction

Results

In order to examine the behaviour of the building in response to horizontal loads, the wind loads previously calculated in accordance with the current standard were introduced into the analytical model. This was done by considering the wind to be blowing once in the X-direction and once in the Y-direction.

- Case 1: Wind blowing in the Y-direction

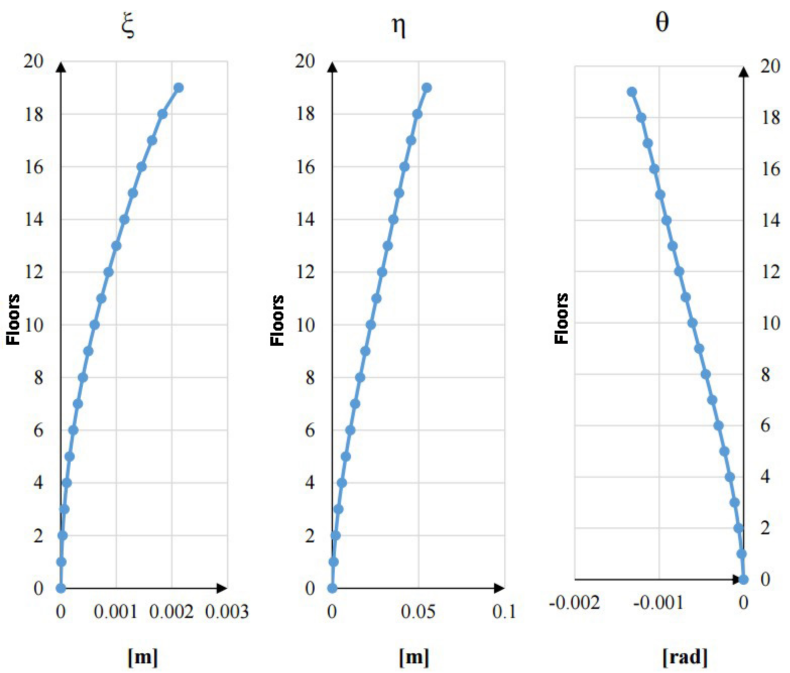

Figure 4.100: Displacements in the X-direction (ξ), in the Y-direction (η) and rotations (ϑ)

The maximum displacement at the top is 2.1 mm in the X-direction and 5.5 cm in the Y-direction, which is the direction in which the wind blows (Figure 4.100).

In accordance with NTC18, the maximum permissible lateral displacement of steel constructions due to horizontal actions is equal to *H/500*, where *H* is the height of the building. In the case under consideration, the height of the tower is 72.21 m, thus the maximum lateral displacement limit is 14.4 cm, which is respected.

- Case 2: Wind blowing in the X-direction

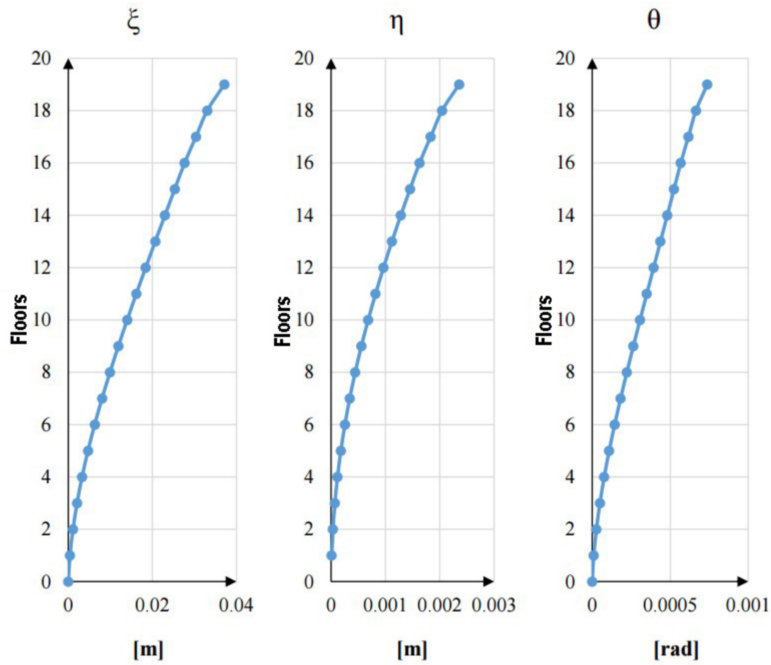

Figure 4.101: Displacements in the X-direction (ξ), in the Y-direction (η) and rotations (ϑ)

In this instance, the displacements at the upper extremity are 3.7 cm in the X direction (the direction in which the wind is blowing) and 2.4 mm in the Y direction. It can be observed that in this instance, the structure exhibits a greater degree of rigidity, which serves to reduce the observed displacements (Figure 4.101).

Furthermore, this case is also within the limits set by NTC18 for lateral displacements.

It is of interest to present the analysis of the internal reactions of the open thin section walls, designated *'VL1'* and *'VL2'* (Figure 4.102 and 4.103).

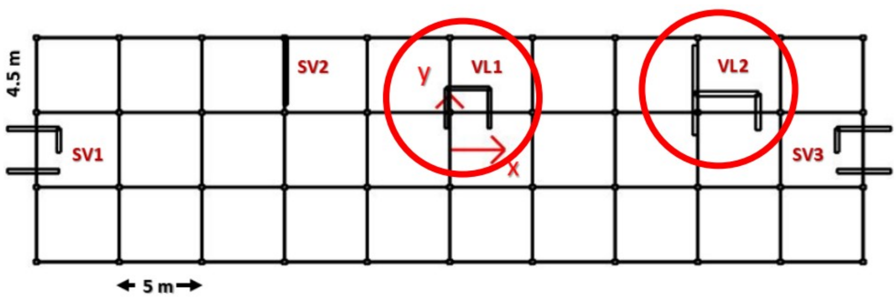

Figure 4.102: Plan position of open thin wall sections

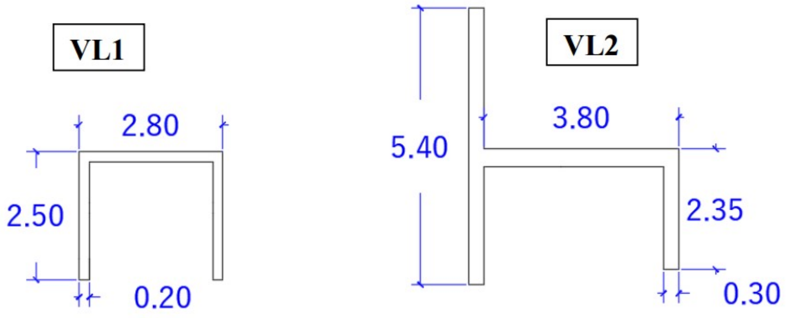

Figure 4.103: Detail of open thin wall sections

- Case 1: Wind blowing in Y-direction

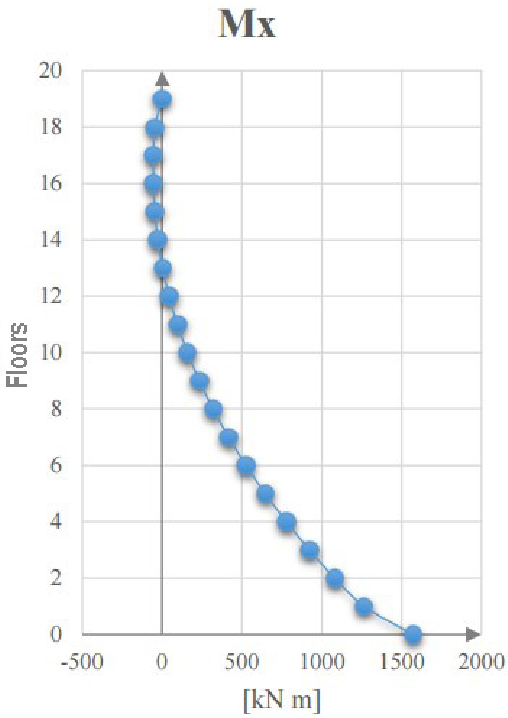

(a) VL1 open thin section

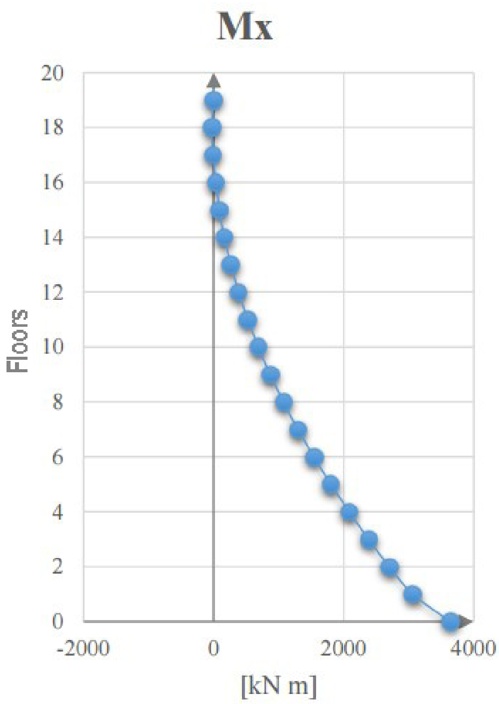

(b) VL2 open thin section

Figure 4.104: Bending moment M_x for wind blowing in Y-direction

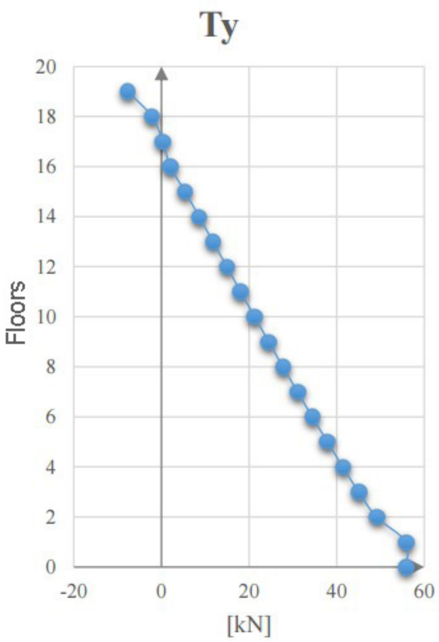

(a) VL1 open thin section

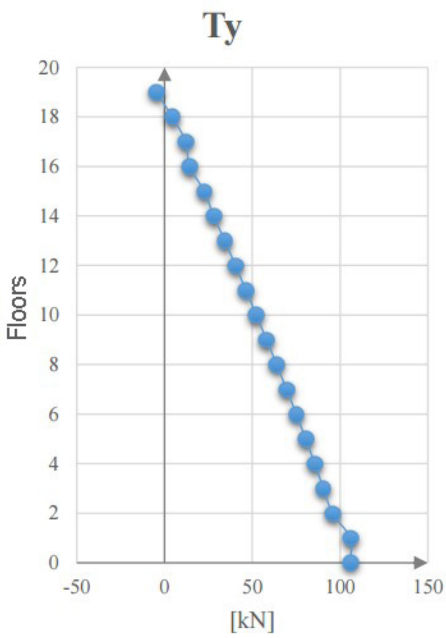

(b) VL2 open thin section

Figure 4.105: Shear T_y in Y-direction

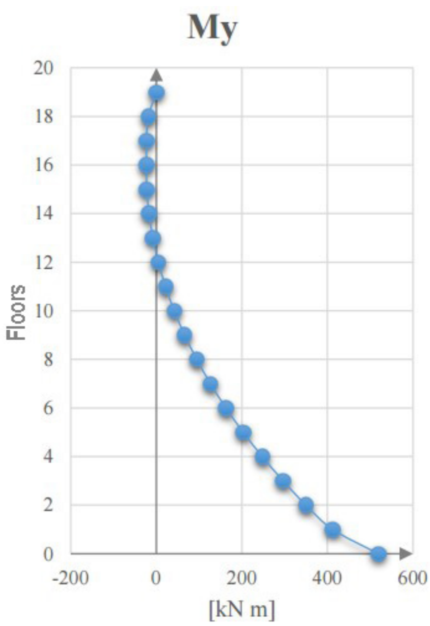

(a) VL1 open thin section

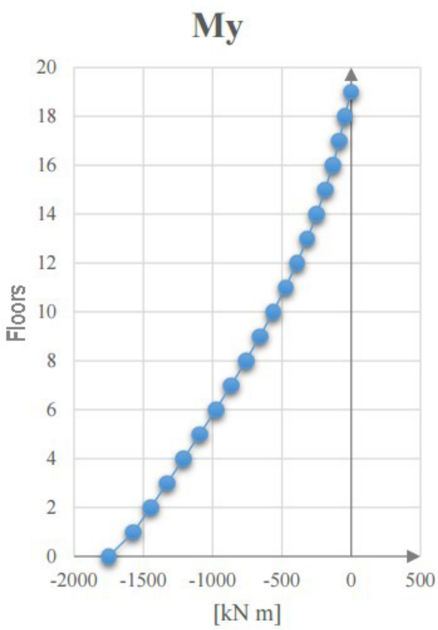

(b) VL2 open thin section

Figure 4.106: Bending moment M_y in Y-direction

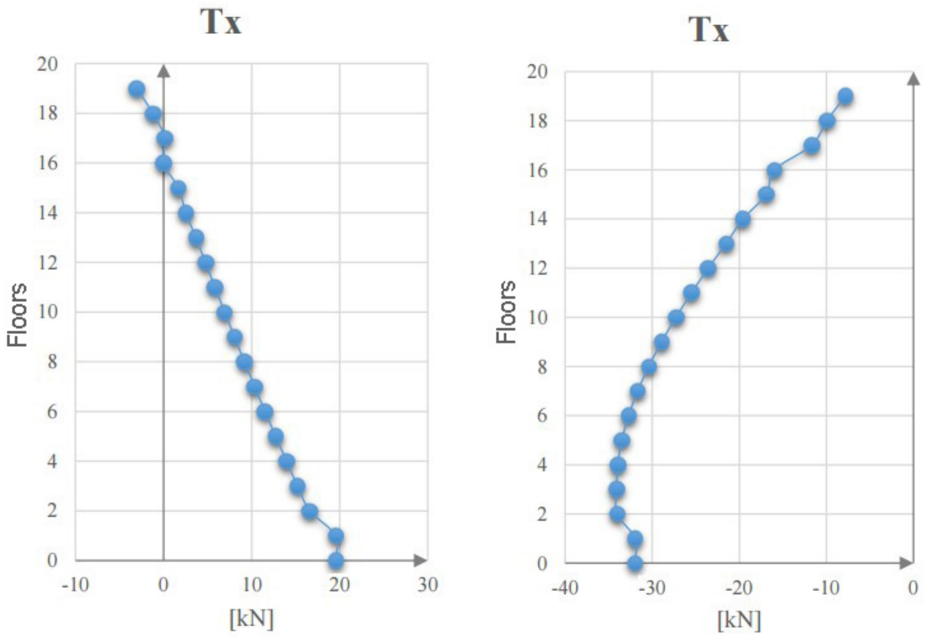

(a) VL1 open thin section **(b)** VL2 open thin section

Figure 4.107: Shear T_x in Y-direction

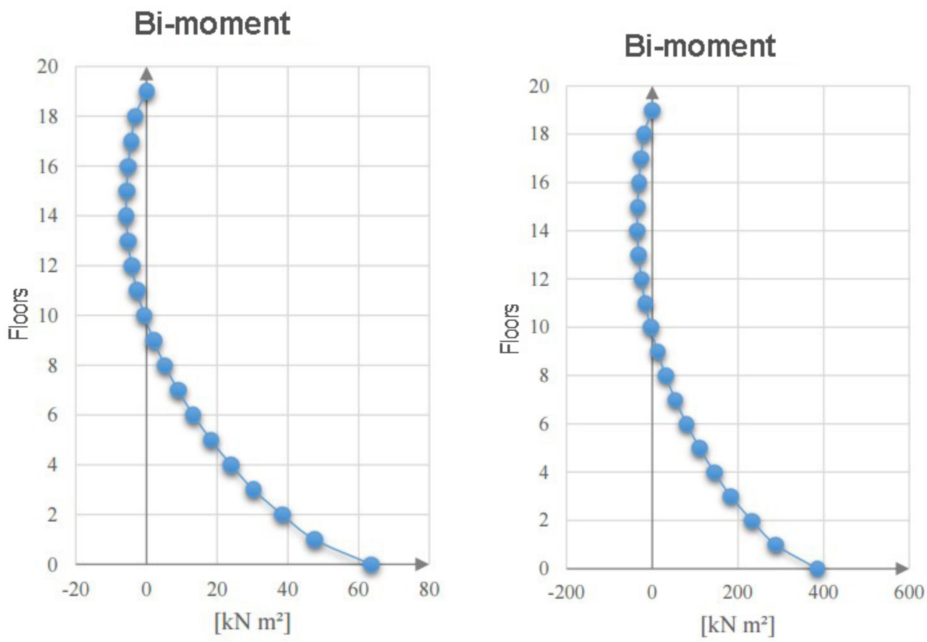

(a) VL1 open thin section **(b)** VL2 open thin section

Figure 4.108: Bi-moment B

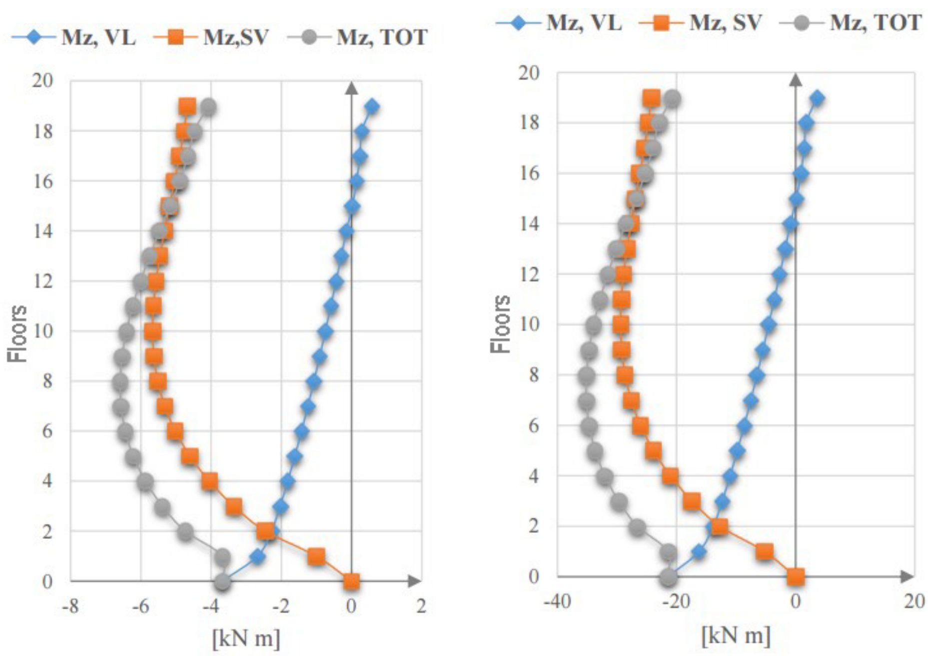

(a) VL1 open thin section

(b) VL2 open thin section

Figure 4.109: Torsional moment M_z in Y-direction

Internal action for VL1								
	M_x [kNm]	M_y [kNm]	B [kNm^2]	T_x [kN]	M_y [kN]	M_z^{VL} [kNm]	M_z^{SV} [kNm]	M_z^{TOT} [kNm]
Min	-54.7	-23.3	-5.7	-3.1	-7.7	-3.7	-5.7	-6.6
Max	1569.7	518.8	63.5	19.6	55.8	0.6	0.0	-3.7

Table 4.21: Internal action for VL1 with wind blowing in Y-direction

Internal action for VL2								
	M_x [kNm]	M_y [kNm]	B [kNm^2]	T_x [kN]	M_y [kN]	M_z^{VL} [kNm]	M_z^{SV} [kNm]	M_z^{TOT} [kNm]
Min	-28.1	-1749.9	-34.8	-34.1	-4.7	-21.4	-29.4	-35.1
Max	3639.0	0.0	385.0	-7.8	105.8	3.6	0.0	-20.7

Table 4.22: Internal action for VL2 with wind blowing in Y-direction

As evidenced by the values presented in Tables 4.21 and 4.22, the VL2 wall demonstrates a greater load absorption capacity than the VL1 wall. This is particularly evident in the bending moment M_x value at the base, which is 3639 kNm for the VL1 wall and 1569.7 kNm for the VL2 wall. Furthermore, the bimoment B is six times greater in the VL2 wall than in the VL1 wall.

- Case 2: Wind blowing in X-direction

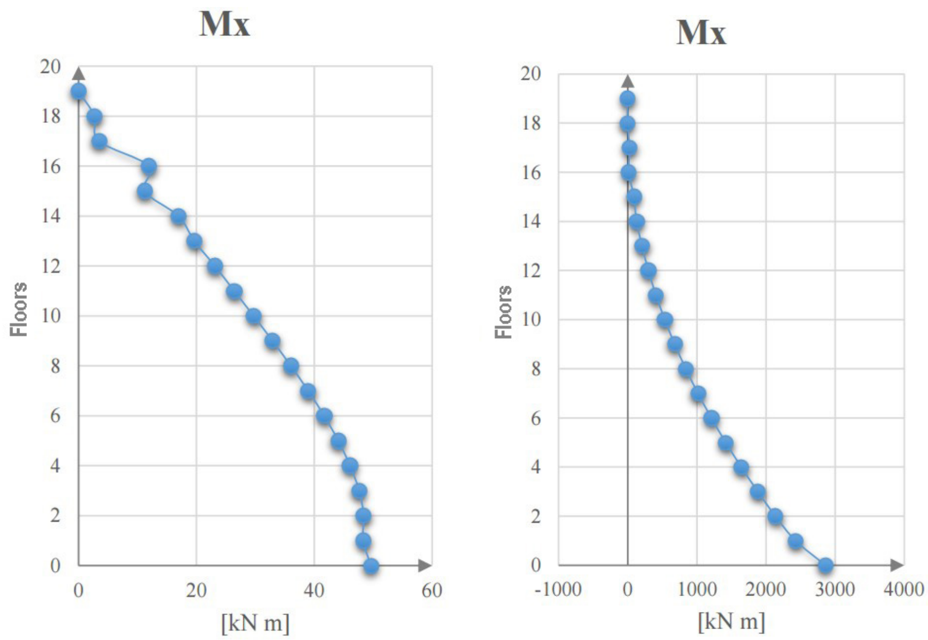

(a) VL1 open thin section **(b)** VL2 open thin section

Figure 4.110: Bending moment M_x in X-direction

Internal action for VL1								
	$\mathbf{M_x}$ [kNm]	$\mathbf{M_y}$ [kNm]	**B** [kNm^2]	$\mathbf{T_x}$ [kN]	$\mathbf{M_y}$ [kN]	$\mathbf{M_z^{VL}}$ [kNm]	$\mathbf{M_z^{SV}}$ [kNm]	$\mathbf{M_z^{TOT}}$ [kNm]
Min	0.0	0.0	-28.3	1.6	-0.2	-0.3	0.0	1.4
Max	49.6	1625.9	1.4	41.4	2.1	1.4	3.1	3.4

Table 4.23: Internal action for VL1 with wind blowing in X-direction

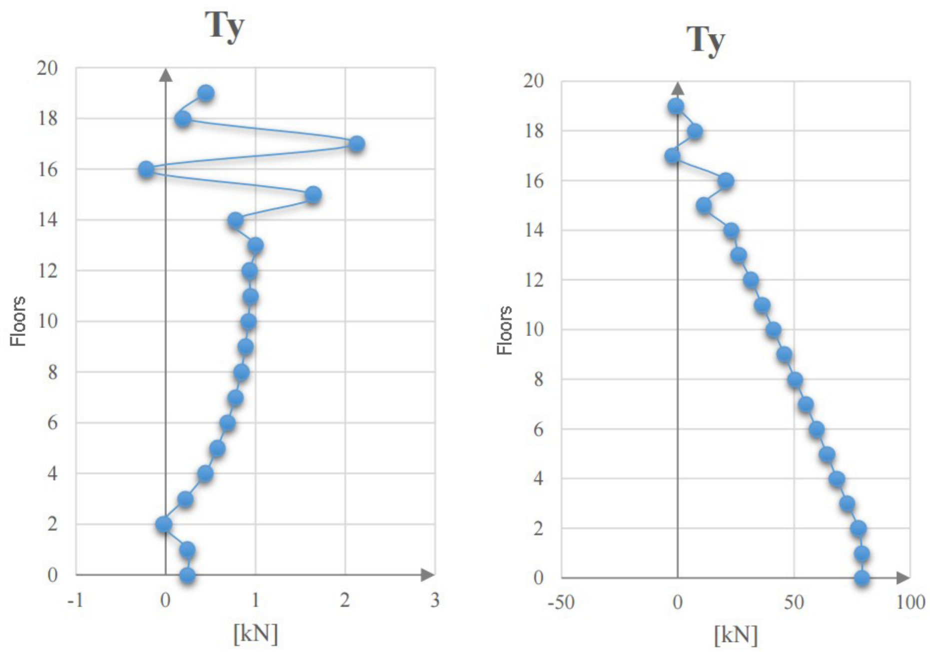

(a) VL1 open thin section

(b) VL2 open thin section

Figure 4.111: Shear T_y in X-direction

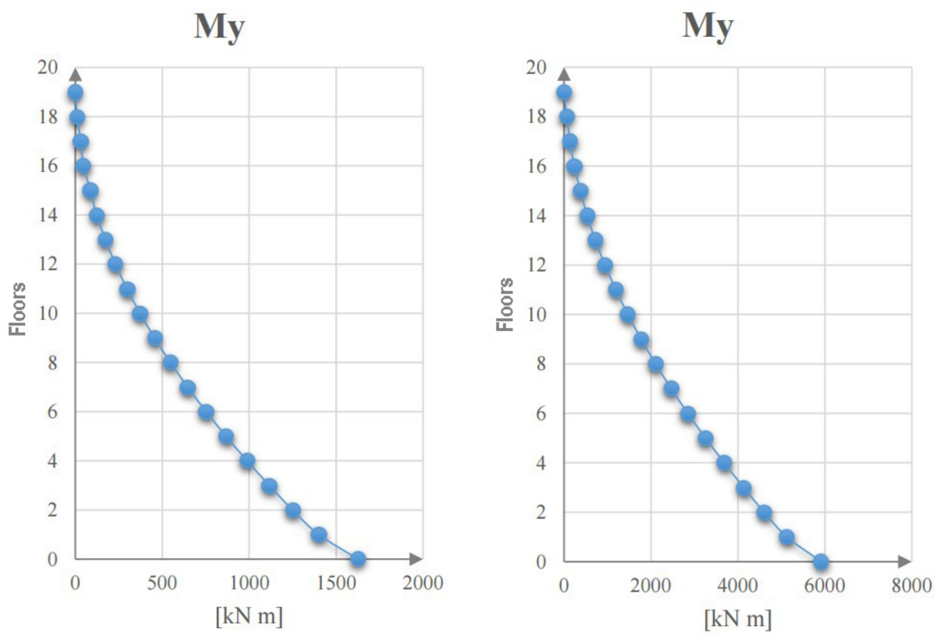

(a) VL1 open thin section

(b) VL2 open thin section

Figure 4.112: Bending moment M_y in X-direction

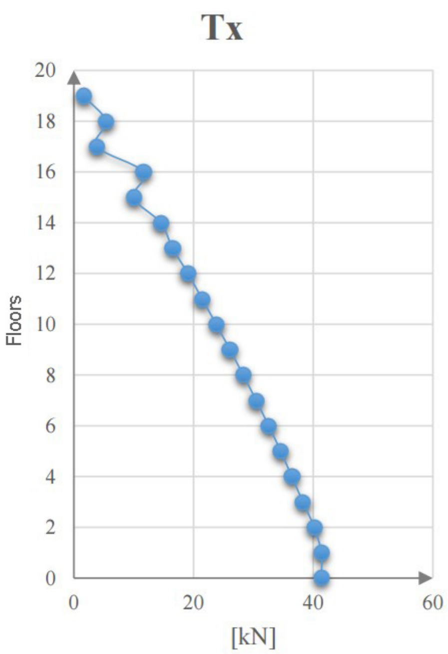

(a) VL1 open thin section

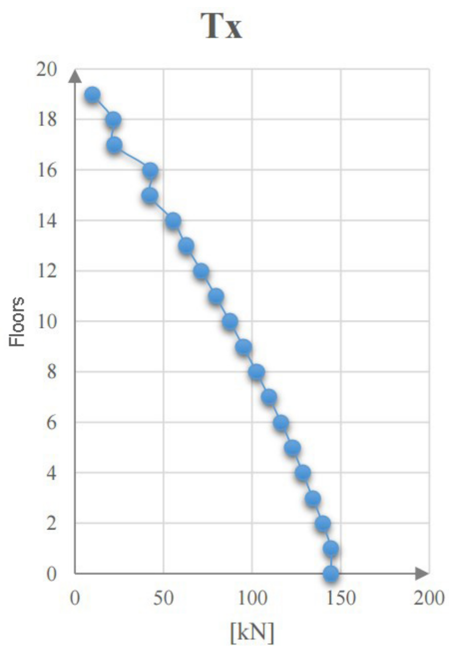

(b) VL2 open thin section

Figure 4.113: Shear T_x in X-direction

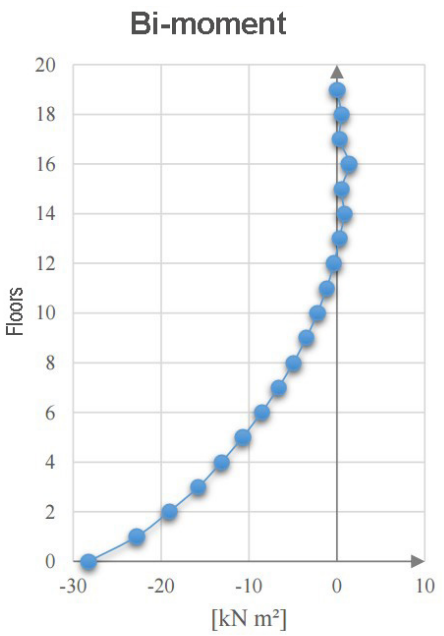

(a) VL1 open thin section

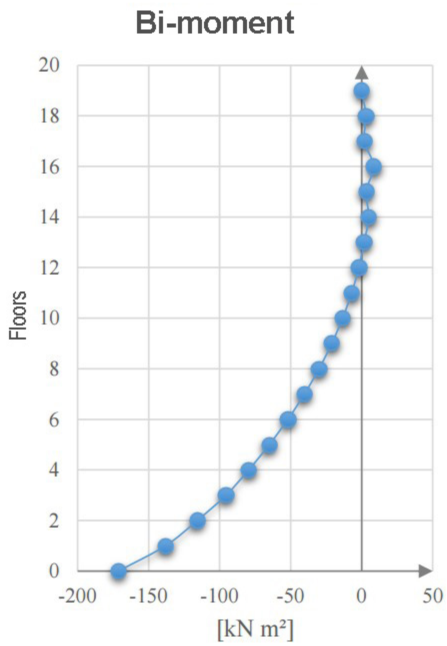

(b) VL2 open thin section

Figure 4.114: Bi-moment B in X-direction

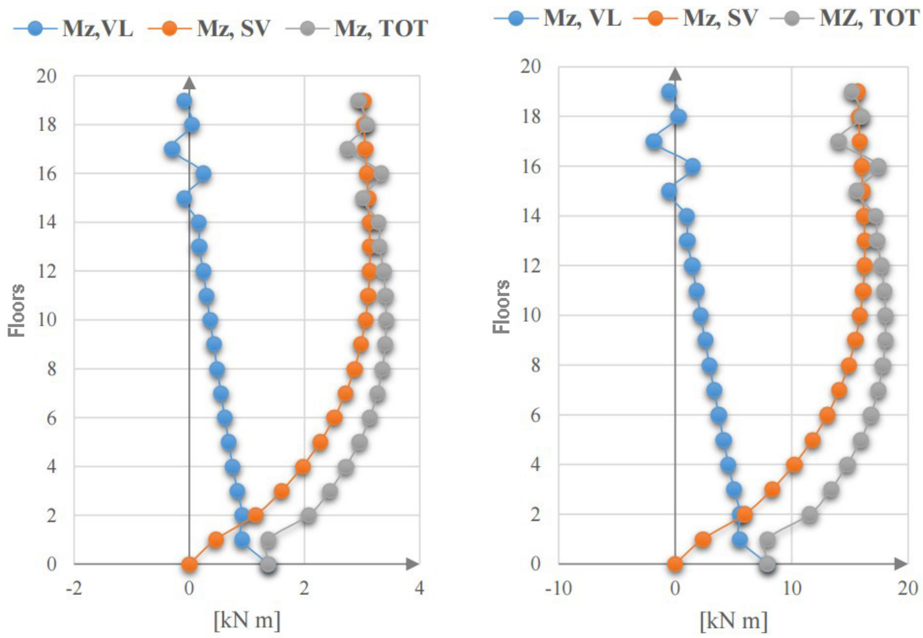

(a) VL1 open thin section

(b) VL2 open thin section

Figure 4.115: Torsional moment M_z in X-direction

Internal action for VL2								
	M_x [kNm]	M_y [kNm]	B [kNm^2]	T_x [kN]	M_y [kN]	M_z^{VL} [kNm]	M_z^{SV} [kNm]	M_z^{TOT} [kNm]
Min	-5.3	0.0	-171.3	9.7	-2.3	-1.8	0.0	7.9
Max	2860.6	5916.7	8.3	144.4	79.3	7.9	16.3	18.1

Table 4.24: Internal action for VL2 with wind blowing in X-direction

Also in this second case, an examination of Tables 4.23 and 4.24 reveals that the wall VL2 is subjected to significantly greater stress than the wall VL1. The maximum moment in the Y direction is 5916.7 kNm for wall VL2, in comparison to 1625.9 kNm for wall VL1.

Stress analysis

The following stress analysis is centred on the section designated as VL1 (Figure 4.116). The calculation code outputs a series of data points, including the barycentre, shear centre, moments of inertia and angle of rotation. The aforementioned data are presented in Table 4.25.

OPEN SHEARWALL 1 'VL1'		
Section barycentre		
x_G	1.1	m
y_G	2.92	m
Shear centre		
x_C	1.1	m
y_C	4.72	m
Moments of inertia		
J_{xx}	9.74E-01	m^4
J_{yy}	1.92E+00	m^4
J_{xy}	0.00E+00	m^4
$J_{\omega\omega}$	1.14E+00	m^6
$J_{x\omega}$	0.00E+00	m^5
$J_{y\omega}$	0.00E+00	m^5
J_t	1.97E-02	m^4
Angle of rotation		
Omega (ω)	0	deg

Table 4.25: Data section of shearwall VL1

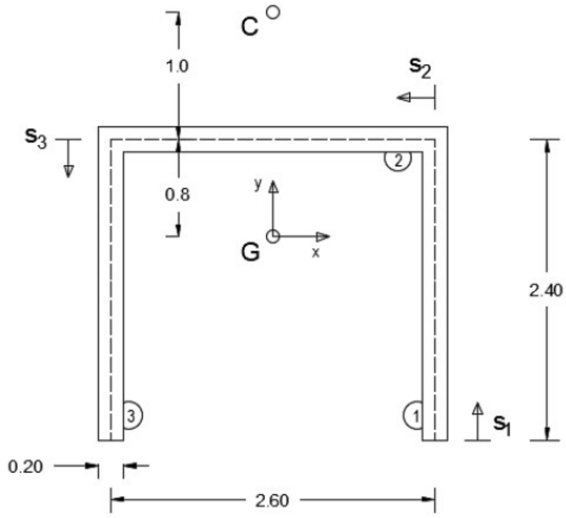

Figure 4.116: Shearwall VL1

In accordance with the stress calculation procedure outlined in Appendix B, the normal stresses σ and tangential stresses τ for the wind blowing in the Y-direction (Table 4.26 and Figures 4.117, 4.118) and in the X-direction (Table 4.27 and Figures 4.119, 4.120) are obtained.

Point	$\sigma_{\mathbf{M_x}}$ [kN/m^2]	$\sigma_{\mathbf{M_y}}$ [kN/m^2]	$\sigma_{\mathbf{B}}$ [kN/m^2]	$\sigma_{\mathbf{z}}$ [kN/m^2]	$\tau_{\mathbf{x}}$ [kN/m^2]	$\tau_{\mathbf{y}}$ [kN/m^2]	τ_{ω} [kN/m^2]	$\tau_{\mathbf{tot}}$ [kN/m^2]
1	-179	-1104	161	-1122	0.0	0.0	0.0	0.0
2	-54	-1104	83	-1074	-44.6	-0.2	-14.2	-58.5
3	-54	1104	-83	967	44.6	-0.2	-14.2	30.1
4	-179	1104	-161	763	0.0	0.0	0.0	0.0

Table 4.26: Stresses of shearwall VL1 for wind blowing in Y-direction

Point	$\sigma_{\mathbf{M_x}}$ [kN/m^2]	$\sigma_{\mathbf{M_y}}$ [kN/m^2]	$\sigma_{\mathbf{B}}$ [kN/m^2]	$\sigma_{\mathbf{z}}$ [kN/m^2]	$\tau_{\mathbf{x}}$ [kN/m^2]	$\tau_{\mathbf{y}}$ [kN/m^2]	τ_{ω} [kN/m^2]	$\tau_{\mathbf{tot}}$ [kN/m^2]
1	-5677	-352	-362	-6391	0.0	0.0	0.0	0.0
2	-1697	-352	-187	-2236	-21	-45	38	-28
3	-1697	352	187	-1157	21	-45	38	14
4	-5677	352	362	-4963	0.0	0.0	0.0	0.0

Table 4.27: Stresses of shearwall VL1 for wind blowing in X-direction

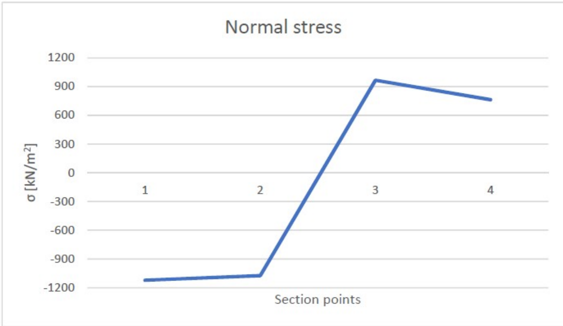

Figure 4.117: Normal stress in Y-direction

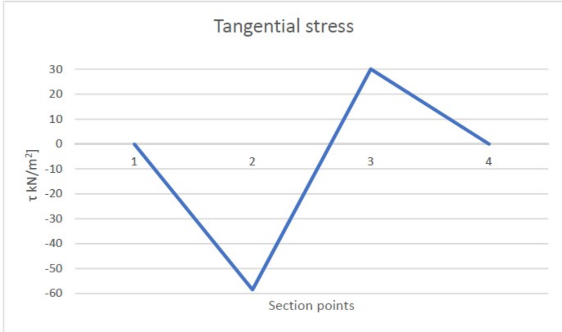

Figure 4.118: Tangential stress in Y-direction

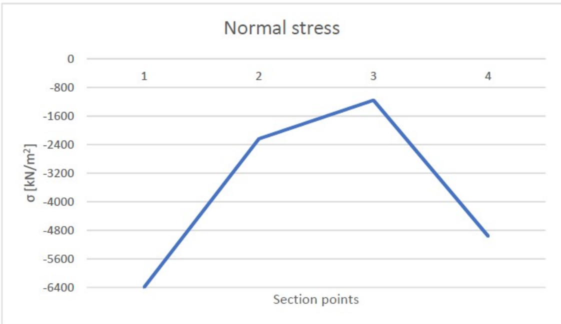

Figure 4.119: Normal stress in X-direction

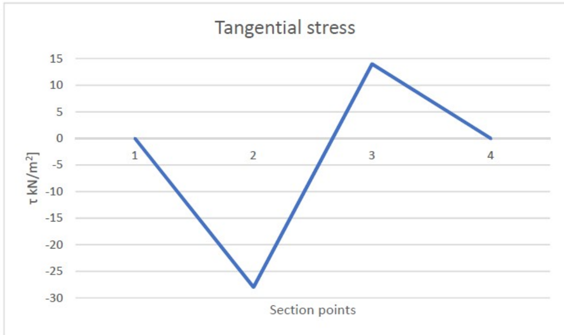

Figure 4.120: Tangential stress in X-direction

Dynamic analysis

The objective of the dynamic analysis is to identify the first three modes of vibration exhibited by the structure. In order to conduct this analysis, it was assumed that the floor weight would be 10 kN/m^3. The natural frequencies for the first three modal shape of the structure were obtained using the calculation code (see Table 4.28).

	Frequency [Hz]	**Period** [s]
1^{st} modal shape	0.24	4.17
2^{nd} modal shape	0.32	3.12
3^{rd} modal shape	0.43	2.33

Table 4.28: Natural frequencies and periods for the first 3 modal shape

4.4.3 FEM model

The finite element model (FEM) of the structure, illustrated in Figure 4.121 and 4.122, was developed using the finite element software *SAP2000*. The initial step involved defining the structure's geometry, utilising *joints*, *frame* elements and *shell elements* to represent the reinforced concrete walls. Ultimately, the interlocking constraint at the base of the edifice and the diaphragm constraint at each floor were imposed to guarantee the latter's stiffness.

The materials employed are concrete (with a modulus of elasticity of 28000 MPa) for the partitions and steel (with a modulus of elasticity of 196133 MPa) for the beams and columns.

The sections employed for the various elements are as follows:

- Pillars with rectangular hollow bases
- Main beams and internal secondary beams with double-T section
- Secondary perimeter beams with C-section
- Walls with thickness varying from 20 to 30 cm

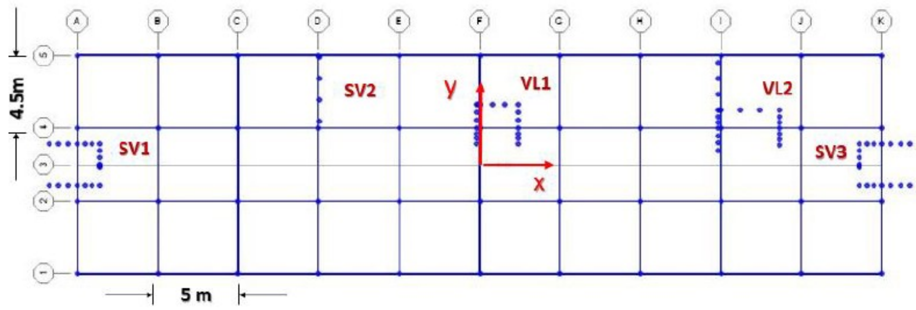

Figure 4.121: Floor plan of the FEM model

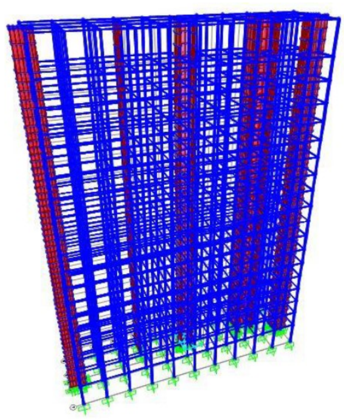

Figure 4.122: 3D of the structure

Static analysis and results

In order to conduct a static analysis, the wind loads in the X and Y directions, as defined in 4.4.2, are applied to the numerical model.

- Case 1: Wind blowing in Y-direction

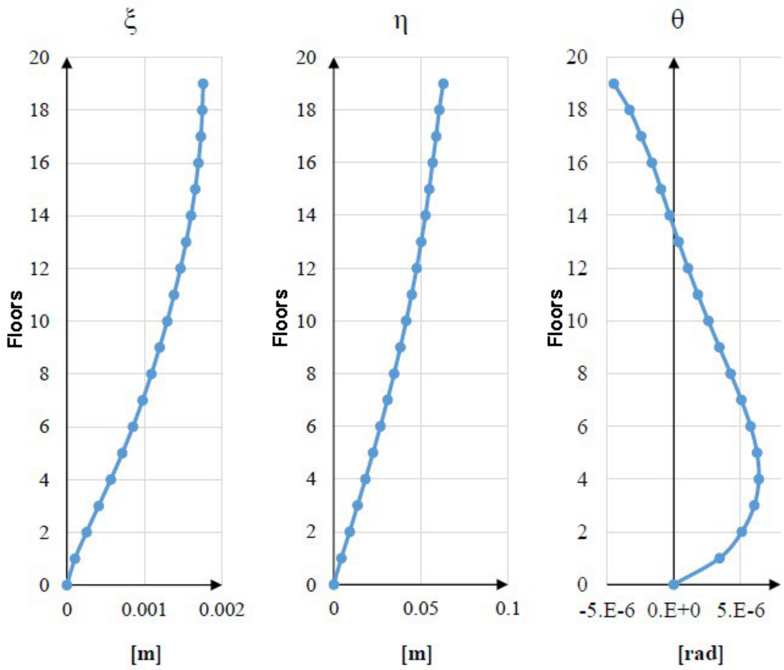

Figure 4.123: Displacements due to wind blowing in Y-direction

Figure 4.123 illustrates that the maximum displacement occurs at the top of the building, with a value of 1.8 mm in the X-direction and 6.8 cm in the Y-direction (in the same direction as the applied load).

- Case 2: Wind blowing in X-direction

Figure 4.124 illustrates that the maximum displacement occurs at the top of the building, with a value of 5.7 mm in the X direction (in line with the applied load) and 2.1 mm in the Y direction.

It can be observed that, in this instance, the structure presents a more rigid behaviour.

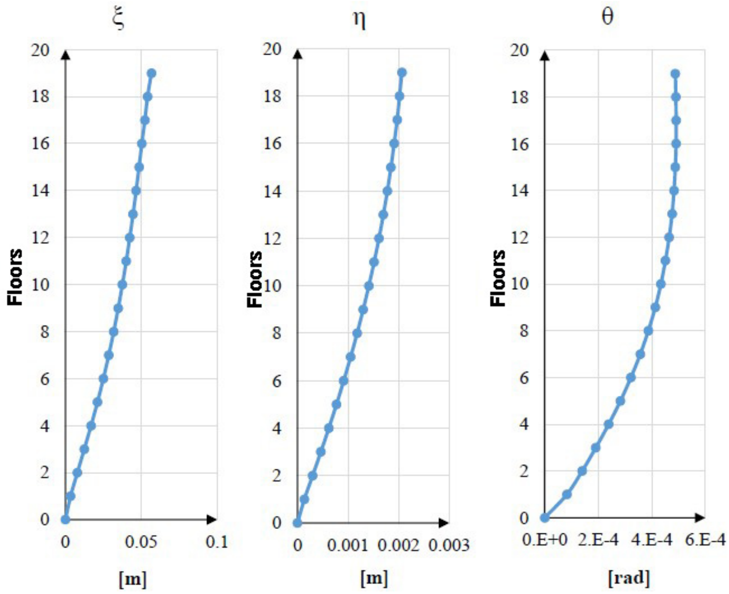

Figure 4.124: Displacements due to wind blowing in X-direction

Comparison between analytical and FEM models

The following section presents a comparative analysis of the displacement results obtained from the analytical and numerical models for wind blowing in Y-direction (Figure 4.125 and Table 4.29) and in X-direction (Figure 4.126 and Table 4.30).

- Case 1: Wind blowing in Y-direction

Displacements at the top			
	ξ [cm]	η [cm]	ϑ [rad]
FEM model	0.18	6.3	-4.5E-06
Analytical model	0.21	5.5	-1.3E-03

Table 4.29: Displacement at the top of the structure for wind blowing in Y-direction

- Case 2: Wind blowing in Y-direction

From the graphs shown in Figure 4.125 and 4.126, it can be observed that there is a slight discrepancy between the displacements in the X and Y directions and the rotations in the plane obtained through the two distinct models.

In particular, it can be observed that the corresponding displacement in the analytical model is reduced by approximately 12% with respect to the numerical model in the direction of the applied load. Conversely, an increase of between 17%

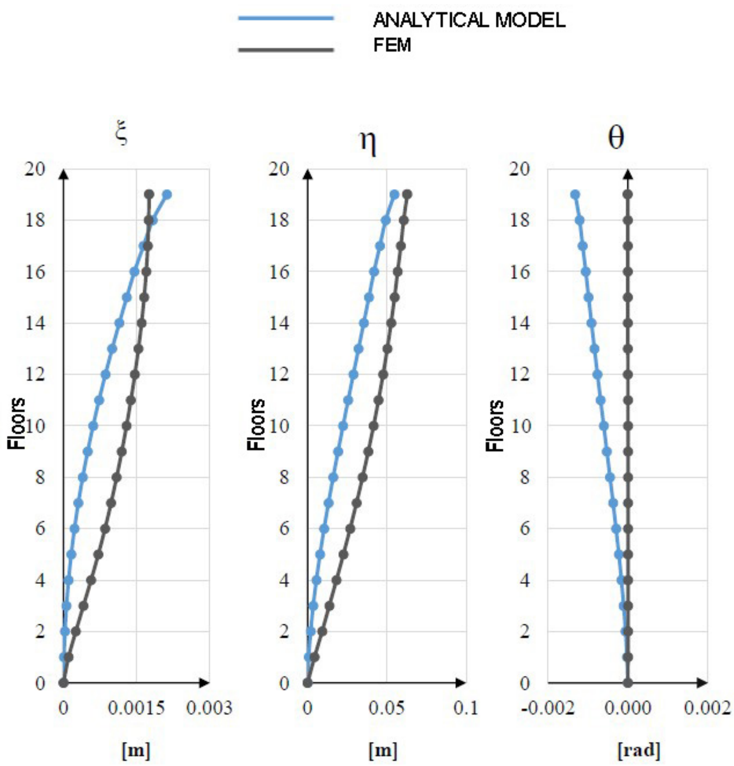

Figure 4.125: Comparsion of displacements in Y-direction

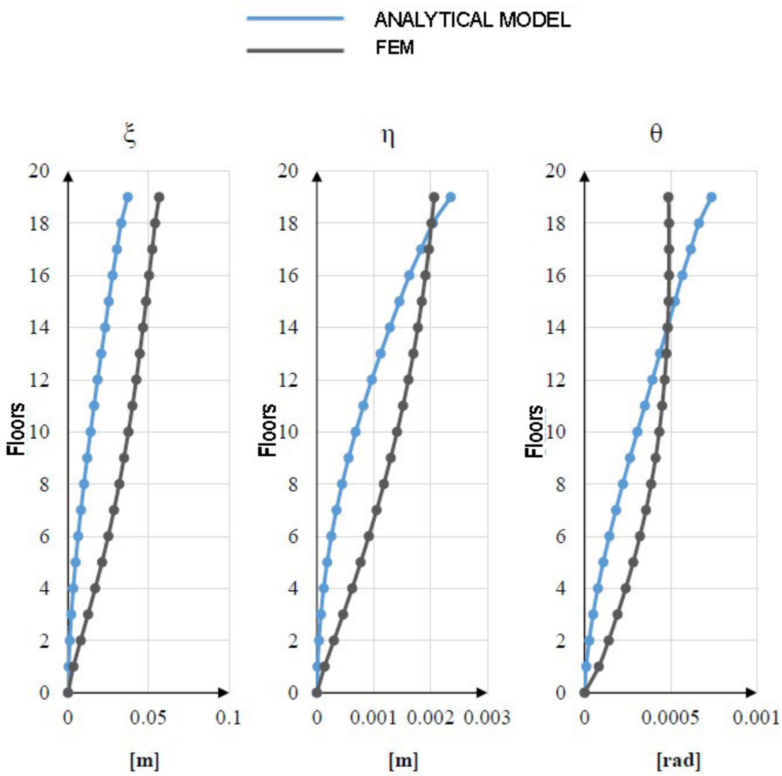

Figure 4.126: Comparsion of displacements in X-direction

Displacements at the top			
	ξ [cm]	η [cm]	ϑ [rad]
FEM model	5.7	0.21	7.4E-04
Analytical model	3.7	0.24	4.9E-04

Table 4.30: Displacement at the top of the structure for wind blowing in X-direction

and 34% is seen in the analytical model with respect to the numerical model for the displacement orthogonal to the direction of application of the load. With regard to rotations, it is observed that the order of magnitude remains constant in both models for a load applied along the most rigid part of the structure. However, considerable variation is evident in the case of a load applied in an orthogonal direction.

Ultimately, the results of the dynamic analysis yielded comparable outcomes with respect to the structure's natural periods (Figure 4.127).

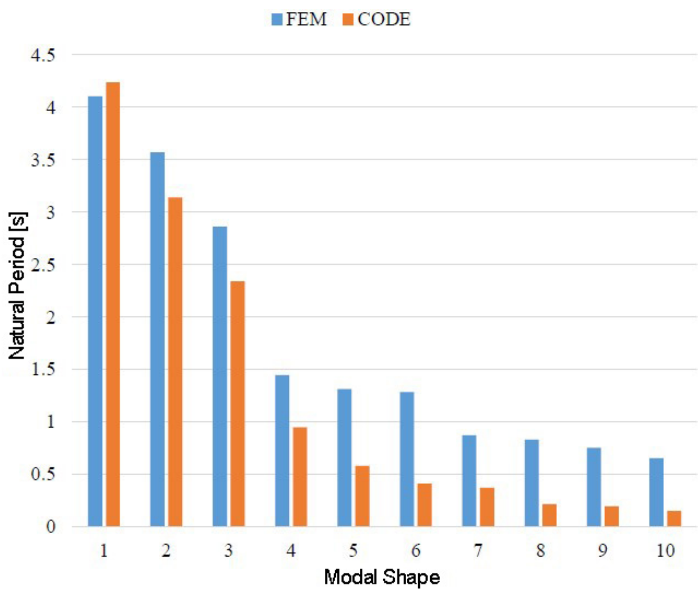

Figure 4.127: Comparsion of natural periods

The comparison reveals that the calculation code views the building in question as consisting of a series of separate frames,whereas the FEM software treats the three-dimensional structure as a unified entity. Moreover, it is evident that the outcomes yielded by the analytical model are highly comparable to those of the numerical model. Additionally, the former offers more comprehensive insights into the internal reactions of the walls.

4.5 Sanpaolo Tower

In 2005, the City of Turin, which encompassed an area of 7,000 square meters between Corso Inghilterra and Corso Vittorio Emanuele, held an auction for the concession of building rights on this area. The tender was won by the banking company Sanpaolo IMI, which proceeded to construct a tower that would serve as its headquarters.

A competition was announced for the design of the Intesa Sanpaolo Tower (Figure 4.128), the central theme of which was the design of a building of great verticality in Turin, a city characterised by a predominantly horizontal architectural and urban layout. The project had to respect sustainable development issues and contain greenhouse gas emissions. The competition was won by the project presented by *Renzo Piano Building Workshop*.

In his remarks, architect Renzo Piano observed that skyscrapers are often regarded as rhetorical symbols of power and arrogance. However, he noted that in this project, the objective is to achieve a sense of lightness. He also highlighted that the building would be open to the city, referencing the restaurants and rooftop terrace planned for the summit area.

The presentation of the project prompted a significant response from the city's public opinion, with many expressing concern that the proposed construction would exceed the height of the Mole Antonelliana, the city's monumental symbol. In addition, a number of associations and committees were established, the most notable of which was "No Grat", whose slogan was "Let's not scratch the sky of Turin". The objective of this group was to oppose the construction of the Sanpaolo Tower due to the potential impact on the city's landscape. This resulted in a partial revision of the project, with the height of the tower reduced from 200 meters to 166.26 meters, which is one meter less than the Mole Antonelliana.

Figure 4.128: Sanpaolo Tower

4.5.1 The structural system of the Sanpaolo Tower

The tower is characterised by its slender, linear shape and its particular external structure, comprising metal and crystal. This structure is a kind of 'double skin' in extra-white crystal, which reduces the time taken to switch on the artificial lighting and favours ventilation in the summer months. The skin is designed to 'breathe' thanks to sophisticated mobile slats located on the external layer and Venetian blinds placed on the internal layer. This meets the request to reduce energy consumption and gives the building lightness and luminosity, which is thus less impactful. It is only the façades facing east and west that will be equipped with this double wall.

The tower has multiple entrances and corresponding halls to facilitate access to the tower. As previously stated, the tower includes not only bank offices but also conference centres with rooms for conferences and exhibitions, restaurants, and a public belvedere at the top.

The staircase building, which runs the full height of the structure on the north side, provides an escape route.

The south side is home to the 'winter gardens', which provide a natural and restful environment for visitors on each floor in the form of green spaces. The specific orientation of the façade permitted the installation of approximately 1,600 square meters of photovoltaic cells.

At the pinnacle of the structure, one encounters a bioclimatic greenhouse comprising three levels. The roof is home to a zen garden and a panoramic restaurant, while the lower levels accommodate an exhibition hall and a cafeteria with a gallery.

The implementation of these measures is projected to result in a reduction of the building's energy consumption by over 30%.

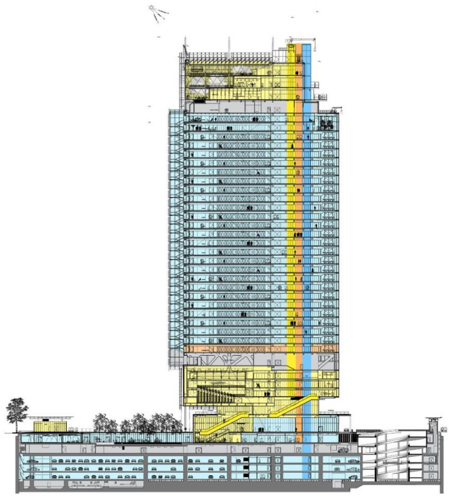

Figure 4.129: Section of the Sanpaolo Tower

The structure comprises 44 vertical storeys, 38 of which are above ground, reaching a height of 166.26 m, and 6 below ground. The subterranean levels accommodate an underground garden, a nursery and a company restaurant.

The foundation of the building is constituted by a slab situated at an approximate elevation of -24 meters above ground level. The primary vertical structure is comprised of reinforced concrete stiffening elements, the so-called *'core'*, which includes the lift cores and the main plant backbones. Additionally, steel elements such as the six mega-columns, each 44 meters in height, situated along the perimeter of the east and west façades, and the supporting structures of beams, pillars, and braces, contribute to the overall stability of the structure. The aforementioned mega-columns are composed of a double steel shell filled on-site with a concrete casting.

Level 6 is occupied for its entire height by the *south and north transfer*. The south transfer is comprised of four orthogonal lattice girders, formed by components with a Π and box section, welded to the mega-columns. Between the first and fifth floors, the auditorium is suspended by a pendant structure.

The north transfer comprises an edge truss beam connected to the reinforced concrete core by two square cantilevers anchored by 12 'Macalloy' bars. Its function is to support the cantilevered offices from the 7th to the 33rd floor and to support, in a hanging configuration, the 3rd, 4th and 5th floors.

The secondary structure located above the south transfer comprises, for each floor, a steel frame that supports a deck formed of 81 inverted pre-stressed reinforced concrete Π tiles.

The upper level of the structure incorporates a bioclimatic greenhouse, comprising a series of perimeter reticular pillars, with a height of approximately 15 meters, positioned in a linear arrangement along the west, south and east façades. The aforementioned pillars serve to support the truss beams, which in turn form a *'shed'* roof system.

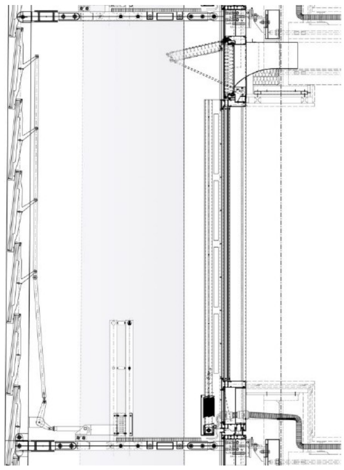

Figure 4.130: Detail of the double-skin façade

Thus, the structural peculiarity of the Sanpaolo Tower consists of the various stiffening elements (shear walls, thin-walled open section shear walls, frames and braced frames) and the presence of the huge trusses that allow the transfer of vertical loads from the upper floors to the external steel columns. The presence of these "transfers" also creates a discontinuity of stiffness between the frames.

4.5.2 Wind action

In accordance with the specifications outlined in Appendix A, the wind forces exerted on the structure were calculated and are presented in Table 4.31.

Floor No.	Storey height (m)	Wind actions		
		$\mathbf{F_x}$ (kN)	$\mathbf{F_y}$ (kN)	$\mathbf{M_z}$ (kNm)
39	6.75	299.60	513.50	9453.76
38	5.03	297.50	510.00	9390.38

Floor No.	Storey height (m)	Wind actions		
		$\mathbf{F_x}$ (kN)	$\mathbf{F_y}$ (kN)	$\mathbf{M_z}$ (kNm)
37	5.10	295.40	506.40	9324.09
36	5.10	293.20	502.70	9256.72
35	5.53	291.00	498.90	9186.45
34	3.89	288.70	495.00	9115.10
33	3.74	286.40	491.00	9040.84
32	3.74	284.00	486.80	8962.60
31	3.74	281.50	482.60	8868.18
30	3.74	279.00	478.30	8806.85
29	3.74	276.40	473.80	8723.54
28	3.74	273.70	469.20	8639.15
27	3.74	270.90	464.40	8550.77
26	3.74	268.00	459.50	8461.30
25	3.74	265.10	454.40	8366.04
24	3.74	262.00	449.10	8268.60
23	3.74	258.80	443.60	8167.18
22	3.74	255.50	438.00	8064.68
21	3.74	252.00	432.00	7954.20
20	3.74	248.40	425.90	7842.64
19	3.74	244.70	419.40	7721.30
18	3.74	240.70	412.70	7599.60
17	3.74	236.60	405.60	7468.11
16	3.74	232.20	398.10	7330.47
15	3.74	227.60	390.20	7184.86
14	3.74	222.70	381.80	7030.20
13	3.74	217.60	372.90	6864.66
12	3.74	212.00	363.40	6690.80
11	3.74	206.00	353.20	6503.90
10	3.74	199.60	342.10	6298.16
9	3.74	192.50	330.00	6076.13
8	3.74	184.70	316.70	5832.60
7	5.46	176.10	301.90	5558.89
6	5.69	166.30	285.10	5249.56
5	3.74	155.00	265.70	4892.05
4	3.74	141.60	242.70	4468.26

Floor No.	Storey height (m)	Wind actions		
		$\mathbf{F_x}$ (kN)	$\mathbf{F_y}$ (kN)	$\mathbf{M_z}$ (kNm)
3	2.64	124.90	214.10	3941.97
2	4.84	102.70	176.00	3240.00
1	7.40	187.30	321.20	5915.31

Table 4.31: Wind pressures

4.5.3 Analytical model

The distribution of the structural elements that guarantee the lateral stability of the work is shown in Figure 4.131.

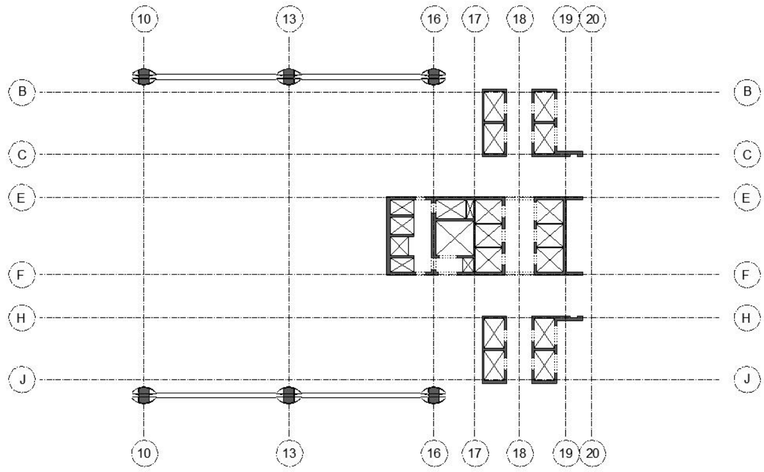

Figure 4.131: Standard floor plan above ground

The left section of the edifice, comprising the six mega-columns and the bracings, was modelled using a series of frames that were orthogonal to one another. The right-hand side of the building, comprising the stairwells and lift shafts, was modelled using shear walls or open shear walls.

It can thus be observed that the structure of the building can be traced back to a coupled frame-shear wall structure. The reinforced concrete core system plays an essential role in reducing displacements and supporting the steel frame system on the lower floors, while the frame system contributes significantly to reducing displacements on the upper floors and to stabilising the concrete part facing north. The lateral stability and reduction of displacements of the building are further ensured by the numerous bracings and transfers.

The reinforced concrete cores were modelled as shear walls or open shear walls, characterised by properties in the short term. It should be noted that shrinkage and creep phenomena were not considered in the analysis, as it refers to wind action (Table 4.32).

Material	ρ [kg/m^3]	**E** [N/mm^2]	ν
Steel	7850	205000	0.3
Concrete short term (C70/85)	2500	40000	0.2
Concrete short term (C45/55)	2500	36000	0.2

Table 4.32: Wind forces

In order to most accurately represent the three-dimensional behaviour of the building, a series of orthogonally interconnected frames, represented by equivalent cantilevers, was employed as a modelling technique.

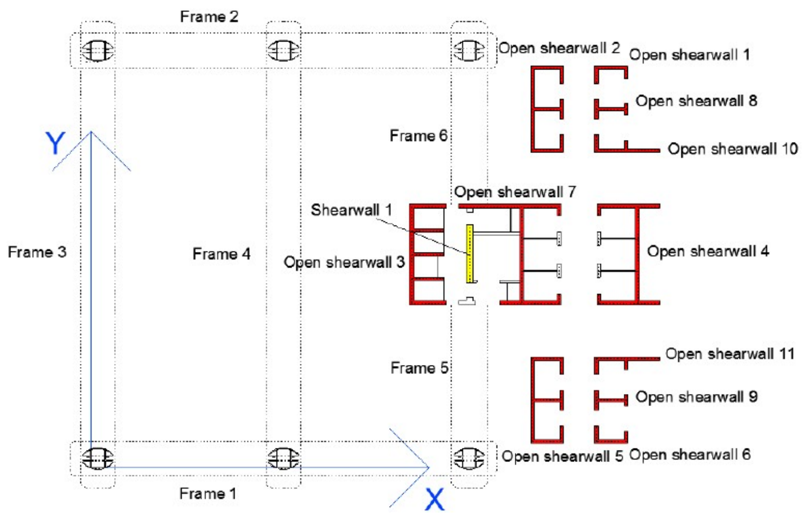

Figure 4.132: Frames and shear walls distribution

The incorporation of bracing systems within the analytical model is a particularly intricate process, as they comprise groups of four floors. It is thus essential to extend the stiffness matrices of the frames in order to accurately take into account the role of the bracing systems in determining the overall stability of the structure.

In order to evaluate the stiffness contribution provided by the diagonals, reference is made to the diagram shown in Figure 4.133.

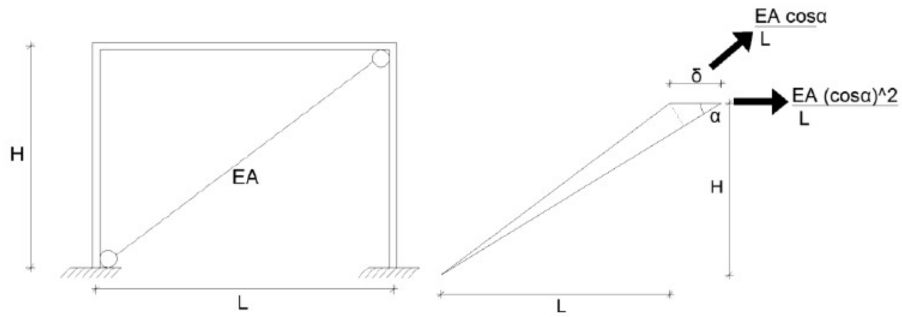

Figure 4.133: Scheme for evaluating the contribution of diagonals of bracing systems

By imposing a displacement δ, the diagonal is deformed by stretching by an amount equal to $\delta cos\alpha$. This force is parallel to the diagonal and can be expressed as follows:

$$F = \frac{EA}{l}\delta cos\alpha$$

In order to evaluate the contribution to the horizontal translation, it is necessary to project this force along the horizontal axis.

$$F = \frac{EA}{l}\delta cos^2\alpha$$

This value should be entered within the stiffness matrices.

In light of the fact that the bracings do not connect two successive planes, it is necessary to study an equivalent frame in which the planes that are not affected by the connection of the bracings are not considered. The frame in question will therefore be characterised by a number of floors equal to 9, rather than the previously stated value of 40.

Two distinct stiffness matrices have been formulated to examine the problem:

- A matrix that considers the contribution of the bracings alone and is constituted by sub-matrices, such as K_{AA}, K_{AB}, and so forth. This matrix has dimensions 9×9.
- A matrix that represents a frame without bracings and is constituted by sub-matrices of size 40×40.

The first matrix is initially constructed, expanded to size 40×40, and then added to the second matrix. The aforementioned relation is then applied to the matrix that has been obtained, resulting in the following:

$$K^* = K_{AA} - K_{AB}K_{BB}^{-1}K_{BA}$$

The sub-matrices of dimension (40×40), which form the reduced stiffness matrix, are obtained.

$$[K^*] = \begin{bmatrix} K_u^* & 0 & 0 \\ 0 & K_v^* & 0 \\ 0 & 0 & K_\vartheta \end{bmatrix}$$

The reduced matrix is evaluated in the global reference system, but through a rotation process it is brought back into the local reference system.

Furthermore, the vectors of forces and displacements must be expanded from the order n to the order N (number of degrees of freedom). This is achieved by defining an expansion matrix [A] of size N×n.

4.5.4 FEM Model

In order to create a model of the tower, the concrete cores were represented using equivalent *beam* elements and *shell* elements. This was done in two different ways: firstly, without including the foundation block, and secondly, by including the foundation block and simulating it using simplified modelling of equivalent elements. Additionally, a foundation model was constructed utilising *shell* elements supported by springs (Figure 4.134).

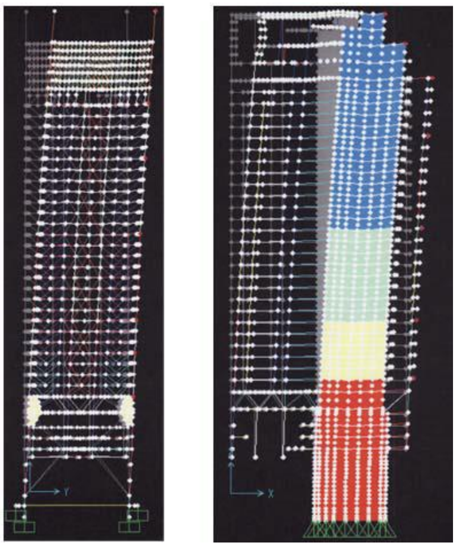

Figure 4.134: FEM model

The model was then subjected to a stress test utilising the wind action forces described in Chapter 4.5.2.

4.5.5 Comparison of the results

The following section presents a comparison between the displacements along the X and Y directions and the rotations, as determined by the algorithmic approach, and the corresponding values reported in the executive project, led by FE simulation [5].

As illustrated in Figures 4.135, 4.136 and 4.137, the analytical method achieves a satisfactory accuracy. It can be seen that the gap in the range is no more than $\pm 0.015\,m$ and the main differences arise next to the level of the huge truss beam, the sections of the structure that exhibit greater irregularity.

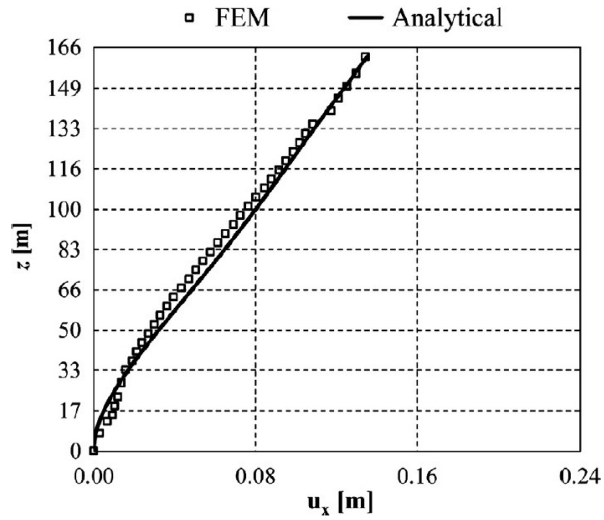

Figure 4.135: Displacements in X-direction

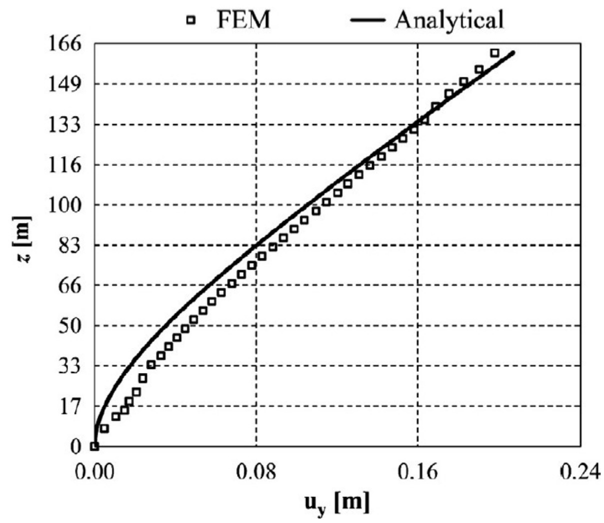

Figure 4.136: Displacements in Y-direction

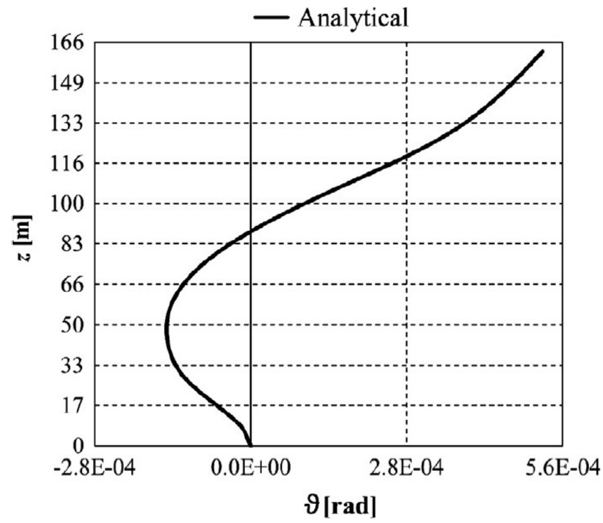

Figure 4.137: Rotation

In Figures 4.138, 4.139 and 4.140 are presented the lateral load distribution of the internal actions between braced frames and shear walls.

An examination of the graphs reveals that the structural discontinuity of the frames in both the principal directions gives rise to elevated interaction forces between the shear walls and the frames. In the X direction, additional high interactions are induced by the presence of highly rigid steel beams.These structural design choices exert a significant influence on the torque distribution.The curves demonstrate the substantial contribution of braced frames in the upper part of the building and the predominance of shear walls in the lower part.

Looking at Figures 4.141 and 4.142, it can be seen that the analytical formulation is also able to evaluate the main internal effects of a generic stiffener. In this way, it is possible to assess which of the stiffeners is the most suitable structural arrangement for the specific loading case.

For the open section shear wall No. 7 in Figure 4.141a) the components of the internal torsional moment are highlighted: the first is related to pure torsion according to De Saint Venant's theory, while the second is related to non-uniform torsion according to Vlasov's theory. It is also possible to see the discontinuities caused by the change in geometry and material of the frames, which particularly affects the non-uniform component. They also modify the evolution of the bimoment (Figure 4.141b).

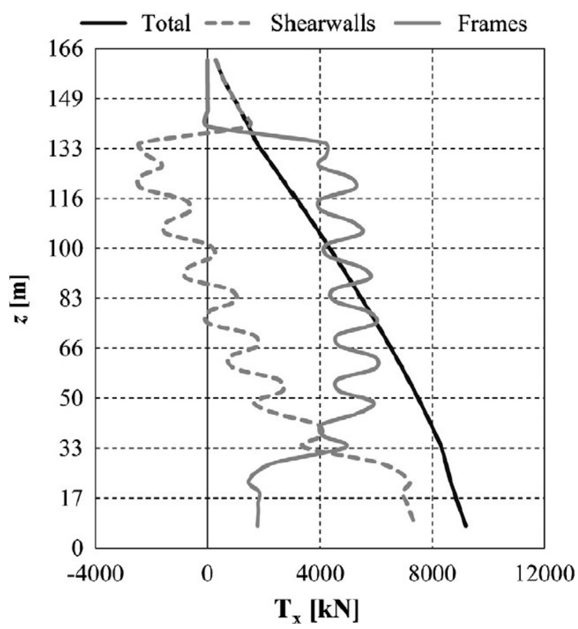

Figure 4.138: Shear in X-direction

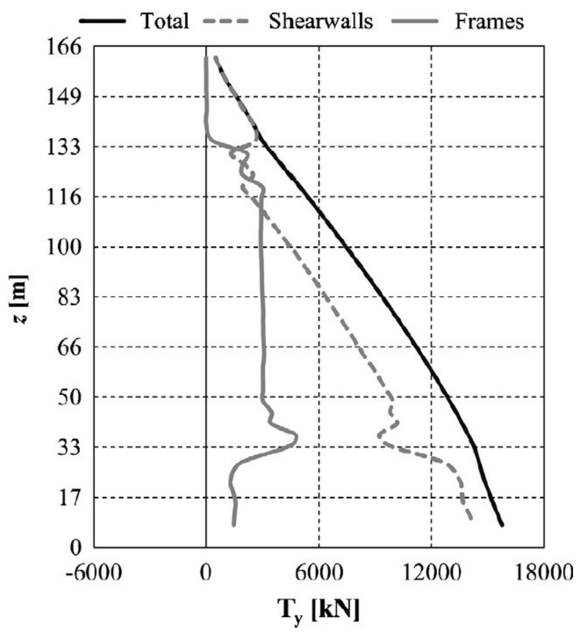

Figure 4.139: Shear in Y-direction

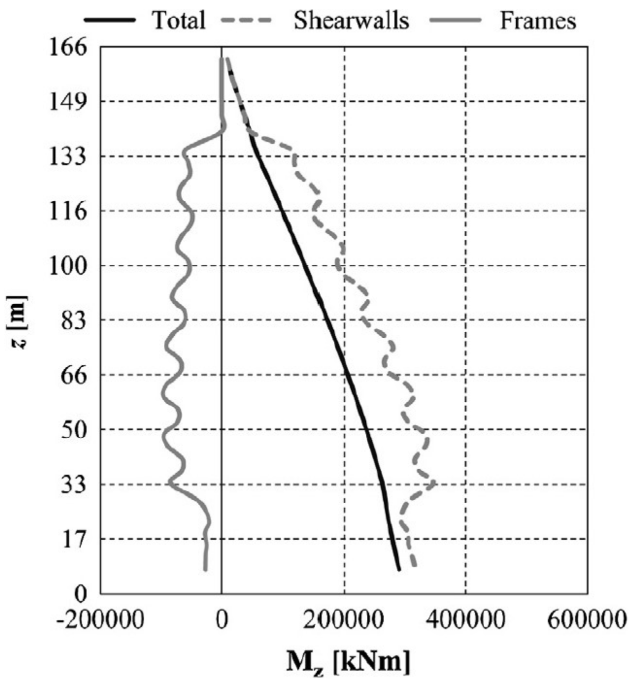

Figure 4.140: Torsional moment

Finally, in Figure 4.142, the same curves are related to the open section shear wall No. 3, showing a more reduced contribution of the non-uniform component of the torsional moment, followed by a lower bimoment action.

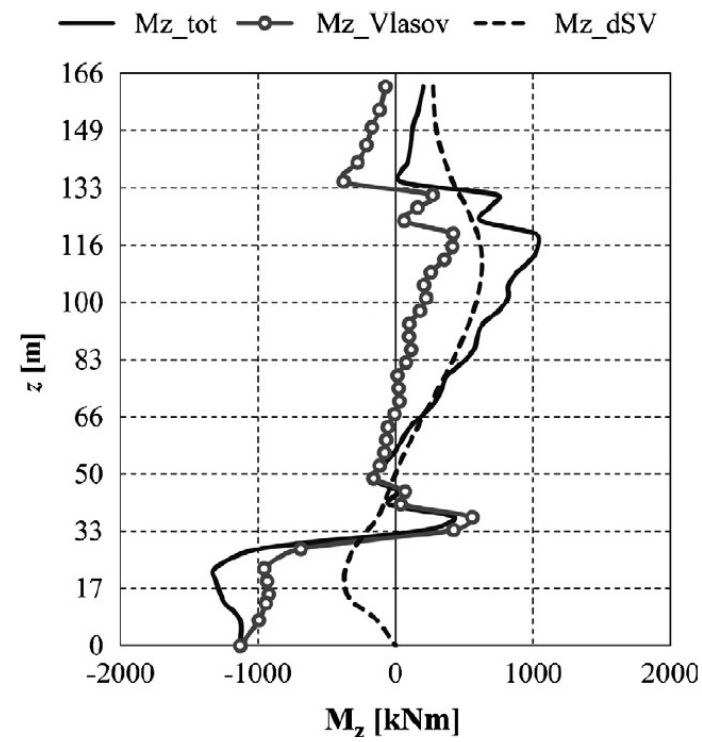

(a)

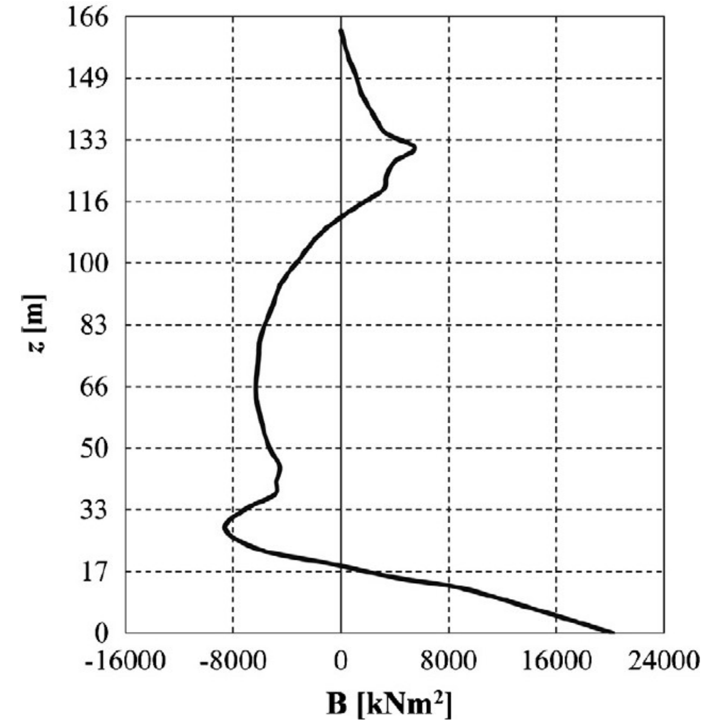

(b)

Figure 4.141: Internal actions in thin-walled open section bracing No.7: torsional moment (a) and bimoment (b)

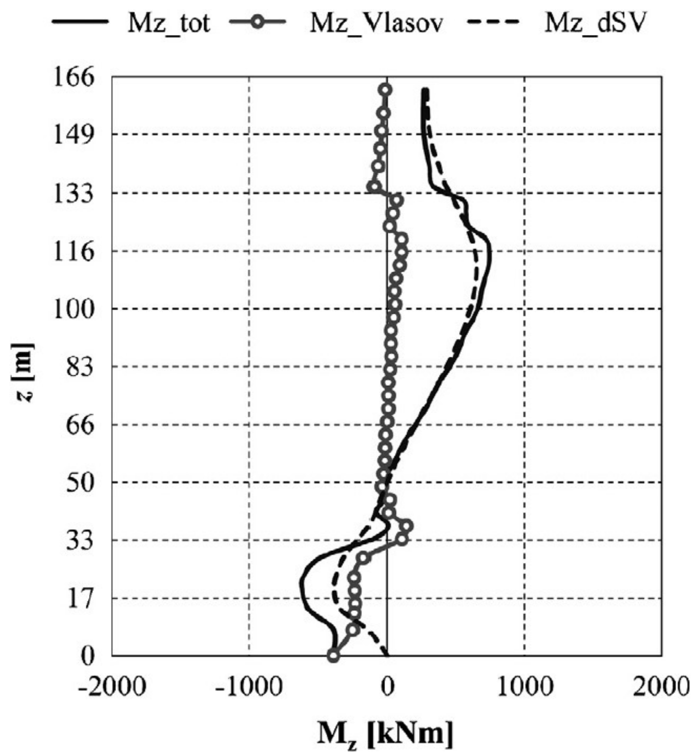

(a)

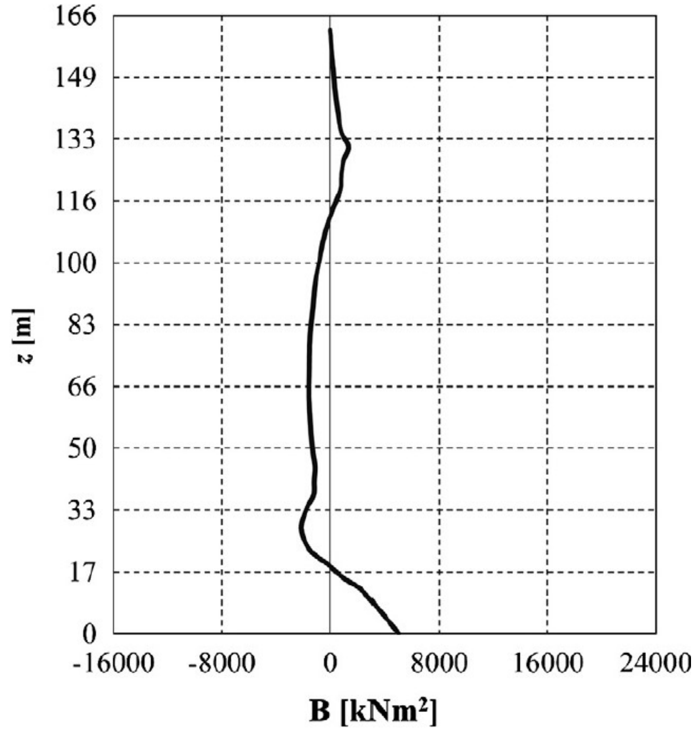

(b)

Figure 4.142: Internal actions in thin-walled open section bracing No.7: torsional moment (a) and bimoment (b)

4.5.6 Equivalent Static Analysis

An equivalent linear static analysis has been carried out to model the inertial forces caused by a design earthquake. It should be noted that this application is of a purely experimental nature, since the structure under consideration does not meet the requirements of the Italian regulations; it would therefore be appropriate to carry out a dynamic analysis. In fact, the NTC18 stipulates that the equivalent static analysis can be carried out if the period of the first mode in the direction under consideration does not exceed the value of $2.5T_C$ or T_D and if the structure is regular in height. In the case of the Sanpaolo Tower, the principal period far exceeds the above condition.

The eigenfrequencies of the structure, in the X and Y directions and for torsion, provided by the designer, Prof. Ing. Ossola, are:

- $F_1 = 0.208$ Hz - North/South (X direction);
- $F_2 = 0.210$ Hz - East/West (Y direction);
- $F_3 = 0.330$ Hz - Torsion.

The value of the equivalent static forces is obtained from the ordinate of the design response spectrum corresponding to the period of the first mode and taking into account the masses present in the structure. The formula to derive the equivalent static force in the i-th plane is as follows:

$$F_i = F_h \cdot \frac{z_i W_i}{\sum_j z_j W_j}$$

$$F_h = S_d(T_1) \cdot \lambda \cdot W/g$$

where:

W_i and W_j are the weights of mass i and mass j, respectively;

z_i and z_j are the heights, with respect to the foundation level, of masses i and j;

$S_d(T_1)$ is the ordinate of the design spectrum at period T_1;

W is the total weight of the construction;

λ is a coefficient equal to 0.85 if the construction has at least three horizons and if $T_1 < 2T_C$, and equal to 1 in all other cases. In the case under consideration it is assumed to be open to 1;

g is the acceleration of gravity.

Following the determination of the design spectrum as shown in Appendix C, the equivalent static forces were derived (Table 4.33).

Floor	**h [m]**	**Mass [t]**	**Weight [kN]**	zW_j **[kNm]**	F_i **[kN]**
L40	166.25	60.00	588	97755	23.62
L39	158.95	250.00	2450	389427.5	94.10
L38	155.55	450.00	4410	685975.5	165.76
L37	150.45	1000.00	9800	1474410	356.28
L36	145.35	1939.00	19002.2	2761969.77	667.42
L35	140.25	1939.24	19004.552	2665388.418	644.08
L34	134.64	1874.76	18372.648	2473693.327	597.76
L33	130.90	1874.76	18372.648	2404979.623	581.15
L32	127.16	1874.76	18372.648	2336265.92	564.55
L31	123.42	1874.76	18372.648	2267552.216	547.94
L30	119.68	1874.76	18372.648	2198838.513	531.34
L29	115.94	1874.76	18372.648	2130124.809	514.74
L28	112.20	1874.76	18372.648	2061411.106	498.13
L27	108.46	1874.76	18372.648	1992697.402	481.53
L26	104.72	1874.76	18372.648	1923983.699	464.92
L25	100.98	1874.76	18372.648	1855269.995	448.32
L24	97.24	1874.76	18372.648	1786556.292	431.71
L23	93.50	1874.76	18372.648	1717842.588	415.11
L22	89.76	1874.76	18372.648	1649128.884	398.51
L21	86.02	1874.76	18372.648	1580415.181	381.90
L20	82.28	1874.76	18372.648	1511701.477	365.30
L19	78.54	1874.76	18372.648	1442987.774	348.69
L18	74.80	1874.76	18372.648	1374274.07	332.09
L17	71.06	1874.76	18372.648	1305560.367	315.48
L16	67.32	1874.76	18372.648	1236846.663	298.88
L15	63.58	1874.76	18372.648	1168132.96	282.27
L14	59.84	1874.76	18372.648	1099419.256	265.67
L13	56.10	1874.76	18372.648	1030705.553	249.07
L12	52.36	1874.76	18372.648	961919.8493	232.46
L11	48.62	1874.76	18372.648	893278.1458	215.86
L10	44.88	1874.76	18372.648	824634.4422	199.25
L9	41.14	1874.76	18372.648	755850.7387	182.65
L8	37.40	1874.76	18372.648	687137.0352	166.04
L7	33.66	468.70	4593.26	154609.1316	37.36

Floor	h [m]	Mass [t]	Weight [kN]	zW_j [kNm]	F_i [kN]
L6	28.05	1406.10	13779.78	386522.829	93.40
L5	22.44	1434.19	14055.062	315395.5913	76.21
L4	18.70	1434.19	14055.062	262829.6594	63.51
L3	14.96	1434.19	14055.062	210263.7275	50.81
L2	12.41	1434.19	14055.062	174423.3194	42.15
L1	7.48	604.90	5928.02	44341.5896	10.71

Table 4.33: equivalent static forces

Introducing the forces thus derived into the calculation algorithm produces diagrams of the displacements in the X and Y directions (Figures 4.143 and 4.144).

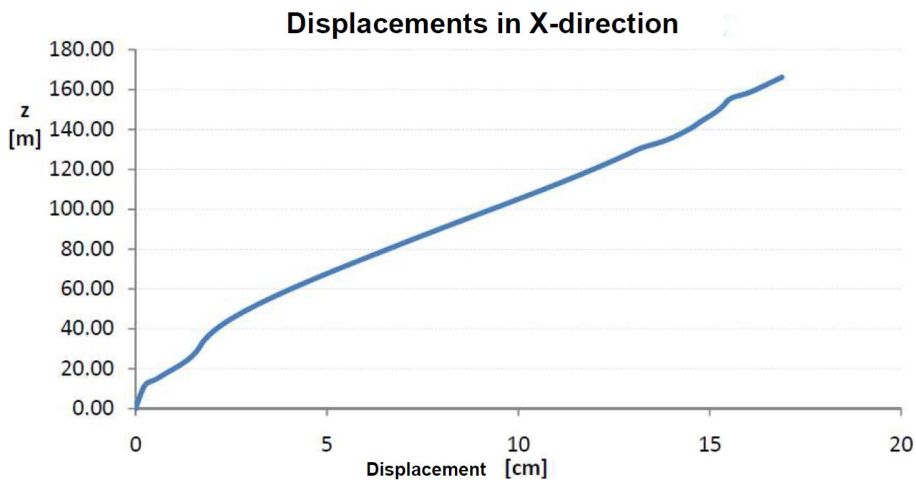

Figure 4.143: Displacements in the X-direction from the equivalent static analysis

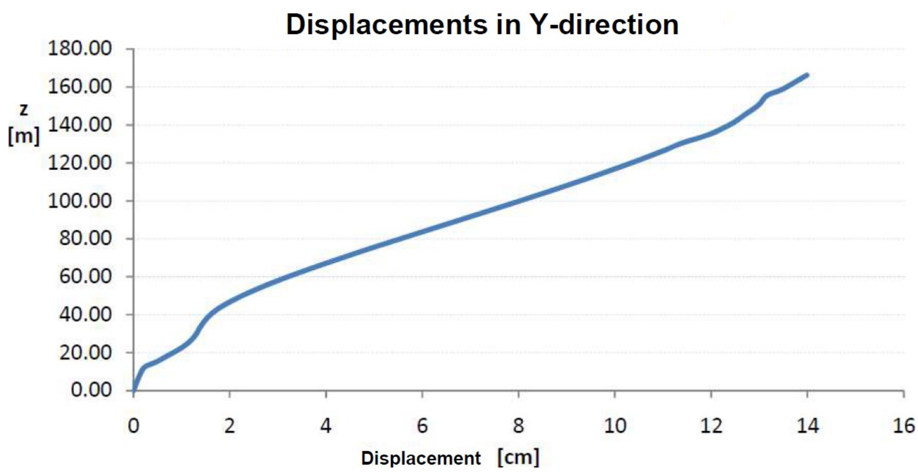

Figure 4.144: Displacements in the Y-direction from the equivalent static analysis

4.6 Piedmont Region Headquarters Tower

In 2006, the Regional Council decided to redevelop the former industrial area of Nizza Millefonti (Avio-Oval area). The task was to redesign the entire area, bounded by Via Nizza to the east, Via Passo Buole to the south, the Turin-Lingotto railway station to the west and the Lingotto trade fair and shopping centre to the north. In 2007, the architect Massimiliano Fuksas presented a project for the construction of a 200-meter tower,thanks to a 2006 variant to the Master Plan and the City of Turin's Urban Planning Division, which limited the obligation not to raise buildings taller than the Mole Antonelliana to the city's historic centre.

In 2022, the Piedmont Region Headquarters Tower (Figure 4.145) will be inaugurated in Piazza Piemonte 1. The tower is part of the so-called "Sede Unica", a complex consisting of an office tower, a service centre and a car park.

The skyscraper, which houses the Region's offices, has 42 floors above ground and reaches a height of 200 m. Above these are technical volumes that bring the total height of the building to 209 m. The service centre is located to the west of the tower.

The Service Centre, located on the west side, is connected to the tower by a suspended glass tunnel. This building houses the Conference Centre of the Piedmont Region and the libraries of the Regional Council and Ires.

The subterranean car park is constructed on three levels, two of which are accessible to the general public and the third is utilized as a regional service car park.

The remaining free area, which is not affected by the headquarters, will be developed with new residential, commercial and service complexes, as well as a large urban park.

Figure 4.145: Piedmont Region Headquarters Tower

4.6.1 The structural system of the Piedmont Region Headquarters Tower

The building has a square floor plan with a side length of 45 m and a total height of 209 m. There are 42 above-ground storeys, with a storey height of 4.27 m, and two basement storeys, with a storey height of 4.30 m. The extrados of the last floor stands at a height of 183.61 m, with the remaining approximately 25 m characterised by a glass roof containing a roof garden.

The eastern side of the building features a series of protrusions, so-called *"satellites"*, that extend 10 meters beyond the main façade. These protrusions, which are not connected to the main structure, have varying inclinations, creating a void from the ground floor up to the 35th floor. This distinctive design element characterizes the elevation of the main façade.

The east façade is comprised of a self-supporting steel frame, connected to the reinforced concrete structure by a limited number of connections and rising up to 180 m. The vertical resistant structure is entirely made of reinforced concrete and consists of four central cores formed by open thin sections and three perimeter frames, with columns arranged with a 6 m pitch, located on the north, south and west sides. The floors are composed of concrete and have a thickness of 34 cm (see Figure 4.148).

The structural solution identified is the result of a study aimed at optimising the

Figure 4.146: Architectural model of the tower

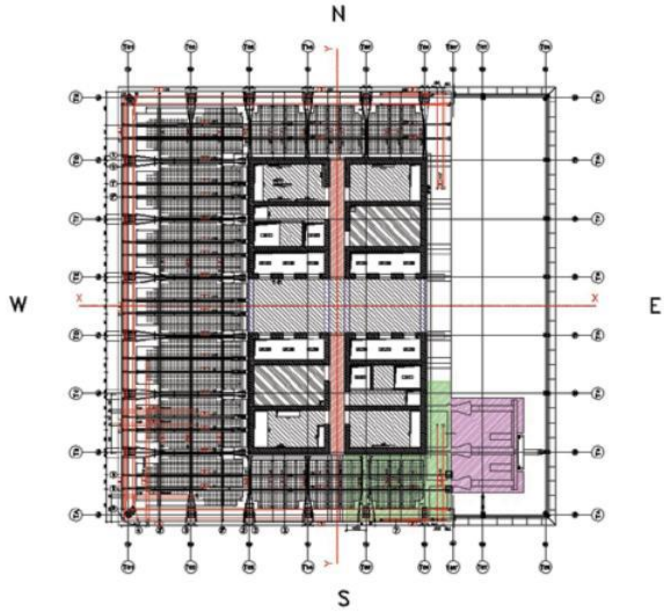

Figure 4.147: Standard floor plan

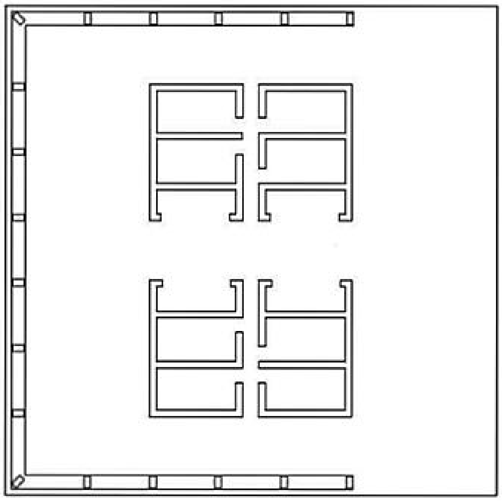

Figure 4.148: Structural system plan

net floor area and ensuring sufficient overall stiffness of the building. The decision to use concrete for the entire structural system ensures uniform behaviour towards deferred effects and rigid connections between the different resistant elements, thereby reducing the deformability of the structure. However, a detailed analysis of the interaction between the concrete structure and the steel east façade was necessary due to rheological effects.

The columns are made of reinforced concrete and have a rectangular cross-section of 110×60 cm for all levels, with the exception of the first six levels, where composite sections were employed (Figure 4.149). Steel profiles were incorporated into these sections to accommodate the elevated stress levels and to mitigate potential structural instability concerns within the hall, which reaches a height of 17 meters. Additionally, the steel profiles serve to restrict the rheological effects of the concrete.

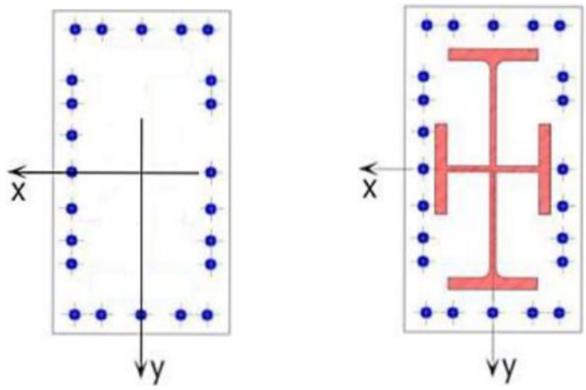

(a) RC column section

(b) Composite column section

Figure 4.149: Columns sections

In order to minimise the occurrence of deferred deformations between columns and cores, concretes with varying characteristic strengths were employed at different elevations.

The floors are constituted of pre-stressed reinforced concrete slab, lightened with PE-HD spheres (*'bubble deck'* type), and have a constant thickness of 34 cm throughout. In contrast, the slab cantilevers are constructed with post-tensioned T-beams and have a reduced thickness of 20 cm.

The slab between the east and west cores is 50 cm thick and consists of solid casting (Figure 4.150). The addition of this thickness results in the creation of stiffeners between the cores, which serve to reduce the overall deformability of the structure in response to horizontal loads.

This stiffening of the portion of the floor between the central cores is the structural peculiarity of the Piedmont Region Headquarters Tower

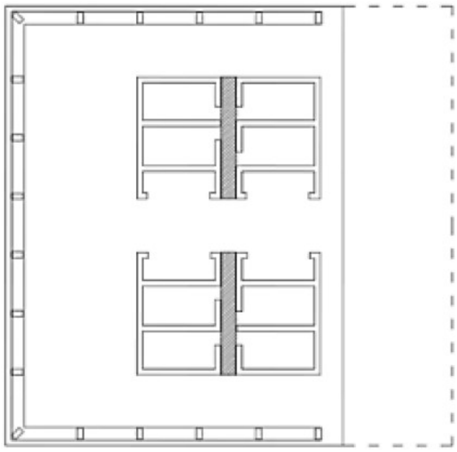

Figure 4.150: Floor thickening in the area between the cores

4.6.2 Analitical model

The model constructed for the analytical analysis is a simplified model in which the thicknesses of the cores and the mechanical properties along the height of the resisting elements were considered to be constant.

A barycentric global reference system was employed for the static analysis (Figure 4.151), whereas a global reference system centred at the geometric centre of gravity of the floors was utilised for the dynamic analysis (Figure 4.152).

The elastic moduli employed are 39 GPa for the columns and 35 GPa for the cores, with a Poisson's coefficient of 0.18. Figure 4.153 illustrates the geometric characteristics of the resisting elements, while Table 4.34 presents the geometric properties of the cores, calculated with respect to the mean line of the sections.

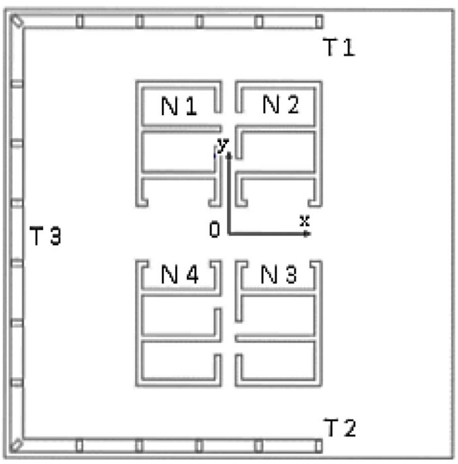

Figure 4.151: Reference system for static analysis

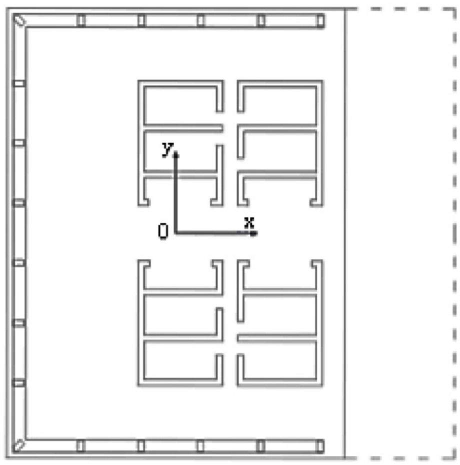

Figure 4.152: Reference system for dynamic analysis

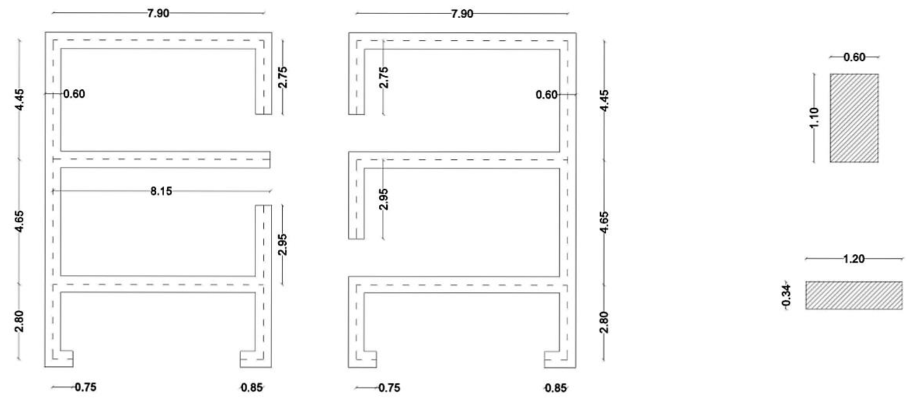

Figure 4.153: Geometrical characteristics of resisting elements

Core	1	2	3	4
Area [m^2]	27.03	27.06	27.03	27.06
Inertia J_{xx} [m^4]	417.31	408.90	417.31	408.90
Inertia J_{yy} [m^4]	277.05	274.38	277.05	274.38
Sectorial inertia $J_{\omega\omega}$ [m^6]	7408.60	4844.69	7408.60	4844.69
De Saint-Venant torsional stiffness [m^4]	3.31	3.28	3.31	3.28
Shear centre coordinates				
x_C [m]	-12.53	12.14	12.53	-12.14
y_C [m]	9.73	11.19	-9.73	-11.19
Barycentre coordinates				
x_0 [m]	-5.26	5.30	5.26	-5.30
y_0 [m]	9.43	9.53	-9.43	-9.53

Table 4.34: Core geometric properties

4.6.3 FEM model

A finite element analysis was conducted using the *"Straus7"* software. In order to model the frames, *beam*, elements were employed, whereas *shell* elements were utilised for the cores. Furthermore, *rigid connection* elements were incorporated into the XY plane to emulate the rigid in-plane behaviour. This resulted in the automatic generation of a master node for each plane, to which the in-plane forces were applied (Figure 4.154).

For the dynamic analysis, a second node was introduced for each floor, constrained by rigid connections, at the centre of gravity of the floor, and in which the entire floor mass was concentrated.

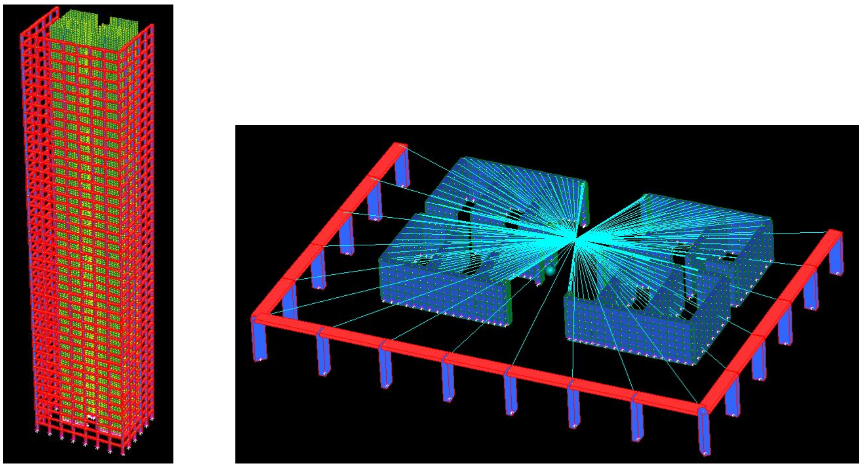

Figure 4.154: FEM model

Additionally, for the dynamic analysis, only the masses of the structural elements of the floor were considered, which were determined by considering each floor homogenous and with a specific weight of 18.75 kN/m^3. This value corresponds to a concrete with a specific weight of 25 kN/m3, lightened by 25%.

4.6.4 Wind action

In accordance with the methodology delineated in Appendix A, the forces exerted by the wind on the building facades were calculated. Two distinct load combinations were considered: one to maximize bending and one to maximize torsion.

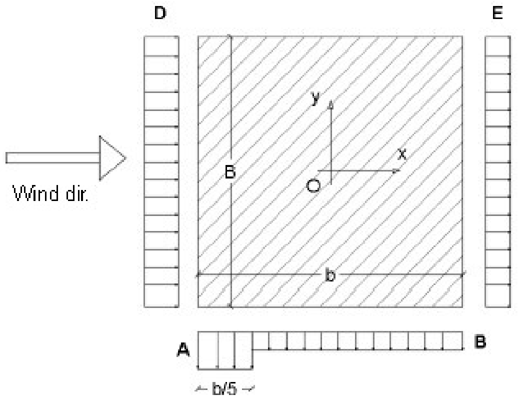

Figure 4.155: Combination 1

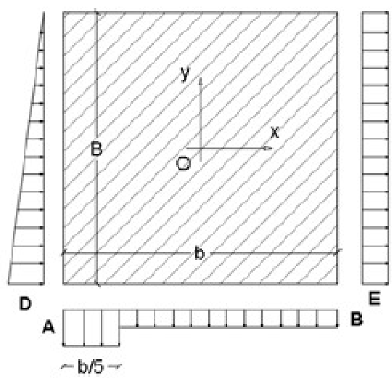

Figure 4.156: Combination 2

Table 4.35 illustrates the forces that maximize the bending (referred to as 'Combination 1'), while Table 4.36 depicts the forces that maximize the torsion (referred to as 'Combination 2').

COMBINATION 1									
Fl	**Floor height**	**F_x**	**F_y**	**M_z**	**Fl**	**Floor height**	**F_x**	**F_y**	**M_z**
[n°]	[m]	[kN]	[kN]	[kNm]	[n°]	[m]	[kN]	[kN]	[kNm]
44	22.14	2867.56	1289.76	186795.66	22	4.27	453.31	265.94	10215.41
43	4.46	572.87	257.66	37317.30	21	4.27	447.31	262.77	10093.74
42	4.27	548.46	321.77	12359.77	20	4.27	442.26	259.46	9966.53
41	4.27	548.46	321.77	12359.77	19	4.27	436.35	255.99	9833.15
40	4.27	548.46	321.77	12359.77	18	4.27	430.13	252.34	9693.00
39	4.27	548.46	321.77	12359.77	17	4.27	423.57	248.50	9545.29
38	4.27	518.03	303.91	11673.88	16	4.27	416.64	244.43	9389.12
37	4.27	514.81	302.02	11061.38	15	4.27	409.29	240.12	9223.38
36	4.27	511.51	300.09	11527.04	14	4.27	401.45	235.52	9046.76
35	4.27	508.13	298.10	11450.77	13	4.27	393.06	230.59	8857.62
34	4.27	504.65	296.06	11372.45	12	4.27	384.02	225.29	8655.94
33	4.27	501.08	293.97	11291.96	11	4.27	379.60	222.70	8554.37
32	4.27	497.41	291.81	11209.19	10	4.27	379.60	222.70	8554.37
31	4.27	493.63	289.59	11123.97	9	4.27	379.60	222.70	8554.37
30	4.27	489.73	287.31	11036.17	8	4.27	379.60	222.70	8554.37
29	4.27	485.71	284.95	10945.61	7	4.27	379.60	222.70	8554.37
28	4.27	481.56	282.52	10852.09	6	4.27	379.60	222.70	8554.37

Fl	**Floor height**	$\mathbf{F_x}$	$\mathbf{F_y}$	$\mathbf{M_z}$	**Fl**	**Floor height**	$\mathbf{F_x}$	$\mathbf{F_y}$	$\mathbf{M_z}$
[n°]	[m]	[kN]	[kN]	[kNm]	[n°]	[m]	[kN]	[kN]	[kNm]
27	4.27	477.27	280.00	10755.42	5	4.27	379.60	222.70	8554.37
26	4.27	472.83	277.39	10655.35	4	4.27	379.60	222.70	8554.37
25	4.27	468.23	274.69	10511.62	3	4.27	379.60	222.70	8554.37
24	4.27	463.45	271.89	10443.95	2	4.27	379.60	222.70	8554.37
23	4.27	458.48	268.98	10332.01	1	2.14	189.80	111.35	4277.19

Table 4.35: Wind actions for 'Combination 1'

COMBINATION 2									
Fl	**Floor height**	$\mathbf{F_x}$	$\mathbf{F_y}$	$\mathbf{M_z}$	**Fl**	**Floor height**	$\mathbf{F_x}$	$\mathbf{F_y}$	$\mathbf{M_z}$
[n°]	[m]	[kN]	[kN]	[kNm]	[n°]	[m]	[kN]	[kN]	[kNm]
44	22.14	2084.98	1289.76	320277.05	22	4.27	332.43	265.94	31497.53
43	4.46	420.10	257.66	64212.58	21	4.27	328.47	262.77	31122.38
42	4.27	402.21	321.77	38109.28	20	4.27	324.33	259.46	30730.07
41	4.27	402.21	321.77	38109.28	19	4.27	319.99	255.99	30318.86
40	4.27	402.21	321.77	38109.28	18	4.27	315.43	252.34	29886.74
39	4.27	402.21	321.77	38109.28	17	4.27	310.62	248.50	29431.32
38	4.27	379.89	303.91	35994.47	16	4.27	305.54	244.43	28949.78
37	4.27	377.53	302.02	35770.92	15	4.27	300.14	240.12	28438.76
36	4.27	375.11	300.09	35541.71	14	4.27	294.40	235.52	27894.18
35	4.27	372.63	298.10	35306.53	13	4.27	288.24	230.59	27311.00
34	4.27	370.08	296.06	35065.04	12	4.27	281.61	225.29	26682.97
33	4.27	367.46	293.97	34816.89	11	4.27	278.37	222.70	26375.98
32	4.27	364.77	291.81	34561.66	10	4.27	278.37	222.70	26375.98
31	4.27	361.99	289.59	34298.92	9	4.27	278.37	222.70	26375.98
30	4.27	359.14	287.31	34028.19	8	4.27	278.37	222.70	26375.98
29	4.27	356.19	284.95	33748.95	7	4.27	278.37	222.70	26375.98
28	4.27	353.15	282.52	33460.62	6	4.27	278.37	222.70	26375.98
27	4.27	350.00	280.00	33162.53	5	4.27	278.37	222.70	26375.98
26	4.27	346.74	277.39	32853.99	4	4.27	278.37	222.70	26375.98
25	4.27	343.37	274.69	32534.18	3	4.27	278.37	222.70	26375.98
24	4.27	339.86	271.89	32202.19	2	4.27	278.37	222.70	26375.98

Fl	Floor height	F_x	F_y	M_z	Fl	Floor height	F_x	F_y	M_z
[n°]	[m]	[kN]	[kN]	[kNm]	[n°]	[m]	[kN]	[kN]	[kNm]
23	4.27	336.22	268.98	31857.03	1	2.14	139.19	111.35	13187.99

Table 4.36: Wind actions for 'Combination 2'

It is observed that the upper floor has a height of influence of approximately 22 meters, given that the upstand height of 20 meters has been accounted for.

4.6.5 Comparison of results between analytical model and numerical model

The following section presents a comparative analysis of the results obtained from the static analysis conducted with the analytical and numerical models. The comparison was based on the analysis of displacements, stresses and strains on the vertical resistant elements. Furthermore, the displacements obtained through the algorithm were compared with the real displacements provided by the designers, derived from the finite element model used for the design of the structure.

Finally, the dynamic analysis carried out by means of the algorithm determined the trend of the frequencies of the structure as a function of the relative vibration modes. A comparison was also made with the frequencies of the simplified numerical model and those relative to the model implemented for the design of the building.

Static analysis - Combination 1

- **Displacements and stresses**

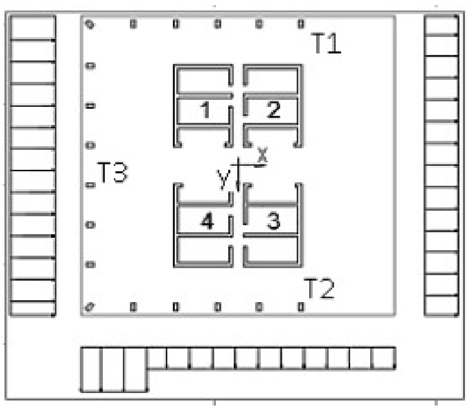

Figure 4.157: Combination 1

Figure 4.158 illustrates the comparison of the displacements in the X- and Y-directions, as determined by the analytical and FEM models.

It can be observed that the algorithm produces a congruent trend with the results of the numerical model, with a maximum deviation of 4% and 7% respectively for the translations along the X and Y axes.

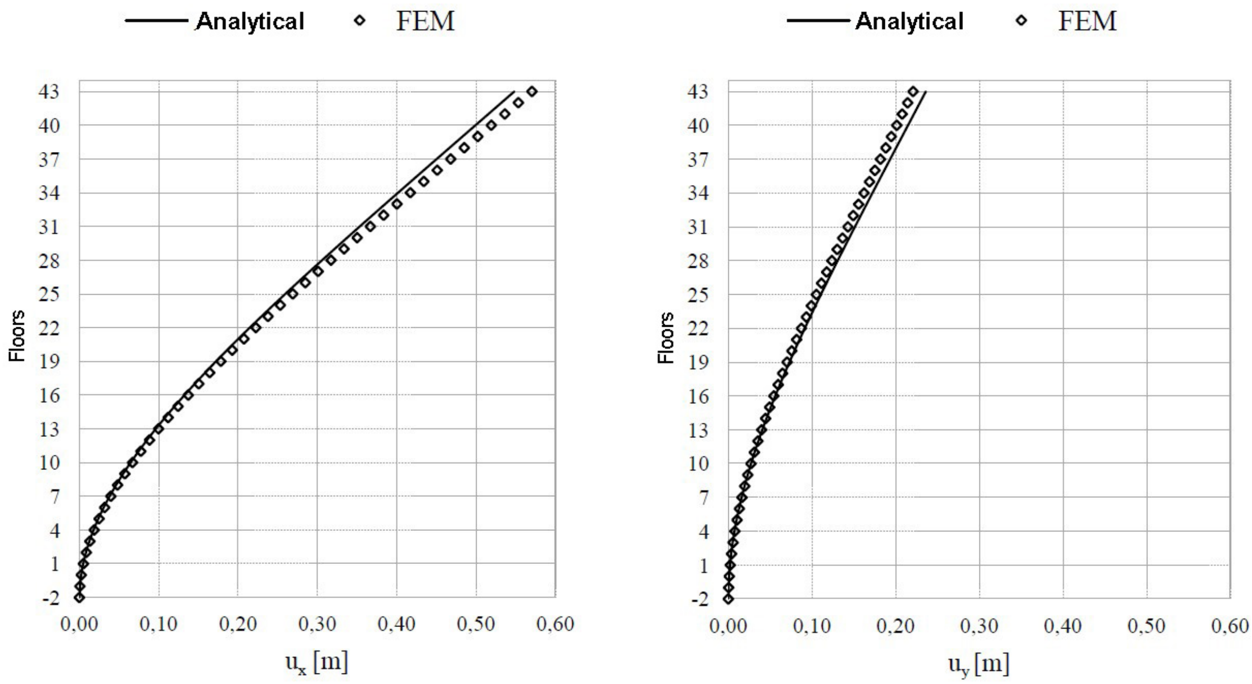

Figure 4.158: Displacements in X- and Y-direction

Figure 4.159 shows the rotations.

Figure 4.160 illustrates the bi-momentum trend. Given that this function is proportional to the rotation, which is equal for each point in the plane, the bi-moment arising in cores 1 and 3 and cores 2 and 4 is identical, as these have the same sectoral stiffness.

An examination of the shear behaviour between the various stiffening systems (Figure 4.161 and 4.162) reveals that it is the core system that absorbs the horizontal forces, as evidenced by the fact that the sum of the four shears acting on each core is nearly equal to the total shear acting.

Furthermore, it can be observed that the frame system exhibits a greater rate of shear absorption as the height increases, until the sign is inverted at the top of the cantilever. This phenomenon occurs when the frame stiffness is sufficiently high.

In the X direction, the cantilevers exhibit reduced flexural stiffness and are supported by two resistant frames. In contrast, in the Y direction, the cantilevers display enhanced flexural stiffness and are supported by a single resistant frame.

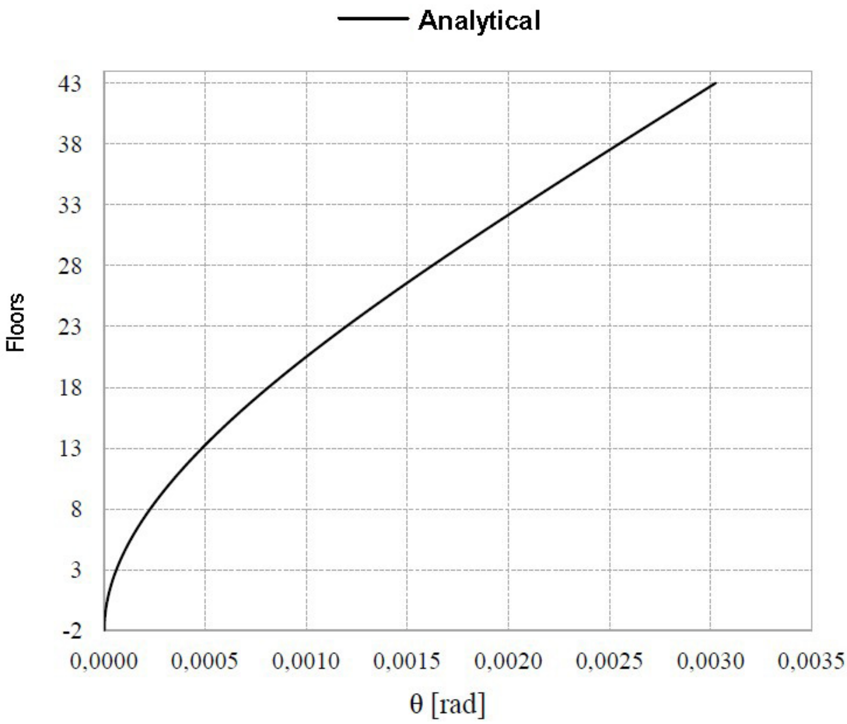

Figure 4.159: Rotations in X- and Y-direction

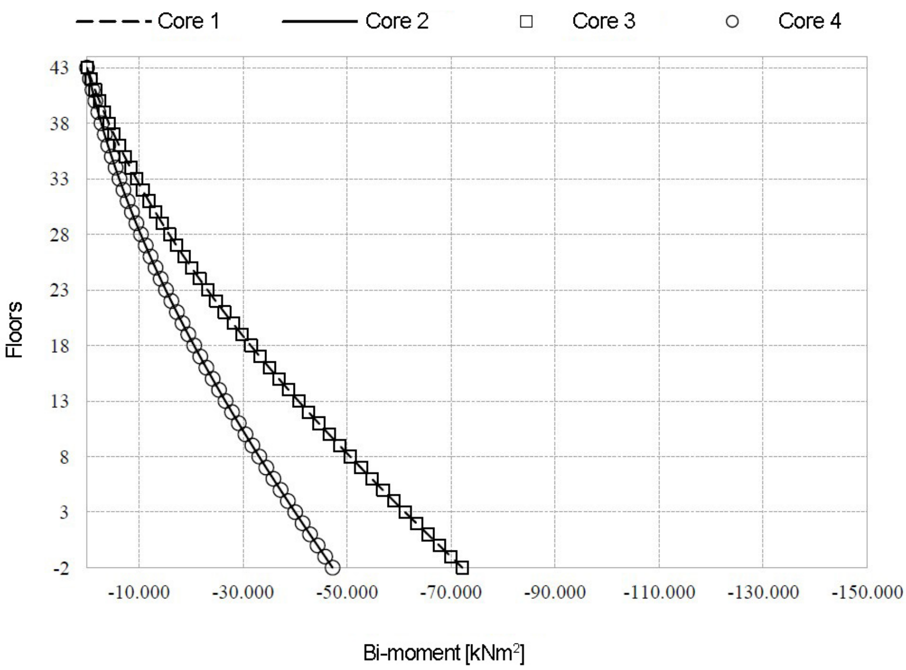

Figure 4.160: Bi-moment

Consequently, in the X direction, the incidence of the frames is more pronounced than in the Y direction, leading to shear reversal on the bracing system. In the Y direction, the frame is practically negligible.

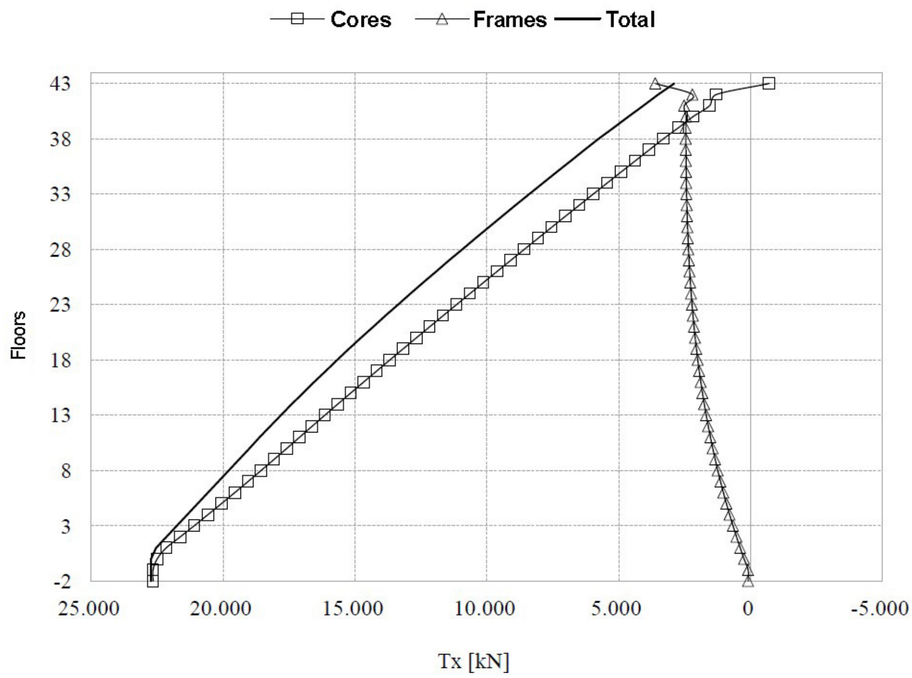

Figure 4.161: Shear T_x on stiffening systems

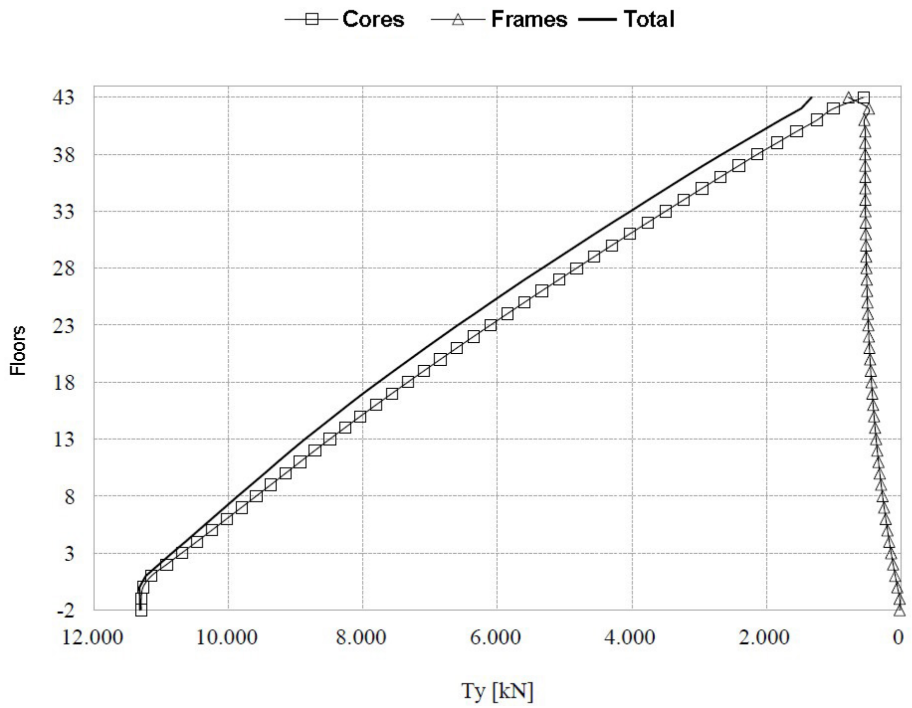

Figure 4.162: Shear T_y on stiffening systems

In order to perform an analysis of individual resisting elements and thereby determine their tensional state, it is essential to understand the distribution of external forces in terms of shear, bending moments and acting torsional moments.

From an examination of the shear graphs (Figure 4.163 and 4.164), it is possible

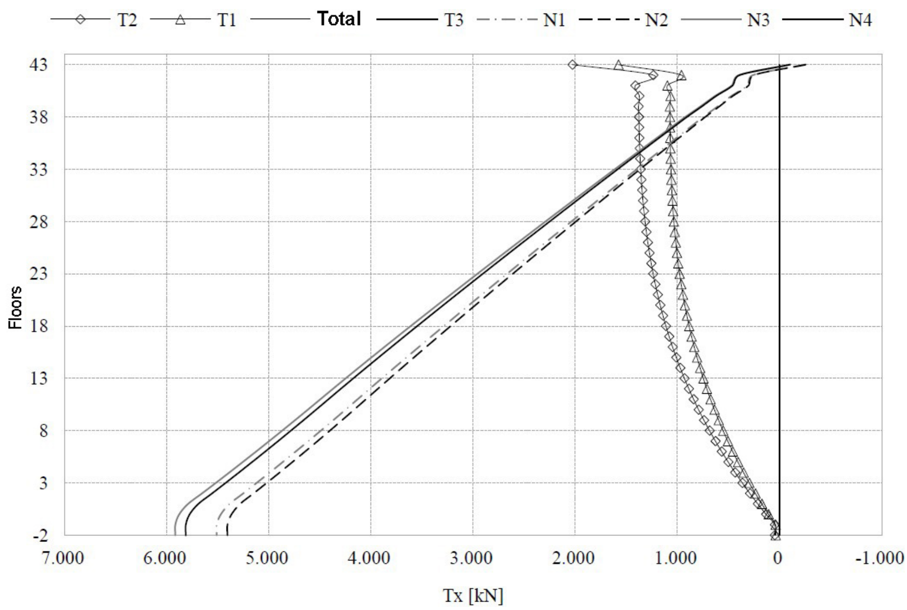

Figure 4.163: Shear T_x on individual elements

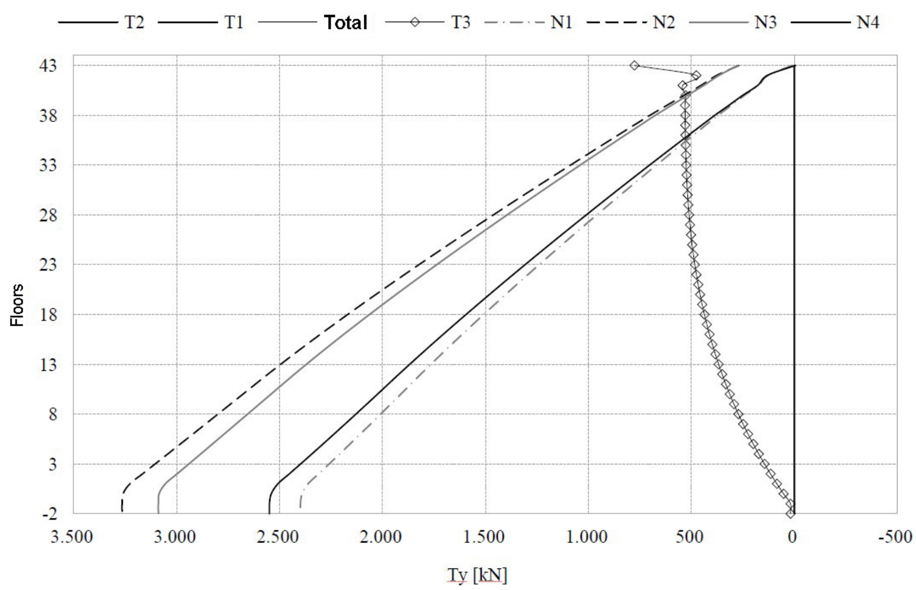

Figure 4.164: Shear T_y on individual elements

to identify the presence of torque by considering the difference between the shear trends in the X direction, both between the two resisting frames and between the cores with the same shear strength. The shears in the Y-direction demonstrate a more pronounced disparity between the cores, as the external horizontal force in that direction is comparatively diminished, thereby precipitating a heightened incidence of torque. This is due to the fact that the distance between the cores is smaller, which results in a smaller arm of the resisting torque and therefore higher shear forces.

The presence of shear stress implies the presence of bending moment. Figure 4.165 and 4.166 show the bending moments on each core for the X and Y directions, respectively.

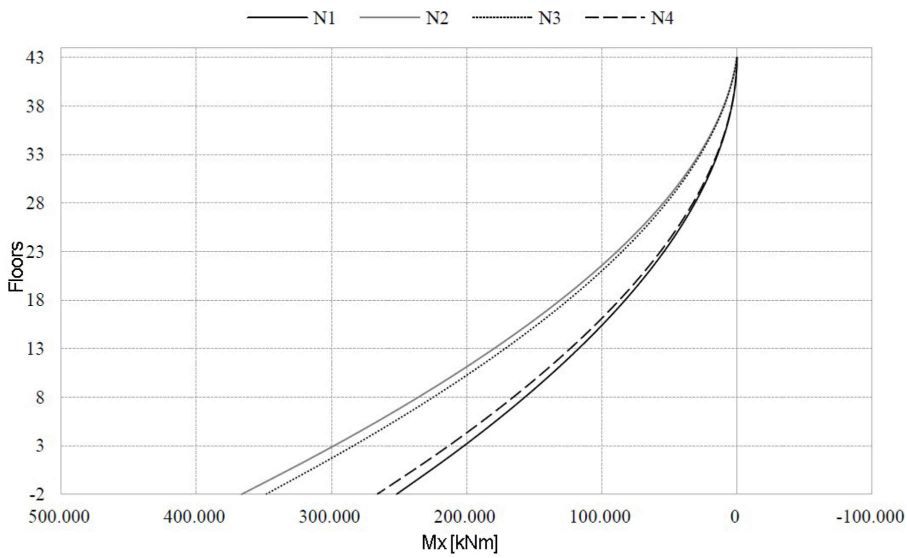

Figure 4.165: Bending moment M_x on the cores

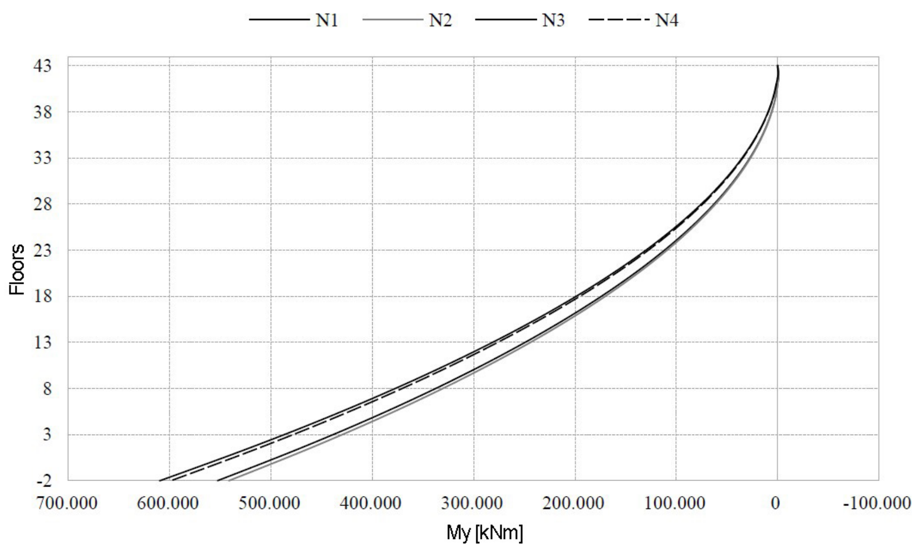

Figure 4.166: Bending moment M_y on the cores

The graphs in Figure 4.167 and 4.168 illustrate the contribution of primary torsion, linked to the De Saint-Venant theory, and the contribution of secondary torsion, linked to the Timoshenko-Vlasov theory.

It has been observed that the maximum value of the secondary torsion varies between approximately 30 and 50% of the maximum value of the torsion due to the primary torsion.

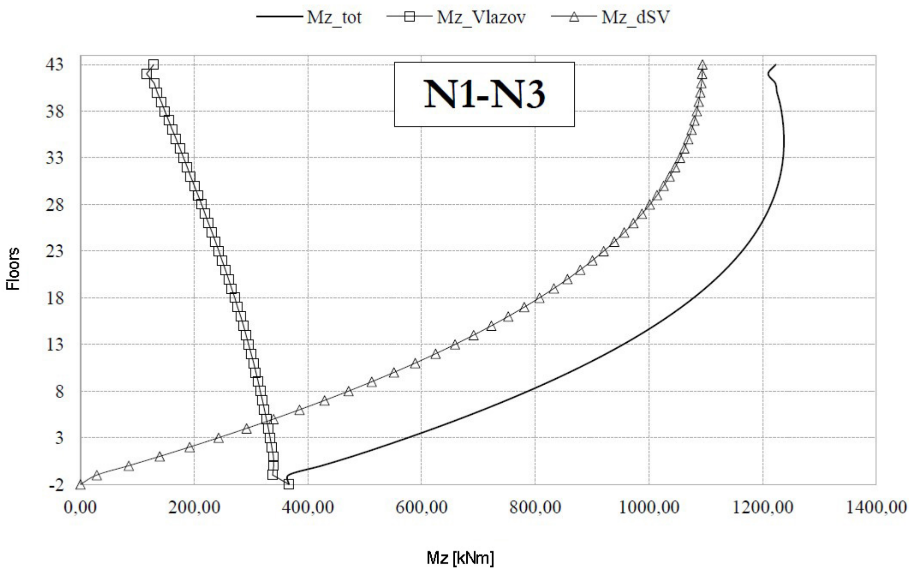

Figure 4.167: Torsional moment M_z on the cores N1 and N3

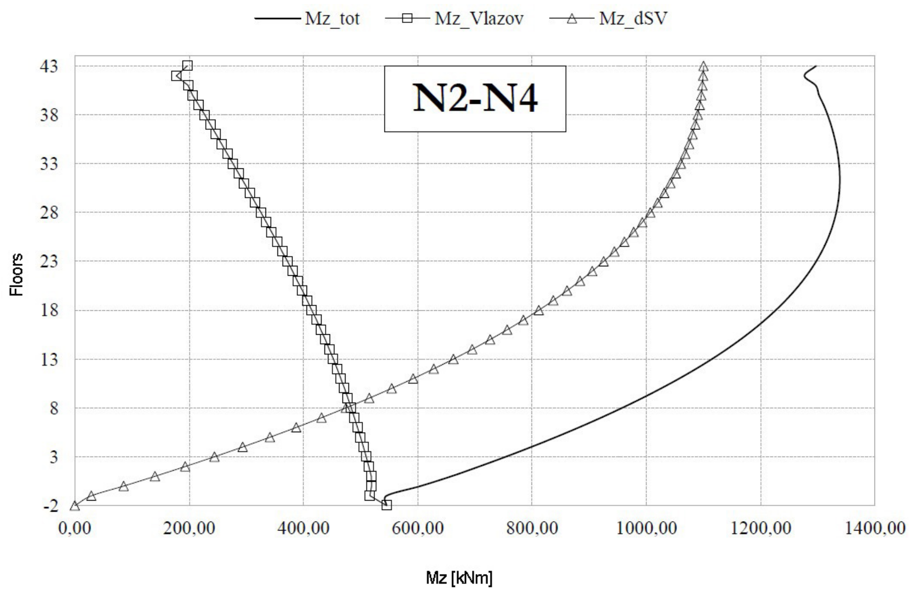

Figure 4.168: Torsional moment M_z on the cores N2 and N4

- **Stress analysis**

A comparison of the longitudinal stresses at the base of the cores due to bending moments and bi-momentum is shown below.

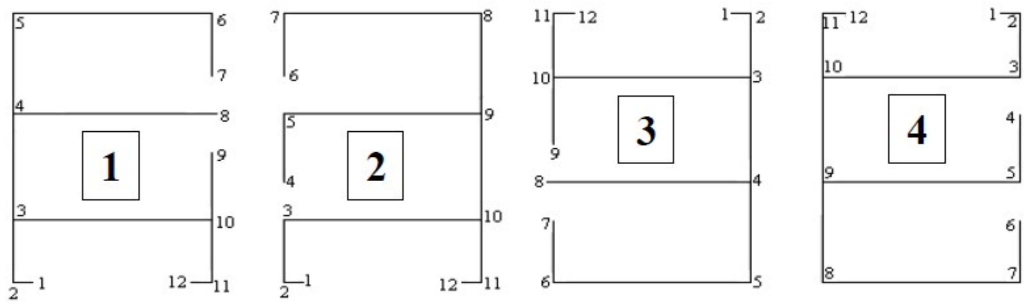

Figure 4.169: Core element numbering

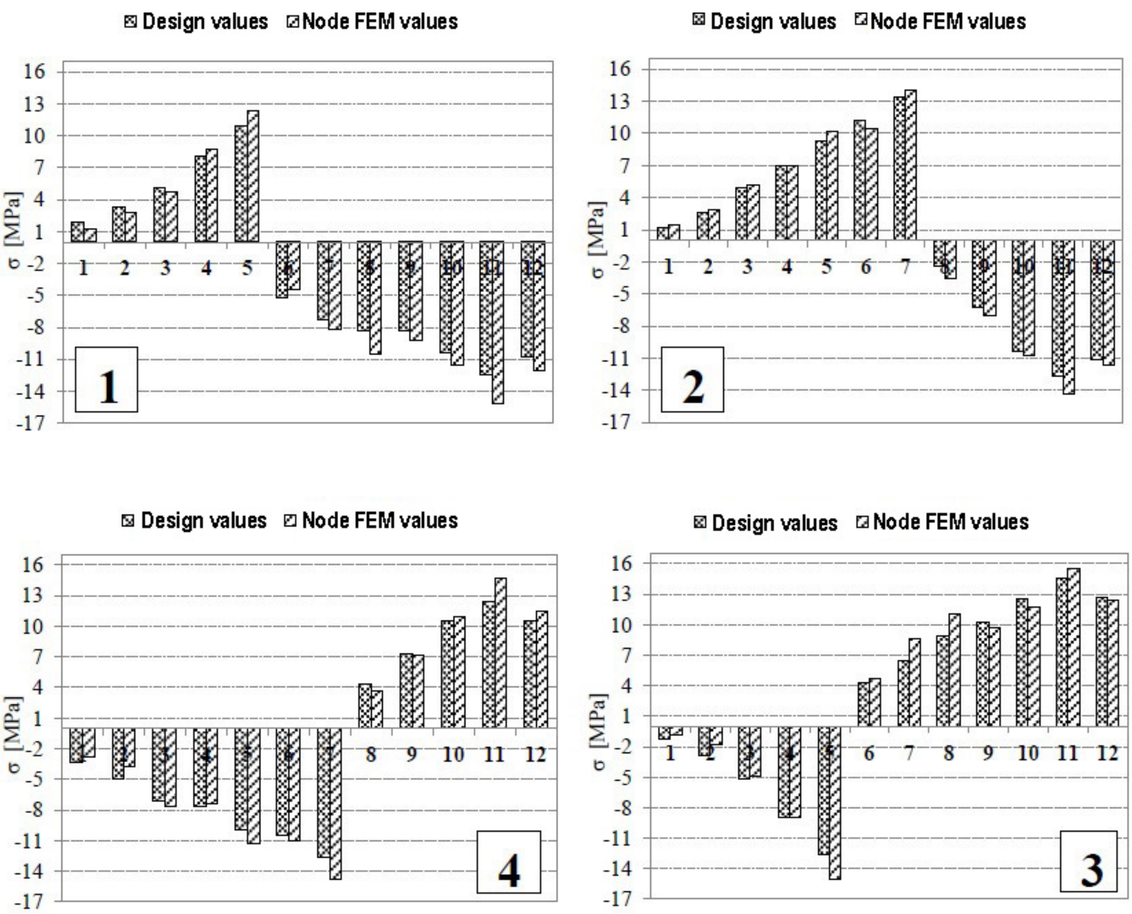

Figure 4.170: Tension comparison in cores

Figure 4.170 demonstrates a strong correlation between the stresses calculated by the algorithm and those determined by the finite element method (FEM). The discrepancy is approximately 15 per cent, which is deemed to be largely acceptable in light of the underlying assumptions of the analytical calculation, namely the planarity of the sections after deformation and the consequent neglect of shear lag.

Figure 4.171 shows the comparisons between the stresses induced by bi-moment and bending moments.

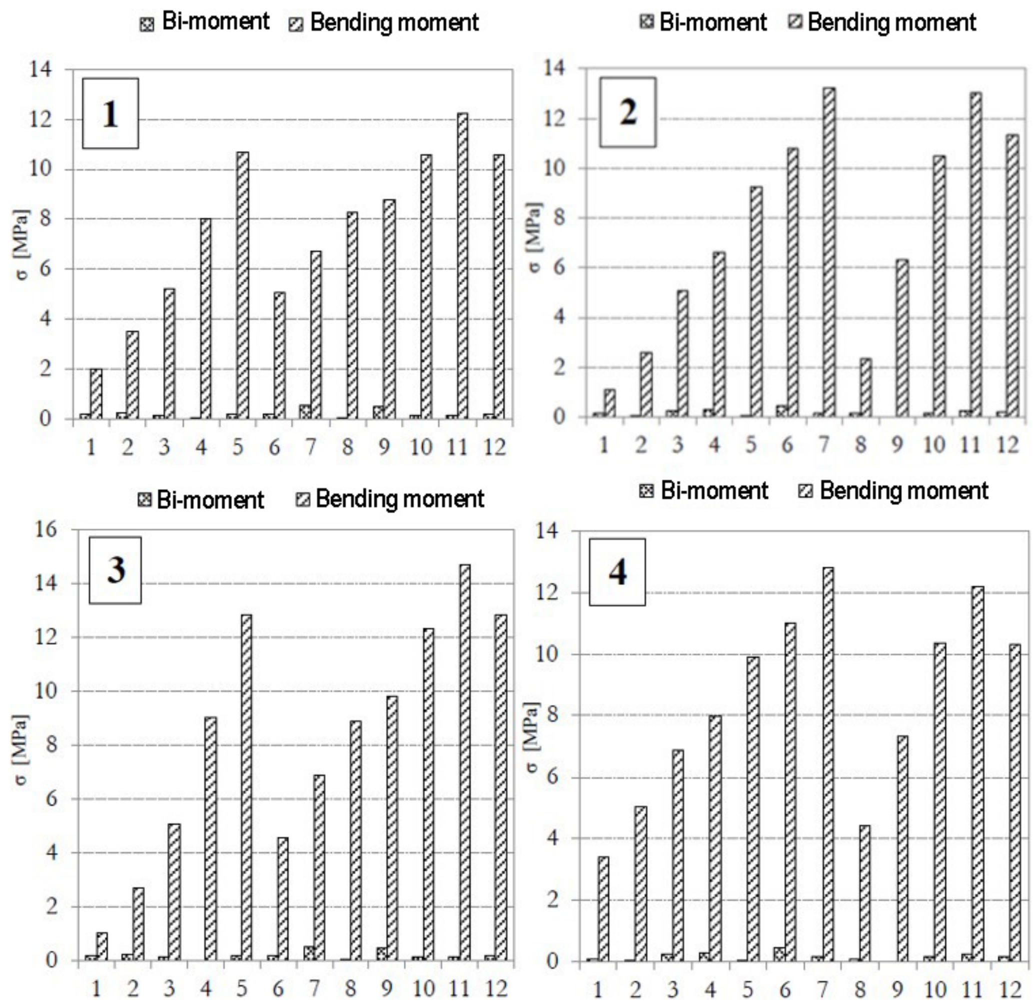

Figure 4.171: Comparison of bi-moment and bending stresses

It is evident that the bi-momentum stresses have a negligible influence on the structure under consideration for this load combination. This was to be expected, since the load combination considered results in a predominantly flexural regime of the structure, with torsional stresses being insignificant for the structural system under consideration.

Static analysis - Combination 2

- Displacements and stresses

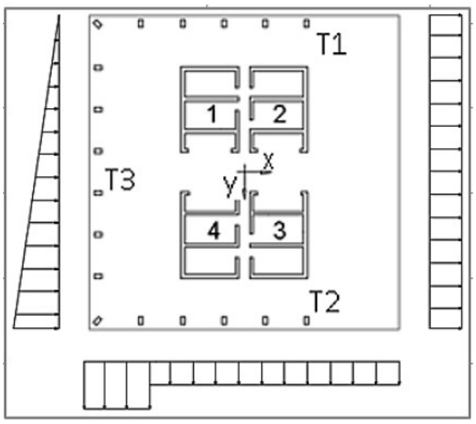

Figure 4.172: Combination 2

The load combination under consideration leads to a decrease in the horizontal forces in the X-direction, but at the same time increases the torque acting on the structure.

A comparison of the displacements in the X- and Y-directions determined by the analytical model and the FEM model (Figra 4.173) reveals that the algorithm produces a trend that is consistent with the results of the numerical model. However, there are minor discrepancies, with deviations of 3% for translations along the X-axis and -6.5% for those along the Y-axis.

An increase in the torsional moment does not affect the distribution of rotations with height; rather, it merely amplifies their magnitude. As illustrated in 4.174, the trajectory of rotations exhibits a similarity to that of Combination 1, yet the values are amplified. Consequently, the values of the bi-momentum will also increase, yet its trend will remain unaltered (Figure 4.175).

The structural functionality remains unaltered in response to varying in external loads. As evidenced by the patterns observed in the data (Figure 4.176 and 4.177), it is evident that the cores continue to bear the largest proportion of the horizontal loads.

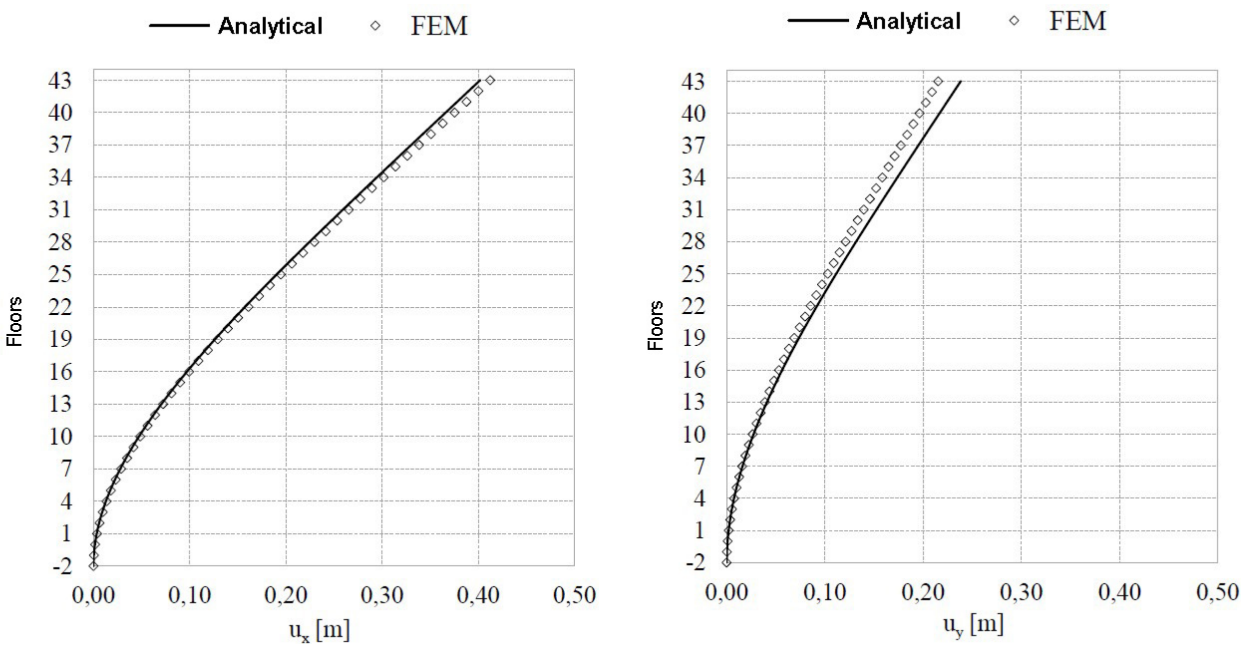

Figure 4.173: Displacements in X- and Y-direction

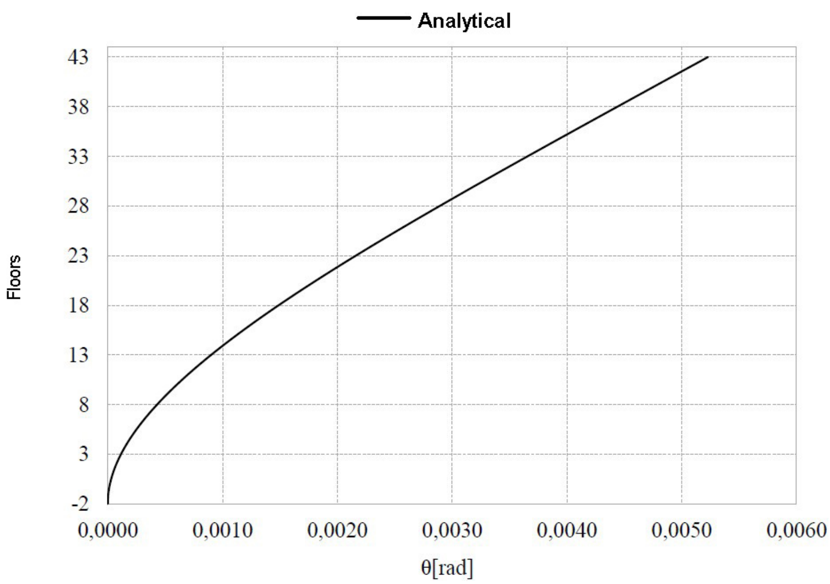

Figure 4.174: Rotations in X- and Y-direction

A further analysis of the individual resisting elements is required in order to determine their tensional state. This analysis reveals a significant difference in behaviour between the two pairs of cores in the case of the shears (Figure 4.178 and 4.179). This is due to the fact that the torque is greater, resulting in a greater value for the balancing shear couple. When this is added to the shear due to the external horizontal forces, it causes a greater total shear difference between the two core systems.

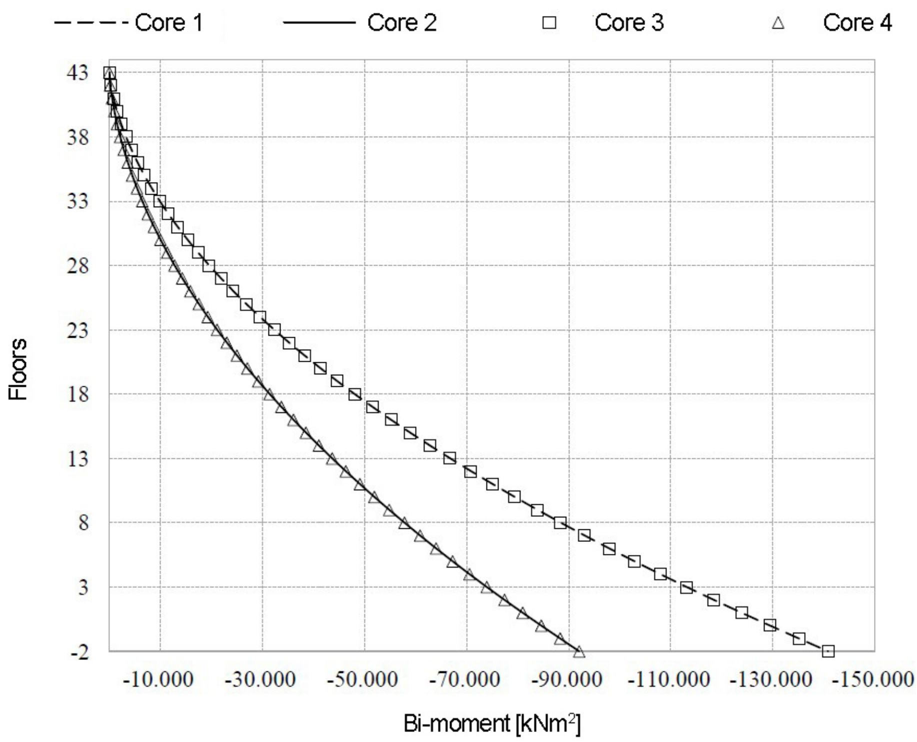

Figure 4.175: Bi-moment

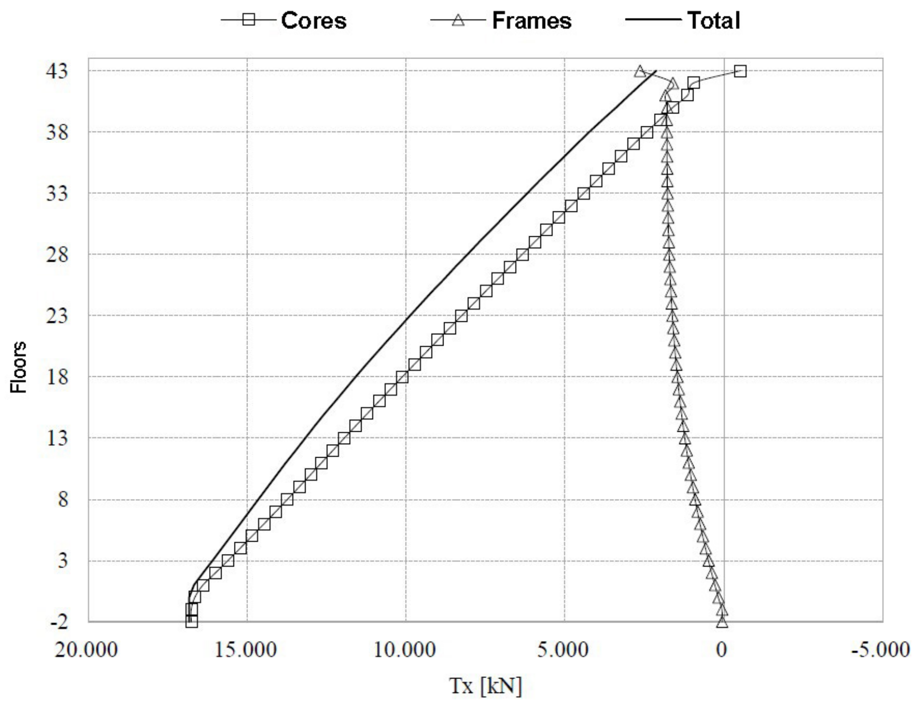

Figure 4.176: Shear T_x on stiffening systems

The presence of shear stress gives rise to the presence of a bending moment, as illustrated in Figures 4.180 for the X-direction and 4.181 for the Y-direction.

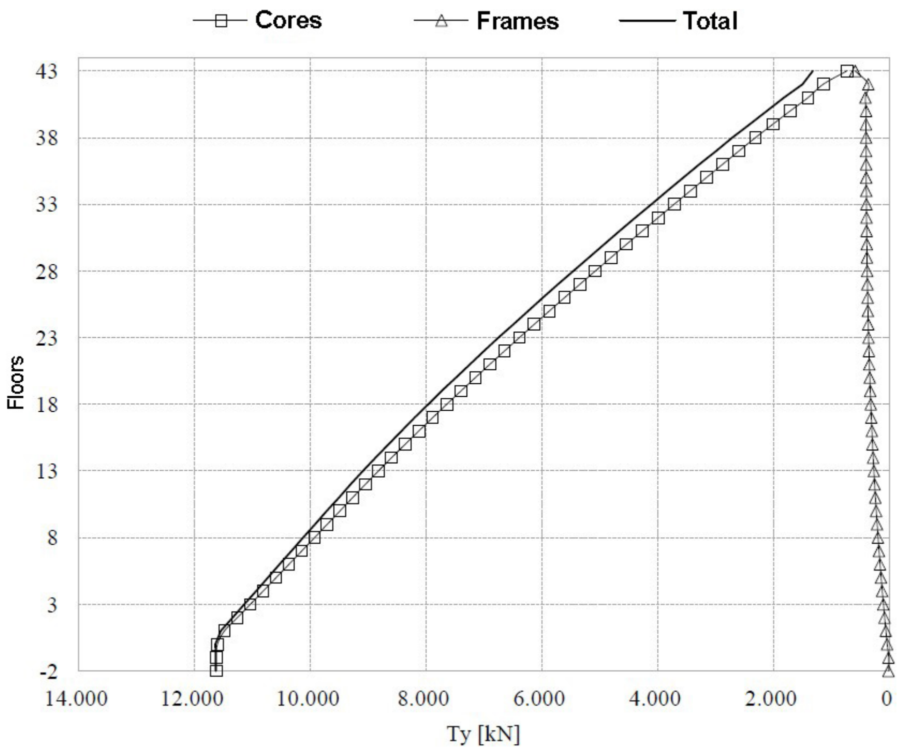

Figure 4.177: Shear T_y on stiffening systems

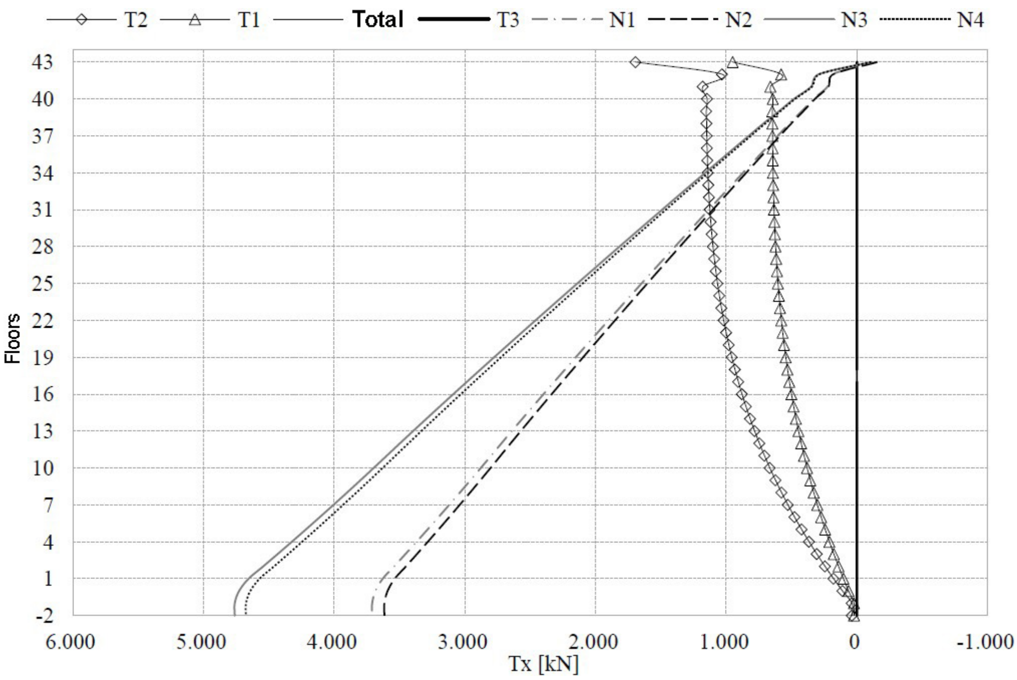

Figure 4.178: Shear T_x on individual elements

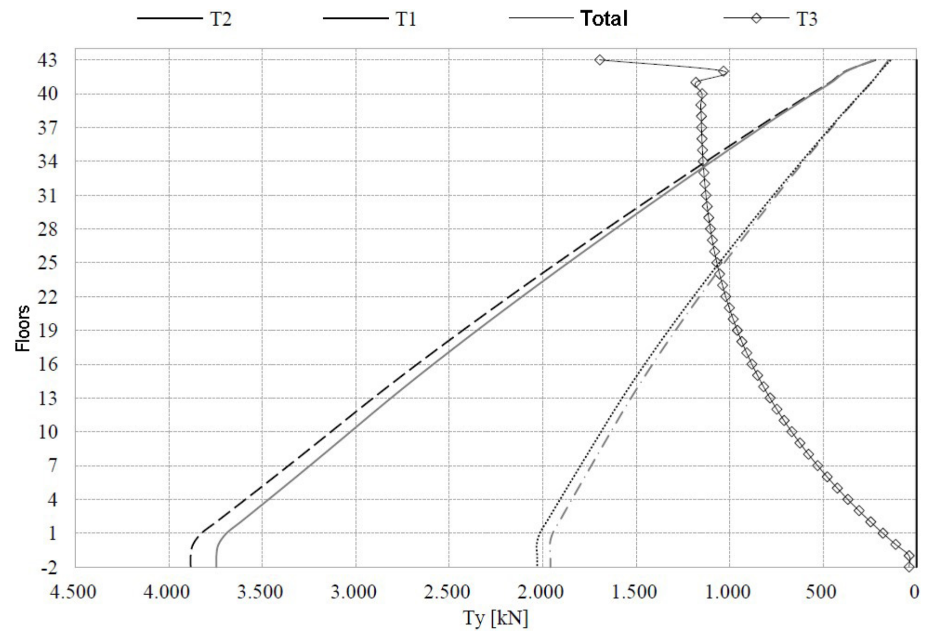

Figure 4.179: Shear T_y on individual elements

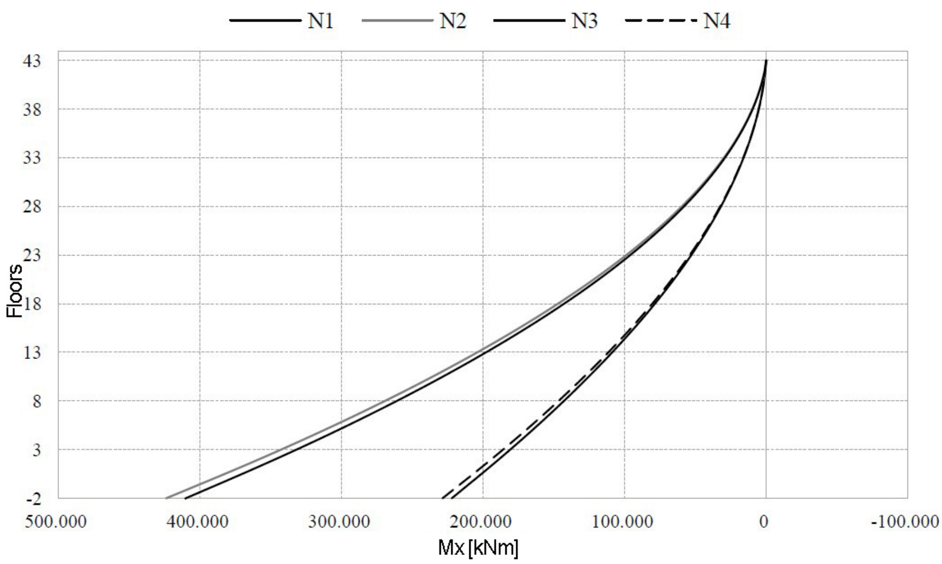

Figure 4.180: Bending moment M_x on the cores

As illustrated in Figures 4.182 and 4.183, the influence of primary and secondary torsion can be discerned. It is evident that the maximum value of secondary torsion, between the two core systems, oscillates between approximately 50 and 70% of the maximum value of the torque associated with primary torsion.

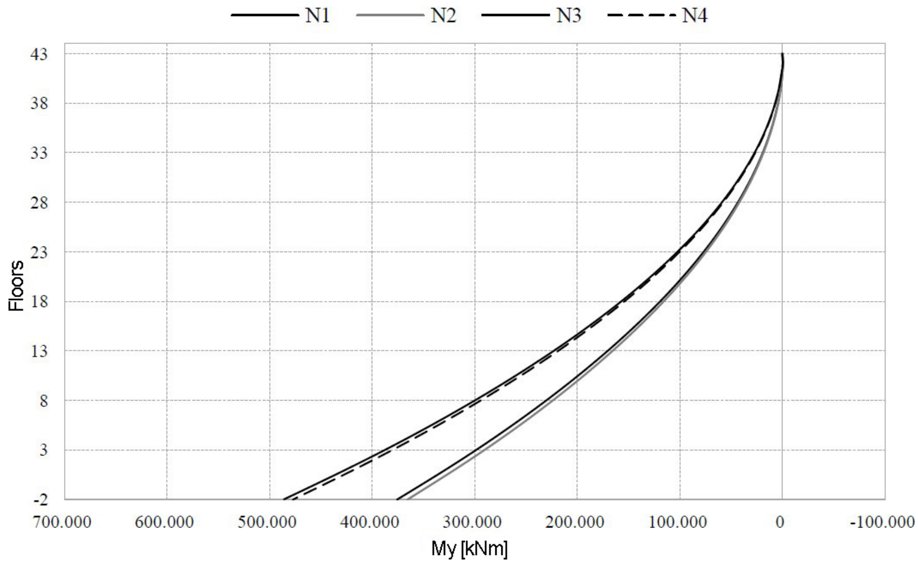

Figure 4.181: Bending moment M_y on the cores

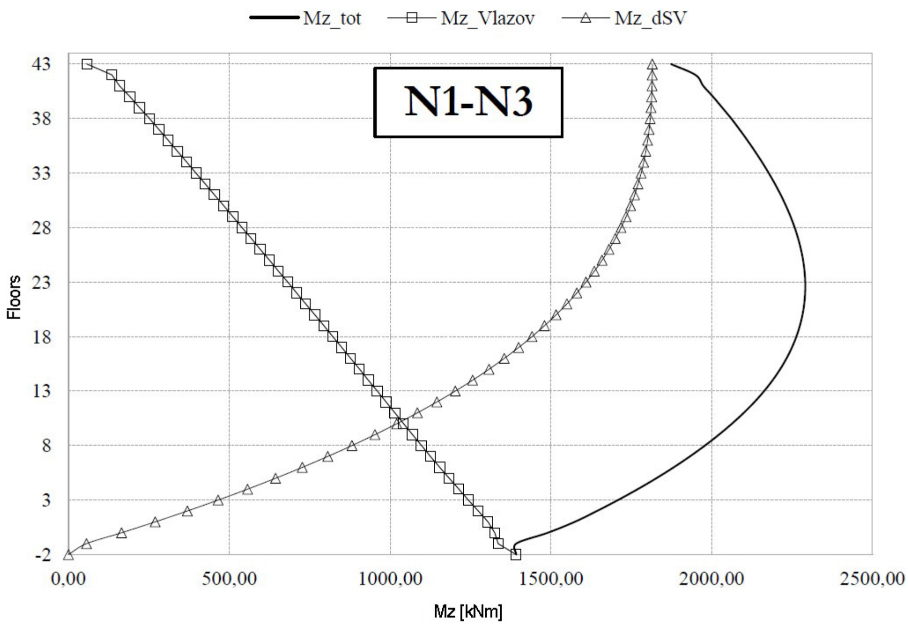

Figure 4.182: Torsional moment M_z on the cores N1 and N3

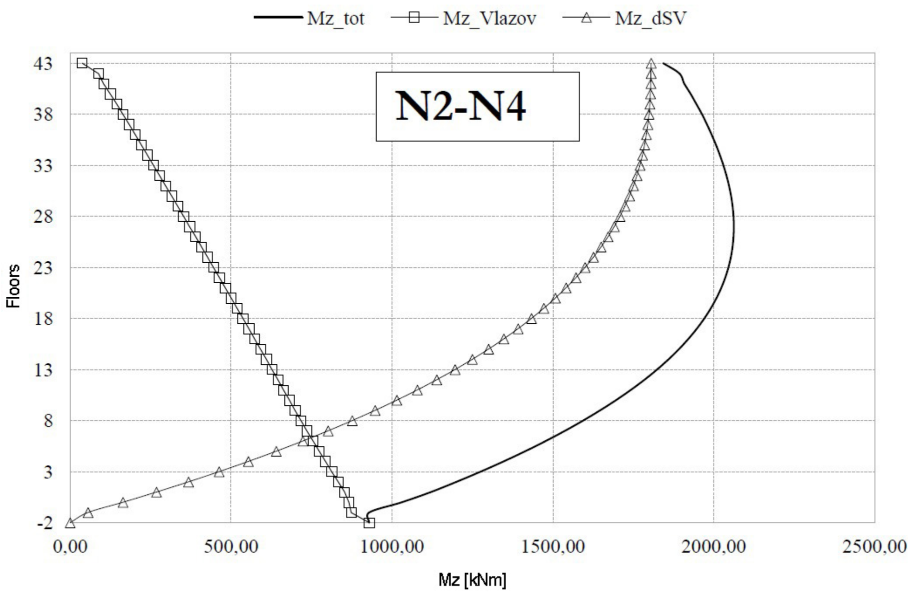

Figure 4.183: Torsional moment M_z on the cores N2 and N4

- **Stress analysis**

In accordance with the illustration depicted in Figure 4.169, the comparative analysis of the tensile forces exerted on each core is presented, with a focus on the contributions from bending moments and bi-momentum.

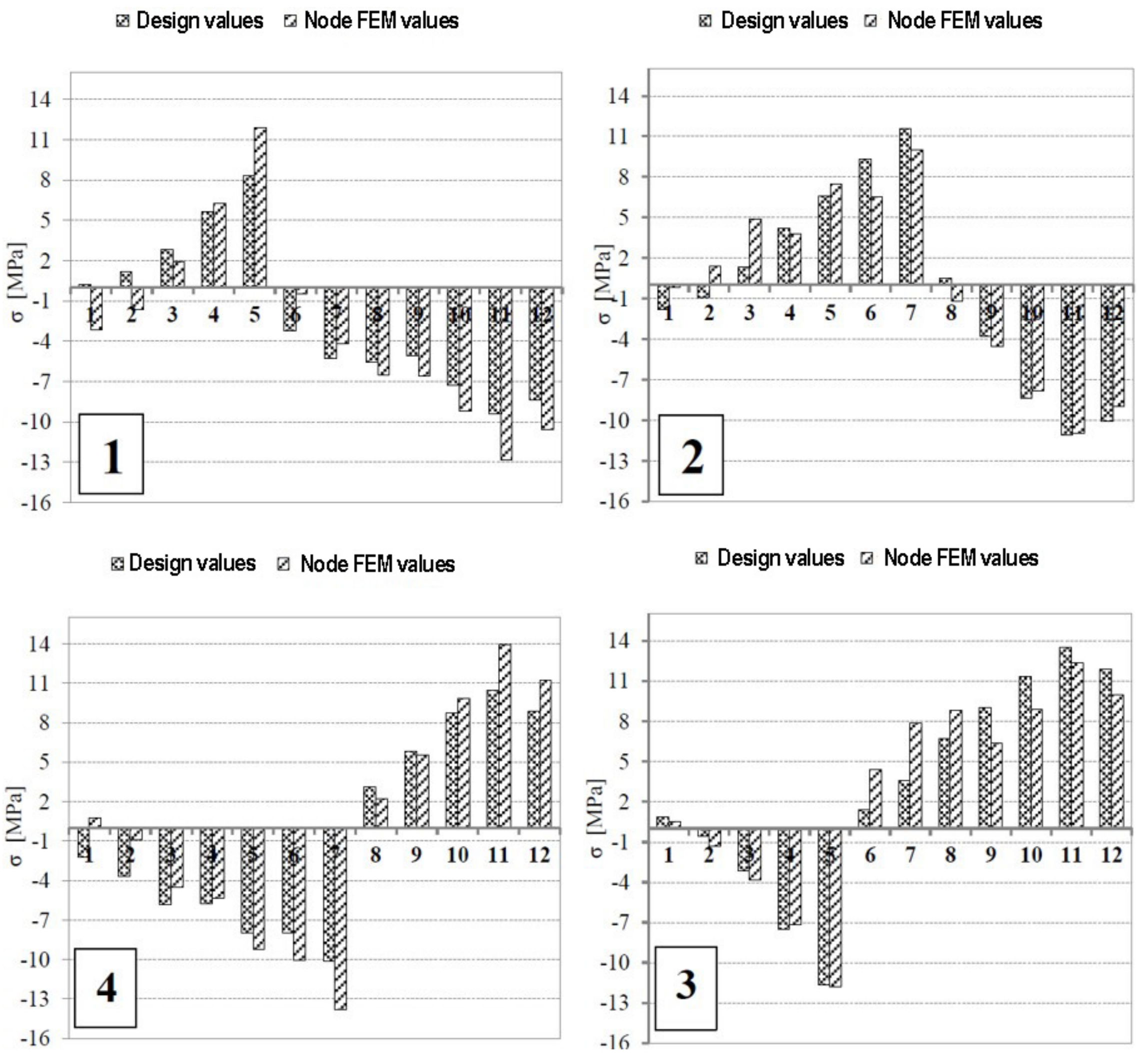

Figure 4.184: Tension comparison in cores

Figure 4.184 illustrates the comparison between the voltages determined using the algorithm and those calculated using the finite element method (FEM) software. It can be observed that, in comparison to Combination 1, the trend in stresses is relatively similar, yet the discrepancy between the two measurements is considerably amplified. This suggests that, as the torsional stresses intensify, the margin of deviation provided by the algorithm also increases.

Figure 4.185 illustrates the comparison between the stresses induced by bi-moment and those resulting from bending moments.

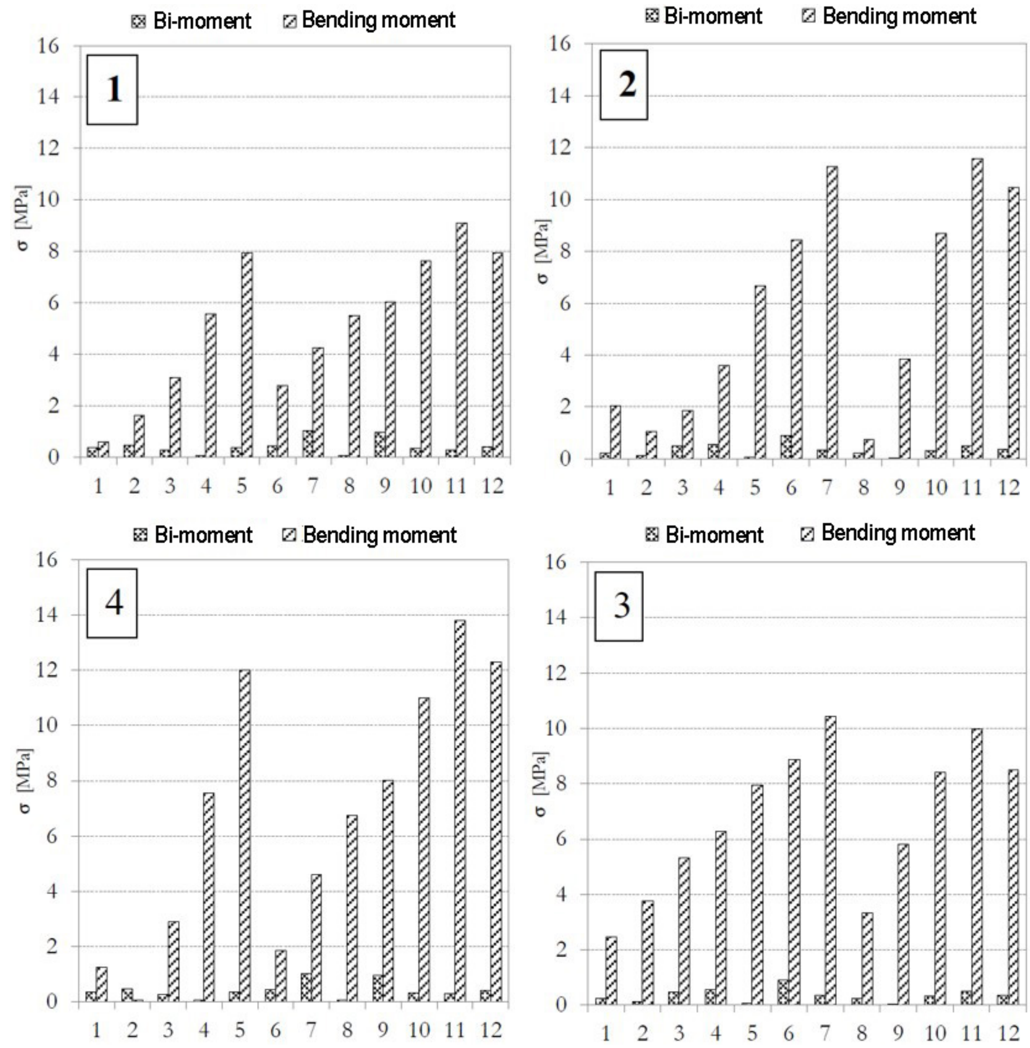

Figure 4.185: Comparison of bi-moment and bending stresses

It can be observed that the tensions induced by the bi-moment are greater for Combination 2, as the torsion is greater. However, even in this case, their influence is not significant, except at some points where they reach 35% of the bending stresses.

4.6.6 Comparison between analytical model and real structure data

In order to ascertain the degree of correspondence between the analytical and the real models, the displacements yielded by the algorithm were compared with the head displacement values declared by the designers (Figure 4.186).

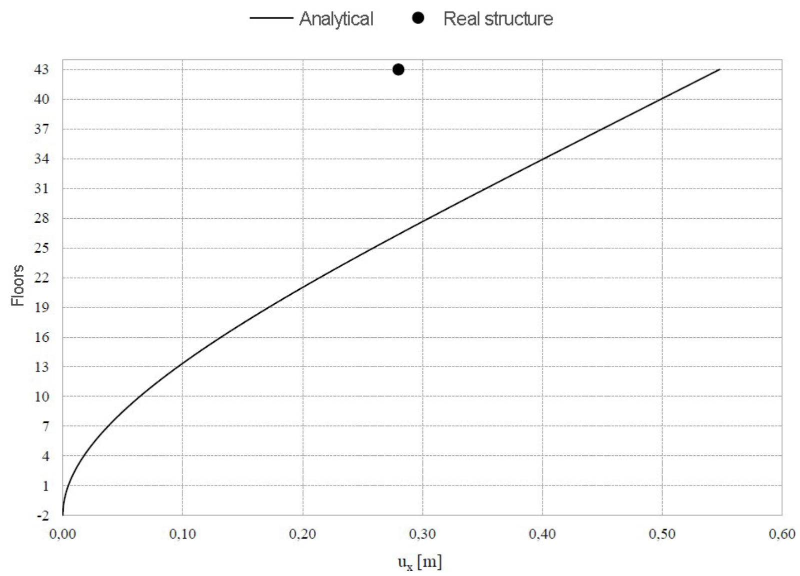

Figure 4.186: Comparison of analytical and real displacement

The graph illustrates that the actual structure exhibits a markedly higher degree of stiffness than the analytical model. This discrepancy can be attributed to the fact that the displacement recorded by the model employed for the design incorporates the deformation of the foundation, which results in an increase in displacement. Furthermore, loads derived from a wind tunnel analysis were utilised, which differed from those employed in the analytical model. Nevertheless, these discrepancies would not have resulted in outcomes that differ significantly from those depicted in the graph.

A more detailed examination of the structure revealed the impact of slab thickenings at the cores (Figure 4.150). At each floor, slab thickenings were provided, forming solid concrete elements with a thickness of 50 cm, a length of 160 cm and a width equal to that of the cores. The aforementioned thickenings have been implemented with the objective of establishing rigid connections that can effectively stiffen the structural system responsible for absorbing horizontal loads.

In order to verify their effective influence, the limit situation in which these elements are non-deformable was studied. For this purpose, the previously created finite element model was modified, adding planes with infinite stiffness along all directions and in correspondence with the thickenings (Figure 4.187).

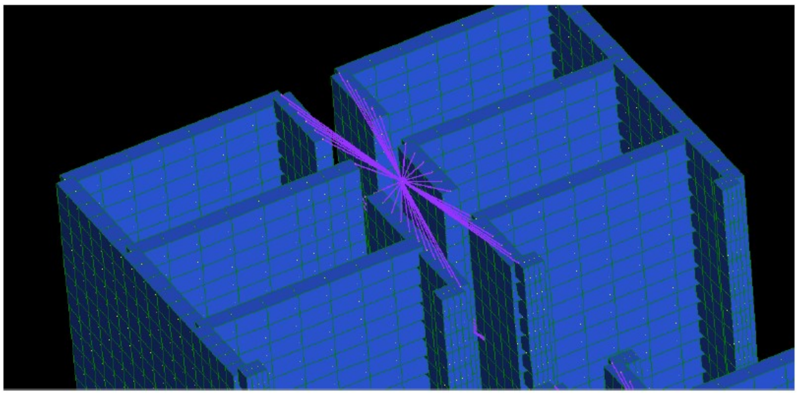

Figure 4.187: Floor thickening modelled in the FEM

The displacements obtained through the analysis of this model are shown in Figure 4.188, where they were compared with the real structure and the unstiffened structure.

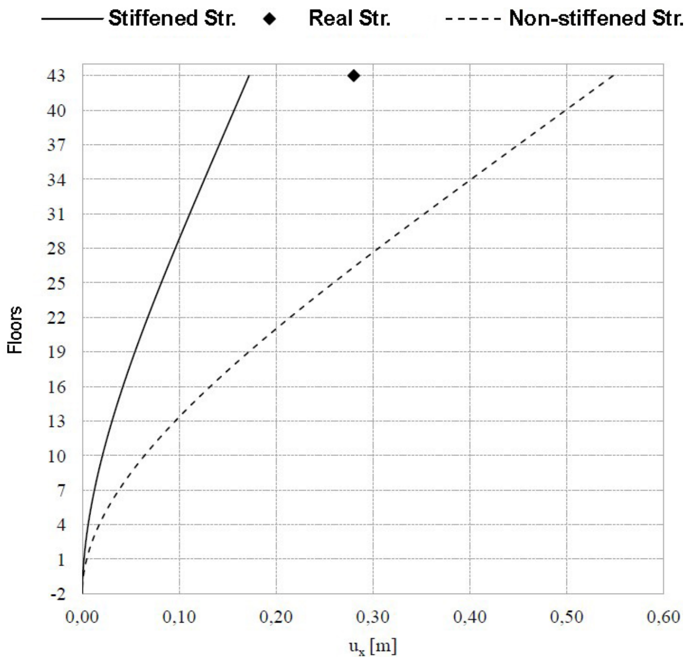

Figure 4.188: Floor thickening modelled in the FEM

The graph shows that the presence of the stiffeners , which are assumed to possess infinite stiffness, would result in displacements of approximately one-third the magnitude of those observed in the system devoid of stiffeners. Furthermore, the actual structure is more closely aligned with the condition of infinitely stiff elements, particularly after accounting for the quantities attributable to the deformation of the foundation and the elevated loads resulting from the wind tunnel analysis.

The incorporation of infinitely rigid elements markedly enhances the overall stiffness of the system, as the structure behaves as if it were composed of only two vertical resistant elements, each comprising the union of two of the four cores. This results in a markedly higher inertia.

The selected solution for the actual structure thus permits the structural system to be stiffened against horizontal actions without altering the occupancy ratio of the resistant elements.

4.6.7 Dynamic analysis

The dynamic analysis is based on the finite element model without the stiffeners and considers the mass concentrated at the centre of gravity of the floors. This calculation is made by neglecting the weight of the structural elements and considering a floor with a weight of 18.75 kN/m^3.

Furthermore, the out-of-plane stiffness of the slabs and the axial deformability of the resisting elements were also neglected. These assumptions deviate from the actual conditions and, consequently, the solution is not an accurate representation of the real system. The slabs partially constrain the deformation due to the warping of the open thin sections, which increases the overall stiffness of the system.

To ascertain the veracity of the results yielded by the algorithm, a comparison was conducted with the outcomes of a FEM model wherein the longitudinal deformation is unconstrained (Figure 4.189).

The graph (Figure 4.189) illustrates a higher degree of accuracy for the initial two vibration modes, while notable discrepancies are evident in the remaining instances.

Finally, Figure 4.190 provides a comparison between the frequencies obtained through the algorithm for the structure without stiffeners and the structure with stiffeners, and the real frequencies derived from the model used in the design phase.

As illustrated in the graph (Figure 4.190), the actual structure displays greater stiffness than the two analytical models, yet its behaviour is more closely aligned with that of the stiffened configuration. This demonstrates that the incorporation of stiffening elements is an effective method for imparting increased rigidity to the structure in response to horizontal forces.

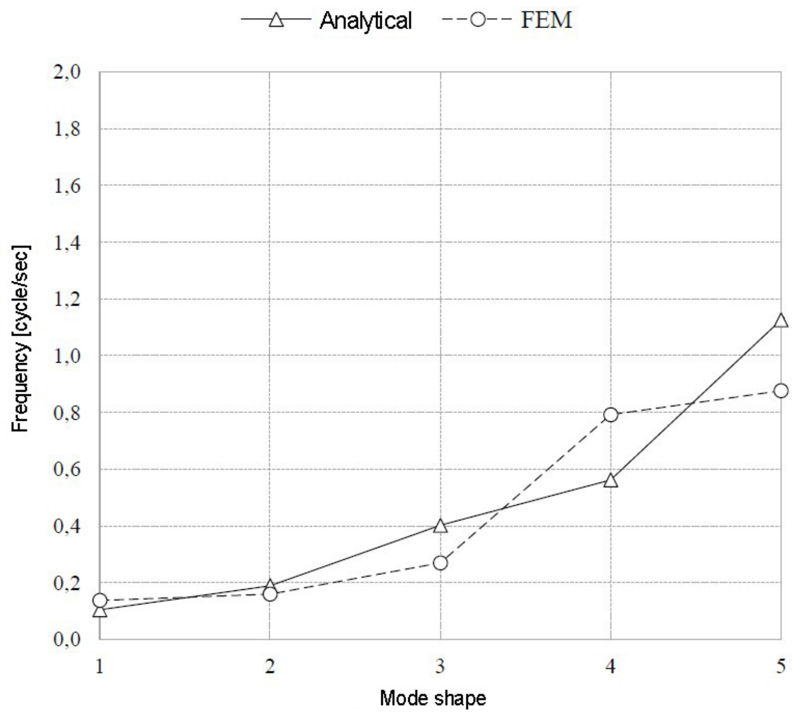

Figure 4.189: Frequencies of simplified FE and analytical models

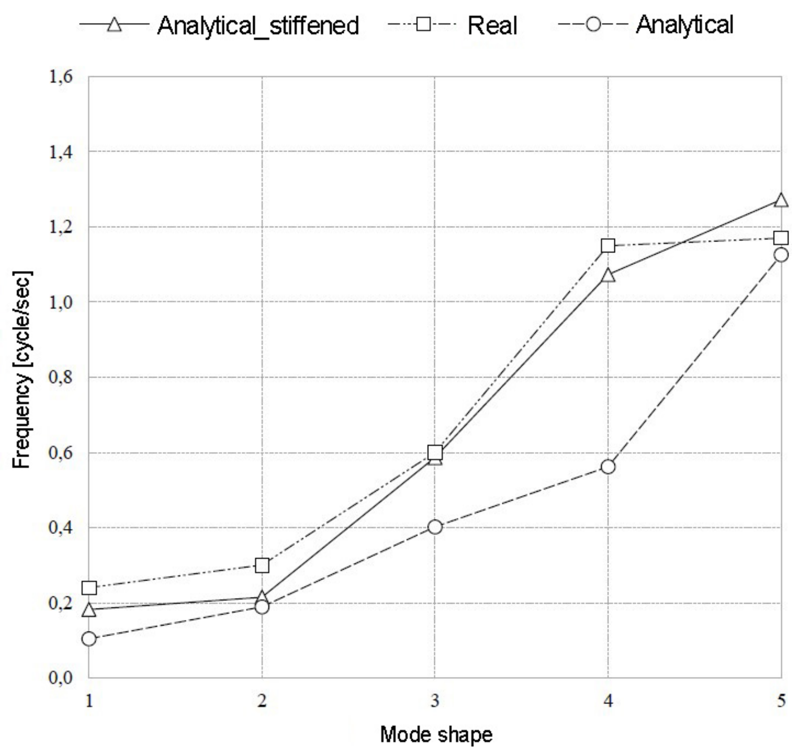

Figure 4.190: Frequencies of real model and FE and analytical stiffened models

Furthermore, it is evident that these elements exert a considerable influence with regard to bending along an axis and torsion. An examination of the frequency trends of the analytical models reveals that the initial mode of vibration corresponds to the flexural mode, in which the stiffening elements are involved. The frequencies of the stiffened structure are observed to be higher than those of the structure devoid of these elements. In contrast, the second mode of vibration corresponds to the flexural mode alone along the direction in which the stiffeners have a minimal impact, resulting in superimposable outcomes. In the remaining modes of vibration, in which torsion is always present, the two curves differ significantly. This is due to the fact that the stiffening elements have a strong stitching effect, causing the cores to tend towards the behaviour of closed sections, which are characterised by a much higher torsional stiffness.

5 Conclusions

The study conducted in this thesis work analyzes five tall buildings in the city of Turin. This analysis highlights the advantages of using the General Algorithm in the design of tall buildings.

From a structural point of view, tall buildings present the challenging issue of formulating an efficient resisting system that can ensure the structure adequate stiffness and lateral stability when subjected to horizontal actions resulting from wind and earthquake.

Currently, the most widely used software for structural analysis of a building, and thus for obtaining a detailed global description of its behavior in terms of stresses and deformations, are FEM software, based on the finite element method.

Structural analysis using FEM software, although it is very detailed, whatever the structure under study, can require substantial computational time, particularly for complex structures such as tall buildings; additionally, the formulation of a numerical model is often a time-consuming process, primarily due to the requirement of providing a substantial amount of data as inputs.

The General Algorithm, as illustrated in this paper, makes it possible to carry out static and dynamic analysis of tall buildings characterized by different resistant structural systems and to check their reliability. Through this algorithm, the creation of a calculation model is easier and faster than with FEM software, and the outcomes derived from this approach are highly reliable. Beyond the provision of the conventional stresses, including normal stress, shear, and bending moment, the algorithm also returns bimoment and torque stresses. In addition, it provides the necessary elements to perform tension calculations in the sections of resisting elements and allows the load distribution between the structural elements to be determined.

A further difference between the two models, the numerical and the analytical, is that in the model created using FEM software the structure is considered as a three-dimensional entity, whereas the algorithm considers the building to be composed of a series of separate elements (frames or cantilevers) that work in parallel with the other components of the resisting system by providing a contribution that is a function of its own stiffness. This discrepancy is evident in the computational times of the two types of programs: in FEM software, the number of unknowns, and consequently the number of equations to be solved, is high and corresponds to the number of nodes multiplied by the number of degrees of freedom they have in space (6 DoF); in the analytical code, on the other hand, the number of unknowns is greatly reduced because of the simplifying hypothesis of infinite rigid floors in their plane, that allows only the degrees of freedom in the plane to be considered (3 DoF). This difference is reflected in significantly different calculation times, as these are proportional to the square of the ratio of the number of degrees of freedom.

The algorithm's simplicity facilitates the rapid modification of the model in response to design variations, thereby enhancing its utility in the preliminary design phase. During this phase, the identification of forces, the structure's overall response, and the distribution of horizontal loads among the various resisting elements are of particular concern. Consequently, the algorithm is a highly effective and dependable instrument for identifying optimal design alternatives and achieving effective predimensioning of the resisting elements.

In summary, the General Algorithm has been demonstrated to be a beneficial tool that supports the structural engineers in the design and predimensioning of tall buildings, simplifying the calculation and model realization and providing sufficiently accurate solutions quickly. Such a calculation code can be combined with the use of finite element programs, which are useful when the final structural design has been reached and the overall behavior of the structure and its characteristics are known, for the refinement of the results obtained through the algorithm.

The purpose of this thesis is to conclude by reflecting on the ability of the city of Turin to become a modern city comparable to other overseas metropolises.

The city of Turin is situated whitin a unique geographical context with strong peculiarities, characterized by its position in a low plain between the Alpine arc, which with its wide semicircle embraces the horizon, and the hills. The confluence of these elements, when viewed from within the city, serves as a unifying architectural motif that is integral to the city's urban fabric. The city's primary thoroughfares, in this regard, function as *"perspective telescopes"* [24], metamorphosing the urban landscape into a seamless extension of the surrounding topography, thereby integrating the mountains and hills into the city's very identity.

From an urban planning perspective, Turin exhibits remarkable cohesion, with its architectural culture spanning a century and a half of recent history. The city's architectural heritage boasts evidence of various styles, including Eclecticism, Art

Nouveau, and the Modern Movement, reflecting a rich and evolving urban landscape.

The concept of vertical city development, in conjunction with the prevailing interest in compact urbanism as a contrast to diffuse urban expansion, has dominated urban development over the past four decades.

The city landscape characteristics give rise to the issue of landscape as a form of *value*,that is, the responsibility to care for and preserve the landscape, which serves as an expression of the life and culture of multiple generations. This responsibility is addressed through the conceptualization of an *"architecture of places"*, rooted in its own territories, in local cultural and social magisteria and choices, capable of responding to the needs of citizens, planning the construction of tall buildings while respecting historic views and a controllable urban sprawl, in light of the richness of historic urban design.

In conclusion, Turin possesses the potential to evolve into a modern city. However, it is imperative to undertake a comprehensive study that explores the integration of tall buildings within the *"urban landscape"*. This study must encompass the visual and social ramifications, employing an approach that safeguards the unique character of the city and prevents the pitfalls of *modernization*, which often entails the implementation of scientific and technological advancements that may not necessarily promote societal progress and development.

Appendix

A Wind Action Calculation

The wind is the movement of air masses with a randomly varying velocity field over time.

In the case of buildings, the actions induced by the wind are aerodynamic in nature, as they are generated by the incident flow and the swirling wakes produced by the bodies hit, which generate precisely dynamic effects. In particular cases, generally with highly deformable buildings, the oscillation of the latter can generate wind-structure interaction phenomena that amplify or reduce the actions of the wind itself.

For ordinary buildings in Italy, i.e. those structures with sufficient stiffness and damping to cancel out such interactions, the standard allows the effects produced by the wind to be modelled by means of equivalent static actions. These actions are described by means of pressures and depressions to be applied to the internal and external surfaces of the structure. In the case of buildings with large lateral surfaces, the associated tangent actions must also be considered.

The wind actions must be applied along the symmetry axes of the structure and, when there are particular buildings, the possible torsional effects generated by these actions must also be taken into account.

The NTC18 reports the procedure for the definition of such equivalent static actions, which consists of the following steps:

- definition of the geography of the site;
- calculation of the design speed and peak kinetic pressure;
- definition of the mechanical properties of the construction;
- definition of the equivalent static actions.

A.1 Reference base speed

The reference speed v_b is the characteristic value of the wind speed at 10 m above the ground on a level and homogeneous site of exposure category II, averaged over 10 minutes and referring to a return period of 50 years. In the absence of specific and adequate statistical investigations, the reference base speed v_b is expressed as:

$$v_b = v_{b,0} \cdot c_a$$

where:

$v_{b,0}$ is the reference base velocity at sea level, assigned in Table 3.3.I according to the area in which the building stands

c_a is the altitude coefficient provided by the relationship:

$$c_a = \begin{cases} 1 & \text{if } a_s \leq a_0 \\ 1 + k_s \left(\dfrac{a_s}{a_0} - 1 \right) & \text{if } a_0 < a_s \leq 1500\, m \end{cases}$$

where

a_0, k_s are parameters given in Table 3.3.I depending on the area in which the building is located (Fig. 3.3.1);

a_s is the altitude above sea level of the site where the building is located.

Zona	Descrizione	$v_{b,0}$ [m/s]	a_0 [m]	k_s
1	Valle d'Aosta, Piemonte, Lombardia, Trentino Alto Adige, Veneto, Friuli Venezia Giulia (con l'eccezione della provincia di Trieste)	25	1000	0,40
2	Emilia Romagna	25	750	0,45
3	Toscana, Marche, Umbria, Lazio, Abruzzo, Molise, Puglia, Campania, Basilicata, Calabria (esclusa la provincia di Reggio Calabria)	27	500	0,37
4	Sicilia e provincia di Reggio Calabria	28	500	0,36
5	Sardegna (zona a oriente della retta congiungente Capo Teulada con l'Isola di Maddalena)	28	750	0,40
6	Sardegna (zona a occidente della retta congiungente Capo Teulada con l'Isola di Maddalena)	28	500	0,36
7	Liguria	28	1000	0,54
8	Provincia di Trieste	30	1500	0,50
9	Isole (con l'eccezione di Sicilia e Sardegna) e mare aperto	31	500	0,32

Figure A.1: Table 3.3.I in the NTC18 - Values of parameters $v_{b,0}, a_0, k_s$

A.2 Wind pressure

Wind pressure is given by the expression:

$$p = q_r \cdot c_e \cdot c_p \cdot c_d$$

where:

q_r is the reference kinetic pressure;

c_e is the exposure coefficient;

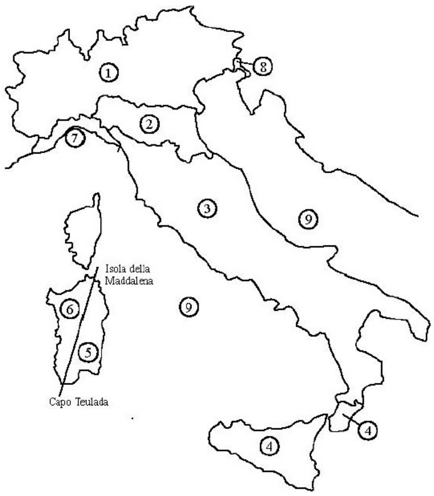

Figure A.2: Figure 3.3.1 in the NTC18 - Map of the zones into which Italy is divided

c_p is the pressure coefficient;
c_d is the dynamic coefficient.

A.2.1 Reference kinetic pressure

The reference kinetic pressure q_r is given by the expression:

$$q_r = \frac{1}{2}\,\rho\, v_r^2$$

where
v_r is the reference speed of the wind;
ρ is the air density conventionally assumed to be constant and equal to 1.25 kg/m^3.

A.2.2 Exposure coefficient

The exposure coefficient c_e depends on the height z above ground of the point considered, the topography of the ground and the exposure category of the site where the construction is located. In the absence of specific analyses taking into account the wind direction and the actual roughness and topography of the site surrounding the construction, for heights above ground not greater than z = 200 m, it is given by the formula:

$$c_e(z) = \begin{cases} k_r^2\, c_t\, ln(z/z_0)[7 + c_t\, ln(z/z_0)] & \text{for } z \geq z_{min} \\ c_e(z_{min}) & \text{for } z < z_{min} \end{cases}$$

where

k_r, z_0, z_{min} are assigned in Table 3.3.II according to the exposure category of the construction site;
c_t is the topography coefficient.

Categoria di esposizione del sito	K_r	z_0 [m]	z_{min} [m]
I	0,17	0,01	2
II	0,19	0,05	4
III	0,20	0,10	5
IV	0,22	0,30	8
V	0,23	0,70	12

Figure A.3: Table 3.3.II in the NTC18 - Parameters for the definition of the exposure coefficient

The exposure category is assigned in Figure A.5 as a function of the geographical position of the site where the construction is located and the soil roughness class defined in Tab. 3.3.III (Figure A.4). In the bands within 40 km from the coast, the exposure category is independent of the altitude of the site.

The topography coefficient c_t is generally set equal to 1 for both flat and undulating, hilly and mountainous areas.

In this case, Figure A.6 shows the variation laws of c_e for the different exposure categories.

Classe di rugosità del terreno	Descrizione
A	Aree urbane in cui almeno il 15% della superficie sia coperto da edifici la cui altezza media superi i 15 m
B	Aree urbane (non di classe A), suburbane, industriali e boschive
C	Aree con ostacoli diffusi (alberi, case, muri, recinzioni,....); aree con rugosità non riconducibile alle classi A, B, D
D	a) Mare e relativa fascia costiera (entro 2 km dalla costa); b) Lago (con larghezza massima pari ad almeno 1 km) e relativa fascia costiera (entro 1 km dalla costa) c) Aree prive di ostacoli o con al più rari ostacoli isolati (aperta campagna, aeroporti, aree agricole, pascoli, zone paludose o sabbiose, superfici innevate o ghiacciate, ...)

Figure A.4: Table 3.3.III in the NTC18 - Ground roughness classes

A.2.3 Pressure coefficient

The pressure coefficient c_p depends on the type and geometry of the construction and its orientation with respect to the wind direction. This coefficient can be

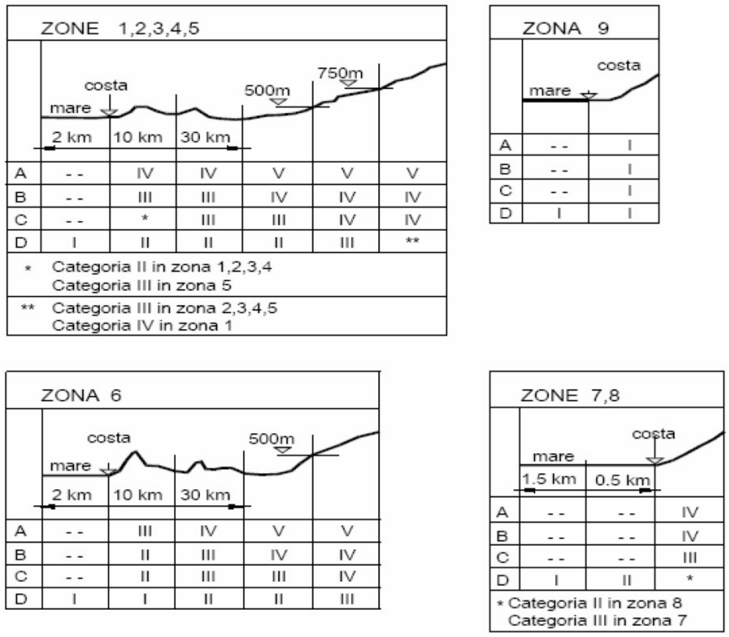

Figure A.5: Figure 3.3.2 in the NTC18 - Definition of exposure categories

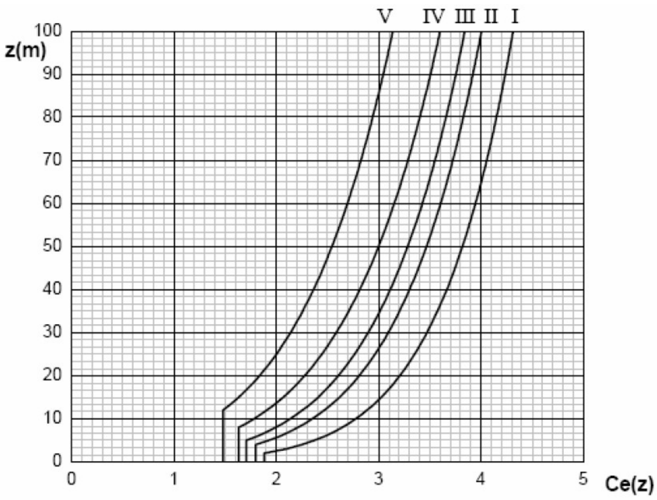

Figure A.6: Figure 3.3.3 in the NTC18 - Trend of the exposure coefficient c_e as a function of height above ground (for $c_t = 1$)

derived from data supported by appropriate documentation or from experimental wind tunnel tests.

A.2.4 Dynamic coefficient

The dynamic coefficient c_d takes into account the reductive effects associated with the non-contemporaneity of the maximum local pressures and the amplifying effects due to the dynamic response of the structure. It may be conservatively assumed to be equal to 1 in buildings of a recurring type, such as buildings of regular shape not exceeding 80 m in height and industrial sheds, or it may be determined by specific analyses or by reference to data of proven reliability.

A.3 Wind action on rectangular buildings

The wind action exercises on the building faces an external pressure distribution p_e and an internal pressure distribution p_i, linked to the definitions of the external pressure coefficients c_{pe} and internal pressure coefficient c_{pi}. The first coefficient depends on the shape of the building, the direction of the incident wind and the size of the area considered.

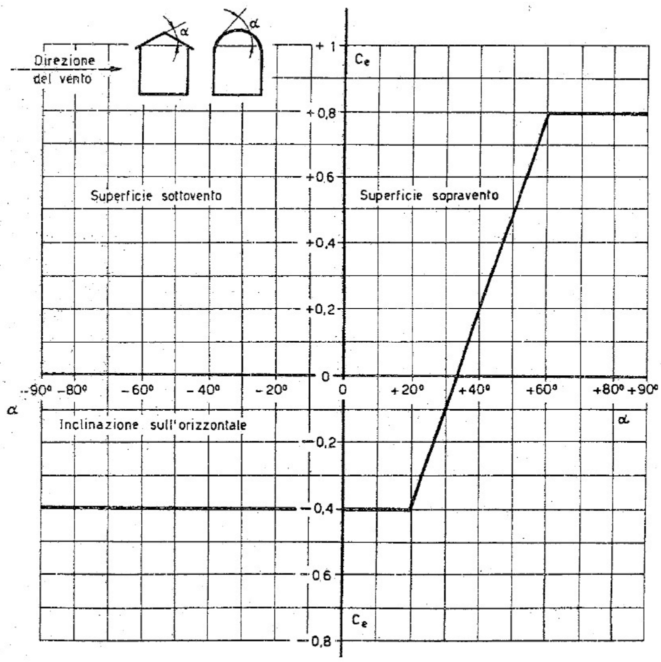

Figure A.7: Figure C3.3.2 in the NTC18 - Values assumed by c_{pe} as α changes

These coefficients are obtained by means of a simplified definition and provide a solution for the pressure field in favour of safety.

The internal pressure, on the other hand, is almost uniform over all the internal surfaces of the building and, for this reason, gives rise to a self-balancing action that does not affect the structure as a whole, but can create considerable aerodynamic actions on certain structural elements or portions of the structure.

When dealing with civil buildings with high internal volumes identified by partitions, the effect of internal pressure can be neglected in structural analyses. This effect has been neglected in this thesis.

A.4 Torsional effects

In the case of particular buildings, it is possible to take twisting actions into account in an approximate way by changing the distribution of wind pressures on the windward face only.

This consideration of the torsional actions takes place by considering a further distribution of pressures; in this particular situation, the course of the pressures on one face of the structure is not constant, but has a linear course, as shown in Figure A.8

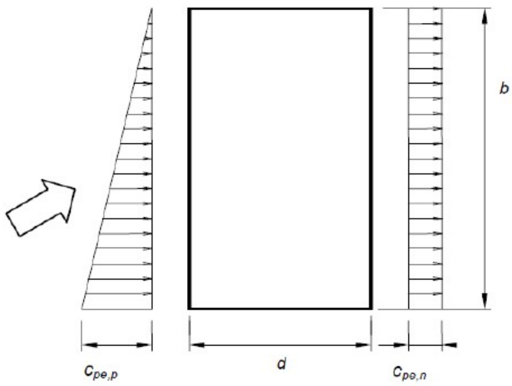

Figure A.8: Pressure distribution to take into account torsional actions

B Stress analysis of an open thin section

The stress analysis of an open thin section is conducted by determining the following:

- Normal axial tension acting along the longitudinal fibres

$$\sigma_z = \frac{M_y}{J_{yy}}x + \frac{M_x}{J_{xx}}y + \frac{B}{J_{\omega\omega}}\omega \tag{B.1}$$

- Tangential tension acting along the midline of the cross-section

$$\tau_{zs} = \frac{1}{b}\left[\frac{T_x}{J_{yy}}S_y(s) + \frac{T_y}{J_{xx}}S_x(s)\frac{M_z^{VL}}{J_{\omega\omega}}S_\omega(s)\right] \tag{B.2}$$

- Primary tangential stress (due to pure torsion), linearly variable along the wall thickness of the section

$$\tau(s,T) = \frac{M_z^{SV}}{J_t}b(s) \tag{B.3}$$

where:

- J_{xx}, J_{yy} are the moments of inertia and $J_{\omega\omega}$ is the sectorial moment of inertia, all referred to the barycentric reference system

$$J_{yy} = I_{yy} - Ax_G^2 \tag{B.4a}$$

$$J_{xx} = I_{xx} - Ay_G^2 \tag{B.4b}$$

$$J_{\omega\omega} = I_{\omega\omega} - A\omega_0^2 \tag{B.4c}$$

  where:

  I_{xx}, I_{yy} are the moments of inertia and $I_{\omega\omega}$ is the sectorial moment of inertia

$$I_{yy} = \int_A x^2\,dA \tag{B.5a}$$

$$I_{xx} = \int_A y^2\,dA \tag{B.5b}$$

$$I_{\omega\omega} = \int_A \omega^2\,dA \tag{B.5c}$$

- $\omega = \int_0^s h(s)\,ds$ = sectorial coordinate or *warping area*

  with: h(s) = ray-vector

- b(s) = thickess of the section
- S_x, S_y are the static moments and S_ω is the sectorial static moment

$$S_y = \int_A x\,dA \tag{B.6a}$$

$$S_x = \int_A y\,dA \tag{B.6b}$$

$$S_\omega = \int_A \omega\,dA \tag{B.6c}$$

- J_t is the torsional moment of inertia

$$J_t = \frac{M_z L}{G\vartheta} \tag{B.7}$$

with:

G = tangential modulus of elasticity or shear modulus
ϑ = torsional angle
L = length of the element

The sectorial coordinate is first calculated in relation to the barycentre of the section $\omega(s_1; s)$, then is calculated in relation to the geometric centre of gravity $\omega(s_0; s)$:

$$\omega(s_0; s) = \omega(s_1; s) - \omega(s_1; s_0) = \omega(s_1; s) - \frac{S_\omega(s_1)}{A} \tag{B.8}$$

Since the stresses and moments of inertia provided by the calculation code refer to the shear centre of the section, it is necessary to express the sectorial coordinate with reference to the shear centre:

$$\omega_c = \omega + c_y(x - x_0) - c_x(y - y_0) \tag{B.9}$$

where:

c_y and c_x are the coordinates of the section shear center with respect to the sectorial barycentre

x_0 and y_0 are are the coordinates of the sectorial barycentre with respect to the geometric barycentre

C Calculations and results

C.1 Reale Mutua Tower

With reference to the chapter on the Reale Mutua Tower, in particular the calculation of wind actions 4.2.3, below are the results of calculations carried out for wind action in the case of wind blowing along the directions of the symmetry axes of the structure (case 1) and in the case where torsional moment is also present (case 2).

WIND ACTION: CASE 1									
Direction X - Windward									
Floor [-]	**Z** [m]	q_b [N/m^2]	c_e [-]	c_p [-]	c_d [-]	**p** [N/m^2]	L_{Wall} [mm]	$H_{Interp.}$ [mm]	F_x [kN]
PT	-	-	-	-	-	-	-	-	-
Basement	4.66	391	1.48	0.8	1	462	18656	4050	35
1	8.10	391	1.48	0.8	1	462	18656	3520	30
2	11.7	391	1.48	0.8	1	462	18656	3600	31
3	15.3	391	1.65	0.8	1	514	18656	3600	35
4	18.9	391	1.80	0.8	1	561	18656	3600	38
5	22.5	391	1.92	0.8	1	601	18656	3800	43
6	26.5	391	2.04	0.8	1	639	18656	3600	43
7	29.7	391	2.13	0.8	1	666	15873	3400	36
8	33.3	391	2.22	0.8	1	694	15873	3600	40
9	36.9	391	2.30	0.8	1	719	15873	3550	40
10	40.4	391	2.37	0.8	1	741	14280	3550	34
11	43.9	391	2.44	0.8	1	762	13000	3500	32
12	47.4	391	2.50	0.8	1	782	13000	3500	36
13	50.9	391	2.56	0.8	1	800	13000	3500	36
14	54.4	391	2.61	0.8	1	817	13000	3500	37
15	57.9	391	2.67	0.8	1	833	13000	3500	38
16	61.4	391	2.72	0.8	1	849	13000	3500	39
17	64.9	391	2.76	0.8	1	863	13000	3500	42
18	68.4	391	2.81	0.8	1	877	13000	3700	43
19	72.3	391	2.85	0.8	1	892	13000	1950	23

WIND ACTION: CASE 1									
Direction X - Leeward									
Floor [-]	**Z** [m]	q_b [N/m^2]	c_e [-]	c_p [-]	c_d [-]	**p** [N/m^2]	L_{Wall} [mm]	$H_{Interp.}$ [mm]	F_x [kN]
PT	-	-	-	-	-	-	-	-	-
Basement	4.66	391	1.48	-0.4	1	-231	18656	4050	-17
1	8.10	391	1.48	-0.4	1	-231	18656	3520	-15
2	11.7	391	1.48	-0.4	1	-231	18656	3600	-16
3	15.3	391	1.65	-0.4	1	-257	18656	3600	-17
4	18.9	391	1.80	-0.4	1	-280	18656	3600	-19
5	22.5	391	1.92	-0.4	1	-300	18656	3800	-21
6	26.5	391	2.04	-0.4	1	-319	18656	3600	-21
7	29.7	391	2.13	-0.4	1	-333	15873	3400	-18
8	33.3	391	2.22	-0.4	1	-347	15873	3600	-20
9	36.9	391	2.30	-0.4	1	-359	15873	3550	-20
10	40.4	391	2.37	-0.4	1	-371	13000	3550	-17
11	43.9	391	2.44	-0.4	1	-381	13000	3500	-17
12	47.4	391	2.50	-0.4	1	-391	13000	3500	-18
13	50.9	391	2.56	-0.4	1	-400	13000	3500	-18
14	54.4	391	2.61	-0.4	1	-408	13000	3500	-19
15	57.9	391	2.67	-0.4	1	-417	13000	3500	-19
16	61.4	391	2.72	-0.4	1	-424	13000	3500	-20
17	64.9	391	2.76	-0.4	1	-432	13000	3500	-20
18	68.4	391	2.81	-0.4	1	-439	13000	3700	-21
19	72.3	391	2.85	-0.4	1	-446	13000	1950	-11

WIND ACTION: CASE 1									
Direction Y - Windward									
Floor	**Z**	q_b	c_e	c_p	c_d	**p**	L_{Wall}	$H_{Interp.}$	F_y
[-]	**[m]**	**[N/m²]**	**[-]**	**[-]**	**[-]**	**[N/m²]**	**[mm]**	**[mm]**	**[kN]**
PT	-	-	-	-	-	-	-	-	-
Basement	4.66	391	1.48	0.8	1	462	49148	4050	92
1	8.1	391	1.48	0.8	1	462	49148	3520	80
2	11.7	391	1.48	0.8	1	462	49148	3600	82
3	15.3	391	1.65	0.8	1	514	49148	3600	91
4	18.9	391	1.80	0.8	1	561	49148	3600	99
5	22.5	391	1.92	0.8	1	601	49148	3800	112
6	26.5	391	2.04	0.8	1	639	47950	3600	110
7	29.7	391	2.13	0.8	1	666	47950	3400	109
8	33.3	391	2.22	0.8	1	694	47950	3600	120
9	36.9	391	2.30	0.8	1	719	47950	3550	122
10	40.4	391	2.37	0.8	1	741	14280	3550	37
11	43.9	391	2.44	0.8	1	762	14280	3500	38
12	47.4	391	2.50	0.8	1	782	14280	3500	39
13	50.9	391	2.56	0.8	1	800	14280	3500	39
14	54.4	391	2.61	0.8	1	817	14280	3500	41
15	57.9	391	2.67	0.8	1	833	14280	3500	42
16	61.4	391	2.72	0.8	1	849	14280	3500	43
17	64.9	391	2.76	0.8	1	863	14280	3500	43
18	68.4	391	2.81	0.8	1	877	14280	3700	44
19	72.3	391	2.85	0.8	1	892	14280	1950	25

WIND ACTION: CASE 1									
Direction Y - Leeward									
Floor [-]	**Z** [m]	q_b [N/m^2]	c_e [-]	c_p [-]	c_d [-]	**p** [N/m^2]	L_{Wall} [mm]	$H_{Interp.}$ [mm]	F_y [kN]
PT	-	-	-	-	-	-	-	-	-
Basement	4.66	391	1.48	-0.4	1	-231	49148	4050	-46
1	8.1	391	1.48	-0.4	1	-231	49148	3520	-40
2	11.7	391	1.48	-0.4	1	-231	49148	3600	-41
3	15.3	391	1.65	-0.4	1	-257	49148	3600	-45
4	18.9	391	1.80	-0.4	1	-280	49148	3600	-50
5	22.5	391	1.92	-0.4	1	-300	49148	3800	-56
6	26.5	391	2.04	-0.4	1	-319	47950	3600	-55
7	29.7	391	2.13	-0.4	1	-333	47950	3400	-54
8	33.3	391	2.22	-0.4	1	-347	47950	3600	-60
9	36.9	391	2.30	-0.4	1	-359	47950	3550	-61
10	40.4	391	2.37	-0.4	1	-371	14280	3550	-19
11	43.9	391	2.44	-0.4	1	-381	14280	3500	-19
12	47.4	391	2.50	-0.4	1	-391	14280	3500	-20
13	50.9	391	2.56	-0.4	1	-400	14280	3500	-20
14	54.4	391	2.61	-0.4	1	-408	14280	3500	-20
15	57.9	391	2.67	-0.4	1	-417	14280	3500	-21
16	61.4	391	2.72	-0.4	1	-424	14280	3500	-21
17	64.9	391	2.76	-0.4	1	-432	14280	3500	-22
18	68.4	391	2.81	-0.4	1	-439	14280	3700	-23
19	72.3	391	2.85	-0.4	1	-446	14280	1950	-12

WIND ACTION: CASE 2									
Direction X - Windward									
Floor [-]	**Z** [m]	q_b [N/m^2]	c_e [-]	c_p [-]	c_d [-]	**p** [N/m^2]	L_{Wall} [mm]	$H_{Interp.}$ [mm]	F_x [kN]
PT	-	-	-	-	-	-	-	-	-
Basement	4.66	391	1.48	0.8	1	462	18656	4050	17
1	8.10	391	1.48	0.8	1	462	18656	3520	15
2	11.7	391	1.48	0.8	1	462	18656	3600	16
3	15.3	391	1.65	0.8	1	514	18656	3600	17
4	18.9	391	1.80	0.8	1	561	18656	3600	19
5	22.5	391	1.92	0.8	1	601	18656	3800	21
6	26.5	391	2.04	0.8	1	639	18656	3600	21
7	29.7	391	2.13	0.8	1	666	15873	3400	18
8	33.3	391	2.22	0.8	1	694	15873	3600	20
9	36.9	391	2.30	0.8	1	719	15873	3550	20
10	40.4	391	2.37	0.8	1	741	14280	3550	17
11	43.9	391	2.44	0.8	1	762	13000	3500	17
12	47.4	391	2.50	0.8	1	782	13000	3500	18
13	50.9	391	2.56	0.8	1	800	13000	3500	18
14	54.4	391	2.61	0.8	1	817	13000	3500	19
15	57.9	391	2.67	0.8	1	833	13000	3500	19
16	61.4	391	2.72	0.8	1	849	13000	3500	19
17	64.9	391	2.76	0.8	1	863	13000	3500	20
18	68.4	391	2.81	0.8	1	877	13000	3700	21
19	72.3	391	2.85	0.8	1	892	13000	1950	11

WIND ACTION: CASE 2									
Direction X - Leeward									
Floor [-]	**Z** [m]	q_b [N/m^2]	c_e [-]	c_p [-]	c_d [-]	**p** [N/m^2]	L_{Wall} [mm]	$H_{Interp.}$ [mm]	F_x [kN]
PT	-	-	-	-	-	-	-	-	-
Basement	4.66	391	1.48	-0.4	1	-231	18656	4050	-9
1	8.10	391	1.48	-0.4	1	-231	18656	3520	-8
2	11.7	391	1.48	-0.4	1	-231	18656	3600	-8
3	15.3	391	1.65	-0.4	1	-257	18656	3600	-9
4	18.9	391	1.80	-0.4	1	-280	18656	3600	-9
5	22.5	391	1.92	-0.4	1	-300	18656	3800	-11
6	26.5	391	2.04	-0.4	1	-319	18656	3600	-11
7	29.7	391	2.13	-0.4	1	-333	15873	3400	-9
8	33.3	391	2.22	-0.4	1	-347	15873	3600	-10
9	36.9	391	2.30	-0.4	1	-359	15873	3550	-10
10	40.4	391	2.37	-0.4	1	-371	13000	3550	-8
11	43.9	391	2.44	-0.4	1	-381	13000	3500	-9
12	47.4	391	2.50	-0.4	1	-391	13000	3500	-9
13	50.9	391	2.56	-0.4	1	-400	13000	3500	-9
14	54.4	391	2.61	-0.4	1	-408	13000	3500	-9
15	57.9	391	2.67	-0.4	1	-417	13000	3500	-9
16	61.4	391	2.72	-0.4	1	-424	13000	3500	-10
17	64.9	391	2.76	-0.4	1	-432	13000	3500	-10
18	68.4	391	2.81	-0.4	1	-439	13000	3700	-11
19	72.3	391	2.85	-0.4	1	-446	13000	1950	-6

WIND ACTION: CASE 2									
Direction Y - Windward									
Floor [-]	**Z** [m]	q_b [N/m^2]	c_e [-]	c_p [-]	c_d [-]	**p** [N/m^2]	L_{Wall} [mm]	$H_{Interp.}$ [mm]	F_y [kN]
PT	-	-	-	-	-	-	-	-	-
Basement	4.66	391	1.48	0.8	1	462	49148	4050	46
1	8.1	391	1.48	0.8	1	462	49148	3520	40
2	11.7	391	1.48	0.8	1	462	49148	3600	41
3	15.3	391	1.65	0.8	1	514	49148	3600	45
4	18.9	391	1.80	0.8	1	561	49148	3600	50
5	22.5	391	1.92	0.8	1	601	49148	3800	56
6	26.5	391	2.04	0.8	1	639	47950	3600	55
7	29.7	391	2.13	0.8	1	666	47950	3400	54
8	33.3	391	2.22	0.8	1	694	47950	3600	60
9	36.9	391	2.30	0.8	1	719	47950	3550	61
10	40.4	391	2.37	0.8	1	741	14280	3550	19
11	43.9	391	2.44	0.8	1	762	14280	3500	19
12	47.4	391	2.50	0.8	1	782	14280	3500	20
13	50.9	391	2.56	0.8	1	800	14280	3500	20
14	54.4	391	2.61	0.8	1	817	14280	3500	20
15	57.9	391	2.67	0.8	1	833	14280	3500	21
16	61.4	391	2.72	0.8	1	849	14280	3500	21
17	64.9	391	2.76	0.8	1	863	14280	3500	22
18	68.4	391	2.81	0.8	1	877	14280	3700	23
19	72.3	391	2.85	0.8	1	892	14280	1950	12

WIND ACTION: CASE 2									
Direction Y - Leeward									
Floor [-]	**Z** [m]	q_b [N/m^2]	c_e [-]	c_p [-]	c_d [-]	**p** [N/m^2]	L_{Wall} [mm]	$H_{Interp.}$ [mm]	F_y [kN]
PT	-	-	-	-	-	-	-	-	-
Basement	4.66	391	1.48	-0.4	1	-231	49148	4050	-23
1	8.1	391	1.48	-0.4	1	-231	49148	3520	-20
2	11.7	391	1.48	-0.4	1	-231	49148	3600	-20
3	15.3	391	1.65	-0.4	1	-257	49148	3600	-23
4	18.9	391	1.80	-0.4	1	-280	49148	3600	-25
5	22.5	391	1.92	-0.4	1	-300	49148	3800	-28
6	26.5	391	2.04	-0.4	1	-319	47950	3600	-28
7	29.7	391	2.13	-0.4	1	-333	47950	3400	-27
8	33.3	391	2.22	-0.4	1	-347	47950	3600	-30
9	36.9	391	2.30	-0.4	1	-359	47950	3550	-31
10	40.4	391	2.37	-0.4	1	-371	14280	3550	-9
11	43.9	391	2.44	-0.4	1	-381	14280	3500	-10
12	47.4	391	2.50	-0.4	1	-391	14280	3500	-10
13	50.9	391	2.56	-0.4	1	-400	14280	3500	-10
14	54.4	391	2.61	-0.4	1	-408	14280	3500	-10
15	57.9	391	2.67	-0.4	1	-417	14280	3500	-10
16	61.4	391	2.72	-0.4	1	-424	14280	3500	-11
17	64.9	391	2.76	-0.4	1	-432	14280	3500	-11
18	68.4	391	2.81	-0.4	1	-439	14280	3700	-12
19	72.3	391	2.85	-0.4	1	-446	14280	1950	-6

C.2 Sanpaolo Skyscraper

C.2.1 Definition of the design spectrum

In order to define the design spectrum,useful for performing the equivalent static analysis 4.5.6, it is necessary to refer to the NTC18 standard. In particular, the calculation programme *"Spettri-NTC ver.1.0.3"*, provided by the regulations, was used.

This program considers the microzonation of the national territory, as represented by the seismic hazard map provided by the National Institute of Geophysics and Volcanology (Figure C.1).

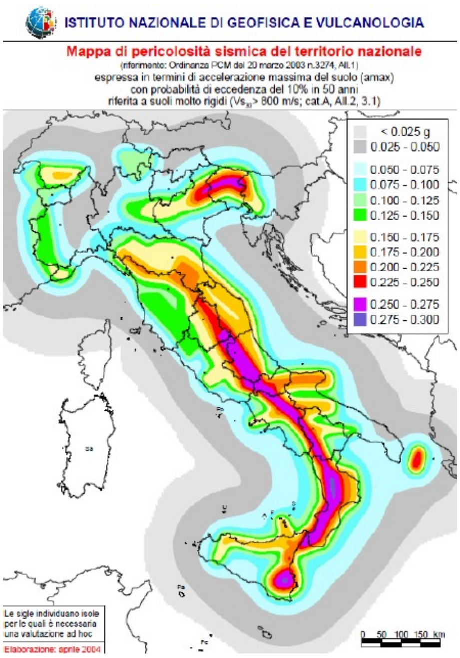

Figure C.1: Seismic hazard map provided by the National Institute of Geophysics and Volcanology

Starting from the building site, the fundamental parameters for defining the response spectrum are obtained by reference to the seismic hazard map. In particular, the parameters are given:

- a_g maximum horizontal acceleration at the site;
- F_0 maximum value of the amplification factor of the spectrum in horizontal acceleration;
- T_C^* reference value for determining the start period of the constant velocity portion of the spectrum in horizontal acceleration.

In the case studied, the parameters obtained by varying the return period are shown in Table C.1.

$\mathbf{T_R}$ [years]	$\mathbf{a_g}$ [g]	$\mathbf{F_0}$ [-]	$\mathbf{T_c^*}$ [s]
30	0.023	2.587	0.177
50	0.029	2.592	0.194
72	0.032	2.630	0.209
101	0.036	2.655	0.220
140	0.039	2.674	0.229
201	0.044	2.688	0.245
475	0.055	2.760	0.272
975	0.065	2.811	0.287
2475	0.079	2.911	0.292

Table C.1: Foundamental parameters by varying the return period

Then, by defining the nominal service life V_N of the structure and the service life coefficient c_U, a return period T_R of 100 years could be obtained. Based on the probability of exceeding the maximum acceleration value a_g in the reference period V_R, the return periods for all limit states were derived (Table C.2).

Limit state	$\mathbf{P_{VR}}$ [-]	$\mathbf{T_R}$ [years]	$\mathbf{a_g}$ [g]	$\mathbf{F_0}$ [-]	$\mathbf{T_c^*}$ [s]
SLO	81%	60	0.030	2.611	0.202
SLD	63%	101	0.036	2.655	0.220
SLV	10%	949	0.064	2.809	0.287
SLC	5%	1950	0.075	2.885	0.290

Table C.2: Foundamental parameters by varying the return period

Finally, the subsoil class, the topographic category and the structure factor are introduced, which in this case are

- Subsoil class: A
- Topographic category: 1 (flat terrain)
- Structure factor: 1

The design spectrum for all limit states is thus derived (Figure C.2).

From this graph, it would be necessary to consider the value that the design

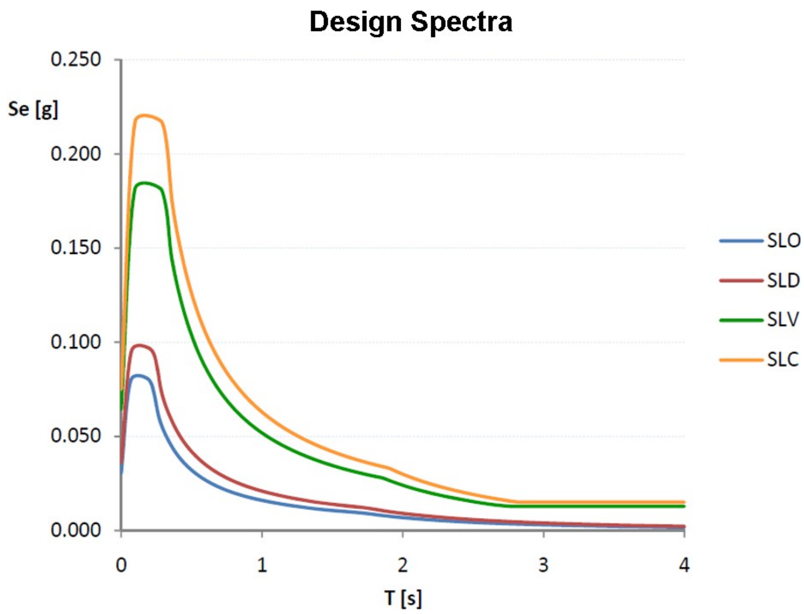

Figure C.2: Design spectra for all limit states

spectrum assumes at the proper period, but since in this case the periods are greater than 4 seconds, the spectral acceleration is evaluated using formula 3.2.10 (NTC18, §3.2.3):

$$S_{De} = S_e(T)\left[\frac{T}{2\pi}\right]^2$$

Solving this equation for the X-direction and Y-direction gives:

$$S_d(T_1) = 0.196\ m/s^2$$

for both forces F_X and forces F_Y.

Finally, applying the equation

$$F_i = F_h \cdot \frac{z_i W_i}{\sum_j z_j W_j}$$

$$F_h = S_d(T_1) \cdot \lambda \cdot W/g$$

it is possible to derive the equivalent static forces.

References

[1] M. Biraghi. *Storia dell'architettura contemporanea II 1945-2023*. Einaudi, 2023.

[2] M. Capurso. "Sul calcolo dei sistemi spaziali di controventamento". In: *Giornale del Genio Civile* (1981).

[3] M. Capurso. "Sul calcolo delle travi in parete sottile in presenza di forze e distorsioni". In: *La Ricerca Scientifica* 6 (1964).

[4] A. Carpinteri. *Advanced structural mechanics*. CRC Press, 2019, pp. 293–319.

[5] A. Carpinteri, Lacidogna G., and S. Cammarano. "Structural analysis of high-rise buildings under horizontal loads: A study on the Intesa Sanpaolo Tower in Turin". In: *Engineering Structures* (2013).

[6] A. Carpinteri, G. Lacidogna, and S. Cammarano. "Conceptual design of tall and unconventionally shaped structures: A handy analytical method". In: *Advances in Structural Engineering* (2014), pp. 757–773.

[7] A. Carpinteri, G. Lacidogna, and G. Nitti. "Open and closed shearwalls in high-rise structural systems: Static and dynamic analysis". In: *Curved Layer. Struct.* (2016), pp. 154–171.

[8] A. Carpinteri, G. Lacidogna, and S. Puzzi. "A global approach for three dimensional analysis of tall buildings". In: *The Structural Design of Tall and Special Buildings* (2010), pp. 518–536.

[9] A. Carpinteri, G. Lacidogna, and S. Puzzi. "A global approach for three-dimensional analysis of tall buildings". In: *The Structural Design of Tall and Special Buildings* (2010).

[10] A. Carpinteri et al. "Lateral load effects on tall shear wall structures of different height". In: *Structural Engineering and Mechanics* (2012), pp. 313–337.

[11] A. Carpinteri et al. "The effect of the warping deformation on the structural behaviour of thin-walled open section shear walls". In: *Thin-Walled Structures* (2014), pp. 335–343.

[12] A. K. Chopra. *Dynamics of structures theory and applications to earthquake engineering*. Prentice Hall, 2014.

[13] M. De Santis. “Verifica statica e cinematica di edifici di grande altezza: Il caso della Torre Reale Mutua in Torino”. Tesi di Laurea Magistrale. Politecnico di Torino, 2017.

[14] G. Faraggiana. *In Fondo Alle Vie Di Torino*. Editris2000, 2005.

[15] M. Fiammingo. “Analisi statica e dinamica degli edifici di grande altezza: Il grattacielo della RAI in Torino”. Tesi di Laurea Magistrale. Politecnico di Torino, 2020.

[18] Società degli Ingegneri e degli Architetti in Torino, ed. *A & RT LXI n.1 - Vicende e dibattiti torinesi* (2007).

[19] Società degli Ingegneri e degli Architetti in Torino, ed. *A & RT LXIV n.3 - Torino verticale* (2010).

[20] G. Lacidogna. “Tall buildings: Secondary effects on the structural behaviour”. In: *Proc. Inst. Civ. Eng. - Struct. Build.* (2017), pp. 391–405.

[21] A. Melis de Villa. “Concorso per il secondo tratto di via Roma in Torino”. In: *L’Architettura Italiana* (1934).

[22] A. Melis de Villa and G. Bernocco. “Ricostruzione dell’isolato di San Emanuele in Via Roma a Torino”. In: *L’Architettura Italiana* (1935).

[23] M. Mezzina. *Fondamenti di tecnica delle costruzioni*. CittàStudi, 2013.

[24] G. Montanari. “Privatizzare il cielo? L’inserimento di edifici alti nel paesaggio urbano storico: il caso di Torino”. In: *Géocarrefour* (2017).

[25] D. Morelli. *Un nuovo palazzo a Torino. La sede della Rai in via Cernaia.* Edizioni G & P, 1968.

[26] G. Nitti, G. Lacidogna, and A. Carpinteri. “Structural Analysis of High-rise Buildings under Horizontal Loads: A Study on the Piedmont Region Headquarters Tower in Turin”. In: *The Open Construction and Building Technology Journal* (2019).

[27] S. Pace. *L’altra torre. Concezione strutturale, architettura e città nell’edificio in corso Francia a Torino (BBPR, Gian Franco Fasana, Giulio Pizzetti: 1955-1959). La concezione strutturale. Ingegneria e architettura in Italia negli anni cinquanta e sessanta.* Allemandi, 2013.

[28] E. J. Paganone. “Ripartizione delle azioni orizzontali negli edifici alti: il grattacielo Intesa San Paolo di Torino”. Tesi di Laurea Magistrale. Politecnico di Torino, 2012.

[30] B. Stafford Smith and A. Coull. *Tall buildings structures: analysis and design*. John Wiley & Sons, 1991.

[31] M. Taggio. "Analisi statica e dinamica degli edifici di grande altezza: La Torre "BBPR" di Piazza Statuto in Torino". Tesi di Laurea Magistrale. Politecnico di Torino, 2020.

[32] B. S. Taranath. *Structural analysis and design of tall buildings*. CRC Press, 1988.

[33] D. Vigorita. "Analisi statica e dinamica dellatorre per i nuovi uffici della Regione Piemonte". Tesi di Laurea Magistrale. Politecnico di Torino, 2016.

[34] V.Z. Vlasov. *Thin-walled Elastic Beams*. National Technical Information Service, 1984.

Sitography

[16] *Geoportale del Comune di Torino*. URL: `http://geoportale.comune.torino.it/web/` (visited on 12/11/2024).

[17] *Il Palazzo della Regione Piemonte*. URL: `https://www.regione.piemonte.it/web/amministrazione/organizzazione/palazzo-della-regione-piemonte` (visited on 11/30/2024).

[29] M. Perello and V. Turini. *Il Grattacielo Intesa Sanpaolo: il progetto e la sua ecosostenibilità*. 2018. URL: `https://www.ingenio-web.it/articoli/il-grattacielo-intesa-sanpaolo-il-progetto-e-la-sua-ecosostenibilita/` (visited on 11/20/2024).